Seasonal Predictability of North American Coastal Extratropical Storm Activity during the Cold Months

by

Katherine A. Pingree-Shippee
B.Sc., Plymouth State University, 2008
M.Sc., University of Maine, Orono, 2010

A Dissertation Submitted in Partial Fulfillment
of the Requirements for the Degree of

DOCTOR OF PHILOSOPHY

in the Department of Geography

Supervisory Committee

Seasonal Predictability of North American Coastal Extratropical Storm Activity during the Cold Months

by

Katherine A. Pingree-Shippee
B.Sc., Plymouth State University, 2008
M.Sc., University of Maine, Orono, 2010

Supervisory Committee

Dr. David Atkinson (Department of Geography)
Co-Supervisor

Dr. Francis Zwiers (Department of Mathematics and Statistics)
Co-Supervisor; Outside Member

Dr. Maycira Costa (Department of Geography)
Departmental Member

Abstract

Supervisory Committee
Dr. David Atkinson (Department of Geography)
Co-Supervisor
Dr. Francis Zwiers (Department of Mathematics and Statistics)
Co-Supervisor; Outside Member
Dr. Maycira Costa (Department of Geography)
Departmental Member

Extratropical cyclones (ETCs) are major features of the weather in the mid- and high-latitudes and are often associated with hazardous conditions such as heavy precipitation, high winds, blizzard conditions, and flooding. Additionally, severe coastal damage and major local impacts, including inundation and erosion, can result from high waves and storm surge due to cyclone interaction with the ocean. Consequently, ETCs can have serious detrimental socio-economic impacts. The west and east coasts of North America are strongly influenced by ETC storm activity. These coastal regions are also host to many land-based, coastal, and maritime socio-economic sectors, all of which can experience strong adverse impacts from extratropical storm activity. Society would therefore benefit if variations in ETC storm activity could be predicted skilfully for the upcoming season. Skilful prediction would enable affected sectors to better anticipate, prepare for, manage, and respond to variations in storm activity and the associated risks.

The overall objective of this dissertation is to determine the seasonal predictability of North American coastal extratropical storm activity during the cold months (3-month rolling seasons – OND, NDJ, DJF, JFM – during which storm activity is most frequent and intense) using Environment and Climate Change Canada's Canadian

Seasonal to Interannual Prediction System (CanSIPS). This dissertation describes research focused on three themes: 1.) reanalysis representation of North American coastal storm activity, 2.) potential predictability of storm activity and climate signal-storm activity relationships for the North American coastal regions, and 3.) seasonal prediction of storm activity in CanSIPS.

Research Theme 1 evaluates six global reanalysis datasets to determine which best reproduces observed storm activity in the North American coastal regions, annually and seasonally, during the 1979-2010 time period using single-station surface pressure-based proxies; ERA-Interim is found to perform best overall.

Research Theme 2, using ERA-Interim, investigates the potential predictability of extratropical storm activity (represented by mean sea level pressure [MSLP], absolute pressure tendency, and 10-m wind speed) during the 1979-2015 time period using analysis of variance. The detected potential predictability provides observation-based evidence showing that it may be possible to predict storm activity on the seasonal timescale. Additionally, using composite analysis, the El Niño-Southern Oscillation, Pacific Decadal Oscillation, and North Atlantic Oscillation are identified as possible sources of predictability in the North American coastal regions. Research Theme 2 provides a basis upon which seasonal forecasting of extratropical storm activity can be developed.

Research Theme 3 investigates the seasonal prediction of North American coastal storm activity using the CanSIPS multi-model ensemble mean hindcasts (1981-2010). Quantitative deterministic, categorical deterministic, and categorical probabilistic forecasts are constructed using the three equiprobable category framework (below-, near-,

and above-normal conditions) and the parametric Gaussian method for determining probabilities. These forecasts are then evaluated against ERA-Interim using the correlation skill score, percent correct score, and Brier skill score to determine forecast skill. Baseline forecast skill is found for the seasonal forecasts of all three storm activity proxies, with MSLP forecasts found to be most skilful and 10-m wind speed forecasts the least skilful. Skilful seasonal forecasting of North American coastal extratropical storm activity is, therefore, possible in CanSIPS.

Table of Contents

List of Tables

List of Figures

Acknowledgements

This research project was funded by the Marine Environmental Observation Prediction and Response (MEOPAR) Network of the Centres of Excellence of Canada, subproject 2.1.2 “Coastal Storm Activity”, PI Francis Zwiers, under Project 2.1 “Climate Change and Extreme Events in the Marine Environment”, PIs Greg Flato, Gordon McBean, Bill Merryfield, Barbara Neis, Ronald Pelot, Jinyu Sheng, and Francis Zwiers. Additional support was provided by the Pacific Climate Impacts Consortium (PCIC) and the University of Victoria’s Department of Geography. Thank you in particular to PCIC for the continued funding as I completed my degree.

Thank you to my co-supervisors, Francis and David, for giving me this PhD opportunity and for taking me on as a student. Thank you both for making me a better researcher, writer, and scientist in general. Thank you David for helping me with programming. Thank you both for all you’ve done over the years, both big and small, as I worked my way to the finish line.

Thank you Maycira for being a committee member and for your support and encouragement throughout the PhD process. Thank you Barbara Casati for being the external examiner and for your amazingly thorough evaluation of the dissertation. Your comments, suggestions, and feedback are invaluable and will help make the manuscripts stronger.

Thank you to everyone at PCIC and PICS for being so welcoming and for your support and encouragement over the years. There was no better preparation for a conference than presenting in front of the members of PCIC. Thank you to everyone in

the Geography Climate Lab and other fellow Geographers Mikaela, Mike, Will, Brandi, Rob, Bryan, Shannon, and others who I'm sure I'm forgetting for your camaraderie.

Thank you to my family, the Pingrees, Shippees, and extended family members, for all your love and support as I completed this PhD adventure. Thank you also to those who have become family over the years, especially Kelly, Brian, and Matt. It's been quite the journey and I'm so thankful for your support along the way. Thanks as well for your visits, it was awesome getting to really go exploring from time to time and truly get a chance to take a break from my work and recharge the mental batteries. And to the Atkinsons, our 'Victoria family', I can't thank you enough for everything you've done for us over the years.

Lastly, very special thanks to Norman, Denali, and BeeBee. It's been quite the journey getting to this point and I'm so thankful to have had you by my side. I love you. On to the next adventure!

Dedication

To Norman, Denali, and BeeBee

and

To my family, for their love and support throughout this PhD adventure.

To Mary Ann.

To all those who have seen potential in me and encouraged me throughout the years,

including (but not limited to) David Smith, Carol Phillips, Daniel Dowe,

Eric Hoffman, Lourdes Aviles, Lisa Doner, Peter Koons, and

David and Francis.

And to M.

1.0 Introduction

Extratropical cyclones (ETCs) play a key role in global atmospheric circulation by transporting heat, moisture, and momentum from the subtropics poleward. ETCs are also major features of the weather in the mid- and high-latitudes, often governing regional patterns of cloud cover, precipitation, and winds. While distinct from tropical cyclones (e.g., hurricanes), mid-latitude cyclones can be as hazardous and damaging. ETCs are frequently associated with hazardous conditions such as heavy precipitation, high winds, blizzard conditions, and flooding. Additionally, severe coastal damage and major local impacts, including inundation and erosion, can result from high waves and storm surge caused by storm interaction with the ocean. Consequently, ETCs can have serious detrimental socio-economic impacts. The west and east coasts of North America are both strongly influenced by ETC storm activity, with the west coast influenced by the North Pacific storm track and atmospheric river events while the east coast is particularly influenced by winter storms following two favoured tracks, the St. Lawrence Valley and the Eastern Seaboard. The North American west and east coastal regions are also host to many socio-economic sectors, including land and marine transportation, aviation, agriculture and fisheries, and the built environment (e.g., infrastructure), all of which can experience strong adverse impacts from ETC storm activity. North American society would therefore benefit substantially if risks associated with seasonal variations in ETC storm activity along the west and east coasts could be skilfully predicted well in advance. Skilful prediction on the seasonal (or longer) timescale would enable affected sectors to

better anticipate, prepare for, manage, and respond to variations in storm activity and the associated risks and impacts.

1.1 Current Operational Seasonal Forecasting

Long-term (seasonal to interannual) patterns and fluctuations in atmospheric variables (e.g., average temperature, total precipitation, and storm track location) are known to be associated with slowly varying large-scale climate signals (i.e., large-scale modes of variability and their teleconnections), such as the El Niño-Southern Oscillation (ENSO), the Pacific Decadal Oscillation (PDO), and the North Atlantic Oscillation (NAO) (Stockdale et al., 2010; Doblas-Reyes et al., 2013). A growing body of research further indicates that several of these teleconnection patterns are predictable on seasonal or longer timescales. At present, ENSO is the most predictable teleconnection, with useful skill at lead times up to 6-12 months (Chen and Cane, 2008; Barnston et al., 2012; Merryfield et al., 2013), and serves as the primary source of seasonal to interannual predictability in operational seasonal forecasting (Stockdale et al. 2010; Doblas-Reyes et al. 2013). Other teleconnections, such as the NAO and PDO, are more regional in extent and have predictive potential on the seasonal timescale (Alexander et al., 2008; Wen et al., 2012; Scaife et al., 2014; Smith et al., 2014; Athanasiadis et al., 2017).

Current operational seasonal forecasting is primarily focused on near surface temperature and total precipitation, producing categorical deterministic and probabilistic forecasts of the likelihood of below-, near-, and above-normal conditions for the upcoming seasons (Stockdale et al., 2010; Doblas-Reyes et al., 2013). Seasonal forecasting is most skilful in the tropics (Stockdale et al. 2010; Doblas-Reyes et al. 2013) since low frequency variability from ENSO and other coupled air-sea interactions forms a

relatively larger fraction of total climate variability in this region than elsewhere. Forecast skill for North America, although often lower due to its mid- to high-latitude location, is also known to originate from coupled air-sea interactions and through teleconnections such as ENSO, PDO, and NAO (Stockdale et al. 2010; Doblas-Reyes et al. 2013).

1.2 Support for Seasonal Predictability of Extratropical Storm Activity

The useful skill of deterministic day-to-day atmospheric variation forecasts (i.e., daily weather and the occurrence of individual storms) is limited to approximately two weeks due to the chaotic nature of the atmosphere. It may be possible, however, to create categorical forecasts of storm activity variability on seasonal (or longer) time scales as storm characteristics (e.g., storm track location and storm intensity) are also known to be associated with teleconnections such as ENSO, PDO, and NAO (Eichler and Higgins 2006; Wang et al. 2006; Lareau and Horel, 2012; Gan and Wu 2013; Grise et al. 2013; Gómara et al. 2016; Kim et al. 2017).

Research performed to date further supports the premise that there is the potential to predict seasonal variations in ETC storm activity. Various studies have investigated the potential predictability of Northern Hemisphere extratropical storm activity at various tropospheric levels (e.g., sea level pressure and 500-hPa geopotential heights) on the monthly or seasonal timescale. Potential predictability investigations identify where the observed year-to-year variance in storm activity exceeds the variability present due to weather noise (i.e., day-to-day weather fluctuations). Any variability in excess of the unpredictable weather noise variability is considered potentially predictable (Madden,

1976). Seminal studies, such as Madden (1976) and Shukla and Gutzler (1983), found potential predictability of monthly mean sea level pressure and monthly mean 500-hPa geopotential heights, respectively, in the extratropics, with the strongest potentially predictable signals found in areas of climatological cyclogenesis (e.g., Kuroshio Current and along the North American east coast). Subsequent studies have found similar patterns of potential predictability on the monthly to seasonal timescales (Zwiers, 1987; Rowell, 1998; Zheng et al., 2000; Hodson and Sutton, 2008).

Studies investigating actual predictability of ETC storm activity, though limited, further support the possibility of extending current seasonal forecasting to include the skilful prediction of ETC storm activity variability. Compo and Sardeshmukh (2004) investigated the predictability of wintertime (JFM) sea surface temperature (SST) forced Northern Hemisphere extratropical storm tracks, with specific focus on the Pacific-North American and North Atlantic-European regions. A multiple linear regression-based "storm track model" trained on atmospheric general circulation model (AGCM)-generated storm track data (consisting of 540 integrations) was used to predict the storm track characteristics associated with the variations in SSTs related to ENSO forcing. Storm tracks in the 500-hPa geopotential height field were defined using the 500-hPa omega (vertical velocity) variance with a 2-7 day bandpass filter. The impact of SST changes on the atmospheric circulation were characterized by the resulting anomalous 200-hPa geopotential height mean flow. Evaluating two winters with modest ENSO SST-forcing, 1987 (El Niño) and 1989 (La Niña), a correlation of 0.9 was obtained between the storm track signal predicted by the linear model and the AGCM-generated 60-member ensemble mean storm track anomalies, indicating success of the empirical storm

track model. Additionally, reasonable correlations (0.4-0.7+) were noted for the 1950-1999 time period in the eastern Pacific, North American, and western Atlantic regions, with a predictable SST-forced storm track signal (on average, "modest" in strength) found for many winters. Years with stronger ENSO signals (i.e., strong El Niño or La Niña events) possessed greater correlation. Compo and Sardeshmukh concluded that the prediction skill of storm track variations is high enough in the Pacific-North American region to be of practical use.

Recently, Yang et al. (2015) investigated the seasonal predictability of extratropical storm tracks in the Geophysical Fluid Dynamics Laboratory (GFDL) high-resolution climate prediction model. Yang et al. defined storm tracks using the seasonal standard deviation of the 24-hr sea level pressure tendency. The average predictability time (APT) optimization method (DelSole and Tippett, 2009a; 2009b) (similar to Empirical Orthogonal Function analysis but patterns are optimized to maximize a predictability metric rather than variance) was applied to a 12-member ensemble seasonal hindcast covering 1982-2014 to identify the predictable patterns of storm tracks. The leading pattern, observable up to 9 months ahead, was found to be strongly related to the ENSO signal, consistent with Compo and Sardeshmukh (2004). Yang et al. also investigated the predictability of extremes (1^{st} and 99^{th} percentiles) by examining how the width of the statistical distribution for selected meteorological variables (wintertime [DJF] sea level pressure, temperature, wind, and precipitation) over North America changes in concert with the ENSO pattern, which also yielded positive results.

Additional studies that have investigated the seasonal predictability of storm activity have focused on specific storm events and/or geographical regions. For example,

Renggli et al. (2011) investigated seasonal predictability of wintertime windstorm frequency in the North Atlantic-European region. Small but statistically significant skill was found both for the December-February and January-April intervals, though lower skill was observed in the January-April interval due to longer lead time. Predictive skill of individual seasons was also found to be related to windstorm frequency, as winters with a higher frequency of windstorms had higher predictive skill. Nevertheless, Renggli et al. report that the predictive skill is "comparatively high and even suggests an economic usability."

1.3 Research Project

The overall objective of this research project is to determine the seasonal predictability of North American coastal extratropical storm activity during the cold months (3-month rolling seasons – OND, NDJ, DJF, and JFM – during which storm activity is most frequent and intense) using Environment and Climate Change Canada's operational Canadian Seasonal to Interannual Prediction System (CanSIPS) (Merryfield et al., 2013), and to develop methods that could be used operationally to produce seasonal storm activity forecasts. To do this, the following research questions (grouped into three research themes) are posed:

1. *Reanalysis Representation of North American Coastal Storm Activity*
    1.1. Which global reanalysis dataset best represents North American coastal storm activity?

2. *Potential Predictability of Storm Activity and Climate Signal-Storm Activity Relationships for the North American Coastal Regions During the Cold Seasons*

    2.1. Is North American coastal storm activity potentially predictable on the seasonal timescale?

    2.2. What are the relationships between large-scale modes of climate variability and North American coastal storm activity on the seasonal timescale?

3. *Seasonal Prediction using the Canadian Seasonal to Interannual Prediction System: Can the potential predictability of North American coastal storm activity during the cold seasons be realized within the CanSIPS dynamical forecasting system?*

    3.1. Are observed North American coastal climate signal-storm activity relationships reproduced in CanSIPS?

    3.2. How can CanSIPS be used to produce seasonal forecasts of North American coastal storm activity?

    3.3. What is the skill of the seasonal forecasts of North American coastal storm activity that can be produced using CanSIPS?

Various global atmospheric datasets, termed *reanalyses*, are examined to determine which best reproduces observed storm activity in the North American coastal regions (Question 1.1). The identified reanalysis is then used conjointly with hindcasts ("forecasts" of past seasons based on initial conditions observed prior to those seasons) from CanSIPS to investigate the potential predictability of North American coastal storm

activity, climate signal-storm activity relationships, and, ultimately, the predictability of storm activity at the seasonal timescale in CanSIPS. Potential predictability of North American coastal storm activity is investigated using the selected reanalysis to provide observation-based evidence indicative of whether it may be possible to predict storm activity on the seasonal timescale (Question 2.1). The identified reanalysis is also used to investigate the relationships between large-scale modes of variability (climate signals) and storm activity to identify possible sources (origins) of the detected potential predictability (Question 2.2). It is then determined how well CanSIPS reproduces these observed modes of variability and climate signal-storm activity relationships (Question 3.1). These climate signal-storm activity relationships provide a basis upon which categorical deterministic and probabilistic seasonal forecasts (below-, near-, and above-normal conditions) can be constructed from the CanSIPS hindcasts (Question 3.2). The seasonal forecasts are evaluated against the identified reanalysis, representative of the true state of the atmosphere, to determine forecast skill and whether that skill is sufficiently high (i.e., if the skill exceeds the climatological forecast, a purely random "chance" forecast that would be, on average, 33.3% correct when using the three equiprobable category framework) to be useful to end-users (Question 3.3).

1.3.1 Canadian Seasonal to Interannual Prediction System (CanSIPS)

CanSIPS is an advanced, one-tier, multi-model seasonal forecasting system that simultaneously forecasts the evolution of the atmosphere and the ocean (Merryfield et al., 2013). It is used operationally at the Canadian Meteorological Centre (CMC) to produce an ensemble of seasonal forecasts that, in turn, are used to make categorical deterministic and probabilistic predictions of the likelihood of below-, near-, and above-normal

seasonal mean temperature and precipitation conditions during the coming seasons (seasonal forecasts at 0-, 1-, 3-, 6-, and 9-month leads). CMC issues CanSIPS-based seasonal forecasts for Canada on a monthly basis. The historical forecast skill of CanSIPS is commensurate with that of its peers (Merryfield et al., 2013). Furthermore, CanSIPS also contributes data to the North American Multimodel Ensemble seasonal forecasting system (Kirtman et al., 2014) and the Climate-system Historical Forecast Project (Tompkins et al., 2017). CanSIPS is supported by the Canadian Centre for Climate Modelling and Analysis (CCCma), a Canadian federal research unit located at the University of Victoria. The extensive collection of hindcasts that is available from CanSIPS, covering the period 1981-2010, provides an excellent basis for the evaluation of the seasonal predictability of storm activity.

1.3.2 North American Coastal Study Domains

The study domains cover substantial portions of the North American west and east coastal regions (Figure 1.1). For Research Theme 1, the study domains encompass the mid-to-high latitude portions of the North American coastal regions (west coast domain: 40°N-60°N, 120°W -140°W; east coast domain: 40°N-65°N, 45°W-75°W). These domains are expanded for Research Themes 2 and 3, to cover the majority of the non-Arctic US and Canadian coastal regions (west coast domain: 30°N-60°N, 115°W-140°W; east coast domain: 25°N-65°N, 50°W-85°W). While used operationally by the Canadian Meteorological Centre to issue public seasonal forecasts only for Canada, CanSIPS is a global prediction system (the reanalyses investigated in Research Theme 1 are also global). This, therefore, allows potential predictability, climate signal-storm activity relationships, and seasonal predictability to be investigated (in Research Themes 2 and 3)

over a broader domain and also allows forecast skill for Canada to be placed into context with regard to North America. Although operational seasonal forecasts are issued Canada-wide and the storm activity seasonal prediction methodology investigated in this project could be expanded to include all of Canada, focus is placed on the coastal regions, which are strongly influenced by extratropical storm activity and are highly populated, socio-economically key, and environmentally sensitive areas.

1.3.3 Extratropical Storm Activity Proxies

Extratropical cyclones (ETCs) are complex features that cannot be summarized with a single variable. Numerous variables have therefore been used to characterize ETCs and extratropical storm activity (e.g., storm tracks), including mean sea level pressure (MSLP) and pressure tendency (the change in pressure [amount and direction] over a specific time interval), relative vorticity (typically at 850-hPa), 500-hPa geopotential heights, and wind speeds (near-surface and aloft) (Compo and Sardeshmukh 2004; Wang et al. 2006; Renggli et al. 2011; Krueger and von Storch 2012; Gan and Wu 2013; Neu et al. 2013; Yang et al. 2015). Analyzing variables at different atmospheric levels, such as MSLP along with 500-hPa geopotential heights and 300-hPa winds, would provide insight into extratropical storm activity throughout the vertical structure of the troposphere. Nevertheless, the majority of end-users would, arguably, be most interested in seasonal forecasts at or near the surface, where the impacts of storm activity are primarily felt. At and near the surface, ETCs still cannot be defined using a single proxy and different end-users put more weight on different proxies. For instance, for fisheries in the North Atlantic, the Laplacian of pressure (representative of a cyclone's intensity) and 10-m wind speed were found to be key factors in maritime incidents (Rezaee et al., 2016)

while tug-and-barge operations in the North Pacific and into the Arctic are primarily focused on 10-m wind speeds (Shippee, 2016).

This research project, therefore, utilizes three variables at or near the surface as proxies to represent extratropical storm activity – MSLP, absolute pressure tendency (ΔMSLP), and 10-m wind speeds. An advantage of these proxies is that they are continuous in space and time, which can simplify analysis in comparison to proxies that are event based. Additionally, information on storm activity characteristics such as frequency and intensity can be derived from these proxies. Since changes in the seasonal mean MSLP are expected to correspond to changes in the number of storms and/or duration of stormy conditions, variations in seasonal mean MSLP provide information on the frequency and/or persistence of storm activity. Alternatively, since changes in the seasonal mean ΔMSLP and 10-m wind speed would be expected to correspond to changes in the strength of storminess (e.g., enhanced cyclogenesis and/or stronger pressure gradients), variations in seasonal mean ΔMSLP and 10-m wind speed provide information on the intensity of storm activity.

1.3.4 Large-scale Climate Signals

Three large-scale climate signals (teleconnections) known to be strongly associated with extratropical storm activity in the Northern Hemisphere are utilized in this study (Research Question 2.2. investigating possible sources of detected ETC storm activity potential predictability): the El Niño-Southern Oscillation (ENSO; Philander, 1983), the Pacific Decadal Oscillation (PDO; Mantua and Hare, 2002), and the North Atlantic Oscillation (NAO; Hurrell et al., 2001). Established climate indices are used to characterize the fluctuations and strength of these teleconnections. In this study, the

Southern Oscillation (SO; Walker, 1924; Bjerknes, 1966;1969) Index (Trenberth, 1984; Ropelewski and Jones, 1987) is used to represent ENSO. Descriptions of these teleconnections and their relationships to extratropical storm activity variability are provided in Chapter 2.

The remainder of this dissertation is divided as follows: Background on extratropical storm activity, reanalysis datasets, and the large-scale climate signals used in this research are provided in Chapter 2. Chapters 3, 4, and 6 are three independent manuscripts presenting the research completed for each Research Theme, respectively:

Chapter 3: "Representation of Mid-latitude North American Coastal Storm Activity by Six Global Reanalyses" [Research Theme 1]

Chapter 4: "Cold Season Extratropical Storm Activity Potential Predictability and its Sources in the Northern Hemisphere with Focus on the North American Coastal Regions" [Research Theme 2]

Chapter 6: " Seasonal Prediction Skill of North American Coastal Storm Activity during the Cold Months of the Canadian Seasonal to Interannual Prediction System (CanSIPS)" [Research Theme 3]

Results from Research Question 3.1 are presented in Chapter 5: "Reproduction of Observed North American Coastal Climate Signal-Storm Activity Relationships in CanSIPS". The overall results of this dissertation are presented in Chapter 7. Additional figures, tables, and supporting information not presented in the manuscripts are provided in the Appendices:

Appendix A: "Additional Research Theme 1 Figures and Tables"

Appendix B: “Additional Research Theme 2 Figures”

Appendix C: “Additional Research Theme 3 Figures and Seasonal Prediction Skill of CanCM3 and CanCM4”

1.4 References

Alexander, M.A., Matrosova, L., Penland, C., Scott, J.D., and Chang, P. (2008) Forecasting Pacific SSTs: Linear Inverse Model Predictions of the PDO. *J. Climate*, 21(2): 385-402.

Athanasiadis, P.J., Bellucci, A., Scaife, A.A., Hermanson, L., Materia, S., Sanna, A., Borrelli, A., MacLachlan, C., and Gualdi, S. (2017) A Multisystem View of Wintertime NAO Seasonal Predications. *J. Climate*, 30(4): 1461-1475.

Barnston, A.G., Tippett, M.K., L’Heureux, M.L., Li, S., and DeWitt, D.G. (2012) Skill of real-time seasonal ENSO model predictions during 2002-11: Is Out Capability Increasing? *Bull. Am. Meteorol. Soc.*, 93(5): 631-651.

Bjerknes, J. (1966) A possible response of the atmospheric Hadley circulation to equatorial anomalies of ocean temperature. *Tellus*, 18(4): 820-829.

Bjerknes, J. (1969) Atmospheric teleconnections from the equatorial Pacific. *Mon. Weather Rev.*, 97(3): 163-172.

Chen, D. and Cane, M.A. (2008) El Niño prediction and predictability. *J. Comput. Phys*., 227(7): 3625-3640.

Compo, G.P. and Sardeshmukh, P.D. (2004) Storm Track Predictability on Seasonal and Decadal Scales. *J. Climate*, 17(19): 3701-3720.

DelSole, T. and Tippett, M.K. (2009a) Average Predictability Time. Part I: Theory. *J. Atmos. Sci.*, 66(5): 1172-1187.

DelSole, T. and Tippett, M.K. (2009b) Average Predictability Time. Part II: Seamless Diagnoses of Predictability on Multiple Time Scales. *J. Atmos. Sci.*, 66(5): 1188-1204.

Doblas-Reyes, F.J., García-Serrano, J., Lienert, F., Biescas, A.P., and Rodrigues, L.R.L. (2013) Seasonal climate predictability and forecasting: status and prospects. *WIREs Clim. Change*, 4(4): 245-268.

Eichler, T. and Higgins, W. (2006) Climatology and ENSO-Related Variability of North American Extratropical Cyclone Activity. *J. Climate*, 19(10): 2076-2093.

Gan, B. and Wu, L. (2013) Seasonal and Long-Term Coupling between Wintertime Storm Tracks and Sea Surface Temperature in the North Pacific. *J. Climate*, 26(16): 6123-6136.

Gómara, I., Rodríguez-Fonseca, B., Zurita-Gotor, P., Ulbrich, S., and Pinto, J.G. (2016) Abrupt transitions in the NAO control of explosive North Atlantic cyclone development. *Clim. Dyn.*, 47(9-10): 3091-3111.

Grise, K.M., Son, S., and Gyakum, J.R. (2013) Intraseasonal and Interannual Variability in North American Storm Tracks and Its Relationship to Equatorial Pacific Variability. *Mon. Weather Rev.*, 141(10): 3610-3625.

Hodson, D.L.R. and Sutton, R.T. (2008) Exploring multi-model atmospheric GCM ensembles with ANOVA. *Clim. Dyn.*, 31(7-8): 973-986.

Hurrell, J.W., Kushnir, Y., and Visbeck, M. (2001) The North Atlantic Oscillation. *Science*, 291(5504): 603-605.

Kim, H.-M., Zhou, Y., and Alexander, M.A. (2017) Changes in atmospheric rivers and moisture transport over the Northeast Pacific and western North America in response to ENSO diversity. *Clim Dyn.*, doi: 10.1007/s00382-017-3598-9

Kirtman, B.P., Min, D., Infanti, J.M., Kinter III, J.L., Paolino, D.A., Zhang, Q., van den Dool, H., Saha, S., Pena Mendez, M., Becker, E., Peng, P., Tripp, P., Huang, J., DeWitt, D.G., Tippett, M.K., Barnston, A.G., Li, S., Rosati, A., Schubert, S.D., Rienecker, M., Suarez, M., Li, Z.E., Marshak, J., Lim, Y.-K., Tribbia, J., Pegion, K., Merryfield, W.J., Denis, B., and Wood, E.F. (2014) The North American Multimodel Ensemble: Phase-I Seasonal-to-Interannual Prediction; Phase-2 toward Developing Intraseasonal Prediction. *Bull. Am. Meteorol. Soc.*, 95(4): 585-601.

Krueger, O. and von Storch, H. (2012) The Informational Value of Pressure-Based Single-Station Proxies for Storm Activity. *J. Atmos. Oceanic Technol.*, 29(4): 569-580.

Lareau, N.P. and Horel, J.D. (2012) The Climatology of Synoptic-Scale Ascent over Western North America: A Perspective on Storm Tracks. *Mon. Weather Rev.*, 140(6): 1761-1778.

Madden, R.A. (1976) Estimates of the Natural Variability of Time-Averaged Sea-Level Pressure. *Mon. Weather Rev.*, 104(7): 942-952.

Mantua, N.J. and Hare, S.R. (2002) The Pacific Decadal Oscillation. *J. Oceanogr*., 58(1): 35-44.

Merryfield, W.J., Lee, W.-S., Boer, G.J., Kharin, V.V., Scinocca, J.F., Flato, G.M., Ajayamohan, R.S., Fyfe, J.C., Tang, Y., and Polavarapu, S. (2013) The Canadian Seasonal to Interannual Prediction System. Part I: Models and Initialization. *Mon. Weather Rev.* 141(8): 2910-2945.

Neu, U., Akperov, M.G., Bellenbaum, N., Benestad, R., Blender, R., Caballero, R., Cocozza, A., Dacre, H.F., Feng, Y., Fraedrich, K., Grieger, J., Gulev, S., Hanley, J., Hewson, T., Inatsu, M., Keay, K., Kew, S.F., Kindem, I., Leckebusch, G.C., Liberato, M.L.R., Lionello, P., Mokhov, I.I., Pinto, J.G., Raible, C.C., Reale, M., Rudeva, I., Schuster, M., Simmonds, I., Sinclair, M., Sprenger, M., TiliNiña, N.D., Trigo, I.F., Ulbrich, S., Ulbrich, U., Wang, X.L. and Wernli, H. (2013) IMILAST: A Community Effort to Intercompare Extratropical Cyclone Detection and Tracking Algorithms. *Bull. Am. Meteor. Soc.*, 94(4): 529-547.

Philander, S.G.H. (1983) El Niño Southern Oscillation phenomena. *Nature*, 302(5906): 295-301.

Renggli, D., Leckebusch, G.C., Ulbrich, U., and Gleixner, S.N. (2011) The Skill of Seasonal Ensemble Prediction Systems to Forecast Wintertime Windstorm Frequency over the North Atlantic and Europe. *Mon. Weather Rev.*, 139(9): 3052-3068.

Rezaee, S., Pelot, R., and Finnis, J. (2016) The effect of extratropical cyclone weather conditions on fishing vessel incidents' severity level in Atlantic Canada. *Safety Sci.*, 85: 33-40.

Ropelewski, C.F. and Jones, P.D. (1987) An Extension of the Tahiti-Darwin Southern Oscillation Index. *Mon. Weather Rev.*, 115(9): 2161-2165.

Rowell, D.P. (1998) Assessing Potential Seasonal Predictability with an Ensemble of Multidecadal GCM Simulations. *J. Climate*, 11(2): 109-120.

Scaife, A.A., Arribas, A., Blockley, E., Brookshaw, A., Clark, R.T., Dunstone, N., Eade, R., Fereday, D., Folland, C.K., Gordon, M., Hermanson, L., Knight, J.R., Lea, D.J., MacLachlan, C., Maidens, A., Martin, M., Peterson, A.K., Smith, D., Vellinga, M., Wallace, E., Waters, J., and Williams, A. (2014) Skillful long-range prediction of European and North American winters. *Geophys. Res. Lett.*, 41, 2514-2519, doi:10.1002/2014GL059637.

Shippee, N.J. (2016) *Developing novel storminess metrics and evaluating seasonal predictability of storminess indicators in the north Pacific and Alaskan regions*. PhD dissertation, Department of Geography, University of Victoria, Victoria, BC, Canada.

Shukla, J. and Gutzler, D.S. (1983) Interannual Variability and Predictability of 500 mb Geopotential Heights over the Northern Hemisphere. *Mon. Weather Rev*., 111(6): 1273-1279.

Smith, D.M., Scaife, A.A., Eade, R., and Knight, J.R. (2014) Seasonal to decadal prediction of the winter North Atlantic Oscillation: emerging capability and future prospects. *Q. J. Roy. Meteorol. Soc*., doi: 10.1002/qj.2479

Stockdale, T.N., Alves, O., Boer, G., Deque, M., Ding, Y., Kumar, A., Kumar, K., Landman, W., Mason, S., Nobre, P., Scaife, A., Tomoaki, O., and Yun, W.T. (2010) Understanding and Predicting Seasonal-to-Interannual Climate Variability - The Producer Perspective. *Procedia Environ. Sci.*, 1: 55-80.

Tompkins, A.M., Inés Ortiz de Zárate, M., Saurral, R.I., Vera, C., Saulo, C., Merryfield, W.J., Sigmond, M., Lee, W.-S., Baehr, J., Braun, A., Butler, A., Déqué, M., Doblas-Reyes, F.J., Gordon, M., Scaife, A.A., Imada, Y., Ishii, M., Ose, T., Kirtman, B., Kumar, A., Müller, W.A., Pirani, A., Stockdale, T., Rixen, M., and Yasuda, T. (2017) The Climate-system Historical Forecast Project: providing open access to seasonal forecast ensembles from centers around the globe. *Bull. Amer. Meteor. Soc*., doi: 10.1175/BAMS-D-16-0209.1

Trenberth, K.E. (1984) Signal Versus Noise in the Southern Oscillation. *Mon. Weather Rev.*, 112(2): 326-332.

Walker, G.T. (1924) Correlation in seasonal variations of weather, IX. A further study of world weather. *Memoirs of the Indian Meteorological Department*, 24(9): 275-333.

Wang, X.L., Wan, H., and Swail, V.R. (2006) Observed Changes in Cyclone Activity in Canada and Their Relationships to Major Circulation Regimes. *J. Climate*, 19(6): 896-915.

Wen, C., Xue, Y., and Kumar, A. (2012) Seasonal Prediction of North Pacific SSTs and PDO in the NCEP CFS Hindcasts. *J. Climate*, 25(17): 5689-5710.

Yang, X., Vecchi, G.A., Gudgel, R.G., Delworth, T.L., Zhang, S., Rosati, A., Jia, L., Stern, W.F., Wittenberg, A.T., Kapnick, S., Msadek, R., Underwood, S.D., Zeng, F., Anderson, W., and Balaji, V. (2015) Seasonal Predictability of Extratropical Storm Tracks in GFDL's High-Resolution Climate Prediction Model. *J. Climate*, 28(9): 3592-3611.

Zheng, X., Nakamura, H., and Renwick, J.A. (2000) Potential Predictability of Seasonal Means Based on Monthly Time Series of Meteorological Variables. *J. Climate*, 13(14): 2591-2604.

Zwiers, F.W. (1987) A Potential Predictability Study Conducted with an Atmospheric General Circulation Model. *Mon. Weather Rev.*, 115(12): 2957-2974.

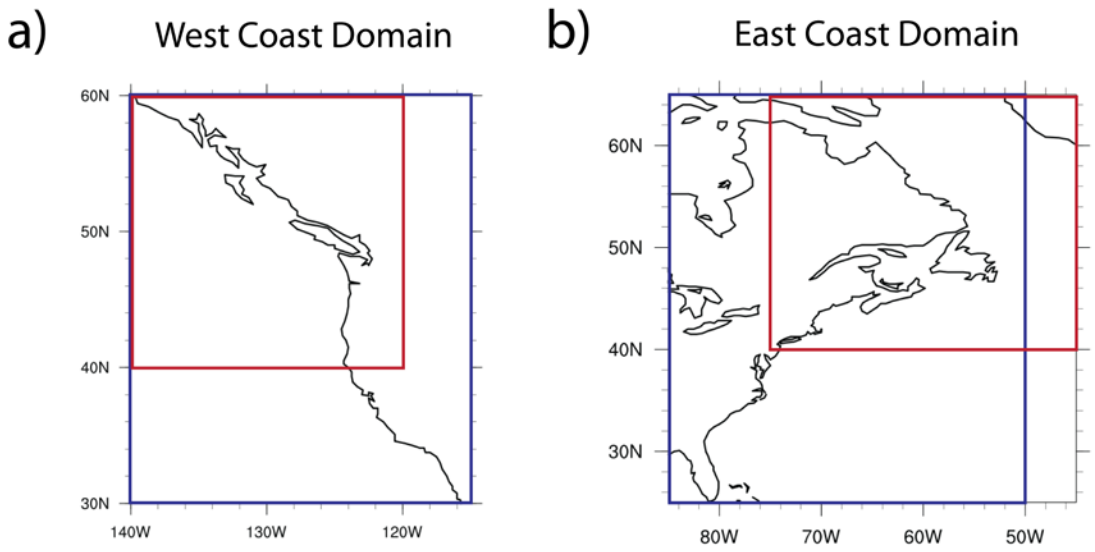

Figure 1.1: The North American (a) west and (b) east coastal study domains as used in Research Theme 1 (red) and Research Themes 2 and 3 (blue).

2.0 Background on Extratropical Storm Activity, Reanalyses, and Large-scale Climate Signals

Extratropical cyclones (ETCs) are synoptic-scale cyclonic circulations ranging in size from approximately 1,000 to 2,000 km with lifespans of a few days to about a week. ETCs are cold-cored, typically closed-contoured, baroclinic low-pressure systems that mirror the Earth's rotation from above (i.e., counterclockwise in the Northern Hemisphere). While ETCs can occur throughout the extratropical latitudes, they grow via baroclinic instability and, as a result, commonly form (cyclogenesis) along mid-latitude frontal boundaries in baroclinic zones (e.g., land-ocean boundary regions with strong horizontal temperature gradients) or in the lee of mountain ranges due to orography-influenced baroclinic instability. ETCs also follow preferred paths (i.e., storm tracks), are influenced by the jet stream and large-scale atmospheric circulation patterns, and dissipate (cyclolysis) in favoured regions. Nevertheless, ETCs are complex features and the characteristics of individual cyclones can vary notably, including size, duration, deepening rates, intensity, trajectory and propagation, vertical structure, and frequency (Stull, 2000; Holton, 2004; Bader et al., 2011; Neu et al., 2013; Lackmann, 2015).

2.1 Reanalyses in Extratropical Storm Activity Research

Due to the complexity of ETCs, various aspects of extratropical storm activity are usually analysed to, e.g., develop climatologies and assess changes in storm activity over time): ETC characteristics commonly evaluated include climatological geographical distribution (regions of cyclogenesis, cyclolysis, and storm tracks), cyclone duration (lifespan), intensity and central pressure, deepening rate, propagation velocity, and frequency

(cyclone counts). ETC storm activity studies also commonly investigate seasonality, interannual variability, and long-term (e.g., 30-year) trends. Gridded data products, such as reanalyses, are typically used to investigate ETC storm activity because they, unlike the conventional observational network, provide representations of the atmospheric state that are continuous in space and time (Dee et al., 2011). Furthermore, gridded data products provide non-observable variables (e.g., potential vorticity), which can be informative to research studies. Reanalyses provide reconstructions of past atmospheric states (meteorological data) that are consistent with both the available observations and atmospheric physics. Reanalyses represent the best estimate of the true state of the atmospheric and are often considered to be equivalent to observations by end-users (though not always justifiable or appropriate) and utilized as such (Dee et al., 2011).

Reanalyses use fixed ("frozen") data assimilation systems, thus preventing model-based inhomogeneities (non-climatic shifts) from influencing the resulting time series (Kalnay et al., 1996; Uppala et al., 2005; Dee et al., 2011). Reanalyses are still affected, however, by changes in the observation network coverage (e.g., pre-satellite vs. satellite eras). Nevertheless, reanalyses provide continuous, observation-based, atmospheric physics-driven reconstructions of the atmosphere state with which long-term investigations of historical storm activity can be completed (Dee et al., 2011). The accuracy and reliability of the reanalysis datasets vary based on assimilation system, the data that are assimilated, model physics, spatial resolution, and the atmospheric variable of interest (Löptien et al., 2008; Ulbrich et al., 2009; Hodges et al., 2011; Tilinina et al., 2013; Wang et al., 2016). Nevertheless, while each reanalysis provides unique estimates of ETC storm activity characteristics, the resulting climatologies are considered reliable

(particularly during the satellite era; i.e., after 1979) and are qualitatively and quantitatively similar (Eichler and Higgins, 2006; Löptien et al., 2008; Ulbrich et al., 2009; Hodges et al., 2011; Tilinina et al., 2013; Wang et al., 2016). The basic climatological geographical distribution of Northern Hemisphere ETC storm activity (storm tracks and regions of cyclogenesis and lysis) and interannual variability are comparable among the reanalyses along with qualitative agreement, but quantitative disagreement, regarding ETC characteristics (Ulbrich et al., 2009; Hodges et al., 2011; Tilinina et al., 2013; Wang et al., 2016). For instance, higher total ETC numbers are generally reported in the higher resolution reanalyses and vice versa (e.g., ERA-40 vs. NCEP-1) (Wang et al., 2006a; Raible et al., 2008; Hodges et al., 2011; Tilinina et al., 2013; Wang et al., 2016). Nevertheless, quantitative agreement is generally strong in the winter season due to the increased frequency and intensity of ETCs as well as among stronger (more intense) ETCs (Wang et al., 2006a; Löptien et al., 2008; Ulbrich et al., 2009; Wang et al., 2016).

2.2 Historical Northern Hemisphere Extratropical Storm Activity

In the Northern Hemisphere extratropics, there are two primary storm tracks extending across the North Pacific and North Atlantic basins, respectively (Figure 2.1). The North Pacific storm track extends from the northwestern Pacific (cyclogenesis in the Kuroshio Current region east of Japan) to the northwestern North American coast, with storms tracking easterly across the ocean basin before curving northward as they mature and ultimately decay (Sickmöller et al., 2000; Graham and Diaz, 2001; Gulev et al., 2001; Bengtsson et al., 2006; Hodges et al., 2011). Maximum cyclogenesis, including rapid

intensification (central pressure drop of 24 hPa/24 hr), is observed in the Kuroshio region while cyclolysis primarily occurs in the Gulf of Alaska and in the southwestern British Columbia region, with the storm track abruptly ending due to the blocking effect of the Rocky Mountains (Sickmöller et al., 2000; Gulev et al., 2001; Bengtsson et al., 2006; Seierstad et al., 2007; Ulbrich et al., 2009; Tilinina et al., 2013). The largest mean intensity and frequency of intense cyclones within the North Pacific storm track is observed over the northeastern Pacific in association with the Aleutian Low (Gulev et al., 2001; Bengtsson et al., 2006; Löptien et al., 2008), with the most intense storms occurring in the autumn season (Eichler and Higgins, 2006; Seierstad et al., 2007). A secondary region of cyclogensis is in the eastern Pacific generating ETCs that impact the west coast of Canada (British Columbia); these eastern Pacific ETCs are less frequent and weaker in intensity (Gulev et al., 2001; Conrad, 2008; Lareau and Horel, 2012).

The North Atlantic storm track extends from the North American east coast (United States east coast/Atlantic Canada), through the Icelandic region, and into northwestern Europe (Sickmöller et al., 2000; Gulev et al., 2001; Bengtsson et al., 2006; Wernli and Schwierz, 2006; Hodges et al., 2011). The cyclogenesis region generally extends along the US east coast from South Carolina to Massachusetts (with a maximum near Cape Hatteras, North Carolina) and includes the potential for cyclones to undergo rapid intensification in the northeast US and Canadian Maritime regions (Gulev et al., 2001; Conrad, 2008; Ulbrich et al., 2009; Hodges et al., 2011; Colle et al., 2013; Tilinina et al., 2013). The most intense storms associated with the North Atlantic storm track occur in the winter season (Eichler and Higgins, 2006; Seierstad et al., 2007), with the

highest frequency of intense cyclones occurring in association with the Icelandic Low (Gulev et al., 2001; Löptien et al., 2008).

While North America is strongly influenced by these primary oceanic storm tracks - the west coast by the exit region of the North Pacific storm track and the east coast by the entrance region of the North Atlantic storm track - the continent is also impacted by substantial regional cyclone activity (Figure 2.2). Over North America, ETCs are generated to the lee (eastern side) of the Rocky Mountains with two peak cyclogenesis regions observed – in Alberta, Canada and the New Mexico-Colorado area of the United States (Gulev et al., 2001; Bengtsson et al., 2006; Eichler and Higgins, 2006; Lareau and Horel, 2012; Grise et al., 2013; Plante et al., 2015). Cyclones can also develop in the Mackenzie River Valley in the Canadian Northwest Territories (Conrad, 2008; Plante et al., 2015). ETCs generated in these three regions track across the continent and into the Great Lakes region where they can intensify or reintensify before tracking up the St. Lawrence valley and impacting northeastern North America (e.g., the New England region of the United States, the Canadian Maritime provinces, Newfoundland-Labrador) (Eichler and Higgins, 2006; Conrad, 2008; Plante et al., 2015). As a result, the Great Lakes region is often considered another area of cyclogenesis (Gulev et al., 2001; Eichler and Higgins, 2006; Conrad, 2008; Plante et al., 2015). The Eastern Seaboard and northeastern North America are also impacted by ETCs generated in the Gulf of Mexico and off the US east coast over the Gulf Stream (e.g., Cape Hatteras, North Carolina region) (Gulev et al., 2001; Conrad, 2008; Colle et al., 2013; Grise et al., 2013; Plante et al., 2015). Furthermore, the ETCs tracking up the Eastern Seaboard have the potential to undergo rapid intensification, developing into intense,

powerful systems (e.g., “nor’easters”) as they impact the northeast US and Canadian Maritime provinces (Conrad, 2008; Seiler and Zwiers, 2016a). As result, North American regional cyclone activity is most frequent over the central plains (US and Canada), Great Lakes region, St. Lawrence Valley, and northeastern North America (Wang et al., 2006b; Colle et al., 2013; Grise et al., 2013). Cyclolysis of North American ETCs occur to the east of the Hudson Bay region of northeastern Canada and as far east as the Greenland Sea (Conrad, 2008; Grise et al., 2013).

The Intergovernmental Panel on Climate Change (IPCC) indicates *low confidence*[1] in the reported changes in extratropical storm activity on the global scale, particularly with regard to extreme extratropical cyclones, due to inconsistences and sensitivities in methods used (e.g., cyclone identification and tracking algorithms and defining a cyclone/extreme cyclone) (Hartmann et al., 2013). Furthermore, Hartmann et al. note that the fidelity of the reported findings is also strongly dependent on the reanalysis product used in the research. Nevertheless, studies have found a ‘general reliability’ of Northern Hemisphere results when using reanalysis datasets, with no sudden shifts in the records that would indicate inhomogeneities due to changes in the observation network coverage (Ulbrich et al., 2009). Over the last half-century, various changes in Northern Hemisphere extratropical storm activity have been detected including an overall decrease in total cyclone numbers, primarily associated with the reduction of relatively shallow cyclones (minimum central pressure of 980-1000 hPa).

[1] The IPCC expresses a level of confidence using five qualifiers: very low, low, medium, high, and very high. In the IPCC report, the respective chapter’s author team determines “confidence in the validity of a finding, based on the type, amount, quality and consistence of evidence (e.g., mechanistic understanding, theory, data, models, expert judgement) and the degree of agreement” (Stocker et al., 2013).

There has been, however, a general intensification observed, particularly of the oceanic storm tracks, with an increase in the number of intense cyclones, including the number of rapidly intensifying cyclones (Gulev et al., 2001; Ulbrich et al., 2008; Ulbrich et al., 2009; Hartmann et al., 2013; Wang et al., 2013; Vose et al., 2014). Furthermore, wintertime storm tracks have undergone a general poleward shift since the 1970s in association with a widening of the tropical belt, contraction of the polar vortex, and a poleward shift of the mid-latitude jet stream (Gulev et al., 2001; Ulbrich et al., 2008; Ulbrich et al., 2009; Bender et al., 2012; Hartmann et al., 2013; Wang et al., 2013).

Alternatively, over North America, an overall increase in cyclone numbers has been observed over the last half-century (despite a summertime decrease in numbers) while no statistically significant changes in cyclone intensity have been detected (Hartmann et al., 2013; Tilinina et al., 2013; Wang et al., 2013). An increase in the number of wintertime cyclones in the North America-North Atlantic mid-latitude storm track has also been reported (Tilinina et al., 2013; Wang et al., 2013). Using hourly mean sea level pressure data from 83 stations across Canada, covering the 1953-2002 time period, Wang et al. (2006b) report a poleward shift of the storm track over central Canada of approximately 260 km in association with an overall reduction in storm activity (frequency and intensity) over southern Canada (south of 60°N) and an overall increase over northern Canada (lower Canadian Arctic). While similar trends in cyclone activity in central Canada can be observed in some reanalysis datasets (e.g., the Twentieth Century Reanalysis [Wang et al., 2013]), a poleward shift is not consistently observed among reanalysis datasets (typically covering the 1979-2010 time period) (Tilinina et al., 2013; Wang et al., 2016).

2.3 Projected Changes in Northern Hemisphere Extratropical Storm Activity

Projected changes in Northern Hemisphere extratropical storm activity through the end of the 21st century indicate a broad continuation of the observed changes since ~1950: An overall reduction in total number of ETCs, an increase in intense cyclones, and a general poleward shift in mid-latitude wintertime storm tracks (Bengtsson et al., 2006; Lambert and Fyfe, 2006; Löptien et al., 2008; Ulbrich et al., 2009; Christensen et al., 2013; Collins et al., 2013; Seiler and Zwiers, 2016b). The Intergovernmental Panel on Climate Change (IPCC) reports that the global number of ETCs is "unlikely to decrease by more than a few percent" under enhanced warming (Christensen et al., 2013; Collins et al., 2013). Similarly, Bengtsson et al. (2006) estimate an overall decrease in total winter ETCs of 4% at the end of the 21st century. Regionally, a 15-20% reduction in wintertime cyclone numbers over North America (e.g., the Great Lakes region) is projected (Löptien et al., 2008; Colle et al., 2013), including a projected decrease in explosive cyclones over the waters adjacent to the North American east coast (Colle et al., 2013; Seiler and Zwiers, 2016b). The frequency of intense cyclones (central pressure below 970 hPa) are projected to increase, however, in some regions (e.g., the North Pacific [particularly the Aleutian Low region], over the eastern USA, and the northeast Atlantic/western Europe region) (Ulbrich et al., 2009; Christensen et al., 2013; Colle et al., 2013; Seiler and Zwiers, 2016b). Cyclone deepening rates are also projected to increase in some regions, contributing to in the increase in the number of intense cyclones, including rapidly intensifying cyclones (Löptien et al., 2008; Colle et al., 2013). Löptien et al. (2008) also report a projected general reduction in propagation velocities and shorter lifespans under enhanced warming. Over North America, an increase in winter precipitation over the

northern half of the continent is projected in associated with a poleward shift in ETC activity (Bengtsson et al., 2006; Christensen et al., 2013).

These overall projected changes are in agreement with the hypothesis (summarized by Lambert and Fyfe, 2006) that enhanced warming is expected to cause a general warming of the lower troposphere. More tropospheric warming is expected to occur at the poles than at low latitudes and to be greatest in the winter. Consequently, a reduction in the lower troposphere pole-to-equator temperature and thickness gradients would be expected. As a result, a reduction of baroclinicity is also to be expected, leading to fewer ETCs, especially during winter. An increase in lower troposphere (surface and near-surface) temperatures, however, has the potential to result in increased precipitation in cyclones, with the associated increased release of latent heat potentially leading to increased development of individual cyclones. Therefore, a decrease in total cyclone numbers but an increase in cyclone intensity could result, and be generally negatively correlated, under enhanced warming.

2.4 Large-scale Climate Signals and Extratropical Storm Activity in the Northern Hemisphere

Variability in Northern Hemisphere extratropical storm activity is strongly associated with dominant large-scale, low-frequency atmospheric circulation patterns. Teleconnection patterns describe these large-scale patterns of atmospheric variability, their preferred phases, and the temporal variations of low-frequency fluctuation (Sickmöller et al., 2000; Panagiotopoulos et al., 2002; Christensen et al., 2013; Hartmann et al., 2013). Additionally, representative of modes of large-scale climate variability

(climate signals), teleconnection patterns also characterize the associated significant simultaneous correlations observed in various meteorological variables and anomalous weather patterns at widely separated, geographically fixed locations around the globe (Wallace and Gutzler, 1981; Panagiotopoulos et al., 2002; Christensen et al., 2013; Hartmann et al., 2013). Subsequently, regional to global climate variability is known to be associated, both directly and indirectly, with teleconnection patterns, resulting in identifiable anomalies in the temperature and precipitation regimes and the location and characteristics of extratropical storm activity (Panagiotopoulos et al., 2002; Christensen et al., 2013).

Three major global or Northern Hemispheric large-scale climate signals (teleconnection patterns) known to be associated with climate variability in the North Pacific, North Atlantic, and North American regions are utilized in this research project – the El Niño-Southern Oscillation (ENSO), the Pacific Decadal Oscillation (PDO), and the North Atlantic Oscillation (NAO). These teleconnection patterns are described in the following subsections along with their relationships with extratropical storm activity variability. Also provided are the definitions of the established climate indices utilized in this research project to characterize the fluctuations and strength of the climate signals.

2.4.1 El Niño-Southern Oscillation

ENSO is the coupled atmosphere-ocean system in the equatorial Pacific, comprised of the Southern Oscillation - a east-west seesaw in surface pressure across the equatorial Pacific between the south-east Pacific High Pressure Zone and the North Australian-Indonesian Low Pressure Zone - and El Niño - the anomalously warm ocean surface temperatures occurring interannually along the coasts of Ecuador and Peru (Philander, 1983;

Christensen et al., 2013; Hartmann et al., 2013) (Figures 2.3 and 2.4). The term “El Niño” originally referred to the annual weak warm current that flows southward along the coast of South America during the boreal winter months but is now typically reserved for the semi-periodic events when the warm sea surface temperatures (SSTs) are much more anomalous and extend across much of the tropical Pacific (Philander, 1983; Trenberth, 1997). There are three preferred phases of ENSO - a warm phase (El Niño), neutral conditions, and a cool phase (La Niña). During El Niño, the east-west pressure gradient across the tropical Pacific weakens, resulting in weakened tradewinds. Consequently, ocean upwelling along the South American coast is significantly reduced and anomalously warm SSTs are able to develop in the eastern tropical Pacific, growing in amplitude and extending westward as the El Niño event develops and matures, and can ultimately result in basin-wide warming of the tropical Pacific (SSTs and surface air temperatures). The eastward displacement in the warm SSTs from the climatological location (the western tropical Pacific) also results in an eastward shift in the upward branch of the Walker Circulation, creating enhanced convection and precipitation over the central-eastern tropical Pacific (Philander, 1983; Trenberth, 1997; Grise et al., 2013). The increased convection influences (intensifies) the Hadley Cell and creates a Rossby wave train that is excited in the low latitudes and extends into the extratropical latitudes (Philander, 1983; Shabbar, 2006; Grise et al., 2013). Anomalous El Niño conditions start to develop in the boreal spring (February-March), gradually build through the summer, and reach maturity in winter (between November and January), with dissipation and normal conditions returning (or possibly La Niña conditions developing) the following spring (February-March) (Philander, 1983; Trenberth, 1997). An El Niño event typically

lasts 12-18 months (Philander, 1983; Trenberth, 1997). Alternatively, during La Niña, tradewinds intensify across the tropical Pacific, increasing ocean upwelling along the South American coast. Consequently, anomalously cool SSTs develop in the eastern tropical Pacific and subsequently extend westward, resulting is a basin-wide cooling of the tropical Pacific (Philander, 1983; Trenberth, 1997). The ENSO cycle is quasi-periodic with El Niño events occurring about once every four-to-five years (Trenberth, 1997; Shabbar, 2006). In this research project, the Southern Oscillation (SO) Index is used to represent ENSO and is defined as the difference between the monthly standardized Tahiti and standardized Darwin sea level pressure anomalies (departures from the 1981-2010 base period). A +/-1 standard deviation cut-off was utilized to define ENSO events vs. neutral conditions and was calculated using the 1951-2015 SO index time series (all months inclusive). SO Index data was obtained from the NOAA Climate Prediction Center: http://www.cpc.ncep.noaa.gov/data/indices/soi.

ENSO is the dominant mode of interannual climate variability and has worldwide influence on climatic conditions, either directly or indirectly (Figure 2.5). The locations of wintertime mid-latitude jet streams and storm tracks are particularly influenced by ENSO and the resulting strength of the Hadley Cell (Eichler and Higgins, 2006; Grise et al., 2013). During El Niño events, the subtropical jet stream that extends over the Pacific and eastward into the subtropical Atlantic is enhanced. Additionally, Shabbar (2006) indicates that the jet stream over the North Pacific is likely to split as it approaches North America, with a weaker branch diverted northward into the Arctic and a stronger branch diverted southward, impacting the California, US region. As a result, the North Pacific storm track is shifted eastward and equatorward, with increased frequency of cyclones

over the north-central Pacific (Eichler and Higgins, 2006; Grise et al., 2013; Plante et al., 2015). Over continental North America, a more zonal storm track and enhanced storm activity is observed across the southwestern US (Lareau and Horel, 2012) along with an enhanced east coast storm track (Gulf of Mexico and up the Eastern Seaboard) (Eichler and Higgins, 2006; Wang et al., 2006b, Grise et al., 2013; Plante et al., 2015). Alternatively, the storm track extending from the lee of the Rocky Mountains to the Great Lakes region is weakened (Eichler and Higgins, 2006; Grise et al., 2013; Plante et al., 2015).

During La Niña events, however, the subtropical jet stream weakens and there is an overall poleward shift in the storm tracks over the North Pacific basin and the North American east coast (Eichler and Higgins, 2006; Plante et al., 2015). Over North America, the storm track extending from the lee of the Rocky Mountains to the Great Lakes region is enhanced (increased frequency of cyclones) (Eichler and Higgins, 2006; Plante et al., 2015). Increased storm activity is also observed over the US Pacific Northwest and British Columbia, Canada (Lareau and Horel, 2012; Grise et al., 2013). Grise et al. (2013) note that storm track changes over North America are weaker and less robust during La Niña events compared to El Niño events.

2.4.2 Pacific Decadal Oscillation

PDO is a long-lived ENSO-like pattern of climate variation in the North Pacific with fluctuations on decadal timescales instead of seasons (Mantua and Hare, 2002). The PDO is characterized by opposing sea surface temperature (SST) dipoles in the north-central North Pacific and the northeast Pacific (Aleutian Islands-Gulf of Alaska region), representing two centres of action (Mantua and Hare, 2002; Christensen et al., 2013)

(Figure 2.6). The PDO is also closely linked to the strength of the wintertime Aleutian Low, which influences the sea level pressure (SLP) anomalies observed in the centres of action (Favre and Gershunov, 2006; Wang et al., 2006b; Christensen et al., 2013). The PDO has two preferred anomalous phases - a positive (warm) phase and a negative (cool) phase. During the positive PDO phase, cooler-than-normal SSTs are observed in the north-central North Pacific while warmer-than-normal SSTs are observed in the northeast Pacific and along the west coast of North America. These SST anomalies are accompanied by higher-than-normal SLP over the northern subtropical Pacific and lower-than-normal SLP over the North Pacific. These SLP anomalies result in enhanced flow around the centres of action and stronger westerlies across the North Pacific (Mantua and Hare, 2002). Alternatively, the reverse SST and SLP conditions and weakened westerlies are observed over the North Pacific basin during the negative PDO phase. PDO events typically persist for 20-30 years (Mantua and Hare, 2002; Christensen et al., 2013). The established PDO Index is defined as the leading principle component of monthly mean sea surface temperature anomalies in the North Pacific Ocean poleward of 20°N. The PDO Index is maintained by Nathan Mantua at the University of Washington, Joint Institute for the Study of the Atmosphere and Ocean (JISAO; http://research.jisao.washington.edu/pdo/PDO.latest) and data was obtained through the NCAR UCAR Climate Data Guide: https://climatedataguide.ucar.edu/climate-data/pacific-decadal-oscillation-pdo-definition-and-indices.

While the PDO's climatic influences are most pronounced in the extratropical North Pacific-North American regions (Mantua et al., 1997; Mantua and Hare, 2002), many of the resulting climatic anomalies are broadly similar to the ENSO-influenced

anomalies, though not as extreme (Mantua and Hare, 2002; Bradbury et al., 2003). Furthermore, PDO fluctuations are found to be associated with ENSO fluctuations, with increased El Niño activity observed during the positive PDO phase and vice versa (Mantua et al., 1997; Bradbury et al., 2003; Favre and Gershunov, 2006; Christensen et al., 2013). During the positive PDO phase, the Aleutian Low is intensified and an enhanced meridional circulation is observed over the North American continent (Mantua et al., 1997; Bradbury et al., 2003; Favre and Gershunov, 2006). Focusing on Canadian extratropical storm activity, Wang et al. (2006b) also found during the positive PDO phase an increased cyclone frequency on the east coast during the summer, increased cyclone frequency on the west coast and southeast coast in spring, and decreased cyclone frequency in the Prairies (to the lee of the Rocky Mountains) in autumn and winter.

2.4.3 North Atlantic Oscillation

NAO is characterized by a seesaw of atmospheric mass (revealed in the sea level pressure field) over the North Atlantic basin between two centres of action - the Icelandic Low and subtropical Azores High (Wallace and Gutzler, 1981; Hurrell et al., 2001; Panagiotopoulos et al., 2002; Grise et al., 2013) (Figure 2.7). In association with this north-south fluctuation of atmospheric mass, the NAO affects the strength and position of the westerlies (jet stream) across the North Atlantic (Grise et al., 2013) (Figure 2.8). The NAO has two preferred phases - positive and negative. During the positive NAO phase, a deeper-than-normal Icelandic Low and higher-than-normal Azores High are observed. The enhanced flow around these centres of action result in strengthened westerlies and a poleward-shifted, northeasterly-oriented jet stream over the North Atlantic (Wallace and Gutzler, 1981; Hurrell et al., 2001; Panagiotopoulos et al., 2002). Alternatively, during

the negative NAO phase, weakened centres of action, weakened westerlies, and an equatorward-shifted, more zonal jet stream are observed over the North Atlantic. The NAO is most pronounced during the boreal winter when the equator-to-pole temperature gradient is strongest. Time series of the NAO index reveal considerable interseasonal and interannual variability and no particular periodicity. Nevertheless, prolonged general persistence of the individual NAO phases is observed (Hurrell, 1995; Hurrell et al., 2001). The established NAO index used in this research project is the seasonal Hurrell station-based NAO Index, which is defined as the difference between the normalized Lisbon, Portugal and normalized Stykkishólmur/Reykjavík, Iceland sea level pressure anomalies (normalized using the 1864-1983 long term mean). Hurrell station-based NAO Index data was obtained from the NCAR UCAR Climate Data Guide: https://climatedataguide.ucar.edu/climate-data/hurrell-north-atlantic-oscillation-nao-index-station-based.

Climate variability in the North Atlantic basin and adjacent coastal regions is known to be associated with the NAO, particularly with regard to wintertime storm activity across the region. Gulev et al. (2001) report a correlation of 0.86 between the NAO and North Atlantic storm frequency in the Atlantic/Arctic sector (defined as longitudes 120°W to 90°E for 10°N to 70°N and all longitudes for 70°N to 90°N). Notable climatic influences (temperature, precipitation, and storm activity) associated with the NAO extend from the North American east coast, across the North Atlantic, and into Europe and the Mediterranean (Gulev et al., 2001; Panagiotopoulos et al., 2002). NAO-associated changes in storm activity mirror the changes in the strength and position of the jet stream (Grise et al., 2013). As such, during the positive NAO phase, the North

Atlantic storm track undergoes a poleward and northeastward shift, with enhanced storm activity extending from the Hudson Bay and Newfoundland, Canada regions, through the Icelandic and Norwegian Sea region, and into northern Europe (Gulev et al., 2001; Pinto et al., 2009; Hurrell and Deser, 2010; Bader et al., 2011; Grise et al., 2013). Additionally, Pinto et al. (2009) found that the occurrence of extreme cyclones (strongest 10% of cyclones) is enhanced under strong positive NAO conditions: Extreme cyclones were found to typically have higher intensities, lower central pressures, longer lifespans, and longer track lengths, suggestive of more intense and/or longer intensification phases associated with the larger area with favourable growth conditions observed extending across the North Atlantic basin during strong positive NAO conditions.

Alternatively, during the negative NAO phase, the North Atlantic storm track is shifted equatorward and has a more zonal orientation, resulting in increased cyclone activity extending eastward from the Cape Hatteras, North Carolina region to southern Europe and the Mediterranean (Gulev et al., 2001; Grise et al., 2013). Enhanced cyclone decay is also observed in the Newfoundland, Canada region associated with cyclones tracking up the North American east coast (Grise et al., 2013). Furthermore, Bernhardt and DeGaetano (2012) found that a negative NAO phase, occurring simultaneously with an positive ENSO phase (El Niño warm event), results in considerably slower wintertime propagation speed of cyclones tracking up the US Eastern Seaboard.

2.5 References

Bader, J., Mesquita, M.D.S., Hodges, K.I., Keenlyside, N. Østerhus, S., and Miles, M. (2011) A review on Northern Hemisphere sea-ice, storminess and the North Atlantic Oscillation: Observations and projected changes. *Atmospheric Res.*, 101(4): 809-834.

Bender, F.A.-M., Ramanathan, V., and Tselioudis, G. (2012) Changes in extratropical storm track cloudiness 1983-2008: observational support for a poleward shift. *Clim. Dyn.*, 38(9-10): 2037-2053.

Bengtsson, L., Hodges, K., and Roeckner, E. (2006) Storm Tracks and Climate Change. *J. Climate*, 19(15): 3518-3543.

Bernhardt, J.E. and DeGaetano, A.T. (2012) Meteorological factors affecting the speed of movement and related impacts of extratropical cyclones along the U.S. east coast. *Nat. Hazards*, 61(3): 1463-1472.

Bradbury, J.A., Keim, B.D., and Wake, C.P. (2003) The Influence of Regional Storm Tracking and Teleconnections on Winter Precipitation in the Northeastern United States. *Ann. Assoc. Am. Geogr.*, 93(3): 544-556.

Christensen, J.H., Krishna Kumar, K., Aldrian, E., An, S.-I., Cavalcanti, I.F.A., de Castro, M., Dong, W., Goswami, P., Hall, A., Kanyanga, J.K., Kitoh, A., Kossin, J., Lau, N.-C., Renwick, J., Stephenson, D.B., Xie, S.-P., and Zhou, T. (2013) Climate Phenomena and their Relevance for Future Regional Climate Change. In: *Climate Change 2013: The Physical Science Basis. Contribution of Working Group I to the Fifth Assessment Report of the Intergovernmental Panel on Climate Change* [Stocker, T.F., Qin, D., Plattner, G.-K., Tignor, M., Allen, S.K., Boschung, J., Nauels, A., Xia, Y., Bex, V., and Midgley, P.M. (eds.)]. Cambridge University Press, Cambridge, United Kingdom and New York, NY, USA.

Colle, B.A., Zhang, Z., Lombardo K.A., Chang, E., Liu, P., and Zhang, M. (2013) Historical Evaluation and Future Prediction of Eastern North American and Western Atlantic Extratropical Cyclones in the CMIP5 Models during the Cool Season. *J. Climate*, 26(18): 6882-6903.

Collins, M., Knutti, R., Arblaster, J., Dufresne, J.-L., Fichefet, T., Friedlingstein, P., Gao, X., Gutowski, W.J., Johns, T., Krinner, G., Shongwe, M., Tebaldi, C., Weaver, A.J., and Wehner, M. (2013) Long-term Climate Change: Projections, Commitments and Irreversibility. In: *Climate Change 2013: The Physical Science Basis. Contribution of Working Group I to the Fifth Assessment Report of the Intergovernmental Panel on Climate Change* [Stocker, T.F., Qin, D., Plattner, G.-K., Tignor, M., Allen, S.K., Boschung, J., Nauels, A., Xia, Y., Bex, V., and Midgley, P.M. (eds.)]. Cambridge University Press, Cambridge, United Kingdom and New York, NY, USA.

Conrad, C.T. (2008) *Severe and Hazardous Weather in Canada: The Geography of Extreme Events*. Oxford University Press, Oxford, United Kingdom. 205 pp.

Dee, D.P., Uppala, S.M., Simmons, A.J., Berrisford, P., Poli, P., Kobayashi, S., Andrae, U., Balmaseda, M.A., Balsamo, G., Bauer, P., Bechtold, P., Beljaars, A.C.M., van

de Berg, L., Bidlot, J., Bormann, N., Delsol, C., Dragani, R., Fuentes, M., Geer, A.J., Haimberger, L., Healy, S.B., Hersbach, H., Holm, E.V., Isaksen, L., Kallberg, P., Kohler, M., Matricardi, M., McNally, A.P., Monge-Sanz, B.M., Morcrette, J.J., Park, B.K., Peubey, C., de Rosnay, P., Tavolato, C., Thepaut, J.N., and Vitart, F. (2011) The ERA-Interim reanalysis: configuration and performance of the data assimilation system. *Q. J. R. Meteorol. Soc*., 137(656): 553-597.

Eichler, T. and Higgins, W. (2006) Climatology and ENSO-Related Variability of North American Extratropical Cyclone Activity. *J. Climate*, 19(10): 2076-2093.

Favre, A. and Gershunov, A. (2006) Extra-tropical cyclonic/anticyclonic activity in North-Eastern Pacific and air temperature extremes in Western North America. *Clim. Dyn.*, 26(6): 617-629.

Graham, N.E. and Diaz, H.F. (2001) Evidence for Intensification of North Pacific Winter Cyclones since 1948. *Bull. Am. Meteorol. Soc*., 82(9): 1869-1893.

Grise, K.M., Son, S., and Gyakum, J.R. (2013) Intraseasonal and Interannual Variability in North American Storm Tracks and Its Relationship to Equatorial Pacific Variability. *Mon. Weather Rev.*, 141(10): 3610-3625.

Gulev, S.K., Zolina, O., and Grigoriev, S. (2001) Extratropical cyclone variability in the Northern Hemisphere winter from the NCEP/NCAR reanalysis data. *Clim. Dyn*., 17(10): 795-809.

Hartmann, D.L., Klein Tank, A.M.G., Rusticucci, M., Alexander, L.V., Br.nnimann, S., Charabi, Y., Dentener, F.J., Dlugokencky, E.J., Easterling, D.R., Kaplan, A., Soden, B.J., Thorne, P.W., Wild, M., and Zhai, P.M. (2013) Observations: Atmosphere and Surface. In: *Climate Change 2013: The Physical Science Basis. Contribution of Working Group I to the Fifth Assessment Report of the Intergovernmental Panel on Climate Change* [Stocker, T.F., Qin, D., Plattner, G.-K., Tignor, M., Allen, S.K., Boschung, J., Nauels, A., Xia, Y., Bex, V., and Midgley, P.M. (eds.)]. Cambridge University Press, Cambridge, United Kingdom and New York, NY, USA.

Hodges, K.I. (1994) A general method for tracking analysis and its application to meteorological data. *Mon. Weather Rev.* 122(11): 2573-2586. doi:10.1175/1520-0493(1994)122<2573:AGMFTA>2.0.CO;2.

Hodges, K.I. (1995) Feature tracking on the unit sphere. *Mon. Weather Rev.* 123(12): 3458-3465. doi:10.1175/1520-0493(1995)123<3458:FTOTUS>2.0.CO;2.

Hodges, K.I. (1999) Adaptive Constraints for Feature Tracking. *Mon. Weather Rev.* 127(6): 1362-1373. doi:10.1175/1520-0493(1999)127<1362:ACFFT>2.0.CO;2.

Hodges, K.I., Lee, R.W., and Bengtsson, L. (2011) A Comparison of Extratropical Cyclones in Recent Reanalyses ERA-Interim, NASA MERRA, NCEP CFSR, and JRA-25. *J. Climate*, 24(18): 4888-4906. doi:10.1175/2011JCLI4097.1.

Holton, J.R. (2004) *An Introduction to Dynamic Meteorology: Fourth Edition*. Elsevier Academic Press, New York, NY, USA. 535 pp.

Hurrell, J.W. (1995) Decadal Trends in the North Atlantic Oscillation: Regional Temperatures and Precipitation. *Science*, 269(5224): 676-679.

Hurrell, J.W., Kushnir, Y., and Visbeck, M. (2001) The North Atlantic Oscillation. *Science*, 291(5504): 603-605.

Hurrell, J.W. and Deser, C. (2010) North Atlantic climate variability: The role of the North Atlantic Oscillation. *J. Mar. Syst.*, 79(3-4): 231-244.

Kalnay, E., Kanamitsu, M., Kistler, R., Collins, W., Deaven, D., Gandin, L., Iredell, M., Saha, S., White, G., Woollen, J., Zhu, Y., Chelliah, M., Ebisuzaki, W., Higgins, W., Janowiak, J., Mo, K.C., Ropelewski, C., Wang, J., Leetmaa, A., Reynolds, R., Jenne, R., and Joseph, D. (1996) The NCEP/NCAR 40-Year Reanalysis Project. *Bull. Am. Meteorol. Soc.*, 77(3): 437-471.

Lackmann, G. (2015) *Midlatitude Synoptic Meteorology: Dynamics, Analysis & Forecasting*. American Meteorological Society, Boston, MA, USA. 345 pp.

Lambert, S.J. and Fyfe, J.C. (2006) Changes in winter cyclone frequencies and strengths simulated in enhanced greenhouse warming experiments: results from the models participating in the IPCC diagnostic exercise. *Clim. Dyn.*, 26(7-8): 713-728.

Lareau, N.P. and Horel, J.D. (2012) The Climatology of Synoptic-Scale Ascent over Western North America: A Perspective on Storm Tracks. *Mon. Weather Rev.*, 140(6): 1761-1778.

Löptien, U., Zolina, O., Gulev, S., Latif, M., and Soloviov, V. (2008) Cyclone life cyclone characteristics over the Northern Hemisphere in coupled GCMS. *Clim. Dyn.*, 31(5): 507-532.

Mantua, N.J., Hare, S.R., Zhang, Y., Wallace, J.M., and Francis, R.C. (1997) A Pacific Interdecadal Climate Oscillation with Impacts on Salmon Production. *Bull. Am. Meteorol. Soc.*, 78(6): 1069-1079.

Mantua, N.J. and Hare, S.R. (2002) The Pacific Decadal Oscillation. *J. Oceanogr.*, 58(1): 35-44.

Neu, U., Akperov, M.G., Bellenbaum, N., Benestad, R., Blender, R., Caballero, R., Cocozza, A., Dacre, H.F., Feng, Y., Fraedrich, K., Grieger, J., Gulev, S., Hanley,

J., Hewson, T., Inatsu, M., Keay, K., Kew, S.F., Kindem, I., Leckebusch, G.C., Liberato, M.L.R., Lionello, P., Mokhov, I.I., Pinto, J.G., Raible, C.C., Reale, M., Rudeva, I., Schuster, M., Simmonds, I., Sinclair, M., Sprenger, M., Tilinina, N.D., Trigo, I.F., Ulbrich, S., Ulbrich, U., Wang, X.L. and Wernli, H. (2013) IMILAST: A Community Effort to Intercompare Extratropical Cyclone Detection and Tracking Algorithms. *Bull. Am. Meteor. Soc.*, 94(4): 529-547.

Panagiotopoulos, F., Shahgedanova, M., and Stephenson, D.B. (2002) A review of Northern Hemisphere winter-time teleconnection patterns. *J. Phys. IV France*, 12(10): 27-47.

Philander, S.G.H. (1983) El Niño Southern Oscillation phenomena. *Nature*, 302(5906): 295-301.

Pinto, J.G., Zacharias, St., Fink, A.H., Leckebusch, G.C., and Ulbrich, U. (2009) Factors contributing to the development of extreme North Atlantic cyclones and their relationships with the NAO. *Clim. Dyn.*, 32(5): 711-737.

Plante, M., Son, S.-W., Atallah, E., Gyakum, J., and Grise, K. (2015) Extratropical cyclone climatology across eastern Canada. *Int. J. Climatol.*, 35(10): 2759-2776.

Raible, C.C., Della-Marta, P.M., Schwierz, C., Wernli, H., and Blender, R. (2008) Northern Hemisphere Extratropical Cyclones: A Comparison of Detection and Tracking Methods and Different Reanalyses. *Mon. Weather Rev.*, 136(3): 880-897. doi:10.1175/2007MWR2143.1.

Seierstad, I.A., Stephenson, D.B., and Kvamstø, N.G. (2007) How useful are teleconnection patterns for explaining variability in extratropical storminess? *Tellus*, 59A(2): 170-181.

Seiler, C. and Zwiers, F.W. (2016a) How well do CMIP5 climate models reproduce explosive cyclones in the extratropics of the Northern Hemisphere? *Clim. Dyn.*, 46(3-4): 1241-1256.

Seiler, C. and Zwiers, F.W. (2016b) How will climate change affect explosive cyclones in the extratropics of the Northern Hemisphere? *Clim. Dyn.*, 46(11-12): 3633-3644.

Shabbar, A. (2006) The impact of El Nino-Southern Oscillation on the Canadian climate. *Adv. Geosci.*, 6: 149-153.

Sickmöller, M., Blender, R., and Fraedrich, K. (2000) Observed winter cyclone tracks in the northern hemisphere in re-analysed ECMWF data. *Q. J. R. Meteorol. Soc.*, 126(563): 591-620.

Stocker, T.F., Qin, D., Plattner, G.-K., Alexander, L.V., Allen, S.K., Bindoff, N.L., Bréon,

F.-M., Church, J.A., Cubasch, U., Emori, S., Forster, P., Friedlingstein, P., Gillett, N., Gregory, J.M., Hartmann, D.L., Jansen, E., Kirtman, B., Knutti, R., Krishna Kumar, K., Lemke, P., Marotzke, J., Masson-Delmotte, V., Meehl, G.A., Mokhov, I.I., Piao, S., Ramaswamy, V., Randall, D., Rhein, M., Rojas, M., Sabine, C., Shindell, D., Talley, L.D., Vaughan D.G., and Xie, S.-P. (2013) Technical Summary. In: *Climate Change 2013: The Physical Science Basis. Contribution of Working Group I to the Fifth Assessment Report of the Intergovernmental Panel on Climate Change* [Stocker, T.F., Qin, D., Plattner, G.-K., Tignor, M., Allen, S.K., Boschung, J., Nauels, A., Xia, Y., Bex, V., and Midgley, P.M. (eds.)]. Cambridge University Press, Cambridge, United Kingdom and New York, NY, USA.

Stull, R. (2000) *Meteorology For Scientists and Engineers: Second Edition*. Brooks/Cole Thomson Learning, Pacific Grove, CA, USA.

Tilinina, N., Gulev, S.K., Rudeva, I., and Kiltermann, P. (2013) Comparing cyclone life cycle characteristics and their interannual variability in different reanalyses. *J. Climate*, 26(17): 6419-6438.

Trenberth, K.E. (1997) The Definition of El Nino. *Bull. Am. Meteorol. Soc.*, 78(12): 2771-2777.

Ulbrich, U., Pinto, J.G., Kupfer, H., Leckebusch, G.C., Spangehl, T., and Reyers, M. (2008) Changing Northern Hemisphere Storm Tracks in an Ensemble of IPCC Climate Change Simulations. *J. Climate*, 21(8): 1669-1679.

Ulbrich, U., Leckebusch, G.C., and Pinto, J.G. (2009) Extra-tropical cyclones in the present and future climate: a review. *Theor. Appl. Climatol*., 96(1-2): 117-131.

Uppala, S.M., Kallberg, P.W., Simmons, A.J., Andrae, U., Da Costa Bechtold, V., Fiorino, M., Gibson, J.K., Haseler, J., Hernandez, A., Kelly, G.A., Li, X., Onogi, K., Saarinen, S., Sokka, N., Allan, R.P., Andersson, E., Arpe, K., Balmaseda, M.A., Beljaars, A.C.M., Van De Berg, L., Bidlot, J., Bormann, N., Caires, S., Chevallier, F., Dethof, A., Dragosavac, M., Fisher, M., Fuentes, M., Hagemann, S., Holm, E., Hoskens, B.J., Isaksen, L., Janssen, P.A.E.M., Jenne, R., McNally, A.P., Mahfouf, J.F., Morcrette, J.J., Rayner, N.A., Saunders, R.W., Simon, P., Sterl. A., Trenberth, K.E., Untch, A., Vasiljevic, D., Viterbo, and Woollen, J. (2005) The ERA-40 re-analysis. *Q. J. Roy. Meteorol. Soc*., 131(612): 2961-3012.

Vose, R.S., Applequist, S., Bourassa, M.A., Pryor, S.C., Barthelmie, R.J., Blanton, B., Bromirski, P.R., Brooks, H.E., DeGaetano, A.T., Dole, R.M., Easterling, D.R., Jensen, R.E., Karl, T.R., Katz, R.W., Klink, K., Kruk, M.C., Kunkel, K.E., MacCracken, M.C., Peterson, T.C., Shein, K., Thomas, B.R., Walsh, J.E., Wang, X.L., Wehner, M.F., Wuebbles, D.J., and Young, R.S. (2014) Monitoring and Understanding Changes in Extremes: Extratropical Storms, Winds, and Waves. *Bull. Am. Meteorol. Soc.*, 95(3): 377-386.

Wallace, J.M. and Gutzler, D.S. (1981) Teleconnections in the Geopotential Height Field during the Northern Hemisphere Winter. *Mon. Weather Rev*., 109(4): 784-812.

Wang, X.L., Swail, V.R., and Zwiers, F.W. (2006a) Climatology and Changes of Extratropical Cyclone Activity: Comparison of ERA-40 with NCEP-NCAR Reanalysis for 1958-2001. *J. Climate*, 19(13): 3145-3166.

Wang, X.L., Wan, H., and Swail, V.R. (2006b) Observed Changes in Cyclone Activity in Canada and Their Relationships to Major Circulation Regimes. *J. Climate*, 19(6): 896-915.

Wang, X.L., Feng, Y., Compo, G.P., Swail, V.R., Zwiers, F.W., Allan, R.J., and Sardeshmukh, P.D. (2013) Trends and low frequency variability of extra-tropical cyclone activity in the ensemble of twentieth century reanalysis. *Clim. Dyn.*, 40(11-12): 2775-2800.

Wang, X.L., Feng, Y., Chan, R., and Isaac, V. (2016) Inter-comparison of extra-tropical cyclone activity in nine reanalysis datasets. *Atmospheric Res.*, 181(15): 133-153. doi: 10.1016/j.atmosres.2016.06.010.

Wernli, H. and Schwierz, C. (2006) Surface Cyclones in the ERA-40 Dataset (1958-2001). Part I: Novel Identification Method and Global Climatology. *J. Atmos. Sci*., 63(10): 2486-2507.

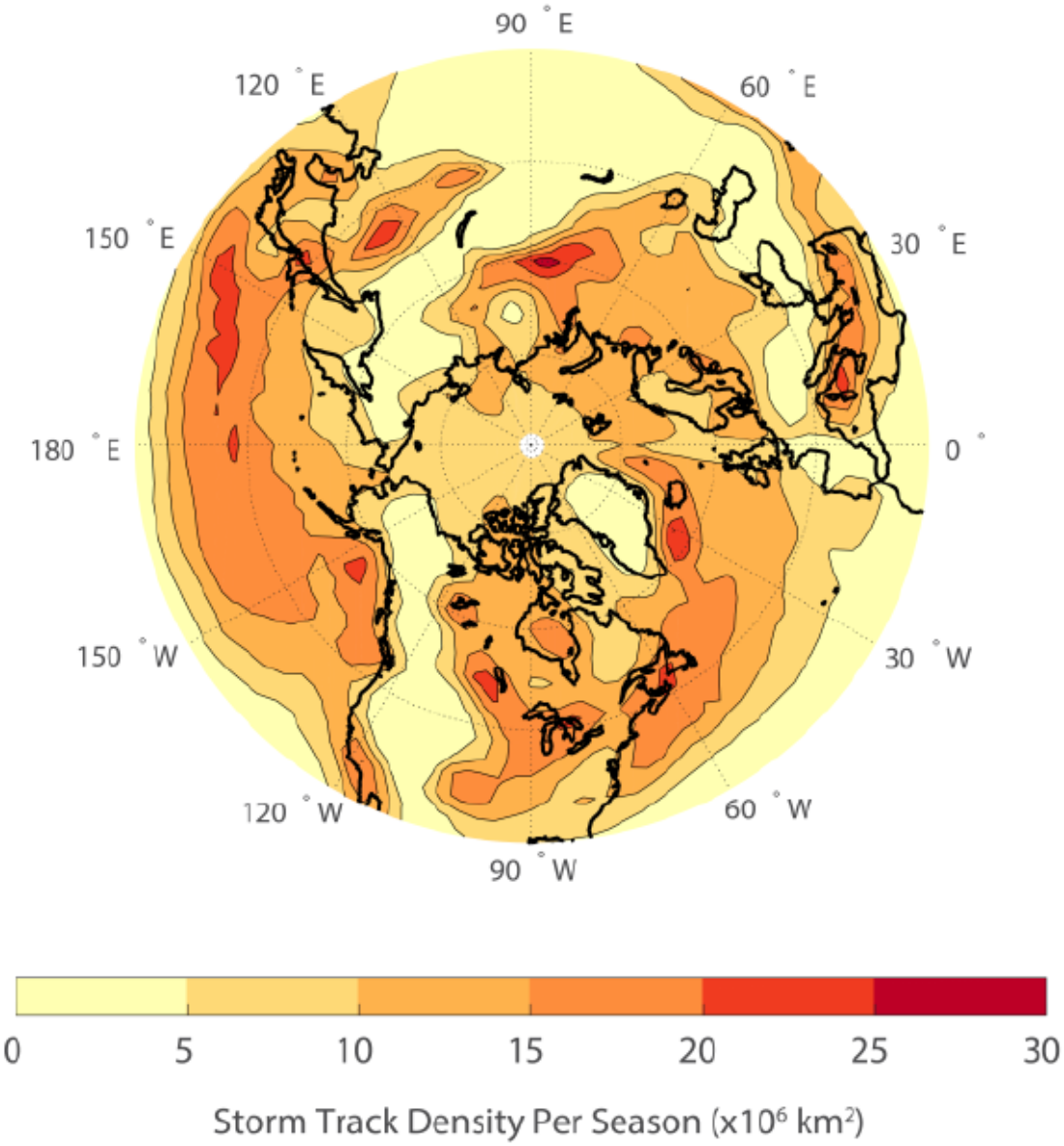

Figure 2.1: Winter (DJF) storm track density for the Northern Hemisphere (30°N-90°N). Storm track density is calculated for the 1980-2010 time period using the Hodges tracking algorithm (Hodges, 1994; 1995; 1999) and 850-hPa relative vorticity from ERA-Interim.

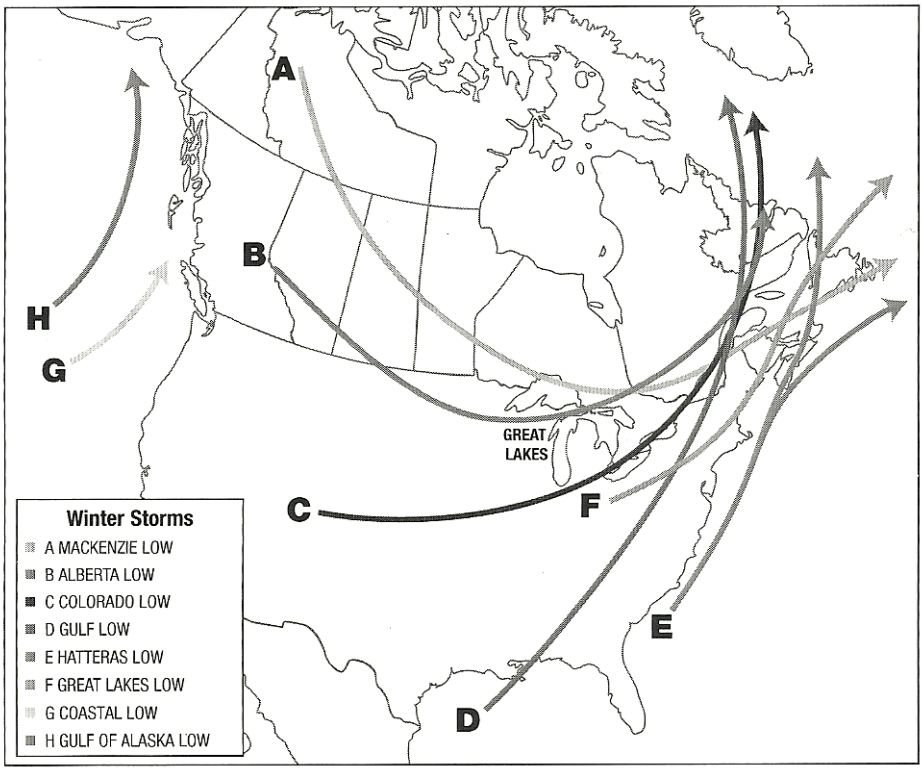

Figure 2.2: Wintertime North American storm tracks. Figure reproduced from Conrad (2008).

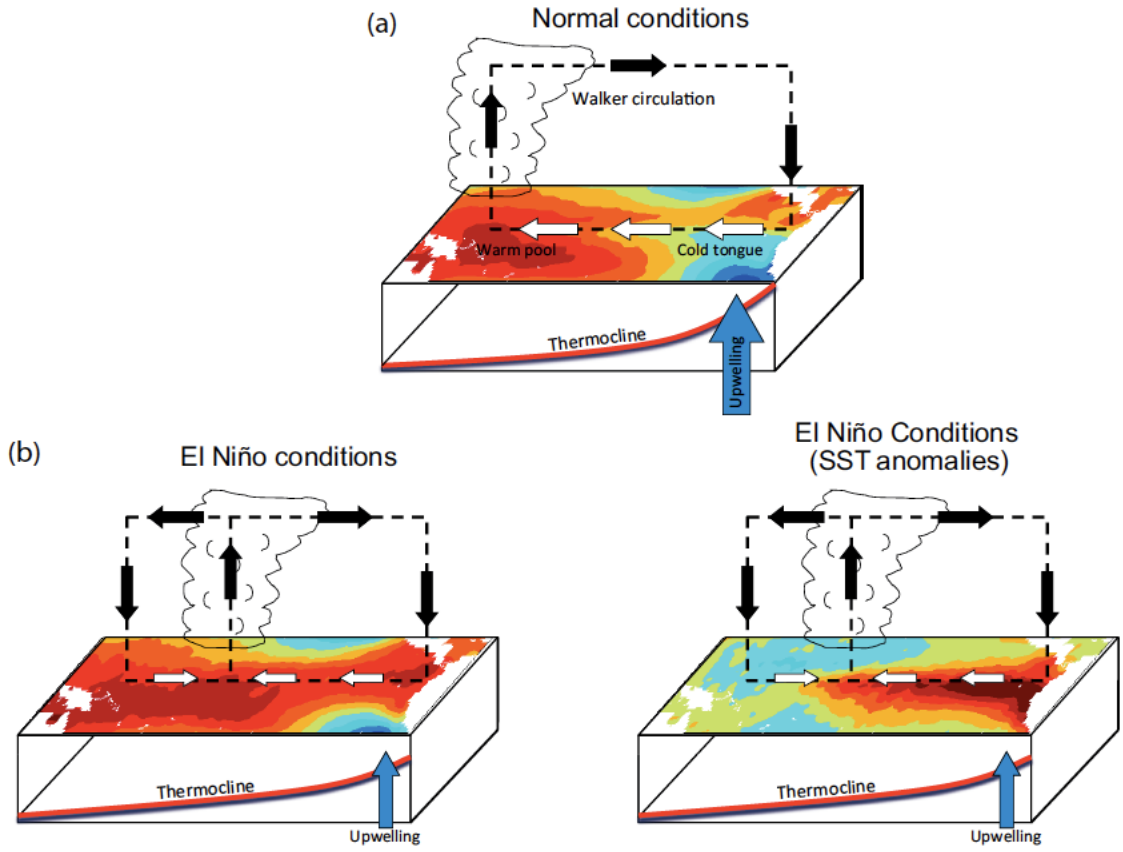

Figure 2.3: Idealized schematic of normal (neutral) and El Niño conditions in the equatorial Pacific. Atmospheric (surface wind stress, Walker Circulation, and convection region) and oceanic (sea surface temperature [and anomalies], thermocline, and strength of upwelling along the Ecuador and Peru coasts) conditions in the equatorial Pacific under neutral and El Niño conditions are displayed. Figure reproduced from Christensen et al. (2013).

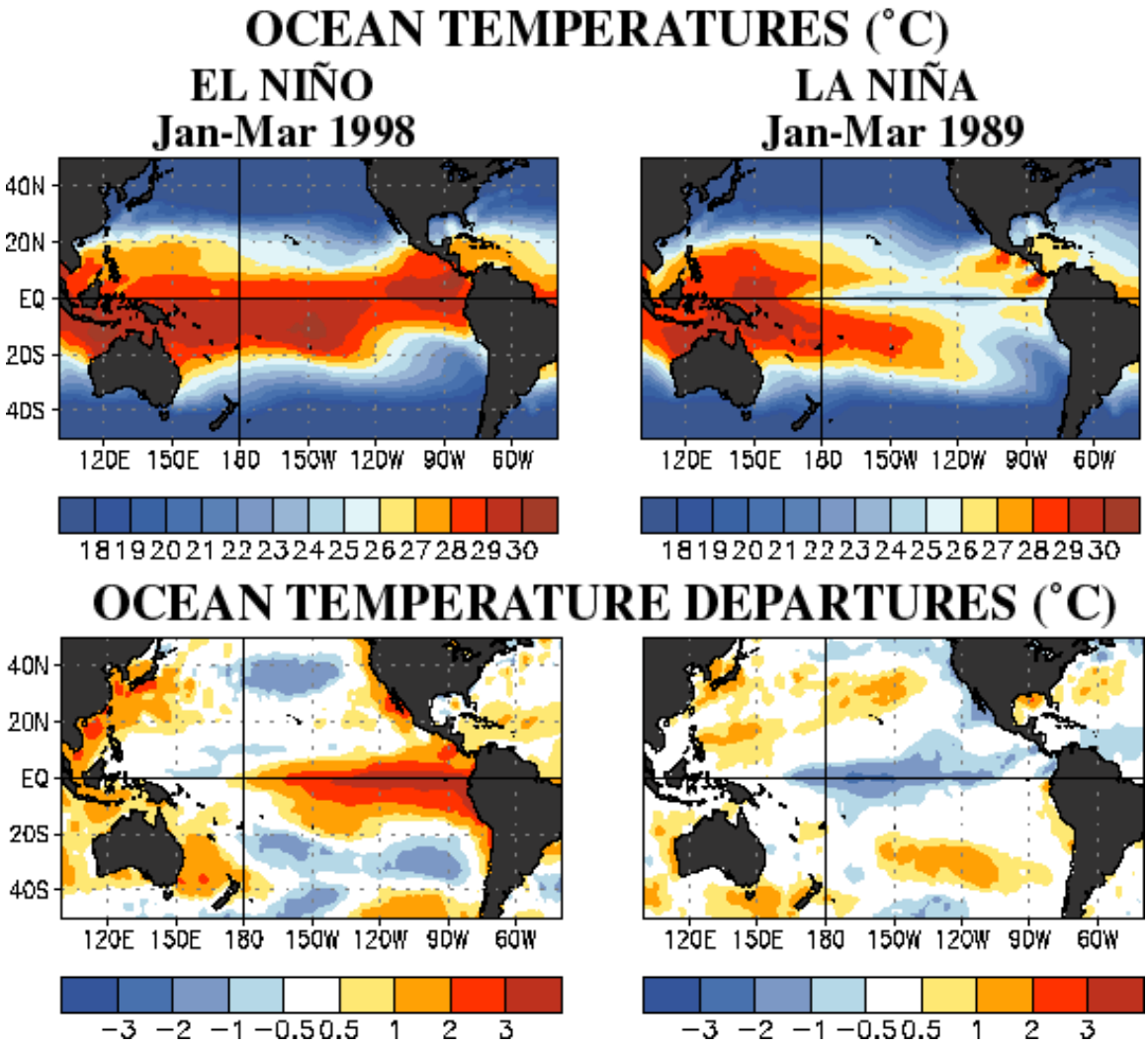

Figure 2.4: Sea surface temperatures and departures (anomalies) associated with a strong El Niño event (JFM 1998) and strong La Niña event (JFM 1989). Figure from NOAA Climate Prediction Center (http://www.cpc.ncep.noaa.gov/products/analysis_monitoring/ensocycle/ensocycle.shtml)

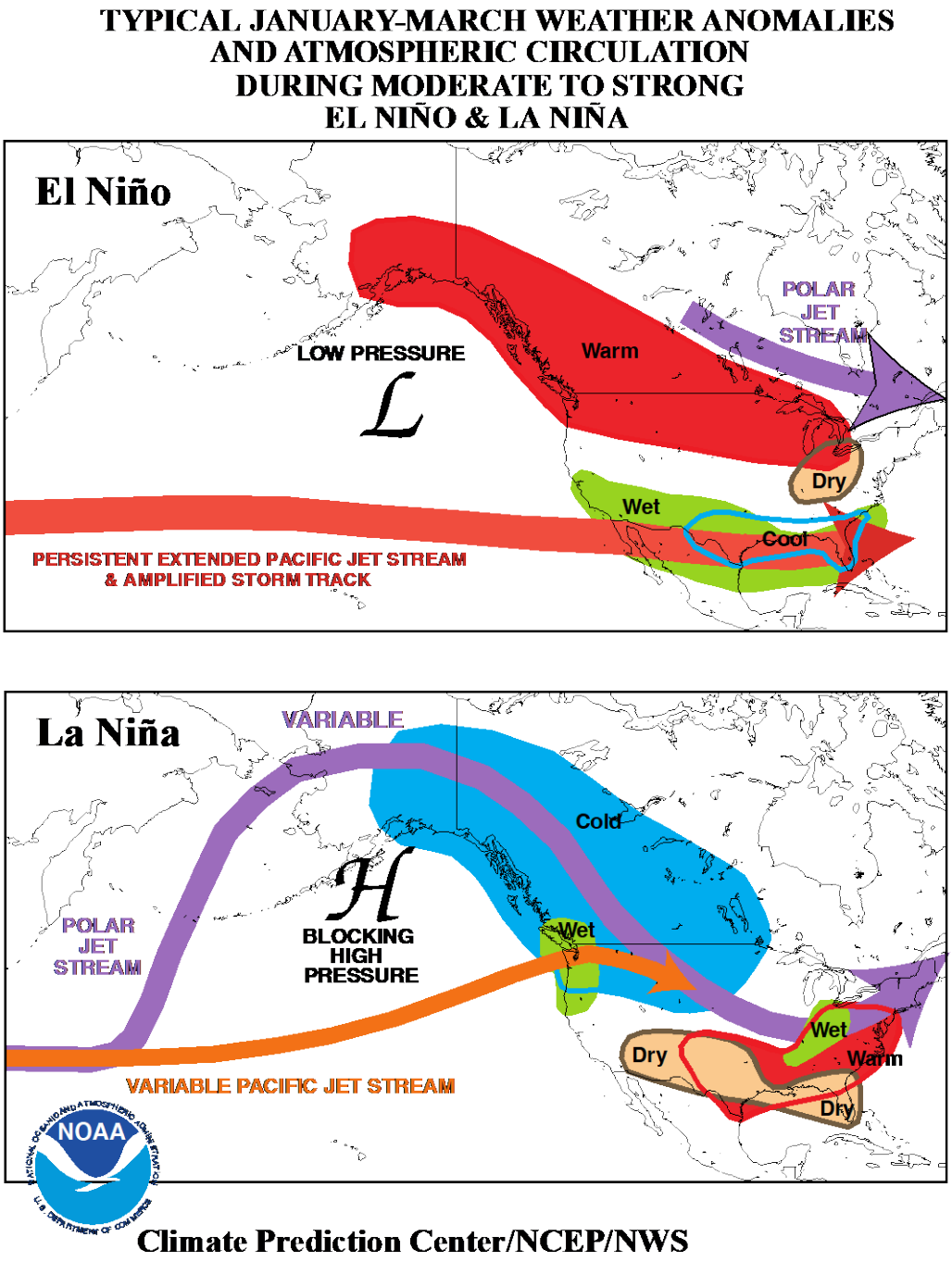

Figure 2.5: Typical JFM atmospheric circulation and weather anomalies associated with the El Niño (top) and La Niña (bottom) phases of ENSO. Figure from NOAA Climate Prediction Center (http://www.cpc.ncep.noaa.gov/products/analysis_monitoring/ensocycle/nawinter.shtml).

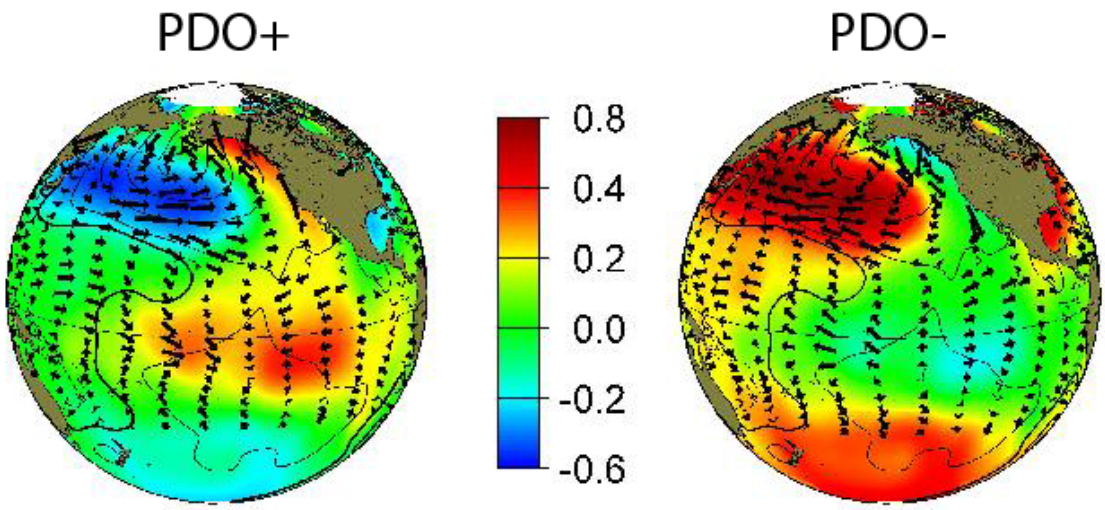

Figure 2.6: Wintertime sea surface temperature (colours), sea level pressure (contours), and surface windstress (arrows) anomalous conditions during the positive (left) and negative (right) phases of the Pacific Decadal Oscillation. Figure from the University of Washington Joint Institute for the Study of the Atmosphere and Ocean (JISAO) (http://research.jisao.washington.edu/pdo/).

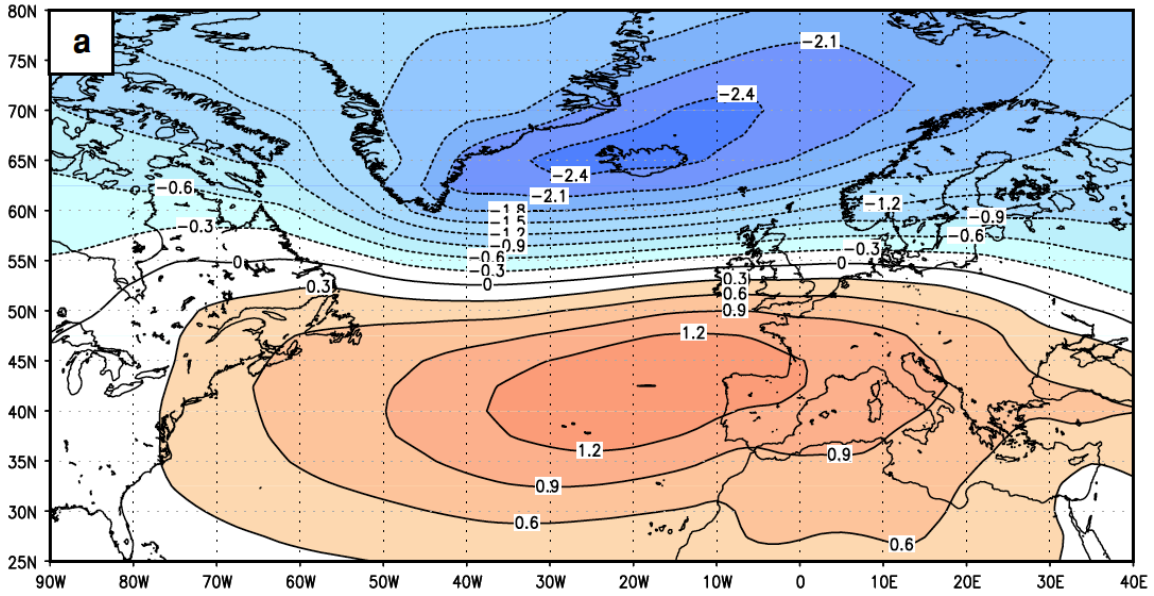

Figure 2.7: The leading principal component (PC) for MSLP for the North Atlantic/Europe region (90°W-50°E, 20°N-80°N), representing the North Atlantic Oscillation. Empirical orthogonal function (EOF) analysis was completed using 1958-1998 NCEP data for the October-March period. Figure reproduced from Pinto et al. (2009).

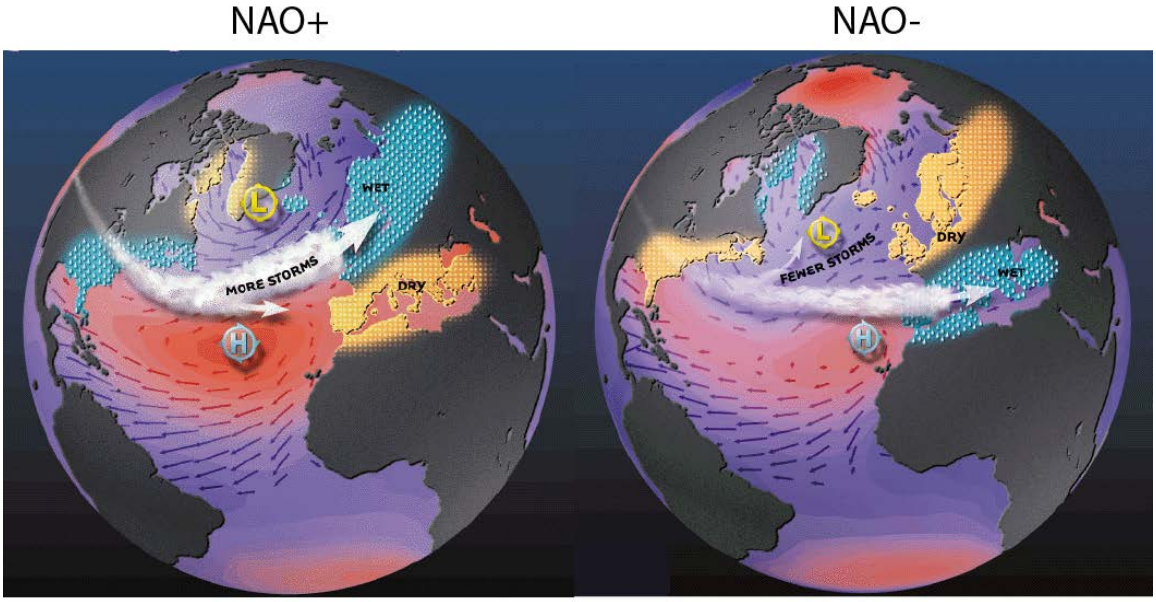

Figure 2.8: The positive (left) and negative (right) phases of the North Atlantic Oscillation and the associated climatic variability. Figures from the Lamont-Doherty Earth Observatory at Columbia University (http://www.ldeo.columbia.edu/res/pi/NAO/).

3.0 Representation of Mid-latitude North American Coastal Storm Activity by Six Global Reanalyses

3.1 Manuscript Information

This manuscript presents research completed in Research Theme 1 and is published in the International Journal of Climatology:

Pingree-Shippee, K.A., Zwiers, F.A., and Atkinson, D.A. (2017) Representation of Mid-latitude North American Coastal Storm Activity by Six Global Reanalyses. *International Journal of Climatology*, 38(2): 1041-1059. doi: 10.1002/joc.5235

Additional Research Theme 1 figures and tables not included in this manuscript are provided in Appendix A of this dissertation.

3.2 Abstract

Extratropical cyclones often produce extreme and hazardous weather conditions, such as high winds, heavy precipitation, blizzard conditions and flooding, all of which have detrimental environmental/physical and socio-economic impacts. Furthermore, storm interaction with the ocean produces additional hazards, with major local impacts, including inundation and coastal erosion. The North American west coast is influenced by the North Pacific storm track and by "atmospheric river" events while the east coast is particularly influenced by winter storms that track along two favoured routes: the St. Lawrence Valley and the Eastern Seaboard. Reanalysis provides an invaluable tool for studying the characteristics of storm events that are identified as causing the most severe

impacts. However, reanalysis products differ substantially in spatial resolution, model physics, assimilation approach and the data that are assimilated. This study evaluates the representation of storm activity along the mid-latitude North American coastlines by six global reanalyses: NCEP-1, NCEP-2, ERA-Interim, MERRA, CFSR, and 20CR. Storm activity representation is evaluated at annual and seasonal timescales (JFM, AMJ, JAS, OND, and "extended winter" ONDFM) during the 1979-2010 time period through comparison with selected meteorological stations using single point surface pressure-based proxies of extratropical storm activity. Stations are selected on the basis of record length, reporting frequency, coastal proximity, and relatively uniform spatial distribution. Comparisons are made using data extracted from the reanalysis grid box centre that is closest to each selected station. All reanalyses are found to successfully represent most aspects of mid-latitude North American coastal strong storm activity, annually and seasonally, along both coasts. Nevertheless, ERA-Interim, MERRA, and CFSR provide the better representations of mid-latitude North American coastal strong storm activity, with ERA-Interim performing best overall.

3.3 Introduction

Extratropical cyclones (ETCs) play a key role in global atmospheric circulation by transporting heat, moisture, and momentum from the subtropics poleward and are major drivers of the weather in the middle and high latitudes, often determining regional patterns of cloud cover, precipitation, and winds. Mid-latitude cyclones are distinct from tropical systems (e.g., hurricanes) but can be equally hazardous and damaging. These systems are often associated with adverse and extreme weather conditions, resulting in

natural hazards such as heavy precipitation, high winds, blizzard conditions, and flooding and, consequently, bringing detrimental socio-economic impacts. Additionally, storm-generated ocean waves and storm surges can cause severe coastal damage and major local impacts such as inundation and erosion. The North American west and east coasts are both strongly influenced by midlatitude storm activity; the west coast is influenced by the North Pacific storm track and by atmospheric river events while the east coast is particularly influenced by winter storms following two favoured tracks, the St. Lawrence Valley and the Eastern Seaboard. Consequently, land-based, coastal, and maritime economic sectors along these coasts, including land and marine transportation, aviation, agriculture, fisheries, and the built environment, all experience strong adverse impacts from ETC storm activity.

Reanalysis provides an invaluable tool for studying the characteristics of storm events associated with the most severe impacts. Reanalyses are sets of meteorological data that provide observation-based, physics-driven reconstructions of the atmospheric state that are complete (i.e., no missing values) in space and time (Dee *et al.*, 2011). These characteristics allow reconstruction of historical global storm activity. The accuracy and reliability of reanalysis datasets differ, however, due to differences in assimilation systems, spatial resolution, and the coverage and types of data that are assimilated (Löptien *et al.*, 2008; Ulbrich *et al.*, 2009; Tilinina *et al*., 2013; Wang et al., 2016). Previous studies have intercompared ETC activity (e.g., climatology, interannual variability, and cyclone characteristics) between different reanalyses, commonly utilizing cyclone identification and tracking algorithms. Hodges *et al*. (2011) compared ERA-Interim, MERRA, CFSR, and JRA-25 winter season synoptic-scale ETC representations

globally for the 1979-2009 time period, including cyclone density and intensity, using the Hodges tracking algorithm (1994; 1995; 1999). Tilinina *et al*. (2013) evaluated reanalysis representation of Northern Hemisphere ETC climatology (cyclone counts) and interannual variability, including rapidly intensifying cyclones, for the 1979-2010 time period in NCEP-2, JRA-25, ERA-Interim, CFSR, and MERRA, using the algorithm of Zolina and Gulev (2002, 2003) and Rudeva and Gulev (2007). Earlier reanalysis intercomparison studies compare older reanalyses, such as NCEP-1 and ERA-40, evaluating ETC climatology and trends (Wang *et al*., 2006a; Raible *et al*., 2008). Key findings of these intercomparison studies are that cyclone representation is, overall, consistent amongst the reanalyses in the Northern Hemisphere but still strongly dependent on spatial resolution and the amount of assimilated data, with lower resolution reanalyses underestimating cyclone frequency and strength.

Reanalyses are commonly considered as "observations" in storm activity studies (Graham and Diaz, 2001; Gulev *et al*., 2001; Eichler and Higgins, 2006; Wang *et al*., 2006a; Ulbrich *et al*., 2009; Wang *et al*., 2013; Eichler *et al*., 2015). Nevertheless, the appropriate choice of reanalysis is not straightforward. While intercomparison studies provide insight into differences between reanalyses, few studies compare reanalyses to observational data; those that do are often 'out-of-date' or consider only individual reanalyses (Harnik and Chang, 2003; Wang *et al*., 2013). This study therefore considers several global reanalyses (NCEP-1, NCEP-2, ERA-Interim, MERRA, CFSR, and 20CR) that represent a range of horizontal resolutions and assimilation systems and evaluate them directly against observational data on annual and seasonal timescales to determine which best represents mid-latitude North American coastal storm activity. Additionally,

this study focuses particularly on faster-moving more severe storms that produce more adverse and extreme weather conditions for which interest in accurate results is arguably highest. Single-station surface pressure-based proxies are utilized in this study, allowing for comparison between observed and reanalyzed storm activity at meteorological stations and the closest reanalysis grid box centres, respectively. The identified reanalysis can then be utilized as "observations" in future studies of mid-latitude North American and Canadian coastal storm activity with higher confidence and provide results of greater accuracy.

Single-station surface pressure-based proxies have been previously utilized to investigate regional storm activity using observations, with the following measures commonly used:

- Number of low pressure readings below a certain threshold
- Low percentiles of pressure readings
- Frequency of absolute pressure tendencies above a certain threshold
- Mean value of absolute pressure tendency
- High percentiles of absolute pressure tendency

These proxies have been used to study storm activity in regions such as the North Atlantic and Europe (Feser *et al*., 2015). For instance, Alexander *et al*. (2005) and Allan *et al*. (2009) studied cold season (October-March) severe storm activity over the United Kingdom and Iceland during the 20th century, defining severe storm activity as pressure tendencies greater than 10 hPa/3 hrs. Using two long-running meteorological stations, Bärring and von Storch (2004) and Bärring and Fortuniak (2009) were able to study storm activity in Scandinavia back to ~1800 using various proxies including the number

of deep lows below 980 hPa, the 95th and 99th percentiles of pressure changes between the stations, and the frequency of absolute pressure tendency above 16 hPa/12 hrs and 25 hPa/24 hrs, respectively. Elsewhere, Wang *et al*. (2006b) used surface pressure proxies of deepening rates and frequency of cyclone deepening events, defining storm activity as mean sea level pressure below 1000 hPa and using 3-hrly pressure tendencies, to study storm activity at 83 meteorological stations throughout Canada from 1953 to 2002.

The remainder of this paper is organized as follows: Descriptions of the study areas, the basis for meteorological station selections, reanalyses evaluated, storm activity proxies utilized, and reanalysis evaluation methods are provided in Section 3.4. Annual and seasonal reanalysis representations of mid-latitude North American coastal storm activity are presented in Section 3.5. A more in-depth evaluation of individual station representations by ERA-Interim and 20CR ensemble mean is also included in Section 3.5. Discussion and conclusions are presented in Section 3.6.

3.4 Methods

3.4.1 Study Areas and Meteorological Station Selections

The study areas encompass the mid-to-high latitude North American west and east coasts, including all of the Canadian and some of the US non-Arctic coastal regions. The west coast domain extends approximately 40°N-60°N, from northern California (USA), through British Columbia (Canada), to southeast Alaska (USA) (Figure 3.1a). The east coast domain extends approximately 40°N-65°N, from the New England region of the United States to southern Baffin Island, Nunavut, Canada (Figure 3.1c). Meteorological stations (Tables 3.1 and 3.2) were selected along each coast to provide synoptic-scale

coverage that intersects the major climatological storm tracks (Figure 3.1b). Station selection criteria included record length (minimum of 1979-2010), reporting frequency (sub-daily), coastal proximity, and a relatively uniform spatial distribution along the coastlines. 00 UTC and 12 UTC mean sea level pressure (MSLP) data from each station were obtained from NOAA's National Centers for Environmental Information (formally the National Climatic Data Center). Linear interpolation was used to fill missing data records, which accounted for 0.01-1.52% of station records (Tables 3.1 and 3.2). The 12-hourly station data were tested for inhomogeneities using the RHtestV3 software (Wang and Feng, 2010); all station records were found to be homogeneous.

3.4.2 Selected Reanalyses

Six global reanalysis datasets were selected for evaluation:

- NCEP-NCAR Reanalysis 1 (NCEP-1) (Kalnay *et al*., 1996; Kistler *et al*., 2001)
- NCEP-DOE Reanalysis-2 (NCEP-2) (Kanamitsu *et al*., 2002)
- ECMWF ERA-Interim (Dee *et al*., 2011)
- NASA Modern-Era Retrospective analysis for Research and Applications (MERRA) (Rienecker *et al*., 2011)
- NCEP Climate Forecast System Reanalysis (CFSR) (Saha *et al*., 2010)
- NOAA Twentieth Century Reanalysis Version 2 (20CR) (Compo *et al*., 2011)

These reanalyses were selected to represent a range of data assimilation approaches, various horizontal resolutions, and datasets commonly utilized in storm activity studies, both presently (e.g., ERA-Interim and CFSR) and during the past 10-15 years (e.g., NCEP-1). 20CR is a 56-member ensemble reanalysis using the Ensemble Kalman Filter

assimilation method. In this study, we use only the 20CR ensemble mean (20CR-em) to investigate the reanalysis' ability to reproduce storm activity, which is reasonable given that 20CR storm activity seems to be well constrained in the Northern Hemisphere by the assimilated observations, at least since the mid-20th century (Wang et al., 2013, Figure 3.4). Only global reanalyses are included in this study because storms impacting the west coast generally form outside the domain of the North American Regional Reanalysis (NARR; Mesinger et al., 2006) and would therefore still be dependent on the underlying global reanalysis. Summary information for the selected reanalyses is provided (Table 3.3) for inter-comparison. Additional information can be found in the respective reference(s) for each reanalysis. 00 UTC and 12 UTC MSLP data for evaluation were extracted from the reanalysis datasets for the closest respective grid box centre corresponding to the meteorological stations (Tables 3.4 and 3.5).

3.4.3 Storm Activity Proxies

Single-station surface pressure-based proxies (following Krueger and von Storch, 2012) allow for comparison between observed and reanalyzed storm activity at meteorological stations and the closest corresponding reanalysis grid boxes. Low pressures and large rates of pressure change (i.e., large pressure tendencies) are linked to the development and passage of synoptic-scale disturbances (i.e., cyclonic activity) and are also associated with strong winds (Kaas *et al*., 1996; Jonsson and Hanna, 2007; Krueger and von Storch, 2012). It is therefore assumed that variations of the pressure proxy statistics correspond to storm activity variations (Krueger and von Storch, 2012). In accordance with a focus on faster-moving, more severe storms, the following single-station surface pressure-based proxies and criteria were utilized to compare the observed and reanalyzed storm activity:

- 1st percentile of pressure readings (1PR); the MSLP value separating the lowest 1% of pressure readings from the remaining 99% of higher pressure readings and, therefore, a single, general indicator of the low MSLPs observed during strong storm activity (calculated annual and seasonal values for the respective reanalysis evaluations)
- 99th percentile of absolute pressure tendencies (99APT); the absolute pressure tendency value separating the highest 1% of absolute pressure tendencies from the remaining 99% of smaller absolute pressure tendencies and, therefore, a single, general indicator of the large pressure tendencies observed during strong storm activity (calculated annual and seasonal values for the respective reanalysis evaluations)
- Number of low pressure readings below 980 hPa (PR980) (calculated for the 1979-2010 time period)
- Frequency of absolute pressure tendencies above 12 hPa/12 hrs (APT12) (calculated for the 1979-2010 time period)

This study does not utilize multi-station proxies, such as the pressure triangle approach (Krueger and von Storch, 2011). The latter uses geostrophic winds calculated from pressure gradients across triangles formed by triples of nearby observing stations to represent synoptic storm activity. The pressure triangle approach is limited to locations with higher spatial coverage, which effectively rules out much of the coastal regions considered in this study.

A limitation of single-station pressure-based proxies is the assumption that variations of the proxy statistics correspond to variations of storm activity, which may not

hold in all circumstances. While the assumption is generally valid in the mid- to high latitudes for the majority of the cold seasons when storm activity is more frequent and intense, phenomena other than the passage of ETCs may cause variations in the pressure proxies. This is particularly true in summer, when the absolute pressure tendency-based proxies, especially APT12, may also reflect other circulation states or events. For instance, rapidly building high-pressure systems can occasionally undergo pressure changes of 12 hPa/12 hr or greater. Thus some care is needed when interpreting proxy-based findings from the perspective of ETC variations. Nevertheless, the pressure reading-based proxies, especially PR980, focus on the passage of synoptic-scale low-pressure systems and will highlight storm activity year-round. Furthermore, the proxy evaluations provide useful information about the ability of the reanalyses to reproduce rapid surface pressure changes.

3.4.4 Reanalysis Evaluation

Reanalysis representations of storm activity were evaluated for the 1979-2010 time period on the annual and seasonal timescales. Seasons were defined as October-November-December (fall), January-February-March (winter), April-May-June (spring), and July-August-September (summer). Additionally, an “extended” winter season of October-March was evaluated. The 1979-2010 time period was chosen based on data availability to provide a consistent time period for evaluation across all reanalyses. Season definition of OND, JFM, etc. allowed for an equal number of years (32) to be evaluated for each season while “extended winter” allows for an evaluation of storm activity representation inclusive of all the cold months during which extratropical storm activity is most frequent and intense. Reanalysis representation of storm activity was

evaluated at each individual station and for each coast as a whole. The overall coastal representation evaluations were performed by comparing observed and reanalyzed proxy anomalies from all stations combined along each coast respectively, where anomalies were obtained by removing the means from the individual time series of observed and reanalysis proxies. Results from the seasonal evaluations were similar and thus we present only those for the extended winter (ONDJFM) and summer (JAS) seasons.

Results from the count/frequency-based proxies (PR980 and APT12) are presented with bar graphs while percentile-based proxy (1PR and 99APT) results are presented with Taylor diagrams. Traditional Taylor diagrams (Taylor, 2001) provide a statistical summary of model (e.g., reanalysis) performance by displaying all at once how well each dataset from the reanalyses compares with a reference dataset (e.g., observations) in terms of correlation, root-mean-square difference, and (normalized) standard deviation of the variable of interest. We have omitted the root-mean-square difference isolines to simplify the plots. In addition to displaying reanalysis performance in the Taylor diagram, a summary skill score can also be calculated, providing a single, quantitative measure of reanalysis skill. Skill scores are based on correlation and standard deviation and can be defined in a number of ways. A desirable characteristic of these skill scores is that, for a given standard deviation, the skill score should increase with increased correlation and, for a given correlation, skill score should increase as the reanalysis standard deviation approaches the observed standard deviation (Taylor, 2001). Taylor (2001) proposed two variants of a skill score that exhibit these properties. We use the variant (Taylor, 2001; Eq. 5) that more heavily penalizes low correlation:

$$S = \frac{4(1+R)^4}{([\hat{\sigma}^2+\hat{\sigma}_o{}^2]/\hat{\sigma}\hat{\sigma}_o)^2(1+R_0)^4} \quad \text{(Eq. 3.1)}$$

where R is the correlation coefficient, $\hat{\sigma}$ is the reanalysis standard deviation, $\hat{\sigma}_o$ is the observed standard deviation, and R_0 is the maximum correlation attainable. In this study, R_0 is set to 1 as the (observation-driven) reanalysis data are being compared to observations. When R_0 = 1, the skill score, S, varies from 0 to 1 with S = 1 indicating the most skilful model representation. Weak, or negative, correlations between reanalyses and observations will result in lower S values, as will large differences between reanalysis and observed standard deviations (even with strong correlations, e.g., $R = R_0$).

3.5 Results

3.5.1 West Coast

3.5.1.1 Annual Storm Activity

Results from the count/frequency-based proxies (PR980 and APT12) show that all six reanalyses accurately reproduce the overall frequency and intensity of the observed strong storm activity along the mid-latitude North American west coast (Figure 3.2). Furthermore, the results indicate that the climatological storm track is well depicted, as stations located close to the main core of climatological storm activity (e.g., Yakutat) have notably higher PR980 counts and APT12 frequencies. Nevertheless, NCEP-1, NCEP-2, CFSR, and 20CR-em underestimate storm activity at all stations for both frequency (PR980) and intensity (APT12). 20CR-em has the largest underestimation of storm activity, particularly at stations located in areas of high storm activity (e.g., Prince Rupert and Yakutat). ERA-Interim and MERRA reproduce PR980 and APT12 most

accurately, by either slightly over- or underestimating frequency and intensity at all stations (with the exception that MERRA notably overestimates frequency at Yakutat).

The percentile-based proxies (1PR and 99APT) also indicate high accuracy of overall representation of strong storm activity by the six reanalyses (Figure 3.3, solid circles; Table S3.1). For 1PR, all reanalyses have correlations higher than 0.9 and, for 99APT, all reanalysis have correlations higher than 0.8, and exceeding 0.9 for ERA-Interim, MERRA, and CFSR. ERA-Interim, MERRA, and CFSR depict both proxies more accurately than NCEP-1, NCEP-2, and 20CR-em, with ERA-Interim and MERRA performing best for 1PR (skill scores of 0.97 and 0.96, respectively) and ERA-Interim providing the most accurate representation of 99APT (skill score of 0.86). NCEP-1, NCEP-2, and 20CR-em skill scores are commonly drawn down by lower correlations, which have a strong influence on the skill score calculation (Eq. 3.1).

Percentile-based proxy results (e.g., skill score) at each individual station are, in general, consistent among the reanalyses (Figure 3.3, open shapes; Table S3.1). Additionally, individual station representations are, largely, consistent with each reanalysis' overall coastal representation, respectively. Nonetheless, 1PR from NCEP-1, NCEP-2, and, in particular, 20CR-em and of 99APT from NCEP-1 and NCEP-2 are notably poorer at Yakutat. Overall, the reanalyses better reproduce storm activity intensity as indicated by 1PR than by 99APT. The accuracy (skill scores) of 1PR in the reanalyses, in general, decreases with increasing climatological storm activity (i.e., along the northward gradient from Arcata to Yakutat) with the exception of ERA-Interim, which is consistently high at all stations. For 99APT, the reanalyses typically perform best at Seattle-Tacoma or Prince Rupert.

3.5.1.2 Seasonal Storm Activity

Seasonal results for the count/frequency-based proxies (PR980 and APT12) are comparable to the annual results, with all six reanalyses accurately reproducing the overall frequency and intensity of the observed strong storm activity along the mid-latitude North American west coast (not shown). Reduced storm activity in the summer season results in considerably lower PR980 counts, decreased APT12 frequencies, and with strong storm activity confined to the higher latitude stations (Prince Rupert and Yakutat). Performance in summer is, nevertheless, generally consistent with annual performance (e.g., underestimation by NCEP-1).

Seasonal evaluations of the reanalyses using the percentile-based proxies for storm activity (1PR and 99APT; Figure 3.4; Table S3.2) are also similar to the annual results (Figure 3.3; Table S3.1); they exhibit comparable skill scores, with ERA-Interim, MERRA, and CFSR outperforming NCEP-1, NCEP-2, and 20CR-em. In extended winter, for both proxies, ERA-Interim performs best overall, followed by MERRA and CFSR, respectively (Figure 3.4a,b, solid circles; Table S3.2a,b). For 1PR, NCEP-1 and NCEP-2 exhibit somewhat lower skill than CFSR (skill scores of 0.93 and 0.92 vs. 0.95, respectively), and 20CR-em is the least skilful (skill score of 0.86) due to notably poor 1PR depictions at Seattle-Tacoma and Yakutat. For 99APT, however, 20CR-em is more accurate than NCEP-1 and NCEP-2 (skill scores of 0.72, 0.66, and 0.59, respectively).

Extended winter performance at individual stations (Figure 3.4a,b, open shapes; Table S3.2a,b) is highly consistent with the overall coastal performance of the respective reanalyses and is very similar among the reanalyses. Frequency (1PR) errors typically increase, however, with increasing storm activity (with the exception of ERA-Interim)

and NCEP-1, NCEP-2, and 20CR-em reproduce 1PR particularly poorly at Yakutat. Compared to 1PR, storm intensity 99APT performance at individual stations is less consistent with the overall coastal assessments and among the reanalyses, particularly for NCEP-1, NCEP-2, and 20CR-em. Furthermore, NCEP-1 and NCEP-2 99APT representations are notably poor, especially NCEP-2 at Yakutat (correlation of 0.62; skill score of 0.43).

During summer (Figure 3.4c,d, solid circles; Table S3.2c,d), the overall 1PR and 99APT results are similar to that of extended winter. Summer 99APT, however, is more accurately reproduced (higher correlations and skill scores) compared to extended winter. In the summer, ERA-Interim again performs best for both percentile-based proxies. ERA-Interim is followed closely by CFSR (skill scores of 0.98 and 0.97, respectively) for 1PR and is tied with MERRA (skill scores of 0.90) for 99APT. While ERA-Interim, MERRA, and CFSR clearly perform better than NCEP-1, NCEP-2, and 20CR-em, the overall coastal representations are more consistent amongst the reanalyses for 1PR than for 99APT.

Summer 1PR at individual stations (Figure 3.4c, open shapes; Table S3.2c) is also strongly consistent with overall coastal performance and among the reanalyses. Individual station representations of 99APT (Figure 3.4d, open shapes; Table S3.2d), however, are considerably less consistent. Furthermore, all reanalyses have notably poor depictions of 99APT at Arcata, with correlations ranging from 0.62 to 0.68 and skills scores ranging from 0.43 to 0.47. Even the best performance at Arcata by MERRA (correlation of 0.82 and skill score of 0.68) is still notably worse than at the other three stations (correlations $\geq$ 0.92 and skill scores $\geq$ 0.84 for MERRA). Subsequently, the

overall coastal assessments of 99APT for all reanalyses suffer due to the poor performance at Arcata, though less so for MERRA.

3.5.2 East Coast

3.5.2.1 Annual Storm Activity

Results from the count/frequency-based proxies (PR980 and APT12) show that all six reanalyses also accurately reproduce the overall frequency and intensity of the observed strong storm activity along the mid-latitude North American east coast (Figure 3.5). Additionally, the results indicate the climatological storm track is sufficiently represented, as stations located in more climatologically stormy locations (e.g., Gander and Goose Bay) have higher PR980 counts and APT12 frequencies. Nevertheless, the reanalyses generally overestimate storm activity frequency as measured by PR980 along the east coast, except 20CR-em which consistently underestimates PR980. In contrast, the frequency of rapid pressure changes (APT12) is more consistent with the observations, again with the exception of 20CR-em, which consistently underestimates storm activity intensity as well. Overall, ERA-Interim, MERRA, and CFSR perform best along the east coast for both PR980 and APT12.

Results from the percentile-based proxies (1PR and 99APT) also indicate high accuracy of overall strong storm activity reproduction, with all reanalyses having correlations higher than 0.9 for 1PR and higher than 0.8 (~0.95 for ERA-Interim, MERRA, and CFSR) for 99APT (Figure 3.6, solid circles; Table S3.3). As with the west coast, however, ERA-Interim, MERRA, and CFSR perform better than NCEP-1, NCEP-2, and 20CR-em. For 1PR, ERA-Interim and CFSR provide very similar assessments of storm activity (both with a skill score of 0.97) and are followed closely by MERRA (skill

score of 0.96). Alternatively, MERRA provides the most accurate depiction of storm activity as indicated by 99APT, followed closely by CFSR and ERA-Interim (skill scores of 0.92, 0.91, and 0.91, respectively).

Skill scores for the percentile-based proxies at individual stations are, in general, consistent among the reanalyses (Figure 3.6, open shapes; Table S3.3), though not as strongly as for the west coast (Figure 3.3; Table S3.1). Assessments at the individual stations are also largely comparable with each reanalysis' overall east coast evaluation. In general, for all reanalyses, 1PR is most accurate at Goose Bay and Gander and the least accurate at Mont-Joli. ERA-Interim, MERRA, and CFSR, however, all have high skill scores (≥0.92) at all the stations. For 99APT, reanalysis performance is typically best at Iqaluit or Charlottetown.

3.5.2.2 Seasonal Storm Activity

Seasonal results for the count/frequency-based proxies (PR980 and APT12) are comparable to the annual evaluation results, with all six reanalyses reproducing the overall frequency and intensity of the observed strong storm activity along the mid-latitude North American east coast (not shown). Reduced storm activity in the summer season results in considerably lower PR980 counts, decreased APT12 frequencies, and with strong storm activity confined to the higher latitude stations, particularly Iqaluit. A notable difference between the summer evaluation and the annual and extended winter evaluation results, however, is the NCEP-2 representation of APT12. In the annual and extended winter evaluations, NCEP-2 typically slightly under- or overestimates storm activity intensity while, during the summer, the reanalysis notably overestimates APT12 at all stations except Iqaluit, where it considerably underestimates APT12.

Seasonal evaluations of the reanalyses using the percentile-based proxies (1PR and 99APT) (Figure 3.7; Table S3.4) are also similar to the annual results (Figure 3.6; Table S3.3) with comparable skill scores, ERA-Interim, MERRA, and CFSR clearly outperforming NCEP-1, NCEP-2, and 20CR-em. During extended winter (Figure 3.7a,b, solid circles; Table S3.4a,b), 1PR assessment is most accurate in ERA-Interim and CFSR followed closely by MERRA (skill scores of 0.97, 0.97, and 0.96, respectively). ERA-Interim, MERRA, and CFSR also reproduce 99ATP comparably, with MERRA providing a slightly better representation based on skill score (0.92 vs. 0.91 for both ERA-Interim and CFSR) and correlation (0.96 vs. 0.95 for both ERA-Interim and CFSR). MERRA, however, does somewhat overestimate the variability of 99ATP relative to station data, with a reanalysis-to-station standard deviation ratio of 1.08 for MERRA compared to 1.04 for ERA-Interim and CFSR. NCEP-1 and NCEP-2 provide the least accurate representations of 99APT (skill scores of 0.73 and 0.71, respectively) and are notably worse than 20CR-em (skill score of 0.80).

Extended winter performances for the percentile-based proxies at individual stations are, in general, comparable with the overall coastal results and are similar among the reanalyses (Figure 3.7a,b, open shapes; Table S3.4a,b), though again not as consistently as for the west coast (Figure 3.4a,b; Table S3.2a,b). Additionally, the extended winter individual station 99APT results have a larger spread than the east coast annual results (Figure 3.6; Table S3.3). For both 1PR and 99APT, the spread is also considerably greater for NCEP-1, NCEP-2, and 20CR-em compared to ERA-Interim, MERRA, and CFSR. 99APT depictions at Boston for NCEP-1 and NCEP-2 are also notably poor (skill scores of 0.58 and 0.55, respectively). For 1PR, ERA-Interim,

MERRA, and CFSR have high skill scores (≥0.92) at all stations. For all six reanalyses, 1PR depiction is typically most accurate at Goose Bay or Gander and the least accurate at Mont-Joli and Boston.

During summer (Figure 3.7c,d, solid circles; Table S3.4c,d), ERA-Interim, MERRA, and CFSR all provide very accurate overall representations of 1PR (correlations of ~0.99; skill scores ≥ 0.97). 1PR depictions in NCEP-1, NCEP-2, and 20CR-em are less accurate but of similar skill level (skill scores of 0.82, 0.81, and 0.83, respectively). For 99APT, ERA-Interim and MERRA provide the best representations, followed closely by CFSR, based on both skill score (0.93 for ERA-Interim and MERRA; 0.92 for CFSR) and correlation (0.97 for ERA-Interim and MERRA; 0.96 for CFSR). NCEP-1, NCEP-2, and 20CR-em 99APT performances, however, are considerably less accurate, with skill scores of 0.68, 0.68, and 0.66, respectively. 20CR-em, in particular, also notably underestimates standard deviation.

Individual station 1PR and 99APT performances during the summer season are, in general, comparable with overall coastal results and are similar among the reanalyses (Figure 3.7c,d, open shapes; Table S3.4c,d), though not as consistently as for the west coast (Figure 3.4c,d; Table S3.2c,d). Strong consistency among the individual stations for 1PR in ERA-Interim, MERRA, and CFSR, however, is quite similar to the summer west coast results and have smaller spreads than the east coast annual and extended winter evaluations. The individual station 99APT results during the summer season, though, have a higher spread than the annual results. Additionally, 99APT performance is particular poor in NCEP-1 and NCEP-2 at Mont-Joli and Goose Bay (skill scores between 0.42 and 0.47). For both proxies, ERA-Interim, MERRA, and CFSR all have

high skill scores (≥0.96 for 1PR and ≥0.87 for 99APT) and consistency among all the stations evaluated.

3.5.3 Evaluation of ERA-Interim and 20CR Ensemble Mean at Individual Stations

More in-depth evaluation of reanalysis representation of strong storm activity at individual stations was also undertaken. In particular, ERA-Interim, a state-of-the-art reanalysis that is strongly constrained by the conventional observation network and satellite data, and 20CR, a tropospheric reanalysis driven only by surface observations, were evaluated at individual stations. Daily (00 UTC) MSLP readings for each reanalysis dataset were compared against those from the meteorological stations to investigate the number and timing of low pressure readings below 980 hPa. Additionally, the timing of daily MSLP readings below the respective annual 1PR and of 24-hr absolute pressure tendencies exceeding the respective annual 99APT for each reanalysis were compared against those from the meteorological stations. Results from the evaluations at Prince Rupert, BC (west coast) and Charlottetown, PE (east coast) are presented (Figures 3.8, 3.9 and 3.10, 3.11, respectively).

In evaluating the number and timing of pressure readings below 980 hPa (Figures 3.8 and 3.10), it is found that, while observed drops in MSLP are reproduced in both ERA-Interim and 20CR-em, the strength of storm events (i.e., the minimum pressure readings) are often underestimated in 20CR-em. As a result, the number of strong storm events, as detected through the MSLP readings-based proxy utilizing the 980 hPa threshold, is under-represented in 20CR-em. Evaluating the storm passages highlighted in Figures 3.8 and 3.10, respectively, 20CR-em is found to underestimate the observed minimum pressure readings of strong storms, on average, by ~5.5 hPa at Prince Rupert

and by ~7 hPa at Charlottetown. Furthermore, the resulting under-representation of strong storm activity frequency (PR980) by 20CR-em is observed at all stations along both coasts (Figures 3.2a and 3.5a), indicating the reanalysis' overall underestimation of storm strength regardless of the synoptic conditions (e.g., cyclogenesis or cyclolysis).

Similarly, while both reanalyses have a success rate of ~80% or better for reproducing the timing of MSLP readings below the respective annual 1PR (MSLP<1PR) and of 24-hr absolute pressure tendencies exceeding the respective annual 99APT (AbsPresTend>99APT) (Figures 3.9 and 3.11), 20CR-em is found to have a lower agreement with the observed data than ERA-Interim. The reduced reanalysis-to-station timing agreement of MSLP<1PR for 20CR-em at both Prince Rupert and Charlottetown (~8% and ~9.5% less than ERA-Interim, respectively) is also influenced by 20CR-em's overall underestimation of storm strength, as the strongest storms (i.e., deepest storms, which dictate the annual 1PR values) are found to have the largest departures from the observations in 20CR-em. The reanalysis-to-station timing agreement of AbsPresTend>99APT is more consistent between ERA-Interim and 20CR-em, particularly at Charlottetown (a 3.5% difference in timing agreement), though 20CR-em continues to have lower agreement with the observations. Both reanalyses are found to have better timing agreement of MSLP<1PR but worse timing agreement of AbsPresTend>99APT at Prince Rupert compared to Charlottetown. Nevertheless, overall, both reanalyses provide better timing agreement with regard to MSLP<1PR (storm frequency) than AbsPresTend>99APT (storm intensity). Subsequently, these more in-depth individual station evaluations provide further support of the coast-wide findings (discussed above) and of the overall success of the reanalyses' depictions of mid-latitude

North American, and in particular Canadian, coastal storm activity regardless of reanalysis specifics.

3.6 Discussion and Conclusions

In this study, reanalysis representation of mid-latitude North American coastal storm activity was investigated using single-station surface pressure-based proxies, with a focus on faster-moving, more severe storm activity. Six global reanalyses (NCEP-1, NCEP-2, ERA-Interim, MERRA, CFSR, and 20CR) were evaluated, representing a range of approaches to data assimilation and selection of input data sources, various horizontal resolutions, and reanalysis datasets commonly utilized in storm activity studies, both presently and during the past 10-15 years. The results reveal that the ***reanalyses using more recent models and assimilation systems, more complete observational data coverage, and higher grid resolutions better represent the observed mid-latitude North American coastal storm activity.*** Additionally, reanalysis performance does not fall along institutional lines and instead is associated with reanalysis characteristics (e.g., high-resolution CFSR vs. low-resolution NCEP-1, both distributed by NCEP). Nevertheless, all six reanalyses successfully reproduce most aspects of strong storm activity (frequency and intensity) along both coasts. ***Overall, ERA-Interim, MERRA, and CFSR performed better than NCEP-1, NCEP-2, and 20CR ensemble mean*** with ERA-Interim, MERRA, and CFSR providing comparable representations of mid-latitude North American coastal storm activity, annually and seasonally. Of these, ***ERA-Interim performs best in most of the cases***, particularly during "extended winter" (October through March), when extratropical storm activity is most frequent and intense and interest in accurate results is

arguably highest. The use of the 20CR ensemble mean may have led to some underestimation of storm activity due to the smoothing effects of averaging over the 56 ensemble members. Use of individual ensemble members in a future study may therefore give a somewhat better assessment. Recall, however, that Wang *et al*. (2013) demonstrate that cyclonic activity in the Northern Hemisphere is well constrained in 20CR by observations during 1979-2010, with cyclonic activity in the ensemble mean being almost as intense as in the individual members. Nevertheless, more in-depth evaluation of ERA-Interim and 20CR ensemble mean at Prince Rupert (west coast) and Charlottetown (east coast) revealed that both reanalyses also possess generally robust capacity to replicate storm event specifics, and therefore provides additional support of the overall success all of the reanalyses exhibited in representing mid-latitude North American, and in particular Canadian, coastal storm activity.

Comparable results are obtained when stations are examined individually. The individual station evaluations further reveal that ***performance among the reanalyses is generally more consistent (i.e., smaller spread) on the west coast than the east coast***, possibly due to the differing synoptic situations on the two coasts (such that cyclolysis and cyclogenesis dominate, respectively). Cyclogenesis, including rapid intensification, is presumably more challenging to reproduce in reanalyses compared to decaying cyclones and cyclolysis. ***The high occurrence of cyclogenesis on the east coast could, therefore, be a main contributor to the larger spread observed.*** The high frequency of cyclogenesis may also be contributing to the interesting results of the count-based and percentile-based proxies: Storm activity frequency, as represented by PR980, along the east coast is overestimated by the majority of the reanalyses, indicating that the reanalyses deepen

cyclones beyond the observed minimum central pressures. Nevertheless, the overall accuracy of 1PR and 99APT in the reanalyses (commonly most accurate at Goose Bay or Gander and Charlottetown, respectively, all located in the main core of the climatological storm activity), indicates that the reanalyses are not over-deepening cyclones excessively and deepening rates are reanalyzed appropriately. Additional investigation that is beyond the scope of this paper would be necessary to determine the reason(s) behind the contrast between the apparent overestimation of PR980 and the appropriate representations of 1PR and 99APT along the east coast.

Reanalysis representation on the east coast could be further challenged by the multiple storm tracks and life cycle stages of the extratropical cyclones impacting the region, resulting in lower skill scores. The two favoured storm tracks that influence the east coast study domain result in extratropical cyclones entering the region at different stages of their life cycles; e.g., systems undergoing cyclogenesis, including rapid intensification, tracking up the Eastern Seaboard vs. mature and decaying cyclones originating in the lee of the Rocky Mountains and tracking up the St. Lawrence Valley. For instance, 1PR on the east coast was, typically, least accurate at Mont-Joli, the furthest inland station and within the St. Lawrence Valley, or Boston, the southern-most station evaluated. Mont-Joli is influenced by multiple storm tracks and cyclones in various life cycle stages, from intensifying to decaying, therefore potentially resulting in a more challenging storm activity picture to reproduce in the reanalyses. The poor representation of 1PR at Mont-Joli may be due to strong cyclones originating from the North America interior decaying too quickly prior to reaching the Gulf of St. Lawrence region. Alternatively, the poor representation may be due to cyclones moving up the Eastern

Seaboard that are tracking incorrectly, not deepening enough prior to moving eastward away from the coast, or not synoptically large enough (i.e., horizontal scale of the system) to register low enough pressures at Mont-Joli. Boston, however, is influenced primarily by cyclones tracking up the Eastern Seaboard, therefore suggesting the poor representation of 1PR there may be due to cyclones tracking too far east of the coast or not deepening quickly enough prior to reaching the northeast US.

In association with the poor performance at select individual stations such as Mont-Joli and Boston on the east coast and Yakutat (1PR and 99APT in NCEP-1, NCEP-2, and 20CR-em) and Arcata (summer 99APT in all reanalyses) on the west coast, ***considerable variations in skill can also be observed along each coast,*** particularly for 99APT in NCEP-1, NCEP-2, and 20CR-em, during the summer. ***These poor individual station performances and coast-wide variations in skill are interesting given that MSLP in the reanalyses (a 'Class A' variable as defined by Kalnay et al., 1996) is strongly constrained by observational data in the assimilation process.*** Furthermore, the observational data from the meteorological stations used in this study would also, presumably, be utilized during the assimilation process in the reanalyses evaluated. Additional investigation is therefore required (e.g., evaluation of additional stations in the region, employing other methods such as cyclone identification and tracking algorithms, investigating data assimilation and model physics, etc.) to determine the reason(s) behind the poorer individual station representations and associated coastal variations in skill found in this research. Nevertheless, this research reveals that, overall, ***all six reanalyses evaluated successfully depict most aspects of mid-latitude North American coastal strong storm activity on both the west and east coasts, annually and seasonally, with***

ERA-Interim, MERRA, and CFSR providing the better representations and ERA-Interim performing best overall.

3.7 Acknowledgements

Funding for this research was provided by the Marine Environmental Observation Prediction and Response (MEOPAR) Network of the Centres of Excellence of Canada, subproject 2.1.2 “Coastal Storm Activity”, PI Francis Zwiers, under Project 2.1 “Climate Change and Extreme Events in the Marine Environment”, PIs Greg Flato, Gordon McBean, Bill Merryfield, Barbara Neis, Ronald Pelot, Jinyu Sheng, and Francis Zwiers. This research was also supported by the University of Victoria’s Department of Geography and the Pacific Climate Impacts Consortium.

3.8 Supporting Information

Skill scores (as calculated using Eq. 3.1) for all presented evaluations (annual, extended winter, and summer) of reanalysis representation of strong storm activity along the mid-latitude North American west and east coasts using the percentile-based proxies (1PR and 99APT) are provided in the Supporting Information:

Table S3.1. Skill scores for the annual evaluations along the North American west coast.

Table S3.2. Skill scores for the extended winter and summer seasonal evaluations along the North American west coast.

Table S3.3. Skill scores for the annual evaluations along the North American east coast.

Table S3.4. Skill scores for the extended winter and summer seasonal evaluations along the North American east coast.

3.9 References

Alexander LV, Tett SFB, Jonsson T. 2005. Recent observed changes in severe storms over the United Kingdom and Iceland. *Geophysical Research Letters* **32**: L13704. doi:10.1029/2005GL022371.

Allan R, Tett S, Alexander L. 2009. Fluctuations in autumn-winter severe storms over the British Isles: 1920 to present. *International Journal of Climatol*ogy **29**: 357-371. doi:10.1002/joc.1765.

Bärring L, von Storch H. 2004. Scandinavian storminess since about 1800. *Geophysical Research Letters* **31**: L20202. doi: 10.1029/2004GL020441.

Bärring L, Fortuniak K. 2009. Multi-indices analysis of southern Scandinavian storminess 1780-2005 and links to interdecadal variations in the NW Europe-North Sea region. *International Journal of Climatology* **29**: 373-384. doi:10.1002/joc.1842.

Compo GP, Whitaker JS, Sardeshmukh PD, Matsui N, Allan RJ, Yin X, Gleason Jr BE, Vose RS, Rutledge G, Bessemoulin P, Bronnimann S, Brunet M, Crouthamel RI, Grant AN, Groisman PY, Jones PD, Kruk MC, Kruger AC, Marshall GJ, Maugeri M, Mok HY, Nordli O, Ross TF, Trigo RM, Wang XL, Woodruff SD, Worley SJ. 2011. The Twentieth Century Reanalysis Project. *Quarterly Journal of the Royal Meteorological Society* **137**: 1-28. doi:10.1002/qj.776.

Dee DP, Uppala SM, Simmons AJ, Berrisford P, Poli P, Kobayashi S, Andrae U, Balmaseda MA, Balsamo G, Bauer P, Bechtold P, Beljaars ACM, van de Berg L, Bidlot J, Bormann N, Delsol C, Dragani R, Fuentes M, Geer AJ, Haimberger L, Healy SB, Hersbach H, Holm EV, Isaksen L, Kallberg P, Kohler M, Matricardi M, McNally AP, Monge-Sanz BM, Morcrette JJ, Park BK, Peubey C, de Rosnay P, Tavolato C, Thepaut JN, Vitart F. 2011. The ERA-Interim reanalysis: configuration and performance of the data assimilation system. *Quarterly Journal of the Royal Meteorological Society* **137**: 553-597. doi:10.1002/qj.828.

Eichler T, Higgins W. 2006. Climatology and ENSO-Related Variability of North American Extratropical Cyclone Activity. *Journal of Climate* **19**: 2076-2093. doi:10.1175/JCLI3725.1.

Eichler TP, Alvarez F, Gottschalck J. 2015. Northern Hemisphere Climatology and Interannual Variability of Storm Tracks in NCEP's CFS Model. *Advances in Meteorology* Vol. 2015, Article ID 720545. doi:10.1155/2015/720545.

Feser F, Barcikowska M, Krueger O, Schenk F, Weisse R, Xia L. 2015. Storminess over the North Atlantic and northwestern Europe - A review. *Quarterly Journal of the Royal Meteorological Society* **141**: 350-382. doi:10.1002/qj.2364.

Graham NE, Diaz HF. 2001. Evidence for Intensification of North Pacific Winter Cyclones since 1948. *Bulletin of the American Meteorological Society* **82**: 1869-1893. doi:10.1175/1520-0477(2001)082<1869:EFIONP>2.3.CO;2.

Gulev SK, Zolina O, Grigoriev S. 2001. Extratropical cyclone variability in the Northern Hemisphere winter from the NCEP/NCAR reanalysis data. *Climate Dynamics* **17**: 795-809. doi:10.1007/s003820000145.

Harnik N, Chang EKM. 2003. Storm Track Variations As Seen in Radiosonde Observations and Reanalysis Data. *Journal of Climate* **16**: 480-495. doi:10.1175/1520-0442(2003)016<0480:STVASI>2.0.CO;2.

Hodges KI. 1994. A general method for tracking analysis and its application to meteorological data. *Monthly Weather Review* **122**: 2573-2586. doi:10.1175/1520-0493(1994)122<2573:AGMFTA>2.0.CO;2.

Hodges KI. 1995. Feature tracking on the unit sphere. *Monthly Weather Review* **123**: 3458-3465. doi:10.1175/1520-0493(1995)123<3458:FTOTUS>2.0.CO;2.

Hodges KI. 1999. Adaptive Constraints for Feature Tracking. *Monthly Weather Review* **127**: 1362-1373. doi:10.1175/1520-0493(1999)127<1362:ACFFT>2.0.CO;2.

Hodges KI, Hoskins BJ, Boyle J, Thorncroft C. 2003. A Comparison of Recent Reanalysis Datasets Using Objective Feature Tracking: Storm Tracks and Tropical Easterly Waves. *Monthly Weather Review* **131**: 2012-2037. doi:10.1175/1520-0493(2003)131<2012:ACORRD>2.0.CO;2.

Hodges KI, Lee RW, Bengtsson L. 2011. A Comparison of Extratropical Cyclones in Recent Reanalyses ERA-Interim, NASA MERRA, NCEP CFSR, and JRA-25. *Journal of Climate* **24**: 4888-4906. doi:10.1175/2011JCLI4097.1.

Jonsson T, Hanna E. 2007. A new day-to-day pressure variability index as a proxy of Icelandic storminess and complement to the North Atlantic Oscillation index 1823-2005. *Meteorologische Zeitschrift* **16**: 25-36. doi:10.1127/0941-2948/2007/0177.

Kaas E, Li T, Schmith T. 1996. Statistical hindcast of wind climatology in the North Atlantic and northwestern European region. *Climate Research* **7**: 97-110. doi:10.3354/cr007097.

Kalnay E, Kanamitsu M, Kistler R, Collins W, Deaven D, Gandin L, Iredell M, Saha S, White G, Woollen J, Zhu Y, Chelliah M, Ebisuzaki W, Higgins W, Janowiak J, Mo KC, Ropelewski C, Wang J, Leetmaa A, Reynolds R, Jenne R, Joseph D. 1996. The NCEP/NCAR 40-Year Reanalysis Project. *Bulletin of the American Meteorological Society* **77**: 437-471. doi:10.1175/1520-0477(1996)077<0437:TNYRP>2.0.CO;2.

Kanamitsu M, Ebisuzaki W, Woollen J, Yang S, Hnilo JJ, Fiorino M, Potter GL. 2002. NCEP-DOE AMIP-II Reanalysis (R-2). *Bulletin of the American Meteorological Society* **83**: 1631-1643. doi:10.1175/BAMS-83-11-1631.

Kistler R, Kalnay E, Collins W, Saha S, White G, Woollen J, Chelliah M, Ebisuzaki W, Kanamitsu M, Kousky V, van den Dool H, Jenne R, Fiorino M. 2001. The NCEP-NCAR 50-Year Reanalysis: Monthly Means CD-ROM and Documentation. *Bulletin of the American Meteorological Society* **82**: 247-267. doi:10.1175/1520-0477(2001)082<0247:TNNYRM>2.3.CO;2.

Krueger O, von Storch H. 2011. Evaluation of an Air Pressure-Based Proxy for Storm Activity. *Journal of Climate* **24**: 1612-2619. doi:10.1175/2011JCLI3913.1.

Krueger O, von Storch H. 2012. The Informational Value of Pressure-Based Single-Station Proxies for Storm Activity. *Journal of Atmospheric and Oceanic Technology* **29**: 569-580. doi:10.1175/JTECH-D-11-00163.1.

Löptien U, Zolina O, Gulev S, Latif M, Soloviov V. 2008. Cyclone life cyclone characteristics over the Northern Hemisphere in coupled GCMS. *Climate Dynamics* **31**: 507-532. doi:10.1007/s00382-007-0355-5.

Mesinger F, DiMego G, Kalnay E, Mitchell K, Shafran PC, Ebisuzaki W, Jović D, Woollen J, Rogers E, Berbery EH, Ek MB, Fan Y, Grumbine R, Higgins W, Li H, Lin Y, Manikin G, Parrish D, Shi W. 2006. North American Regional Reanalysis. *Bulletin of the American Meteorological Society* **87**: 343-360. doi: 10.1175/BAMS-87-3-343.

Raible CC, Della-Marta PM, Schwierz C, Wernli H, Blender R. 2008. Northern Hemisphere Extratropical Cyclones: A Comparison of Detection and Tracking Methods and Different Reanalyses. *Monthly Weather Review* **136**: 880-897. doi:10.1175/2007MWR2143.1.

Rienecker MM, Suarez MJ, Gelaro R, Rodling R, Bacmeister J, Liu E, Bosilovich MG, Schubert SD, Takacs L, Kim G-K, Bloom S, Chen J, Collins D, Conaty A, da Silva A, Gu W, Joiner J, Koster RD, Lucchesi R, Molod A, Owens T, Pawson S, Pegion P, Redder CR, Reichle R, Robertson FR, Ruddick AG, Sienkiewicz M, Woollen J. 2011. MERRA: NASA's Modern-Era Retrospective Analysis for Research and Applications. *Journal of Climate* **24**: 3624- 3648. doi:10.1175/JCLI-D-11-00015.1.

Rudeva I, Gulev SK. 2007. Climatology of cyclone size characteristics and their changes during the cyclone life cycle. *Monthly Weather Review* **135**: 2568-2587. doi:10.1175/MWR3420.1.

Saha S, Moorthi S, Pan H-L, Wu X, Wang J, Nadiga S, Tripp P, Kistler R, Woollen J, Behringer D, Liu H, Stokes D, Grumbine R, Gayno G, Wang J, Hou Y-T, Chuang H-Y, Juang H-MH, Sela J, Iredell M, Treadon R, Kleist D, Van Delst P, Keyser D, Derber J, Ek M, Meng J, Wei H, Yang R, Lord S, van den Dool H, Kumar A, Wang W, Long C, Chelliah M, Xue Y, Huang B, Schemm J-K, Ebisuzaki W, Lin R, Xie P, Chen M, Zhou S, Higgins W, Zou C-Z, Liu Q, Chen Y, Han Y, Cucurull L, Reynolds RW, Rutledge G, Goldberg M. 2010. The NCEP Climate Forecast System Reanalysis. *Bulletin of the American Meteorological Society* **91**: 1015-1057. doi:10.1175/2010Bams3001.1.

Taylor KE. 2001. Summarizing multiple aspects of model performance in a single diagram. *Journal of Geophysical Research* **106**: 7183-7192. doi:10.1029/2000JD900719.

Tilinina N, Gulev SK, Rudeva I, Kiltermann P. 2013. Comparing cyclone life cycle characteristics and their interannual variability in different reanalyses. *Journal of Climate* **26**: 6419-6438. doi:10.1175/JCLI-D-12-00777.1.

Ulbrich U, Leckebusch GC, Pinto JG. 2009. Extra-tropical cyclones in the present and future climate: a review. *Theoretical and Appied. Climatology* **96**: 117-131. doi:10.1007/s00704-008-0083-8.

Wang XL, Swail VR, Zwiers FW. 2006a. Climatology and Changes of Extratropical Cyclone Activity: Comparison of ERA-40 with NCEP-NCAR Reanalysis for 1958-2001. *Journal of Climate* **19**: 3145-3165. doi:10.1175/JCLI3781.1.

Wang XL, Wan H, Swail VR. 2006b. Observed Changes in Cyclone Activity in Canada and Their Relationships to Major Circulation Regimes. *Journal of Climate* **19**: 896-915. doi:10.1175/JCLI3664.1.

Wang XL, Feng Y. 2010. RHtestsV3 User Manual. Available online at http://etccdi.pacificclimate.org/RHtest/RHtestsV3_UserManual.doc. Accessed 1 May 2013.

Wang XL, Feng Y, Compo GP, Swail VR, Zwiers FW, Allan RJ, Sardeshmukh PD. 2013. Trends and low frequency variability of extra-tropical cyclone activity in the ensemble of twentieth century reanalysis. *Climate Dynamics* **40**: 2775-2800. doi:10.1007/s00382-012-1450-9.

Wang XL, Feng Y, Chan R, Isaac V. 2016 Inter-comparison of extra-tropical cyclone activity in nine reanalysis datasets. *Atmospheric Research* **181**: 133-153. doi: 10.1016/j.atmosres.2016.06.010.

Zolina O, Gulev SK. 2002. Improving the accuracy of mapping cyclone numbers and frequencies. *Monthly Weather Review* **130**: 748-759. doi:10.1175/1520-0493(2002)130<0748:ITAOMC>2.0.CO;2.

Zolina O, Gulev SK. 2003. Synoptic variability of ocean-atmosphere turbulent fluxes associated with atmospheric cyclones. *Journal of Climate* **16**: 2717-2734. doi:10.1175/1520-0442(2003)016<2717:SVOOTF>2.0.CO;2.

West Coast				
Station	**Station Name, WMO Id**	**Latitude, Longitude**	**Elevation (m)**	**Percent of Record Filled via Linear Interpolation**
Arcata, CA, USA	Arcata Airport, 725945-24283	40.978°, -124.108°	60.959	1.27
Seattle-Tacoma, WA, USA	Seattle-Tacoma International Airport, 727930-24233	47.444°, -122.314°	132.3	0.01
Prince Rupert, BC, Canada	Prince Rupert, 718980-99999	54.283°, -130.450°	35.349	1.52
Yakutat, AK, USA	Yakutat Airport, 703610-25339	59.512°, -139.671°	10.06	0.05

Table 3.1: Meteorological station selections for the west coast.

East Coast				
Station	**Station Name, WMO Id**	**Latitude, Longitude**	**Elevation (m)**	**Percent of Record Filled via Linear Interpolation**
Boston, MA, USA	Gen E L Logan International Airport, 725090-14739	42.360°, -71.010°	3.66	0.01
Charlottetown, PE, Canada	Charlottetown, 717060-99999	46.283°, -63.133°	48.759	0.83
Mont-Joli, QC, Canada	Mont Joli A, 717180-99999	48.600°, -68.216°	52.419	1.11
Gander, NL, Canada	Gander Intl, 718030-99999	48.936°, -54.568°	151.179	0.72
Goose Bay, NL, Canada	Goose Bay, 718160-99999	53.316°, -60.416°	48.759	0.82
Iqaluit, NU, Canada	Iqaluit, 719090-99999	63.756°, -68.555°	33.520	0.87

Table 3.2: Meteorological station selections for the east coast.

Reanalysis	Complete Reanalyzed Time Period	Resolution (Horizontal; Vertical)	Assimilation System	Observational Data Assimilated
NCEP-NCAR Reanalysis 1 (NCEP-1; Kalnay *et al*., 1996; Kistler *et al*., 2001)	1948-present	T62; 28 vertical levels	3D-variational analysis (3D-Var) spectral statistical interpolation	Conventional observation network and satellite data
NCEP-DOE Reanalysis-2 (NCEP-2; Kanamitsu *et al*., 2002)	1979-present	T62; 28 vertical levels	3D-variational analysis (3D-Var) spectral statistical interpolation	Conventional observation network and satellite data
ECMWF ERA-Interim (Dee *et al*., 2011)	1979-present	T225; 60 vertical levels	4D-variational analysis (4D-Var)	Conventional observation network and satellite data
NASA Modern-Era Retrospective analysis for Research and Applications (MERRA; Rienecker *et al*., 2011)	1979-present	½° lat x ⅔° long; 72 vertical levels	3D-variational data (3D-Var) analysis based on the Gridpoint Statistical Interpolation scheme, includes an incremental analysis update procedure	Conventional observation network and satellite data
NCEP Climate Forecast System Reanalysis (CFSR; Saha *et al*., 2010)	1979-2010	T382; 64 vertical levels	3D-variational data assimilation (3D-Var) analysis based on the Gridpoint Statistical Interpolation scheme	Conventional observation network and satellite data
NCAR Twentieth Century Reanalysis (20CR; Compo *et al*., 2011)	1871-2011	T62; 28 vertical levels	56-member ensemble Ensemble Kalman Filter method	Surface pressure from conventional observational network stations

Table 3.3: Global reanalyses selected for evaluation. Note: While the complete reanalyzed time periods are indicated for each reanalysis dataset in this table, only the 1979-2010 time period was evaluated in this research.

West Coast							
Location		**Meteorological Station**	**NCEP-1, NCEP-2**	**ERA-Interim**	**MERRA**	**CFSR**	**20CR**
Arcata, CA	Lat. (Diff)	40.978° -	40.000° (-0.978°)	41.250° (0.272°)	41.000° (0.022°)	41.000° (0.022°)	40.000° (-0.978°)
	Lon. (Diff)	-124.108° -	-125.000° (-0.892°)	-123.750° (0.358°)	-124.000° (0.108°)	-124.000° (0.108°)	-124.000° (0.108°)
Seattle-Tacoma, WA	Lat. (Diff)	47.444° -	47.500° (0.056°)	47.250° (-0.194°)	47.500° (0.056°)	47.500° (0.056°)	48.000° (0.556°)
	Lon. (Diff)	-122.314° -	-122.500° (-0.186°)	-122.250° (0.064°)	-122.000° (0.314°)	-122.500° (-0.186°)	-122.000° (0.314°)
Prince Rupert, BC	Lat. (Diff)	54.283° -	55.000° (0.717°)	54.000° (-0.283°)	54.500° (0.217°)	54.500° (0.217°)	54.000° (-0.283°)
	Lon. (Diff)	-130.450° -	-130.000° (0.450°)	-130.500° (-0.050°)	-130.667° (-0.217°)	-130.500° (-0.050°)	-130.000° (0.450°)
Yakutat, AK	Lat. (Diff)	59.512° -	60.000° (0.488°)	59.250° (-0.262°)	59.500° (-0.012°)	59.500° (-0.012°)	60.000° (0.488°)
	Lon. (Diff)	-139.671° -	-140.000° (-0.329°)	-139.500° (0.171°)	-140.000° (-0.329°)	-139.500° (0.171°)	-140.000° (-0.329°)

Table 3.4: Latitude-longitude coordinates for west coast meteorological stations and the associated closest reanalysis grid box centres along with the latitudinal/longitudinal difference between the locations.

East Coast							
Location		**Meteorological Station**	**NCEP-1, NCEP-2**	**ERA-Interim**	**MERRA**	**CFSR**	**20CR**
Boston, MA	Lat.	42.360°	42.500°	42.000°	42.500°	42.500°	42.000°
	(Diff)	-	(0.140°)	(-0.360°)	(0.140°)	(0.140°)	(-0.360°)
	Lon.	-71.010°	-70.000°	-71.250°	-71.333°	-71.000°	-72.000°
	(Diff)	-	(1.010°)	(-0.240°)	(-0.323°)	(0.010°)	(-0.990°)
Charlottetown, PE	Lat.	46.283°	47.500°	46.500°	46.500°	46.500°	46.000°
	(Diff)	-	(1.217°)	(0.217°)	(0.217°)	(0.217°)	(-0.283°)
	Lon.	-63.133°	-62.500°	-63.000°	-63.333°	-63.000°	-64.000°
	(Diff)	-	(0.633°)	(0.133°)	(-0.200°)	(0.133°)	(-0.867°)
Mont-Joli, QC	Lat.	48.600°	47.500°	48.750°	48.500°	48.500°	48.000°
	(Diff)	-	(-1.100°)	(0.150°)	(-0.100°)	(-0.100°)	(-0.600°)
	Lon.	-68.216°	-67.500°	-68.250°	-68.000°	-68.000°	-68.000°
	(Diff)	-	(0.716°)	(-0.034°)	(0.216°)	(0.216°)	(0.216°)
Gander, NL	Lat.	48.936°	50.000°	48.750°	49.000°	49.000°	48.000°
	(Diff)	-	(1.064°)	(-0.186°)	(0.064°)	(0.064°)	(-0.936°)
	Lon.	-54.568°	-55.000°	-54.750°	-54.667°	-54.500°	-54.000°
	(Diff)	-	(-0.432°)	(-0.182°)	(-0.099°)	(0.068°)	(0.568°)
Goose Bay, NL	Lat.	53.316°	52.500°	53.250°	53.500°	53.500°	54.000°
	(Diff)	-	(-0.816°)	(-0.066°)	(0.184°)	(0.184°)	(0.684°)
	Lon.	-60.416°	-60.000°	-60.750°	-60.667°	-60.500°	-60.000°
	(Diff)	-	(0.416°)	(-0.334°)	(-0.251°)	(-0.084°)	(0.416°)
Iqaluit, NU	Lat.	63.756°	65.000°	63.750°	63.500°	64.000°	64.000°
	(Diff)	-	(1.244°)	(-0.006°)	(-0.256°)	(0.244°)	(0.244°)
	Lon.	-68.555°	-67.500°	-68.250°	-68.667°	-68.500°	-68.000°
	(Diff)	-	(1.055°)	(0.305°)	(-0.112°)	(0.055°)	(0.555°)

Table 3.5: Latitude-longitude coordinates for east coast meteorological stations and the associated closest reanalysis grid box centres along with the latitudinal/longitudinal difference between the locations.

(a)	***Annual 1st Percentile Skill Scores***					
	NCEP-1	NCEP-2	ERA-Interim	MERRA	CFSR	20CR
Arcata, CA	0.97	0.98	0.97	0.98	0.97	0.93
Seattle-Tacoma, WA	0.93	0.92	0.97	0.97	0.95	0.83
Prince-Rupert, BC	0.88	0.87	0.97	0.95	0.93	0.90
Yakutat, AK	0.81	0.80	0.97	0.95	0.92	0.70
Overall Coastal Representation	0.91	0.90	0.97	0.96	0.95	0.85
(b)	***Annual 99th Percentile Skill Scores***					
	NCEP-1	NCEP-2	ERA-Interim	MERRA	CFSR	20CR
Arcata, CA	0.78	0.73	0.77	0.87	0.79	0.76
Seattle-Tacoma, WA	0.85	0.88	0.87	0.85	0.90	0.80
Prince-Rupert, BC	0.77	0.71	0.89	0.87	0.83	0.76
Yakutat, AK	0.50	0.45	0.89	0.81	0.82	0.73
Overall Coastal Representation	0.70	0.66	0.86	0.85	0.84	0.76

Table S3.1: Skill scores (associated with Figure 3.3 Taylor diagrams; calculated using Eq. 3.1) for annual reanalysis representation of strong storm activity along the mid-latitude North American west coast using the (a) 1st percentile of pressure readings and (b) 99th percentile of absolute pressure tendencies proxies.

(a)	***Extended Winter 1st Percentile Skill Scores***					
	NCEP-1	NCEP-2	ERA-Interim	MERRA	CFSR	20CR
Arcata, CA	0.96	0.97	0.95	0.98	0.96	0.93
Seattle-Tacoma, WA	0.97	0.95	0.98	0.97	0.98	0.79
Prince-Rupert, BC	0.90	0.88	0.98	0.94	0.94	0.92
Yakutat, AK	0.86	0.85	0.98	0.95	0.92	0.79
Overall Coastal Representation	0.93	0.92	0.97	0.96	0.95	0.86
(b)	***Extended Winter 99th Percentile Skill Scores***					
	NCEP-1	NCEP-2	ERA-Interim	MERRA	CFSR	20CR
Arcata, CA	0.75	0.64	0.74	0.82	0.73	0.69
Seattle-Tacoma, WA	0.83	0.88	0.88	0.88	0.86	0.79
Prince-Rupert, BC	0.62	0.53	0.82	0.75	0.75	0.71
Yakutat, AK	0.54	0.43	0.76	0.75	0.68	0.69
Overall Coastal Representation	0.66	0.59	0.81	0.79	0.76	0.72
(c)	***Summer 1st Percentile Skill Scores***					
	NCEP-1	NCEP-2	ERA-Interim	MERRA	CFSR	20CR
Arcata, CA	0.92	0.91	0.87	0.81	0.92	0.85
Seattle-Tacoma, WA	0.97	0.95	0.97	0.96	0.98	0.96
Prince-Rupert, BC	0.97	0.97	0.99	0.99	0.99	0.97
Yakutat, AK	0.83	0.85	0.99	0.96	0.96	0.91
Overall Coastal Representation	0.91	0.91	0.98	0.96	0.97	0.94

Table S3.2: Skill scores (associated with Figure 3.4 Taylor diagrams; calculated using Eq. 3.1) for extended winter (ONDJFM) and summer (JAS) seasonal reanalysis representation of strong storm activity along the mid-latitude North American west coast using the (a and c) 1st percentile of pressure readings and (b and d) 99th percentile of absolute pressure tendencies proxies, respectively. [Table continued on next page.]

(d)	***Summer 99th Percentile Skill Scores***					
	NCEP-1	NCEP-2	ERA-Interim	MERRA	CFSR	20CR
Arcata, CA	0.46	0.47	0.47	0.68	0.43	0.45
Seattle-Tacoma, WA	0.76	0.77	0.81	0.84	0.84	0.65
Prince-Rupert, BC	0.66	0.62	0.95	0.92	0.90	0.81
Yakutat, AK	0.71	0.68	0.95	0.92	0.89	0.75
Overall Coastal Representation	0.68	0.66	0.90	0.90	0.85	0.74

Table S3.2 continued.

(a)	***Annual 1st Percentile Skill Scores***					
	NCEP-1	NCEP-2	ERA-Interim	MERRA	CFSR	20CR
Boston, MA	0.86	0.84	0.95	0.94	0.95	0.87
Charlottetown, PE	0.82	0.81	0.95	0.93	0.95	0.87
Mont-Joli, QC	0.84	0.79	0.92	0.94	0.94	0.74
Gander, NL	0.86	0.87	0.97	0.98	0.98	0.88
Goose Bay, NL	0.93	0.91	0.98	0.97	0.98	0.84
Iqaluit, NU	0.93	0.90	0.98	0.96	0.96	0.90
Overall Coastal Representation	0.88	0.87	0.97	0.96	0.97	0.86
(b)	***Annual 99th Percentile Skill Scores***					
	NCEP-1	NCEP-2	ERA-Interim	MERRA	CFSR	20CR
Boston, MA	0.74	0.70	0.78	0.86	0.92	0.75
Charlottetown, PE	0.63	0.58	0.93	0.95	0.94	0.90
Mont-Joli, QC	0.75	0.70	0.82	0.84	0.83	0.78
Gander, NL	0.73	0.68	0.92	0.95	0.90	0.71
Goose Bay, NL	0.67	0.69	0.93	0.91	0.93	0.77
Iqaluit, NU	0.85	0.79	0.95	0.92	0.93	0.90
Overall Coastal Representation	0.73	0.69	0.91	0.92	0.91	0.80

Table S3.3: Skill scores (associated with Figure 3.6 Taylor diagrams; calculated using Eq. 3.1) for annual reanalysis representation of strong storm activity along the mid-latitude North American east coast using the (a) 1st percentile of pressure readings and (b) 99th percentile of absolute pressure tendencies proxies.

(a)	***Extended Winter 1st Percentile Skill Scores***					
	NCEP-1	NCEP-2	ERA-Interim	MERRA	CFSR	20CR
Boston, MA	0.78	0.76	0.92	0.92	0.97	0.81
Charlottetown, PE	0.79	0.76	0.96	0.95	0.95	0.80
Mont-Joli, QC	0.78	0.73	0.95	0.94	0.94	0.74
Gander, NL	0.87	0.87	0.98	0.98	0.99	0.89
Goose Bay, NL	0.88	0.87	0.97	0.97	0.98	0.88
Iqaluit, NU	0.83	0.81	0.97	0.98	0.95	0.84
Overall Coastal Representation	0.83	0.82	0.96	0.96	0.96	0.84
(b)	***Extended Winter 99th Percentile Skill Scores***					
	NCEP-1	NCEP-2	ERA-Interim	MERRA	CFSR	20CR
Boston, MA	0.58	0.55	0.88	0.92	0.87	0.74
Charlottetown, PE	0.76	0.70	0.88	0.95	0.93	0.90
Mont-Joli, QC	0.69	0.74	0.86	0.79	0.82	0.78
Gander, NL	0.71	0.68	0.95	0.94	0.94	0.70
Goose Bay, NL	0.61	0.55	0.92	0.88	0.90	0.73
Iqaluit, NU	0.83	0.82	0.95	0.96	0.94	0.89
Overall Coastal Representation	0.73	0.71	0.91	0.92	0.91	0.80

Table S3.4: Skill scores (associated with Figure 3.7 Taylor diagrams; calculated using Eq. 3.1) for extended winter (ONDJFM) and summer (JAS) seasonal reanalysis representation of strong storm activity along the mid-latitude North American east coast using the (a and c) 1st percentile of pressure readings and (b and d) 99th percentile of absolute pressure tendencies proxies, respectively. [Table continued on next page.]

(c)	***Summer 1st Percentile Skill Scores***					
	NCEP-1	NCEP-2	ERA-Interim	MERRA	CFSR	20CR
Boston, MA	0.91	0.90	0.97	0.97	0.97	0.91
Charlottetown, PE	0.85	0.86	0.98	0.98	0.98	0.87
Mont-Joli, QC	0.76	0.76	0.97	0.98	0.96	0.84
Gander, NL	0.85	0.86	0.98	0.99	0.99	0.79
Goose Bay, NL	0.75	0.71	0.97	0.98	0.97	0.81
Iqaluit, NU	0.80	0.81	0.99	0.98	0.96	0.83
Overall Coastal Representation	0.82	0.81	0.98	0.98	0.97	0.83
(d)	***Summer 99th Percentile Skill Scores***					
	NCEP-1	NCEP-2	ERA-Interim	MERRA	CFSR	20CR
Boston, MA	0.73	0.76	0.91	0.88	0.89	0.73
Charlottetown, PE	0.75	0.74	0.94	0.94	0.92	0.81
Mont-Joli, QC	0.47	0.46	0.93	0.93	0.89	0.59
Gander, NL	0.78	0.79	0.97	0.97	0.96	0.65
Goose Bay, NL	0.43	0.42	0.87	0.90	0.88	0.54
Iqaluit, NU	0.81	0.79	0.93	0.91	0.92	0.58
Overall Coastal Representation	0.68	0.68	0.93	0.93	0.92	0.66

Table S3.4 continued.

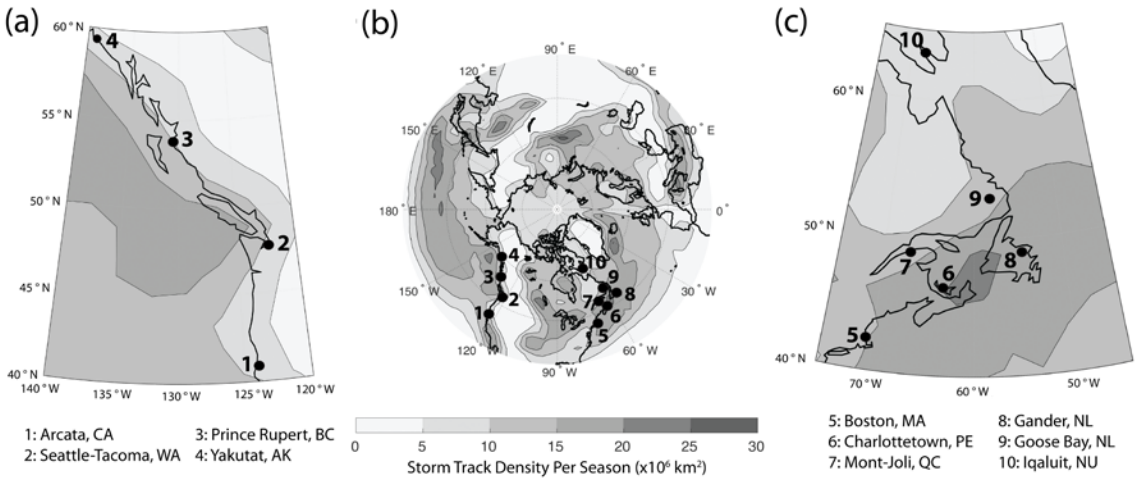

Figure 3.1: Winter (DJF) storm track density for the (b) Northern Hemisphere and the (a) west and (c) east coast study domains with the locations of the meteorological stations utilized in this evaluation indicated. Storm track density per DJF season is calculated for the 1980-2010 time period using the Hodges tracking algorithm (1994; 1995; 1999) and 850-hPa relative vorticity from ERA-Interim.

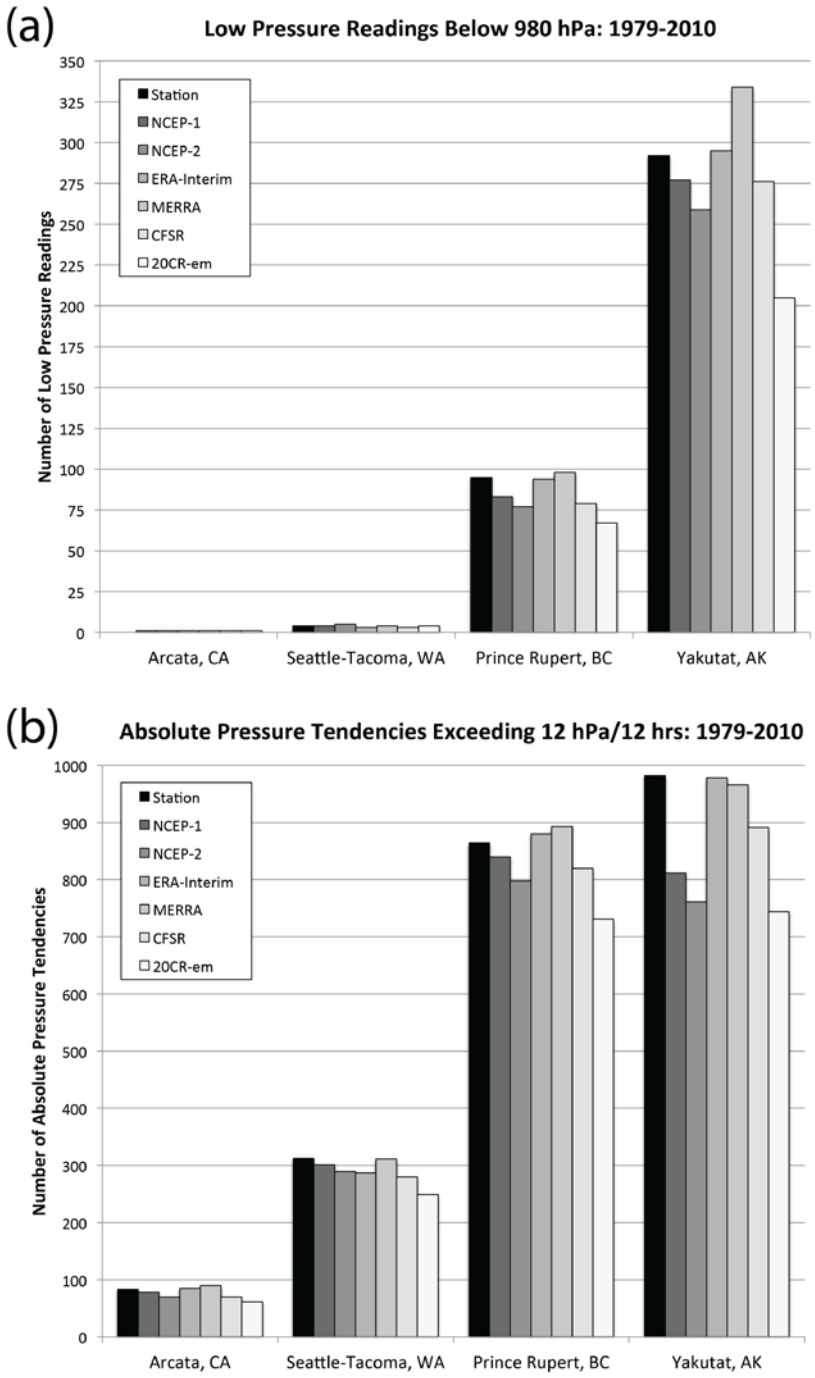

Figure 3.2: Comparison of reanalysis detection of annual strong storm activity along the mid-latitude North American west coast as represented by (a) the number of low pressure readings below 980 hPa and (b) the frequency of absolute pressure tendencies above 12 hPa/12 hrs.

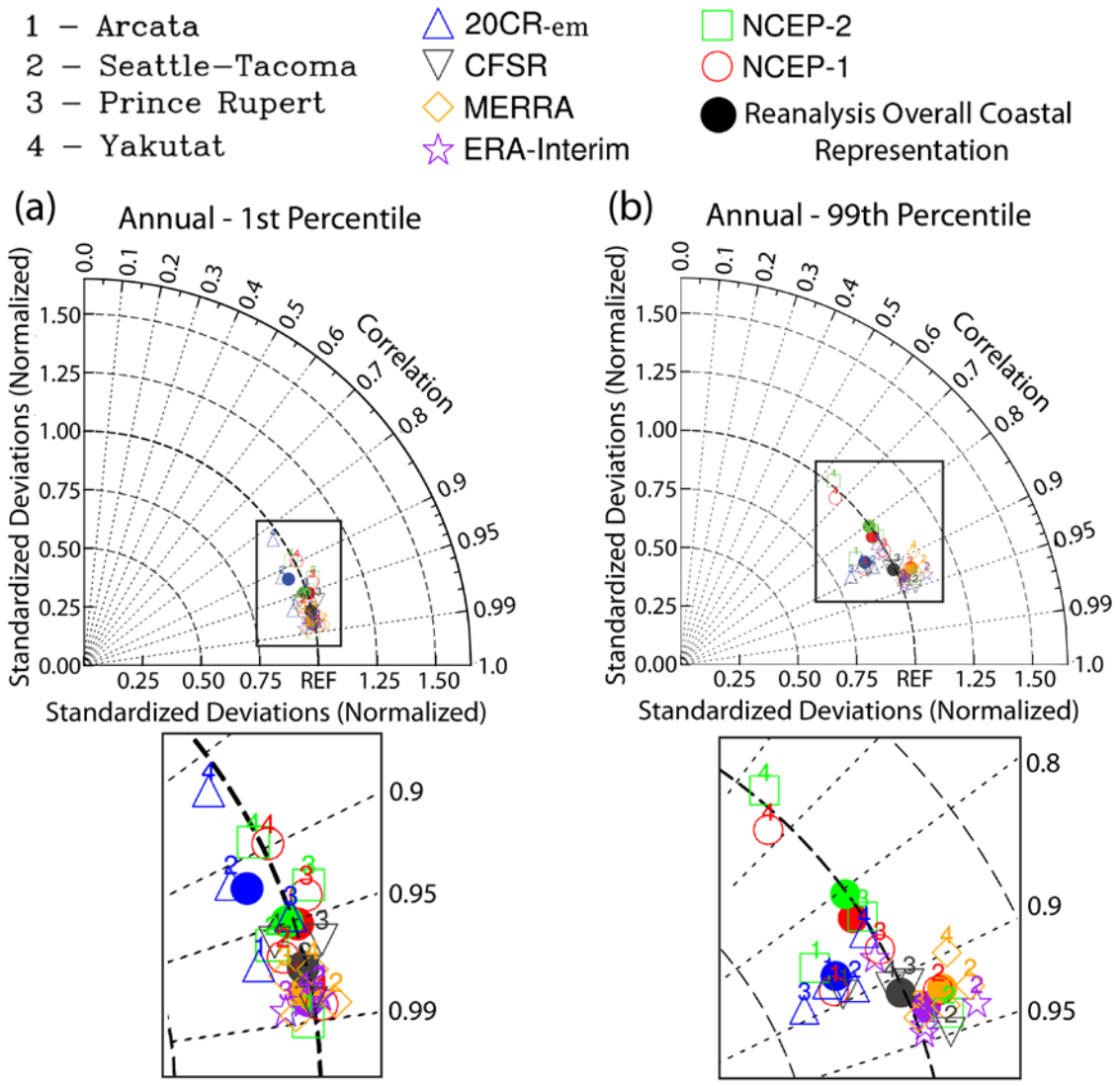

Figure 3.3: Taylor diagrams comparing annual reanalysis representation of strong storm activity along the mid-latitude North American west coast using the (a) 1st percentile of pressure readings and (b) 99th percentile of absolute pressure tendencies proxies. Three parameters are plotted: reanalysis vs. observation ("REF") correlation (radials from origin), root-mean-square difference (arcs from REF), and normalized standard deviation (arcs from origin). Reanalysis representations are displayed for the individual stations (open shapes) and for overall coastal representation (solid circles). The associated skill scores of the reanalysis representations (calculated using Eq. 3.1) are presented in Table S3.1.

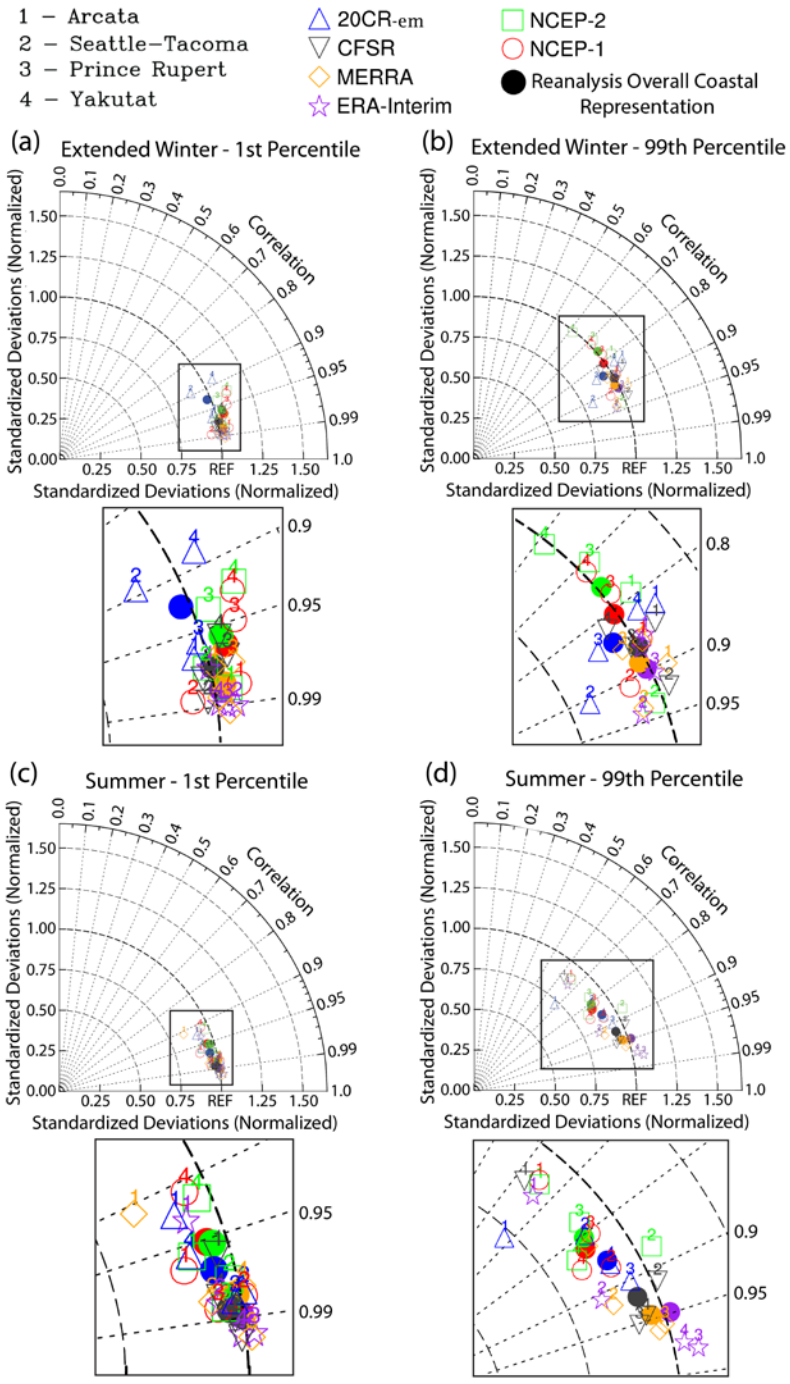

Figure 3.4: As in Figure 3.3, Taylor diagrams comparing reanalysis representation of strong storm activity along the mid-latitude North American west coast but for the extended winter (ONDJFM) and summer (JAS) seasons using (a and c) 1st percentile of pressure readings and (b and d) 99th percentile of absolute pressure tendencies proxies, respectively. Associated reanalysis representation skill scores are presented in Table S3.2.

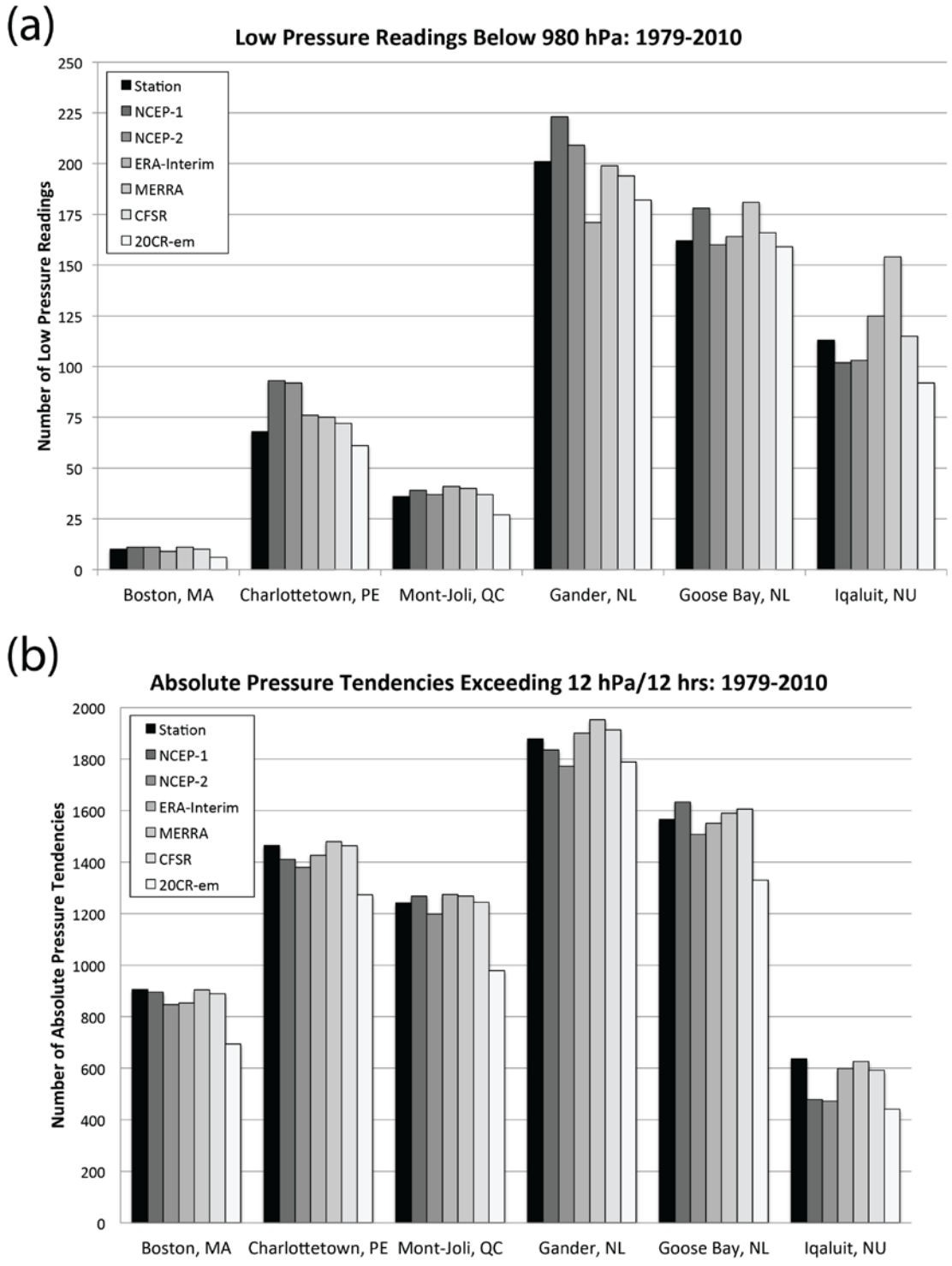

Figure 3.5: As in Figure 3.2 but for the mid-latitude North American east coast.

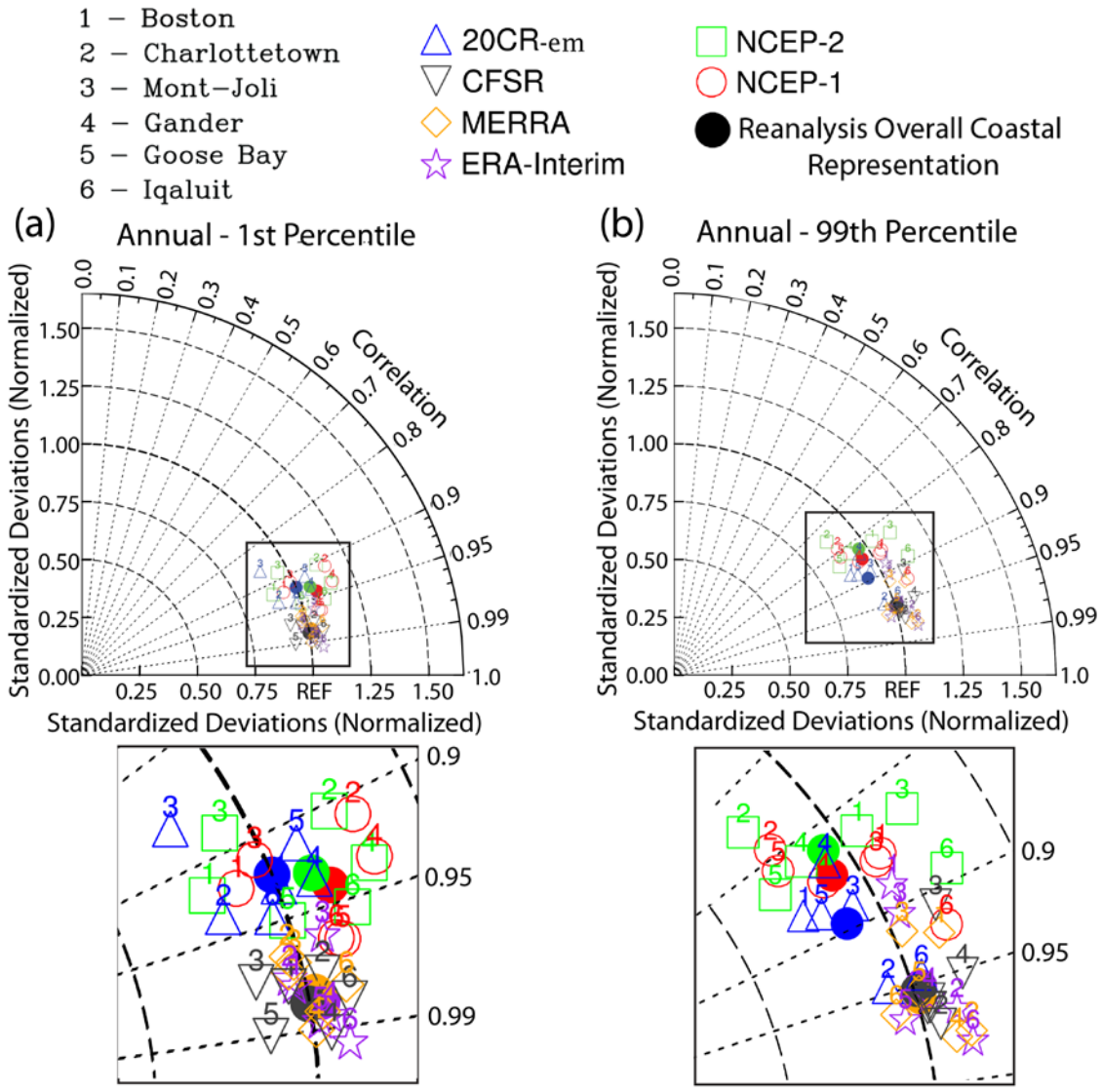

Figure 3.6: As in Figure 3.3 but for the mid-latitude North American east coast. Associated reanalysis representation skill scores are presented in Table S3.3.

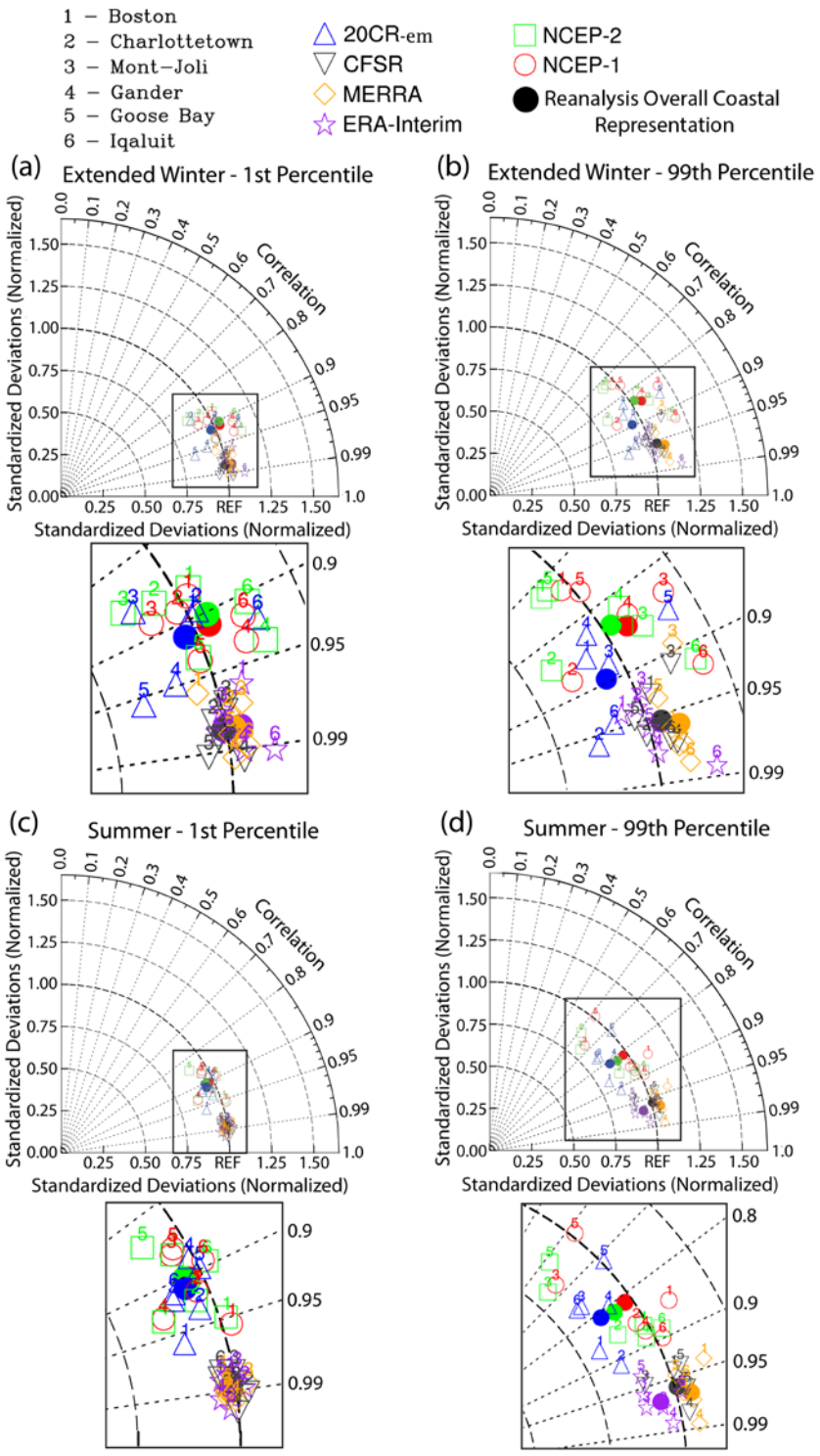

Figure 3.7: As in Figure 3.4 but for the mid-latitude North American east coast. Associated reanalysis representation skill scores are presented in Table S3.4.

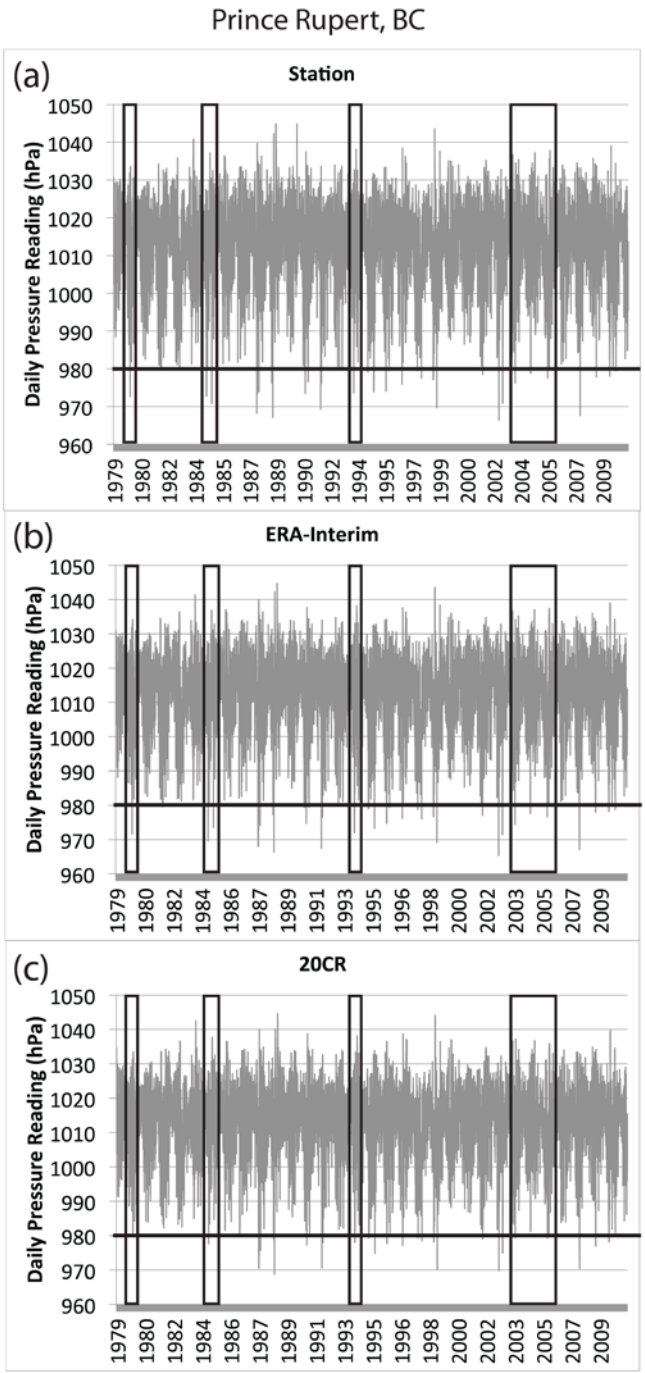

Figure 3.8: Prince Rupert, BC daily (00Z) mean sea level pressure readings (1979-2010), (a) observed and reanalysed in (b) ERA-Interim and (c) 20CR ensemble mean, with the 980 hPa threshold highlighted. Time periods of noticeable differences in detection of strong storms (as represented by low pressure readings) between the station observations and reanalyses are indicated using boxes.

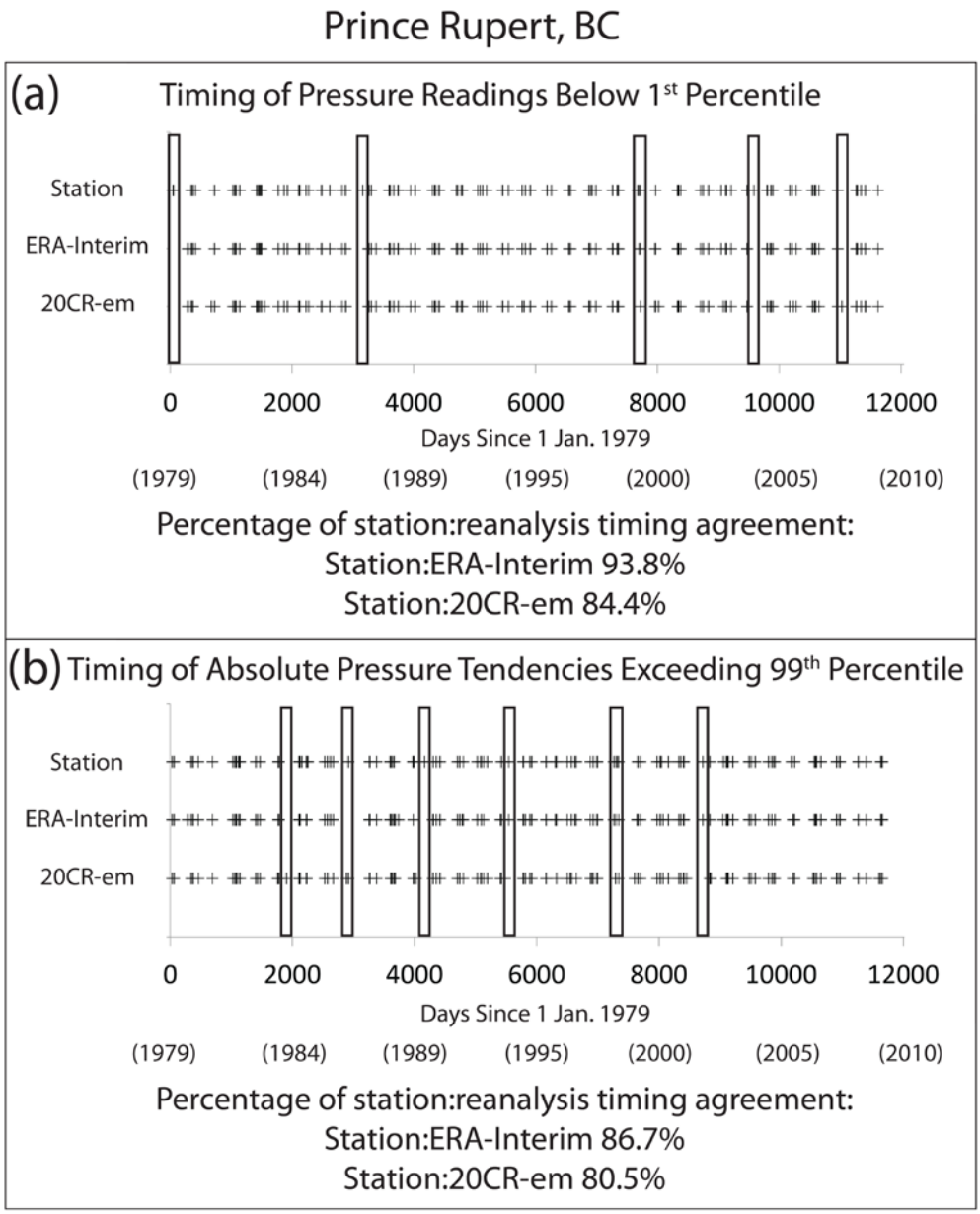

Figure 3.9: Prince Rupert, BC timing of (a) daily (00Z) mean sea level pressure readings below the respective annual 1st percentile of pressure readings and (b) 24-hr absolute pressure tendencies exceeding the respective annual 99th percentile of absolute pressure tendencies. Time periods of noticeable differences in detection of strong storm activity (as represented by deep low pressure readings and large pressure changes, respectively) are indicated using boxes. The percentage of station-reanalysis timing agreement is also noted.

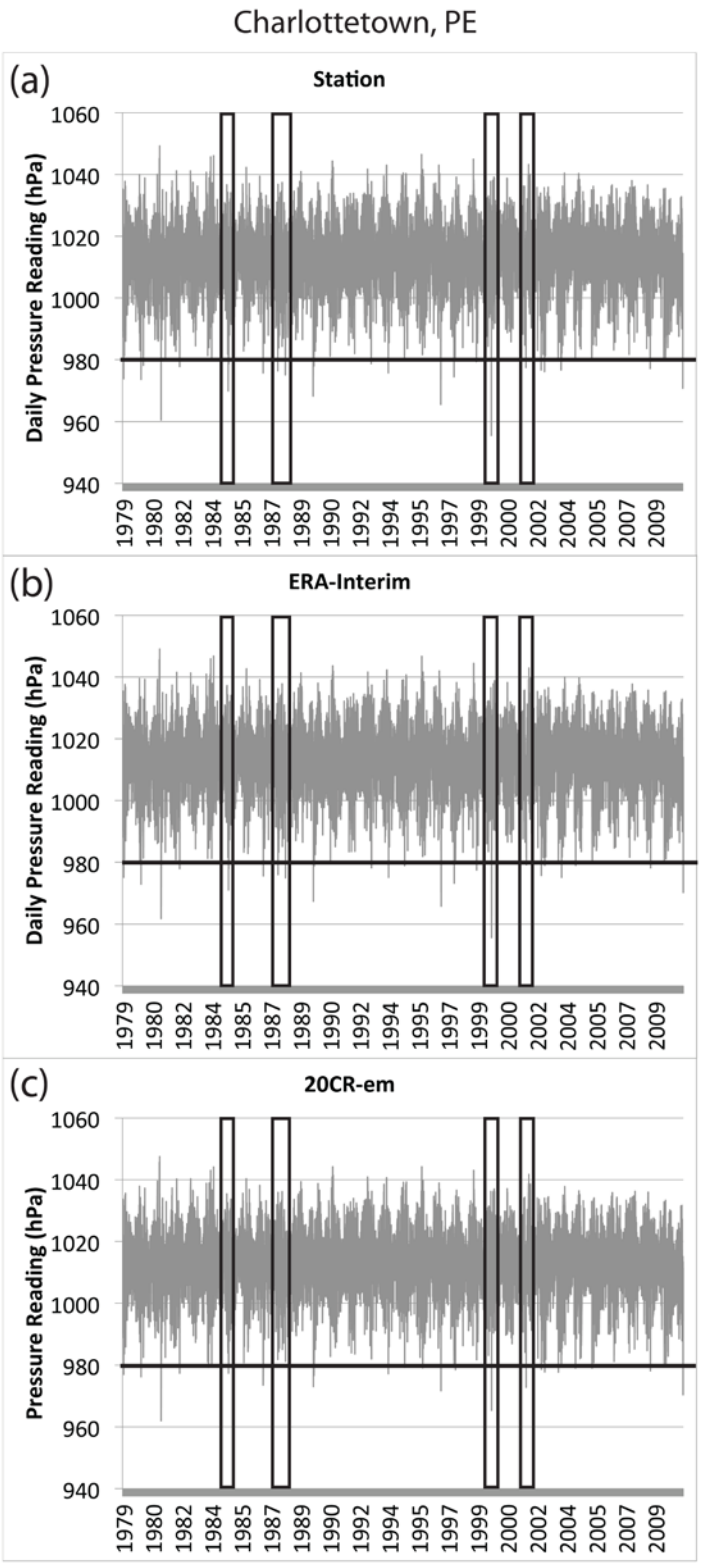

Figure 3.10: As in Figure 3.8 but for Charlottetown, PE.

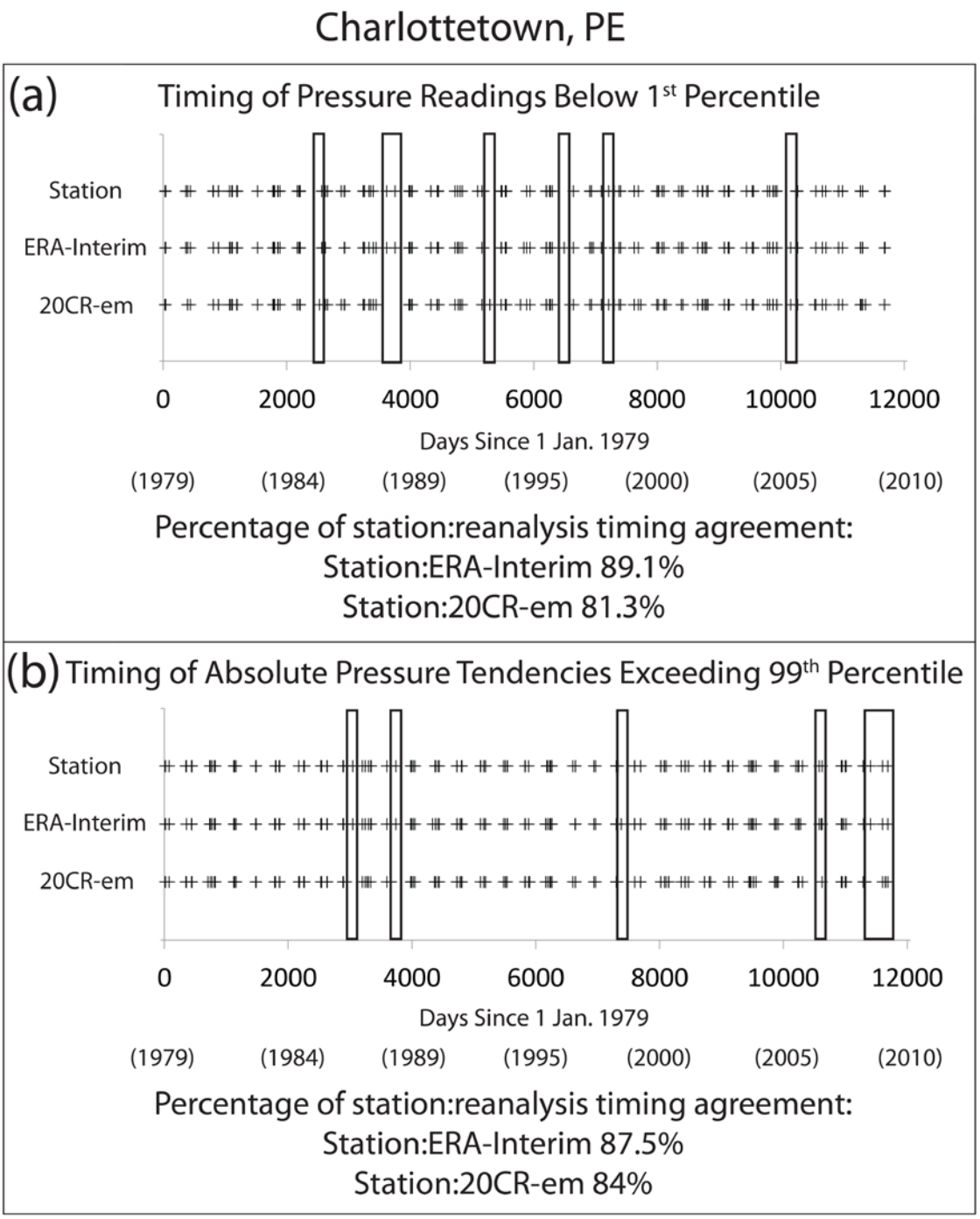

Figure 3.11: As in Figure 3.9 but for Charlottetown, PE.

4.0 Cold Season Extratropical Storm Activity Potential Predictability and its Sources in the Northern Hemisphere with Focus on the North American Coastal Regions

4.1 Manuscript Information

This manuscript presents research completed in Research Theme 2 and is being prepared for submission to the journal Advances in Statistical Climatology, Meteorology and Oceanography:

Pingree-Shippee KA, Zwiers FA, Atkinson DA (in prep) Cold Season Extratropical Storm Activity Potential Predictability and its Sources in the Northern Hemisphere with Focus on the North American Coastal Regions.

Additional Research Theme 2 figures not included in this manuscript are provided in Appendix B of this dissertation.

4.2 Abstract

Society would benefit if variations in extratropical storm activity could be predicted skilfully for the upcoming season. Skilful seasonal prediction would enable socio-economic sectors in regions such as the North American coastal regions to better anticipate, prepare for, manage, and respond to storm activity and the associated risks. Prior to developing seasonal forecasting methods, however, it is useful to determine the potential predictability of extratropical storm activity along with its sources. We find potential predictability in areas strongly influenced by storm activity, with the highest

signals typically found in areas of cyclogenesis. Additionally, three large-scale teleconnections (Southern Oscillation, Pacific Decadal Oscillation, and North Atlantic Oscillation) are identified as possible sources of predictability. With a focus on North American coastal regions, this study therefore provides evidence that seasonal variations of extratropical storm activity are potentially predictable and thus contributes to the basis upon which seasonal forecasts can be developed. The study considers the 1979-2015 time period, uses storm activity indicators based on daily mean sea level pressure, absolute pressure tendency, and 10-m wind speeds, and focuses on overlapping 3-month cold seasons (OND, NDJ, DJF, JFM), during which extratropical storm activity is most frequent and intense.

4.3 Introduction

Extratropical cyclones (ETCs) play a key role in global atmospheric circulation by transporting heat, moisture, and momentum from the subtropics poleward. ETCs are also major drivers of the weather in the mid- and high-latitudes, often governing regional patterns of cloud cover, precipitation, and winds. These systems are frequently associated with hazardous weather conditions such as heavy precipitation, high winds, blizzard conditions, and flooding. Additionally, severe coastal damage and major local impacts, including inundation and erosion, can result from storm interaction with the ocean and the subsequent high waves and storm surge. Consequently, ETCs can have serious socio-economic impacts. The west and east coasts of North America are both strongly influenced by ETC storm activity, with the west coast influenced by the North Pacific storm track and atmospheric river events and the east coast influenced by winter storms

following two favoured tracks, the St. Lawrence Valley and the Eastern Seaboard. These North American coastal regions are also host to many socio-economic sectors, including land and marine transportation, aviation, agriculture and fisheries, and the built environment (e.g., infrastructure), which can all experience strong adverse impacts from ETC storm activity.

Society would benefit if risks associated with ETCs and their variability could be skilfully predicted for the upcoming season (or longer), well in advance of their occurrence. Skilful prediction would enable affected sectors to better anticipate, prepare for, manage, and respond to variations in storm activity and the associated risks and impacts (e.g., through improved contingency planning that accounts for the predicted changes in risk). Currently, operational seasonal forecasting primarily focuses on near surface temperature and total precipitation, producing deterministic and probabilistic forecasts of the likelihood of below-, near-, and above-normal conditions for the upcoming seasons. Seasonal forecasting is most skilful in the tropics, where seasonal to interannual variability, such as the El Niño-Southern Oscillation (ENSO), occur on relatively long timescales (Stockdale et al. 2010; Doblas-Reyes et al. 2013). Forecast skill for North America, although often lower due to its mid- to high-latitude location, is also known to originate from coupled air-sea interactions and through teleconnections such as ENSO, the Pacific Decadal Oscillation (PDO), and the North Atlantic Oscillation (NAO) (Stockdale et al. 2010; Doblas-Reyes et al. 2013). These teleconnections are known to be associated with extratropical storm activity characteristics (e.g., storm track location and storm activity frequency and intensity; Gulev et al. 2001; Eichler and Higgins 2006; Wang et al. 2006; Lareau and Horel 2012; Gan and Wu 2013; Grise et al. 2013) and are

themselves predictable. ENSO predictions have useful skill at lead times up to 6-12 months (Chen and Cane 2008; Barnston et al. 2012; Merryfield et al. 2013) and is currently considered the primary global source of seasonal to interannual predictability in operational seasonal forecasting (Stockdale et al. 2010; Doblas-Reyes et al. 2013). Other teleconnections, such as the NAO and PDO, are more regional in extent and have predictive potential on the seasonal timescale (e.g., lead time of 1-3 months; Alexander et al. 2008; Wen et al. 2012; Scaife et al. 2014; Smith et al. 2014; Dunstone et al. 2016; Athanasiadis et al. 2017).

Prior to developing seasonal forecasting methods for ETC variability, it is useful to determine the potential predictability of extratropical storm activity at the seasonal timescale along with its sources. Investigating potential predictability will identify locations where the observed year-to-year variance in storm activity exceeds the variability present due to weather noise (i.e., day-to-day weather fluctuations), which generally has a limit of predictability on the order of two weeks. Any variability in excess of the unpredictable weather noise variability is considered potentially predictable (Madden 1976) and, therefore, provides quantitative and geographical evidence it may be possible to predict variations in extratropical storm activity on the seasonal timescale. Furthermore, identifying sources of this potential predictability will provide the basis upon which seasonal predictions can be developed.

Previous research supports the premise that there is the potential to predict monthly or longer variations in ETC storm activity. Seminal studies using analysis of variance (ANOVA) to investigate potential predictability, such as Madden (1976) and Shukla and Gutzler (1983), first identified potential predictability of Northern

Hemisphere extratropical storm activity at various tropospheric levels on the monthly timescale. Madden (1976) investigated the monthly potential predictability of sea level pressure using daily data from Historical Weather Maps and digitized grid-point values for the 1899-1972 time period. Shukla and Gutzler (1983) evaluated potential predictability of monthly mean 500-hPa geopotential heights using daily data from NOAA National Meteorological Center (NMC) final analyses for 15 January and 15 July months covering the 1963-1977 time period. Both studies found potential predictability in the extratropics in areas where ETC storm activity is prevalent, such as the North Pacific and North Atlantic storm tracks, and with the strongest potentially predictable signals found in areas of climatological cyclogenesis (e.g., Kuroshio Current and along the North American east coast). Subsequent ANOVA-based potential predictability studies produced similar patterns of potential predictability on monthly to seasonal timescales (Zwiers 1987; Rowell 1998; Zheng et al. 2000; Hodson and Sutton 2008).

ETCs, however, are complex features that cannot be summarized with a single variable. Numerous variables have therefore been used to characterize ETCs and extratropical storm activity (e.g., storm tracks) including mean sea level pressure (MSLP), relative vorticity (typically at 850-hPa), 500-hPa geopotential heights, and wind speeds (near-surface and aloft) (Compo and Sardeshmukh 2004; Wang et al. 2006; Renggli et al. 2011; Krueger and von Storch 2012; Gan and Wu 2013; Neu et al. 2013; Yang et al. 2015). Analyzing variables at different atmospheric levels, such as MSLP along with 500-hPa geopotential heights and 300-hPa winds, would provide insight into the potential predictability of extratropical storm activity throughout the vertical structure of the troposphere. Nevertheless, the majority of end-users would, arguably, be most interested

in seasonal forecasts at or near the surface where the impacts of storm activity are primarily felt. Therefore, this study investigates the potential predictability of ETC storm activity based on surface and near-surface variables.

In this study, potential predictability of seasonal variations in extratropical storm activity and its sources are investigated for the Northern Hemisphere, with specific focus on the highly-populated and environmentally sensitive North American west and east coastal regions. Using daily data from the ECMWF ERA-Interim reanalysis covering the 1979-2015 time period, potential predictability and its sources are evaluated for overlapping 3-month cold seasons (OND, NDJ, DJF, JFM), during which extratropical storm activity is most frequent and intense and, arguably, most hazardous. This evaluation utilizes two ETC storm activity proxies at the surface – mean sea level pressure and 24-hr absolute pressure tendency. A third proxy – 10-m wind speeds – was also evaluated over the oceans to provide additional insight into the potential predictability of extratropical storm activity and its sources. The Southern Oscillation (representative of ENSO), PDO, and NAO are evaluated as possible sources of the detected potential predictability.

The remainder of this manuscript is outlined as follows: Descriptions of the study areas, reanalysis dataset, extratropical storm activity proxies, teleconnections, and the methods used to evaluate potential predictability (analysis of variance) and its sources (composite analysis) are provided in Section 4.4. Results are presented in Section 4.5 while a discussion of the potential predictability detected in the North American coastal regions and its possible sources provided in Section 4.6. Conclusions are presented in Section 4.7. Key findings from the 10-m wind speed-based investigations are included in

this manuscript, with detailed results provided in the Supplementary Material [Section 4.10].

4.4 Data and Methods

4.4.1 Study Areas

Potential predictability of seasonal variations in extratropical storm activity and its sources are evaluated for the Northern Hemisphere (20°N-90°N), with specific focus on the North American west and east coastal regions. The North American study areas encompass the non-Arctic USA and Canadian coastal regions. The west coast domain covers 30°N-60°N, 115°W-140°W, extending from northern Baja California (Mexico), through the contiguous USA west coast and British Columbia (Canada), and into southeast Alaska (USA). The east coast domain covers 25°N-65°N, 50°W-85°W, extending from the southern tip of Florida (USA) northward to southern Baffin Island, Nunavut, Canada, including Newfoundland, Canada.

4.4.2 Reanalysis Dataset, Storm Activity Proxies, Teleconnections

Potential predictability of ETC seasonal variations and its sources are evaluated utilizing the ERA-Interim reanalysis dataset distributed by the European Centre for Medium-Range Weather Forecasts (ECMWF). ERA-Interim (Dee et al. 2011) is a 3rd-generation reanalysis that extends from 1979 to the present, with a horizontal resolution of T255 (0.54° x 0.54°) and 60 vertical levels, and provides 6-hrly output. ERA-Interim was previously determined to have the best representation of mid-latitude North American coastal extratropical storm activity compared to other commonly used global reanalyses (Pingree-Shippee et al. 2017) and, therefore, was chosen for this study.

Since ETCs are complex features and cannot be summarized in a single parameter, three variables – MSLP, 24-hr absolute pressure tendency (ΔMSLP), and 10-m wind speeds – are utilized in this study as proxies to represent extratropical storm activity. T159 horizontal resolution (0.75° x 0.75°) Northern Hemisphere daily (00 UTC) MSLP and 10-m wind speed data (10-m *u*- and *v*-component wind data) for the 1979-2015 time period are utilized from ERA-Interim. Information on storm activity characteristics such as frequency and intensity can be derived from these proxies and, thus, would provide end-users valuable information on ETC variability on the seasonal timescale. Variations in MSLP provide information on the frequency (and/or persistence) of storm activity since an increase in the number of storms (and/or longer-lasting storms) would be expected to correspond to lower (and/or persistently lower) MSLP. Alternatively, ΔMSLP and 10-m wind speeds provide information on the intensity of storm activity since higher seasonal mean absolute pressure tendency and wind speed would be expected to correspond to greater storminess (e.g., enhanced cyclogenesis and/or stronger pressure gradients).

For the potential predictability investigation using analysis of variance, the square root of the 24-hr absolute pressure tendencies is utilized. The distribution of the raw absolute pressure tendencies is strongly right skewed, while the square root of the absolute pressure tendencies has a more symmetric distribution (Figure 4.1). Analysis of variance assumes the variables being evaluated are normally distributed and, if this assumption is not met, the usual *F*-test may be compromised.

In the 10-m wind speed-based investigations (potential predictability and composite analysis), results are considered only over the oceans due to difficulties in

simulating anemometer-height winds over land. In reanalyses, *u*- and *v*-wind components at 10-m, while influenced by observational data, are also strongly influenced by model physics and, over land, are particularly influenced by parameterized sub-grid scale surface properties (e.g., surface roughness) and the representation of surface topography. As such, 10-m winds over land are less reliable than 10-m winds over the oceans and the ERA-Interim land mask is applied. Since the 10-m wind speed investigations are confined to over the oceans, only key results are noted in this manuscript while detailed results are provided in the Supplementary Material.

Three large-scale climate signals known to be strongly associated with extratropical storm activity in the Northern Hemisphere were selected for evaluation as possible sources of the detected potential predictability – the Southern Oscillation (SO [Walker 1924; Bjerknes 1966, 1969]), which is representative of ENSO (Philander, 1983), the PDO (Mantua and Hare 2002), and the NAO (Hurrell et al. 2001). Established climate indices were utilized to characterize the fluctuations and strength of these teleconnections: The monthly Standardized Tahiti – Standardized Darwin sea level pressure anomaly (departure from the 1981-2010 base period) SO Index was obtained from the NOAA Climate Prediction Center (http://www.cpc.ncep.noaa.gov/data/indices/soi). The standardized monthly PDO index (the leading principle component of monthly mean sea surface temperature anomalies in the North Pacific Ocean poleward of 20°N), maintained by Nathan Mantua at the University of Washington, Joint Institute for the Study of the Atmosphere and Ocean (JISAO), was obtained through the NCAR UCAR Climate Data Guide (https://climatedataguide.ucar.edu/climate-data/pacific-decadal-oscillation-pdo-

definition-and-indices; http://research.jisao.washington.edu/pdo/PDO.latest). The seasonal Hurrell station-based NAO Index (normalized Lisbon, Portugal – normalized Stykkishólmur/Reykjavík, Iceland sea level pressure anomalies) was obtained from the NCAR UCAR Climate Data Guide (https://climatedataguide.ucar.edu/climate-data/hurrell-north-atlantic-oscillation-nao-index-station-based).

4.4.3 Methods

4.4.3.1 Potential Predictability

Potential predictability of seasonal variations in extratropical storm activity is investigated using analysis of variance (ANOVA) in the time domain (Madden 1976; Shukla and Gutzler 1983; Trenberth 1985; Zwiers 1987; Boer 2004, 2011; DelSole and Feng 2013). Analysis of variance as applied in potential predictability studies determines whether the observed interannual variance exceeds a level that would be expected based only on weather noise, proceeding from the null hypothesis that there is no potential predictability (observed low frequency variability equals the low frequency component of weather noise variability). Analysis of variance, therefore, provides insight into the likelihood for potentially predictable variability to be present in the climate system.

Analysis of variance in the time domain separates the total observed variation within a time series into the variation observed on the interannual timescale (signal) and that observed on the intraseasonal timescale (weather noise). It is assumed that these two components of variation are statistically independent and that they do not interact. These two components are used to construct two independent estimates of interannual variability of the seasonal mean, one based on the total interannual variability of seasonal

means, and the other based on an estimate of the interannual variability of seasonal means that arises only from short-term weather noise. The former is affected by the low frequency component of weather noise and the potentially predictable low frequency variations, and thus it is expected to be larger if seasonal mean conditions are potentially predictable. The former is calculated as:

$$\hat{\sigma}_m{}^2 = \frac{1}{J-1}\sum_{j=1}^{J} \overline{x}_j{}^2 \qquad \text{(Eq. 4.1)}$$

where J is the number of seasons, and $\bar{x}_j$ is the seasonal mean anomaly in season j. The latter, the low-frequency component of intraseasonal variation, is calculated as:

$$\hat{\sigma}_N{}^2 = \frac{T_0}{N-T_0} s^2 \qquad \text{(Eq. 4.2)}$$

where T_0 is the characteristic time between independent values (which accounts for autocorrelation present in the time series), N is the number of daily values in the season, and s^2 is the mean intraseasonal daily variance. See the Supplementary Material for a detailed mathematical explanation of ANOVA in the time domain. These two independent estimates of variability are then compared using the F-test to evaluate potential predictability, based on the statistic:

$$F = \frac{\hat{\sigma}_m{}^2}{\hat{\sigma}_N{}^2} \qquad \text{(Eq. 4.3)}$$

Under the null hypothesis of no potential predictability we would expect $\hat{\sigma}_m{}^2$ and $\hat{\sigma}_N{}^2$ to be equal to within random variation, and F to have an F-distribution with J - 1 and $J(N_{\text{eff}}$ - 1) degrees of freedom, where N_{eff} is the effective number of independent observations:

$$N_{\text{eff}} = N\frac{\Delta t}{T_o} \qquad \text{(Eq. 4. 4)}$$

(where Δt is the sampling interval; Δt = 1). When the null hypothesis is false, the $\hat{\sigma}_m{}^2/\hat{\sigma}_N{}^2$ ratio will tend to be larger than one, and thus the test is conducted by comparing F with the upper tail critical values from the F-distribution. When the null hypothesis is rejected, F provides an estimate of the signal-to-noise ratio and $F - 1$ providing an indication of the magnitude of the potentially predictable signal. A $p = 0.05$ significance level was chosen to obtain critical F-values for the F-test.

We also accessed the field significance of the storm activity ANOVA results to aid in the interpretations of potential predictability. A challenge that arises in multiple testing, such as when a test is conducted at each of many grid points (e.g., ANOVA), is that there will, inevitably, be locations where rejection occurs even if the null hypothesis is true everywhere. Thus it is useful to assess whether the frequency of rejection across the field of test statistics is greater than would occur by random chance – a somewhat complex question given that the individual grid-point test statistics are likely spatially correlated. While several approaches are available for addressing the multiple testing problem, we follow the method described by Livezey and Chen (1983), which is widely used. To assess field significance, the local hypothesis tests are used as the input to a "meta-test" which tests the "global" null hypothesis that all the individual "local" null hypotheses are true. Local, apparently significant, test results should not be interpreted when the global null hypothesis cannot be rejected because this indicates that the rate of occurrence of local rejection is consistent with the rate due to random chance that is specified via the significance level. Exceptions to this general rule are situations where there is a strong underlying physical basis for the interpretation of a cluster of local

rejections. In order to reject the global null hypothesis, a considerably larger proportion of the local null hypotheses must be rejected than indicated by the local significance level. In this study, the rejection rate of the local null hypothesis, *R*, is calculated using the fraction of the domain where the local test *F*-values are significant (where the local null hypothesis has been rejected in ANOVA using $p = 0.05$). The observed rejection rates are then used to determine the minimum number of independent local tests, *M* (representative of spatial degrees of freedom), that are required for field significance at the 0.05 level using the binomial distribution. Therefore, for a particular *R*, the results would be considered field significant at the 0.05 level (and the individual ANOVA tests not rejecting the null hypothesis by chance) when the number of independent tests in the field is greater than or equal to the calculated *M*.

Potential predictability of the teleconnection indices was also investigated using a variant of the ANOVA method (Zheng et al. 2000; Table 1, 5th equation) that is adapted to monthly time series. The results of the teleconnection ANOVA investigations provide a simple indication of the strength of the climate indices' potential predictability.

4.4.3.2 Sources of Potential Predictability

The sources of the detected potential predictability of seasonal ETC variability are investigated using composite analysis. The seasonal data (OND, NDJ, DJF, JFM) are divided into three subsamples – El Niño, neutral, and La Niña conditions – for the SO analyses and into two subsamples – positive and negative phase - for the PDO and NAO analyses (Tables S4.1-S4.3). A +/-1 standard deviation cut-off was utilized to define ENSO events vs. neutral conditions and was calculated using the complete SO index time series (1951-2015, all months inclusive). For teleconnections with monthly indices (i.e.,

SO and PDO), monthly values were averaged to calculate seasonal index values in order to determine the 'event' classification of each season.

The average conditions for each individual season were first calculated. These were then averaged over each complete subsample of years associated with a particular teleconnection criterion (e.g., the average MSLP field associated with the NAO positive phase). The composites obtained, therefore, represent the 'typical' structures of the ETC proxy associated with each teleconnection phase. Composite anomalies (composite with the seasonal climatology removed) are presented to highlight 'typical' atmospheric changes associated with each teleconnection phase (e.g., changes in the Icelandic Low and Azores High during the NAO phases). The composites are then compared (e.g., NAO positive phase average MSLP field vs. NAO negative phase average MSLP field) to determine if the mean values are statistically different, thus revealing whether or not there is a discernable relationship between the data (i.e., the ETC proxies) and the clustering criteria (i.e., the teleconnections), suggesting that the teleconnections are possible sources of potential predictability. The composites are compared using the Student's *t*-test at the 0.05 significance level.

4.5 Results

4.5.1 Analysis of Variance

Critical *F*-values vary slightly between the variables and seasons due to differences in short term persistence, which affects the calculation of the number of degrees of freedom appropriate for the *F*-test (Eq. 4.4). For all three proxies and seasons evaluated, the critical *F*-value varies between 1.42 and 1.49 (Tables S4.4-S4.6). A fixed critical *F*-value

of 1.5 was, therefore, used to identify areas of statistically significant potential predictability. For each storm activity proxy, similar geographical patterns of statistically significant *F*-values are found throughout the four seasons evaluated. Nevertheless, the spatial extent and, in particular, the strength (*F*-value) of the statistically significant signal detected does vary as the seasons progress (Figures 4.2, 4.3, and S4.2; in Appendix B Figures B.2, B.3, B.4). Regardless, the results can be considered field significant at the 0.05 level for all seasons evaluated. The percent of the domain over which *F*-values are locally significant is 43% or greater (Table 4.1) with the results being considered field significant when there are 5 or more independent local tests (representative of spatial degrees of freedom). With 3200 individual ANOVA tests completed over the Northern Hemisphere (20°N-90°N), it could be expected that more than 5 local tests are independent for the proxies evaluated.

For MSLP (Figure 4.2), high *F*-values (in the range of 3-4) are found in the mid- to high-latitudes, in particular over the North Pacific and North Atlantic in association with the major oceanic storm tracks. High *F*-values (up to ~5) are also found off the southern west coast of North America (Mexico), an extension of high *F*-values in the subtropics (not shown). The *F*-values over the North Pacific are highest in the western Pacific during OND and NDJ (Figure B.2 in Appendix B) before extending across the ocean basin as the *F*-values in the eastern Pacific increase in DJF and JFM. The *F*-values over the North Atlantic are relatively consistent across the ocean basin, extending from the Canadian east coast to the eastern North Atlantic, with the highest values observed in the western North Atlantic where cyclogenesis regularly occurs. *F*-values in the North Atlantic increase as the seasons progress, peaking in DJF, before decreasing again in JFM.

High *F*-values are also found in the high-latitudes in the Svalbard/Iceland region. In general, *F*-values along the North American coastal regions peak during DJF (east coast) and JFM (west coast). During these seasons, statistically significant *F*-values are detected extending along much of the North American west coast, with the highest values (*F*-values of ~2.5 to 5) found off the Mexican and USA coasts. During JFM, weaker but still statistically significant *F*-values (1.5 to 2) also extend over the majority of the western half of the North American continent. Along the North American east coast, during DJF and JFM, statistically significant *F*-values extend along the majority of the coast and inland over both the southeast USA (e.g., Florida) and the Canadian coastal provinces (e.g., Newfoundland and Labrador). The highest *F*-values (~3.5 to 4) are detected off the coast of Newfoundland and Labrador, corresponding with the area of climatological cyclogenesis.

While the results of the analysis of variance using 24-hr absolute pressure tendencies (ΔMSLP; Figure 4.3) are noisier, large-scale patterns are observable, including the major oceanic storm tracks. High *F*-values (3-5.5) in the ΔMSLP analysis are primarily confined to the mid-latitudes (40°N-55°N) and particularly over the ocean basins, corresponding with the storm tracks. These *F*-values are highest in OND and generally decrease as the seasons progress (Figure B.3 in Appendix B). The *F*-values over the North Pacific are highest in the western half of the ocean basin, near the Kuroshio Current region, an area of climatological cyclogenesis, including rapid intensification. *F*-values over the North Atlantic are relatively uniform, extending along the North American east coast and across the ocean basin. High *F*-values are also found in the high-latitudes in the Svalbard/Iceland region. *F*-values along the North American

coasts also peak during OND: Statistically significant *F*-values are detected throughout the west coast study domain and extend over much of the western half of the continent. The highest *F*-values (3-4.5) are found along the USA west coast, peaking in California, an area commonly influenced by atmospheric river events. A secondary peak is also detected inland over Nevada/Utah, where cutoff lows form over the southwestern USA. During OND, statistically significant *F*-values also extend throughout the majority of the North American east coast study domain and over the majority of the eastern half of the continent. The highest *F*-values (2.5 to 3.5) along the east coast are observed over the water adjacent to the Eastern Seaboard, extending from Florida to the Canadian Maritimes, where cyclones regularly form and track up the coast.

High *F*-values (3-4.5) over the North Pacific and North Atlantic, corresponding with the major oceanic storm tracks, are also found in the analysis of variance using 10-m wind speeds (Figure S4.2). Highest *F*-values, both over the ocean basins and along the North American coasts, are observed in OND and, in general, decrease as the seasons progress (Figure B.4 in Appendix B). Peak *F*-values along the North American west and east coasts are found off the coast of British Columbia (*F*-values of 3-3.5) and the New England region of the USA (*F*-values of 3.5-4; corresponding to an area of climatological cyclogenesis, including rapid intensification), respectively.

4.5.2 Potential Predictability of Teleconnection Indices

The critical *F*-values for the teleconnection indices ANOVA investigations are 1.58 (OND and JFM) and 1.59 (NDJ and DJF), due to the different number of years comprising the time series (37 and 36, respectively). *F*-values for all three teleconnection indices and all four seasons exceed the respective critical *F*-values (Table 4.2).

Nevertheless, *F*-values for the NAO are small and considerably lower than those for the SO and PDO. With the exception of the NDJ season, the PDO has the highest *F*-values and are noticeably higher than the SO *F*-values.

4.5.3 Composite Analysis

Similar geographical patterns of statistically significant differences between the composites were found throughout the four seasons evaluated for all three teleconnections investigated (SO, PDO, NAO) and for each storm activity proxy (MSLP, ΔMSLP, 10-m wind speeds), respectively. Nevertheless, similar to the ANOVA results, the spatial extents of the regions where the composites differ with statistical significance do vary throughout the seasons. Within the North American coastal domains, for all three teleconnections, the spatial extent of statistically significant differences increases as the seasons progress (Figures B.5-B.13 in Appendix B), with the greatest spatial extents observed in JFM (Figures 4.4-4.6, S4.3-S4.5).

The SO composites using MSLP highlight the differences in the strength of the Aleutian Low between El Niño and La Niña conditions, with anomalies greater than +/-7 hPa observed (Figure 4.4, top). Considerable anomalies are also seen in the North Atlantic during El Niño conditions, with lower pressures than normal observed in the mid-latitudes (-2 to -4 hPa) and a tripole of higher than normal pressures in the Arctic (+2 to 5 hPa). Statistically significant differences between the SO composites are observed over the majority of the North Pacific and into the North American west coast domain, particularly when comparing El Niño vs. La Niña conditions. A large portion of the eastern North Atlantic, including the southern half of the North American east coast domain, is also found to have statistically significant differents when comparing El Niño

vs. La Niña and El Niño vs. neutral conditions. When comparing La Niña vs. neutral conditions, however, statistically significant differences are primarily confined to the eastern North Pacific.

The SO composites using ΔMSLP also highlight the differences in the Aleutian Low observed between El Niño and La Niña, displaying dipole patterns in the composite anomalies (Figure 4.4, bottom). Within the eastern North Pacific, ΔMSLP anomalies on the order of +/-1 hPa/24 hrs or greater are observed between the ENSO events. A dipole pattern in the ΔMSLP anomalies is also found in the North Atlantic, particularly in association with El Niño conditions. Additionally, over the Western Hemisphere, a strong land-ocean contrast in ΔMSLP anomalies is observed – during El Niño conditions, strong negative anomalies are observed over land while strong positive anomalies are observed over the oceans and the reserve (albeit with weaker anomalies) is seen under La Niña conditions. In general, the patterns of statistically significant differences between composites correspond with those of the ΔMSLP anomalies, particularly when comparing El Niño vs. La Niña and El Niño vs. neutral conditions. Statistically significant differences are observed in the mid-latitudes over the eastern North Pacific, the subtropics in the North Atlantic, and over much of North America when comparing El Niño vs. La Niña and El Niño vs. neutral conditions. When comparing La Niña vs. neutral conditions, however, the main areas of statistically significant differences are limited to the central eastern North Pacific and Aleutian Low-Bering Sea regions.

Similar to the SO composites, the PDO composites using MSLP also highlight the differing strength of the Aleutian Low between the positive and negative PDO phases (PDO+ and PDO-, respectively), with +/-2 hPa anomalies (and greater during PDO-)

observed (Figure 4.5, top). The PDO composite differences are statistically significant over much of the central and eastern North Pacific and over the southern half of the North American west coast (e.g., along the USA coast). Statistically significant differences are also found within the subtropics and mid-latitudes of the western North Atlantic (west of ~60°W), building in spatial extent as the seasons progress (Figures B.8-B.10, top, in Appendix B and Figure 4.5, top), and extending over a large portion of the USA east coast by JFM.

Similar again to the SO composites, the ΔMSLP PDO composites also highlight differences in the Aleutian Low between the PDO+ and PDO- phases, displaying a dipole pattern with anomalies of +/-0.4 hPa/24 hrs (and greater during the PDO- phase) (Figure 4.5, bottom). In concert with the North Pacific anomaly dipole pattern observed, statistically significant differences between the PDO phases are found in the mid-latitudes (centered around ~45°N) of the eastern-central North Pacific and in association with the Aleutian Low and extending into the Bering Sea. Similar to the PDO MSLP analyses, a considerable area of statistically significant differences is also observed within the subtropics and mid-latitudes of the western North Atlantic (west of ~60°W). Over North America, the spatial extent of statistically significant differences is confined to western mountainous regions.

The NAO composites using MSLP strongly highlight the differing strengths of the NAO's centres of action (Icelandic Low and Azores High) between the positive and negative phases (NAO+ and NAO-, respectively), with +/-3 hPa anomalies (and greater during NAO-) observed (Figure 4.6, top [the NAO negative phase is strongest in JFM

while the positive phase is strongest in DJF, Figure B.13, top, in Appendix B]). The NAO composite differences are statistically significant over nearly the entire North Atlantic Ocean basin and over a large portion of the Arctic. In earlier seasons (e.g., OND), the spatial extent of the statistically significant differences is confined to the mid- and high-latitudes of the North Atlantic and the Arctic and then builds as the seasons progress (Figures B.11-B.13, top, in Appendix B and Figure 4.6, top). Nevertheless, statistically significant differences are observed extending across a large portion of the North American east coast during all seasons evaluated. Only the northerly sections of Quebec and Labrador, Canada, consistently do not have statistically significant differences due to these areas being located in a transition zone between the opposing strong anomalies associated with the NAO's centres of action. Statistically significant differences are observed in the North Pacific (e.g., Kuroshio Current and Gulf of Alaska) in the earlier seasons but the spatial extent decreases as the seasons progress (Figures B.11-B.13, top, in Appendix B) until there is minimal coverage in JFM (Figure 4.6, top).

Similar to the PDO composites, the NAO composites using ΔMSLP reveal a dipole pattern in relation to changes in the teleconnection's centres of action (Figure 4.6, bottom [the NAO negative phase is strongest in JFM while the positive phase is strongest in DJF, Figure B.13, middle, in Appendix B]). Over the North Atlantic, a dipole pattern of ΔMSLP anomalies on the order of +/-0.6 hPa/24 hrs (and greater during the NAO- phase) are observed in the subtropics and the mid-to-high latitudes. During the NAO- phase, when these North Atlantic anomalies are strong (e.g., during JFM), large anomalies (+0.4 to 1 hPa/24 hrs) are also observed over the Kuroshio Current, Asia, and central Russia regions. In the North Atlantic, statistically significant differences between

the NAO phases are found in concert with the observed ΔMSLP anomaly dipole pattern. The statistically significant differences in the North Atlantic mid-to-high latitudes also extend over much of the northeastern region of North America (e.g., northeast USA and eastern Canada).

The 10-m wind speed-based composite analyses over the oceans provide additional support for the results from the ΔMSLP analyses (Figures S4.3-S4.5). The anomalous 10-m wind speed conditions observed in the analyses further highlight the differing strengths of the centres of action and related shifts in extratropical storm activity between the teleconnection phases through dipole and tripole patterns. Within the North American coastal regions, statistically significant differences between the composites are found off the USA west coast, primarily off the Pacific Northwest region, in the SO analysis (when comparing El Niño vs. La Niña and El Niño vs. neutral conditions), over the water adjacent to the southern half of the USA east coast in the PDO analysis, and along a large portion of the USA Eastern Seaboard and over the waters northeast of Newfoundland and Labrador, Canada in the NAO analysis.

4.6 Discussion: Potential Predictability and its Possible Sources

For the MSLP and ΔMSLP storm activity proxies, potential predictability is detected throughout a considerable portion of the Northern Hemisphere and within much of the North American west and east coastal regions. Potential predictability of the 10-m wind speed storm activity proxy is also detected over much of the North Pacific and North Atlantic basins. Within the North American coastal domains, the strength (*F*-values) and spatial extent of potential predictability is strongest in DJF and JFM for MSLP (Figure

4.2) and in OND for ΔMSLP and 10-m wind speeds (Figures 4.3 and S4.2, respectively). Noting a critical *F*-value of 1.5, west coast domain *F*-values during these peak seasons are as high as ~3 to 3.5 for MSLP and 10-m wind speeds and ~4 to 4.5 for ΔMSLP. Within the east coast domain, the *F*-values are as high as ~3.5 to 4 for MSLP and 10-m wind speeds and ~3 to 3.5 for ΔMSLP. As such, there is considerable potential predictability detected along both coasts.

Additionally, all three teleconnections evaluated – SO (representative of ENSO), PDO, and NAO – are found to provide possible sources of the detected potential predictability within the Northern Hemisphere (Figures 4.7-4.9). Within the Northern Hemisphere, the structure of the MSLP, ΔMSLP, and 10-m wind speed composites (e.g., centres of action) strongly reflect the three teleconnections, with seasonal variations in the storm activity proxies (highlighted in the composite anomalies) strongly associated with the teleconnection phases (e.g., El Niño vs. La Niña conditions) (Figures 4.4-4.6, S4.3-S4.5, and Figures B.5-B.13 in Appendix B). In the North American coastal domains, for MSLP, the potential predictability detected and the spatial extent of the teleconnections providing possible sources both increase as the seasons progress. For ΔMSLP and 10-m wind speeds, however, while the potential predictability detected is greatest during OND, the spatial extent of the teleconnections providing possible sources peak during JFM. Nevertheless, in general, the SO and PDO provide possible sources of the potential predictability detected within the west coast domain and over, at the least, the southern half of the east coast domain (e.g., the USA coastal region) while the NAO is found to provide another possible source of the potential predictability detected within the east coast domain (Figures 4.7-4.9 and S4.6-S4.7).

Spatially, the SO provides the main possible source of the detected potential predictability along the west coast with the PDO providing a second possible source in the southern half of the domain (USA coastal region). Along the east coast, the NAO provides the main possible source (spatially) of the detected potential predictability, covering a large portion of the domain (USA Eastern Seaboard and into eastern Canada). The SO and PDO also provide additional possible sources within the southern half of the east coast domain (e.g., USA Eastern Seaboard). Furthermore, all three teleconnection indices are found to be potentially predictable themselves, with particularly high *F*-values detected for the SO and PDO (Table 4.2).

The strong association between the MSLP, ΔMSLP, and 10-m wind speed anomalies and the teleconnections observed in the composite analysis, and the potential predictability of the teleconnection indices themselves, suggests the detected potential predictability of the storm activity proxies originates, in large measure, with the teleconnections. Successfully predicting the teleconnections – all of which are potentially predictable and have been demonstrated to be actually predictable on seasonal or longer timescales (Alexander et al. 2008; Chen and Cane 2008; Barnston et al. 2012; Wen et al. 2012; Merryfield et al. 2013; Scaife et al. 2014; Smith et al. 2014; Dunstone et al. 2016; Athanasiadis et al. 2017) – therefore augers well for the prospects of predicting seasonal variations in storm activity.

4.7 Conclusions

In this study, the potential predictability of seasonal variations in extratropical storm activity and possible sources of this potential predictability are investigated during the

cold seasons (OND, NDJ, DJF, JFM), over the 1979-2015 time period, for the Northern Hemisphere with specific focus on the North American west and east coastal regions. Daily MSLP and 24-hr absolute pressure tendency (ΔMSLP) were used to represent extratropical storm activity. 10-m wind speeds were also utilized to provide additional insight into potential predictability and its sources over the oceans. Analysis of variance (ANOVA) in the time domain was utilized to investigate potential predictability. Possible sources of the detected potential predictability were investigated using composite analysis conditioned on large-scale teleconnections known to be strongly associated with extratropical storm activity – the Southern Oscillation (representative of ENSO), the Pacific Decadal Oscillation, and the North Atlantic Oscillation.

When evaluating the MSLP, ΔMSLP, and 10-m wind speed storm activity proxies, potential predictability is observed in the mid- to high-latitudes in areas where extratropical storm activity is prevalent (e.g., the North Pacific and North Atlantic storm tracks). Furthermore, the strongest potentially predictable signals are typically found in areas of cyclogenesis, in particular the Kuroshio Current region and along the east coast of North America. These geographical patterns of potential predictability are in agreement with previous studies (Madden 1976; Shukla and Gutzler 1983; Zwiers 1987; Rowell 1998; Zheng et al. 2000; Hodson and Sutton 2008). Of the four seasons evaluated, potential predictability in the North American west and east coastal regions is greatest during DJF and JFM for MSLP and OND for ΔMSLP and 10-m wind speeds. During these peak seasons, potentially predictable signals extent throughout the majority, if not all, of the coastal study domains, with the largest spatial coverage in both domains

observed when using ΔMSLP. Potential predictability of 10-m wind speeds is found along the immediate North American coastlines and over the waters adjacent.

The anomalous conditions highlighted in the composite analyses mirror changes in atmospheric circulation (e.g., strengths of semi-permanent pressure cells) and in the related extratropical storm activity (e.g., shifts in storm track location and intensity) observed between the teleconnection phases. MSLP composites highlight the changes in the strengths of climatological features such as the Aleutian Low (SO and PDO) and the Icelandic Low and Azores High (NAO) while the ΔMSLP and 10-m wind speed composites highlight shifts in extratropical storm activity through dipole anomaly patterns. In addition to providing insight into the structure of the MSLP, ΔMSLP, and 10-m wind speed anomalies, the teleconnection indices themselves are also found to be potentially predictable. Subsequently, all three teleconnections evaluated are found to provide a possible source of the detected potential predictability, with the potential predictability of the storm activity proxies originating, in large measure, with the potential predictability of the climate signals.

While extratropical storm activity cannot be described completely using only MSLP, ΔMSLP, and 10-m wind speeds as proxies, the results of this study strongly indicate that seasonal variations of extratropical storm activity are potentially predictable along the North American west and east coastal regions. Additionally, while not all of the possible sources of potential predictability can be accounted for using only three large-scale teleconnections (as other teleconnections are also known to be associated with extratropical storm activity), this study has identified three, likely important, possible sources of the detected potential predictability. As such, the SO, PDO, and NAO can be

utilized to provide the basis upon which seasonal extratropical storm activity forecasts can begin to be developed.

Furthermore, the results of this study also provide insight into which storm activity proxy-teleconnection combinations may produce the most promising seasonal forecast development. For instance, the MSLP-SO combination provides the largest extents of potentially predictable signals and a likely source along both North American coastal regions, thus providing a particularly strong basis for developing seasonal forecasting methods. This MSLP-SO combination result is consistent with other research that investigates the predictability of storm track location and strength on the seasonal timescale (Compo and Sardeshmukh 2004; Yang et al. 2015). Additionally, similar to the 'windows of opportunity' associated with ENSO prediction (Troccoli 2010; Doblas-Reyes et al. 2013), this study also found that SO provides a larger (spatial) possible source of the detected North American coastal potential predictability during El Niño conditions than La Niña conditions, therefore suggesting that seasonal forecasts may have a higher possibility of being successful and more skilful during El Niño events. Thus, this study provides strong support and a basis for developing methods to forecast the seasonal variations of extratropical storm activity along the North American west and east coastal regions.

4.8 Acknowledgements

Funding for this research was provided by the Marine Environmental Observation Prediction and Response (MEOPAR) Network of the Centres of Excellence of Canada, subproject 2.1.2 "Coastal Storm Activity", PI Francis Zwiers, under Project 2.1 "Climate

Change and Extreme Events in the Marine Environment", PIs Greg Flato, Gordon McBean, Bill Merryfield, Barbara Neis, Ronald Pelot, Jinyu Sheng, and Francis Zwiers. This research was also supported by the University of Victoria's Department of Geography and the Pacific Climate Impacts Consortium.

4.9 References

Alexander MA, Matrosova L, Penland C, Scott JD, Chang, P (2008) Forecasting Pacific SSTs: Linear Inverse Model Predictions of the PDO. J Clim 21(2): 385-402

Athanasiadis PJ, Bellucci A, Scaife AA, Hermanson L, Materia S, Sanna A, Borrelli A, MacLachlan C, Gualdi S (2017) A Multisystem View of Wintertime NAO Seasonal Predictions. J Clim 30(4): 1461-1475

Barnston AG, Tippett MK, L'Heureux ML, Li S, DeWitt DG (2012) Skill of real-time seasonal ENSO model predictions during 2002-11: Is Out Capability Increasing? Bull Am Meteorol Soc 93(5): 631-651

Bjerknes J (1966) A possible response of the atmospheric Hadley circulation to equatorial anomalies of ocean temperature. Tellus 18(4): 820-829

Bjerknes J (1969) Atmospheric teleconnections from the equatorial Pacific. Mon Weather Rev 97(3): 163-172

Boer GJ (2004) Long time-scale potential predictability in an ensemble of coupled climate models. Clim Dyn 23(1): 29-44

Boer GJ (2011) Decadal potential predictability of twenty-first century climate. Clim Dyn 36(5-6): 1119-1133

Chen D, Cane MA (2008) El Niño prediction and predictability. J Comput Phys 227(7): 3625-3640

Compo GP, Sardeshmukh PD (2004) Storm Track Predictability on Seasonal and Decadal Scales. J Clim 17(19): 3701-3720

Dee DP, Uppala SM, Simmons AJ, Berrisford P, Poli P, Kobayashi S, Andrae U, Balmaseda MA, Balsamo G, Bauer P, Bechtold P, Beljaars ACM, van de Berg L, Bidlot J, Bormann N, Delsol C, Dragani R, Fuentes M, Geer AJ, Haimberger L, Healy SB, Hersbach H, Holm EV, Isaksen L, Kallberg P, Kohler M, Matricardi

M, McNally AP, Monge-Sanz BM, Morcrette JJ, Park BK, Peubey C, de Rosnay P, Tavolato C, Thepaut JN, Vitart F (2011) The ERA-Interim reanalysis: configuration and performance of the data assimilation system. Q J R Meteorol Soc 137(656): 553-597

DelSole T, Feng X (2013) The "Shukla-Gutzler" Method for Estimating Potential Seasonal Predictability. Mon Weather Rev 141(2): 822-831

Doblas-Reyes FJ, García-Serrano J, Lienert F, Biescas AP, Rodrigues LRL (2013) Seasonal climate predictability and forecasting: status and prospects. WIREs Clim Change 4(4): 245-268

Dunstone N, Smith D, Scaife A, Hermanson L, Eade R, Robinson N, Andrews M, Knight J (2016) Skilful predictions of the winter North Atlantic Oscillation one year ahead. Nature 9(11): 809-814

Eichler T, Higgins W (2006) Climatology and ENSO-Related Variability of North American Extratropical Cyclone Activity. J Clim 19(10): 2076-2093

Gan B, Wu L (2013) Seasonal and Long-Term Coupling between Wintertime Storm Tracks and Sea Surface Temperature in the North Pacific. J Clim 26(16): 6123-6136

Grise KM, Son S, Gyakum JR (2013) Intraseasonal and Interannual Variability in North American Storm Tracks and Its Relationship to Equatorial Pacific Variability. Mon Weather Rev 141(10): 3610-3625

Gulev SK, Zolina O, Grigoriev S (2001) Extratropical cyclone variability in the Northern Hemisphere winter from the NCEP/NCAR reanalysis data. Clim Dyn 17(10): 795-809

Hodson DLR, Sutton RT (2008) Exploring multi-model atmospheric GCM ensembles with ANOVA. Clim Dyn 31(7-8): 973-986

Hurrell JW, Kushnir Y, Visbeck M (2001) The North Atlantic Oscillation. Science 291(5504): 603-605

Krueger O, von Storch H (2012) The Informational Value of Pressure-Based Single-Station Proxies for Storm Activity. J Atmos Oceanic Technol 29(4): 569-580

Lareau NP, Horel JD (2012) The Climatology of Synoptic-Scale Ascent over Western North America: A Perspective on Storm Tracks. Mon Weather Rev 140(6): 1761-1778

Livezey RE, Chen WY (1983) Statistical Field Significance and its Determination by Monte Carlo Techniques. Mon Weather Rev 111(1): 46-59

Madden RA (1976) Estimates of the Natural Variability of Time-Averaged Sea-Level Pressure. Mon Weather Rev 104(7): 942-952

Mantua NJ, Hare SR (2002) The Pacific Decadal Oscillation. J Oceanogr 58(1): 35-44

Merryfield WJ, Lee W-S, Boer GJ, Kharin VV, Scinocca JF, Flato GM, Ajayamohan RS, Fyfe JC, Tang Y, Polavarapu S (2013) The Canadian Seasonal to Interannual Prediction System. Part I: Models and Initialization. Mon Weather Rev 141(8): 2910-2945

Neu U, Akperov MG, Bellenbaum N, Benestad R, Blender R, Caballero R, Cocozza A, Dacre HF, Feng Y, Fraedrich K, Grieger J, Gulev S, Hanley J, Hewson T, Inatsu M, Keay K, Kew SF, Kindem I, Leckebusch GC, Liberato MLR, Lionello P, Mokhov II, Pinto JG, Raible CC, Reale M, Rudeva I, Schuster M, Simmonds I, Sinclair M, Sprenger M, Tilinina ND, Trigo IF, Ulbrich S, Ulbrich U, Wang XL, Wernli H (2013) IMILAST: A Community Effort to Intercompare Extratropical Cyclone Detection and Tracking Algorithms. Bull Am Meteor Soc 94(4): 529-547

Philander SGH (1983) El Niño Southern Oscillation phenomena. Nature 302(5906): 295-301

Pingree-Shippee KA, Zwiers FW, Atkinson DE (2017) Representation of Mid-latitude North American Coastal Storm Activity by Six Global Reanalyses. Int J Climatol 38(2): 1041-1059. https://doi.org/10.1002/joc.5235

Renggli D, Leckebusch GC, Ulbrich U, Gleixner SN (2011) The Skill of Seasonal Ensemble Prediction Systems to Forecast Wintertime Windstorm Frequency over the North Atlantic and Europe. Mon Weather Rev 139(9): 3052-3068

Rowell DP (1998) Assessing Potential Seasonal Predictability with an Ensemble of Mutlidecadal GCM Simulations. J Clim 11(2): 109-120

Scaife AA, Arribas A, Blockley E, Brookshaw A, Clark RT, Dunstone N, Eade R, Fereday D, Folland CK, Gordon M, Hermanson L, Knight JR, Lea DJ, MacLachlan C, Maidens A, Martin M, Peterson AK, Smith D, Vellinga M, Wallace E, Waters J, Williams A (2014) Skillful long-range prediction of European and North American winters. Geophys Res Lett 41, 2514-2519. https://doi.org/10.1002/2014GL059637

Shukla J, Gutzler DS (1983) Interannual Variability and Predictability of 500 mb Geopotential Heights over the Northern Hemisphere. Mon Weather Rev 111(6): 1273-1279

Smith DM, Scaife AA, Eade R, Knight JR (2014) Seasonal to decadal prediction of the winter North Atlantic Oscillation: emerging capability and future prospects. Q J Roy Meteorol Soc https://doi.org/10.1002/qj.2479

Stockdale TN, Alves O, Boer G, Deque M, Ding Y, Kumar A, Kumar K, Landman W, Mason S, Nobre P, Scaife A, Tomoaki O, Yun WT (2010) Understanding and Predicting Seasonal-to-Interannual Climate Variability - The Producer Perspective. Procedia Environ Sci 1: 55-80

Trenberth KE (1985) Potential Predictability of Geopotential Heights over the Southern Hemisphere. Mon Weather Rev 113(1): 54-64

Troccoli A (2010) Seasonal climate forecasting: A review. Meteorol Appl 17 (3): 251-268

Walker GT (1924) Correlation in seasonal variations of weather, IX. A further study of world weather. Memoirs of the Indian Meteorological Department 24(9): 275-333

Wang XL, Wan H, Swail VR (2006) Observed Changes in Cyclone Activity in Canada and Their Relationships to Major Circulation Regimes. J Clim 19(6): 896-915

Wen C, Xue Y, Kumar A (2012) Seasonal Prediction of North Pacific SSTs and PDO in the NCEP CFS Hindcasts. J Clim 25(17): 5689-5710

Yang X, Vecchi GA, Gudgel RG, Delworth TL, Zhang S, Rosati A, Jia L, Stern WF, Wittenberg AT, Kapnick S, Msadek R, Underwood SD, Zeng F, Anderson W, Balaji V (2015) Seasonal Predictability of Extratropical Storm Tracks in GFDL's High-Resolution Climate Prediction Model. J Clim 28(9): 3592-3611

Zheng X, Nakamura H, Renwick JA (2000) Potential Predictability of Seasonal Means Based on Monthly Time Series of Meteorological Variables. J Clim 13(14): 2591-2604

Zwiers FW (1987) A Potential Predictability Study Conducted with an Atmospheric General Circulation Model. Mon Weather Rev 115(12): 2957-2974

Percent of Domain with Significant Local F-values			
Season	**MSLP**	**ΔMSLP**	**10-m Wind Speeds**
OND	43	72	52
NDJ	43	66	50
DJF	46	70	52
JFM	58	69	60

Table 4.1: The percent of the Northern Hemisphere domain (20°N-poleward) where the local *F*-values are significant (the null hypothesis of no potential predictability has been rejected in ANOVA) at the $p = 0.05$ critical level for MSLP, ΔMSLP, and 10-m wind speed potential predictability. The ANOVA results can be considered field significant at the $P = 0.05$ level

Teleconnection Indices F-values				
Season	**SO**	**PDO**	**NAO**	**Critical *F*-value**
OND	11.48	17.34	1.86	1.58
NDJ	17.56	17.35	2.16	1.59
DJF	16.85	24.12	1.98	1.59
JFM	11.56	18.49	2.98	1.58

Table 4.2: Potential predictability (*F*-values) of the teleconnection indices, investigated using a variant of the ANOVA method adapted to monthly time series (Zheng et al. 2000; Table 1, 5th equation). The critical *F*-values are calculated using a 0.05 significance level and 35 or 36 numerator degrees of freedom and 72 or 74 denominator degrees of freedom (OND/JFM and NDJ/DJF, respectively). The numerator and denominator degrees of freedom are calculated using $J - 1$ and $2J$, respectively, where J is the number of seasons (Zheng et al. 2000; Equation 8)

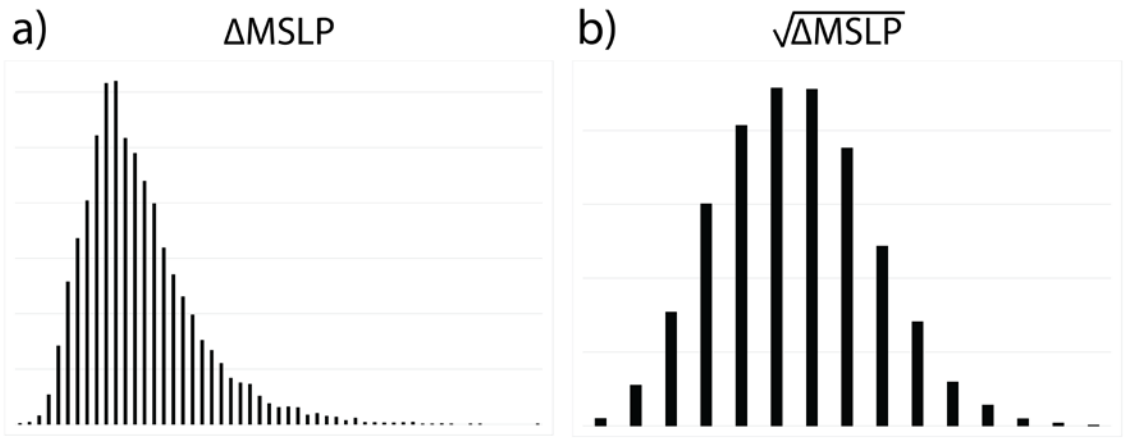

Figure 4.1: Example ΔMSLP distributions exhibiting a) the strongly right skewed distribution of raw absolute pressure tendencies vs. b) the more symmetric distribution of the square root of the absolute pressure tendencies

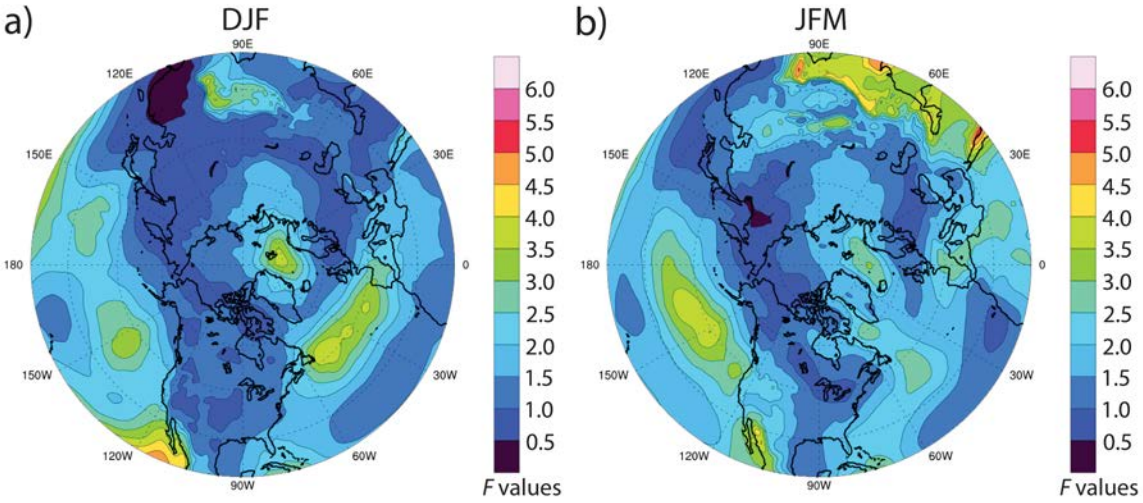

Figure 4.2: Northern Hemisphere (20°N-poleward) MSLP potential predictability for a) DJF and b) JFM. *F*-values above 1.5 are statistically significant at the 0.05 significance level

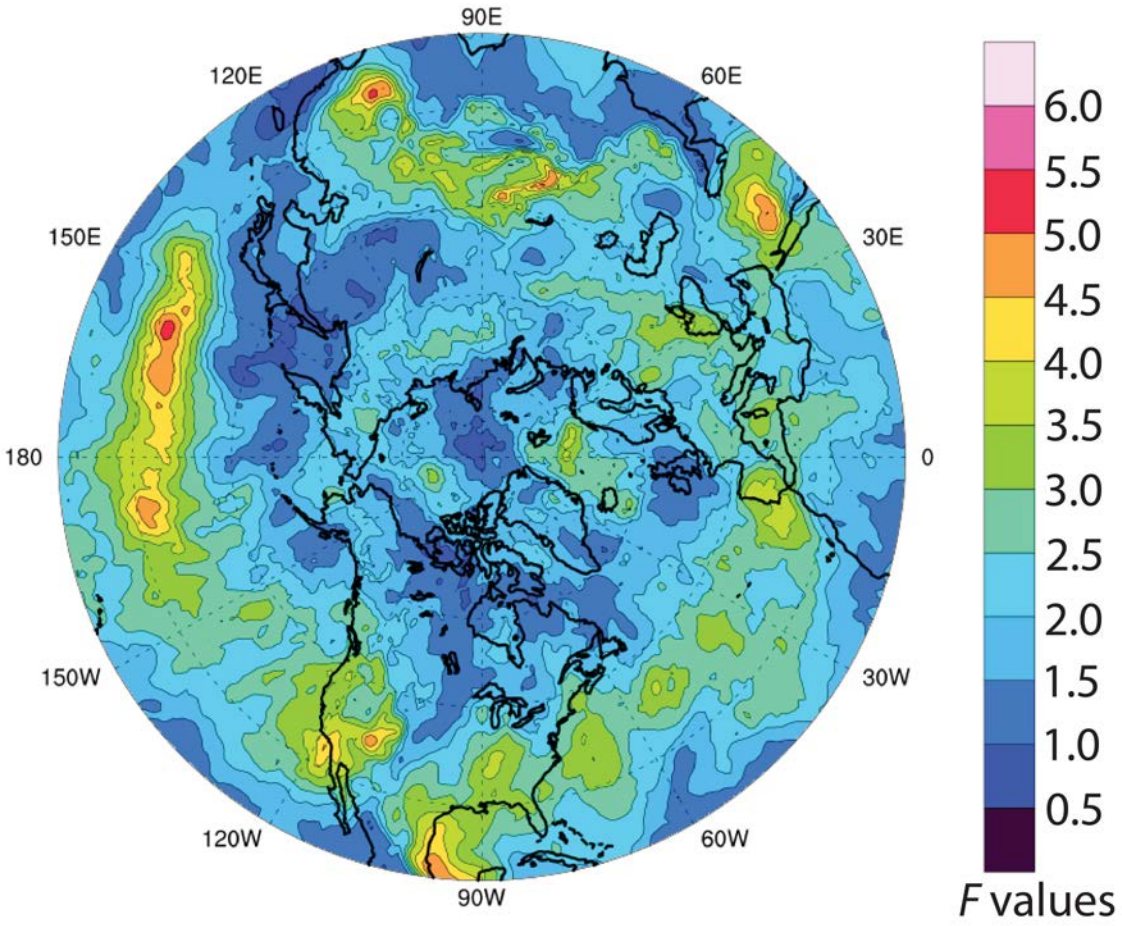

Figure 4.3: Northern Hemisphere (20°N-poleward) ΔMSLP potential predictability for OND. *F*-values above 1.5 are statistically significant at the 0.05 significance level

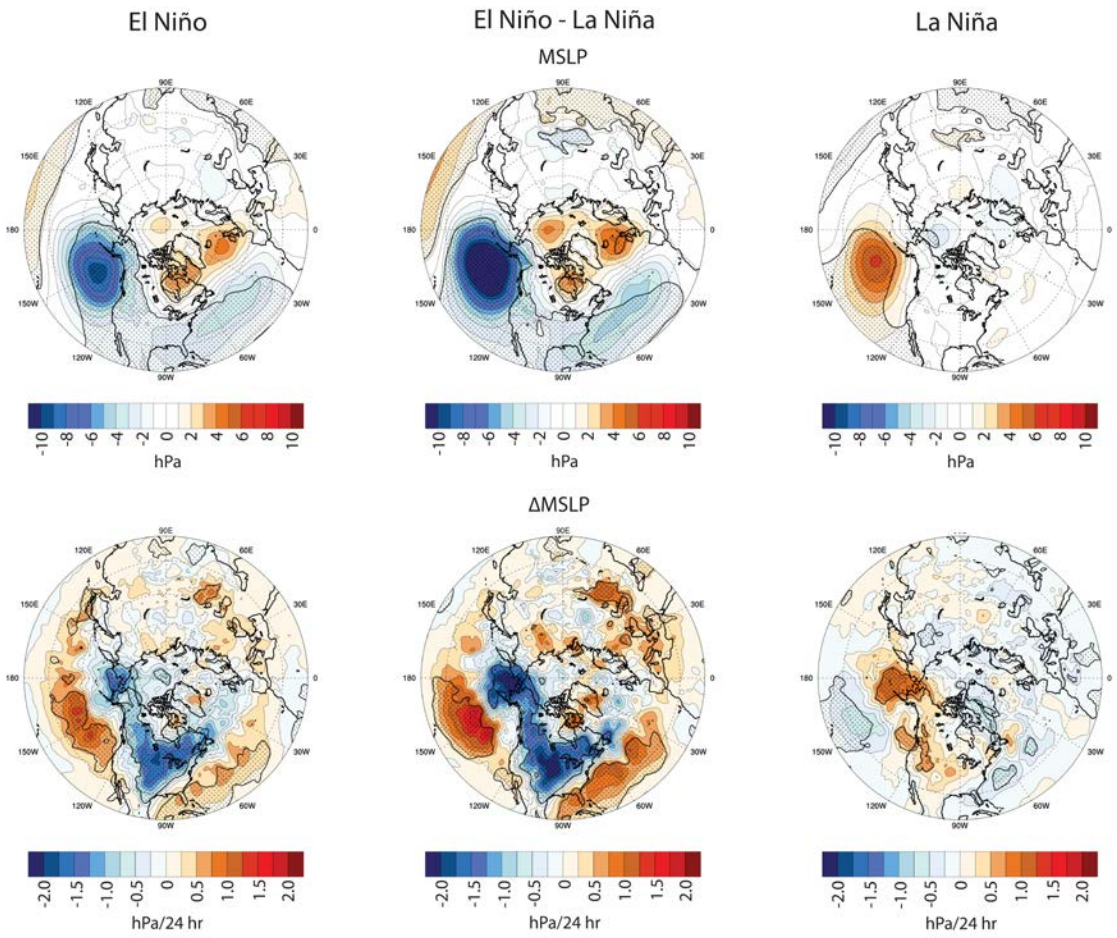

Figure 4.4: Southern Oscillation JFM composite analysis for MSLP (top) and ΔMSLP (bottom). Colours represent MSLP and ΔMSLP anomalies during the El Niño (left) and La Niña (right) phases (composite with the seasonal climatology removed) and differences between the two phases (middle; El Niño composite minus La Niña composite). Shading represents where the composites differ statistically (El Niño vs. neutral conditions [left], El Niño vs. La Niña [middle], La Niña vs. neutral conditions [right])

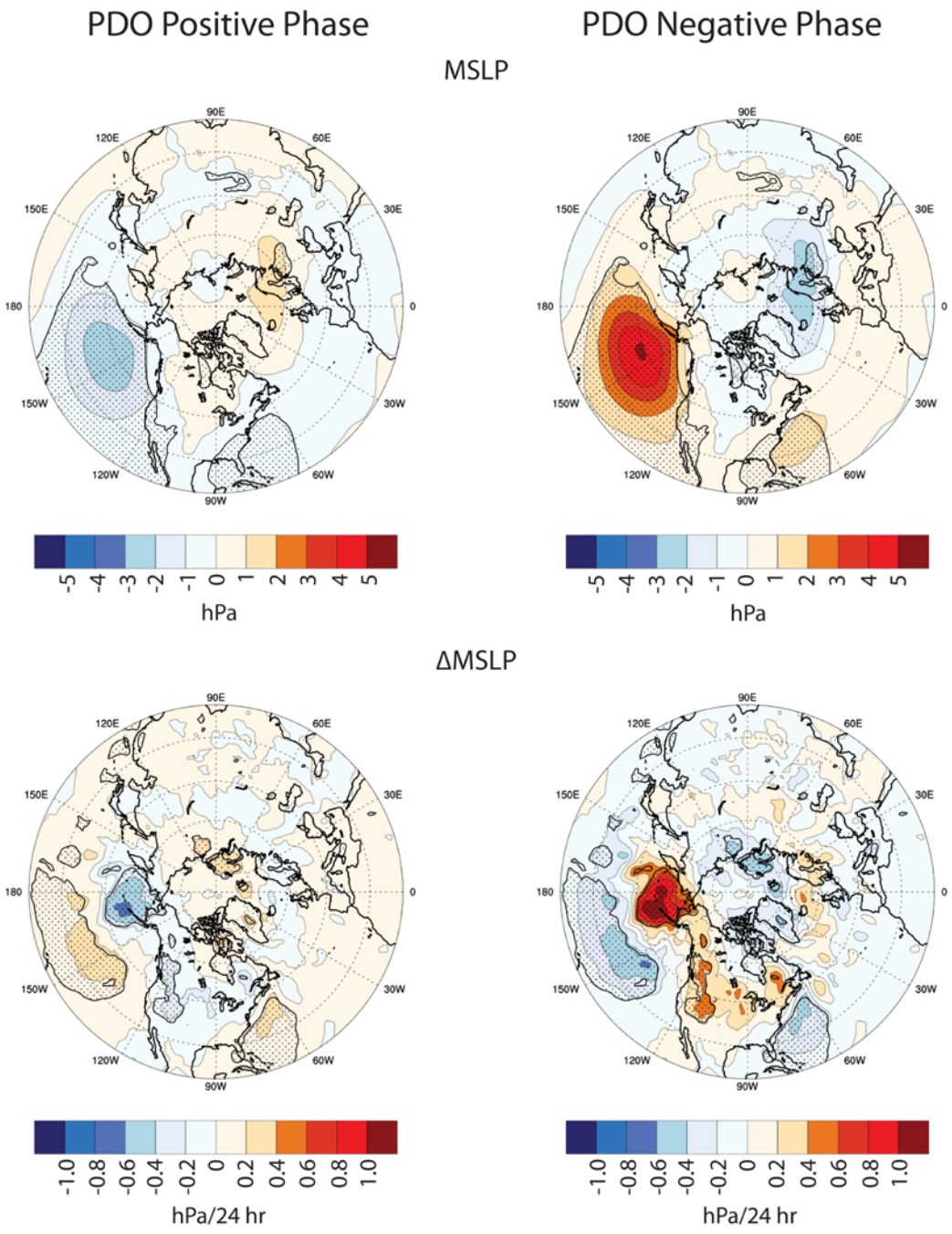

Figure 4.5: Pacific Decadal Oscillation JFM composite analysis for MSLP (top) and ΔMSLP (bottom). Colours represent MSLP and ΔMSLP anomalies during the positive (left) and negative (right) phases (composite with the seasonal climatology removed). Shading represents where the composites differ statistically (positive phase vs. negative phase).

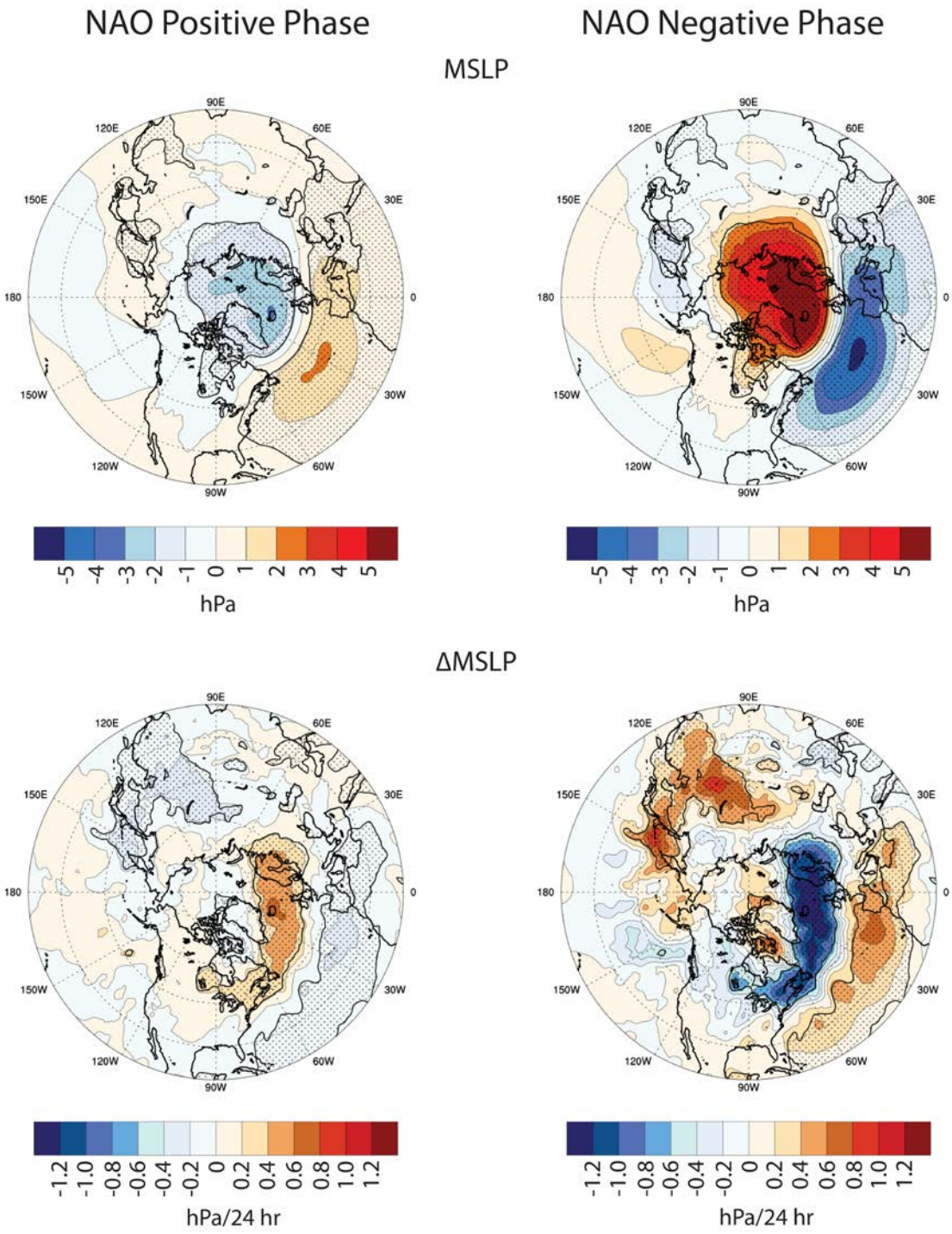

Figure 4.6: As in Fig. 4.5, except for the North Atlantic Oscillation composite analysis

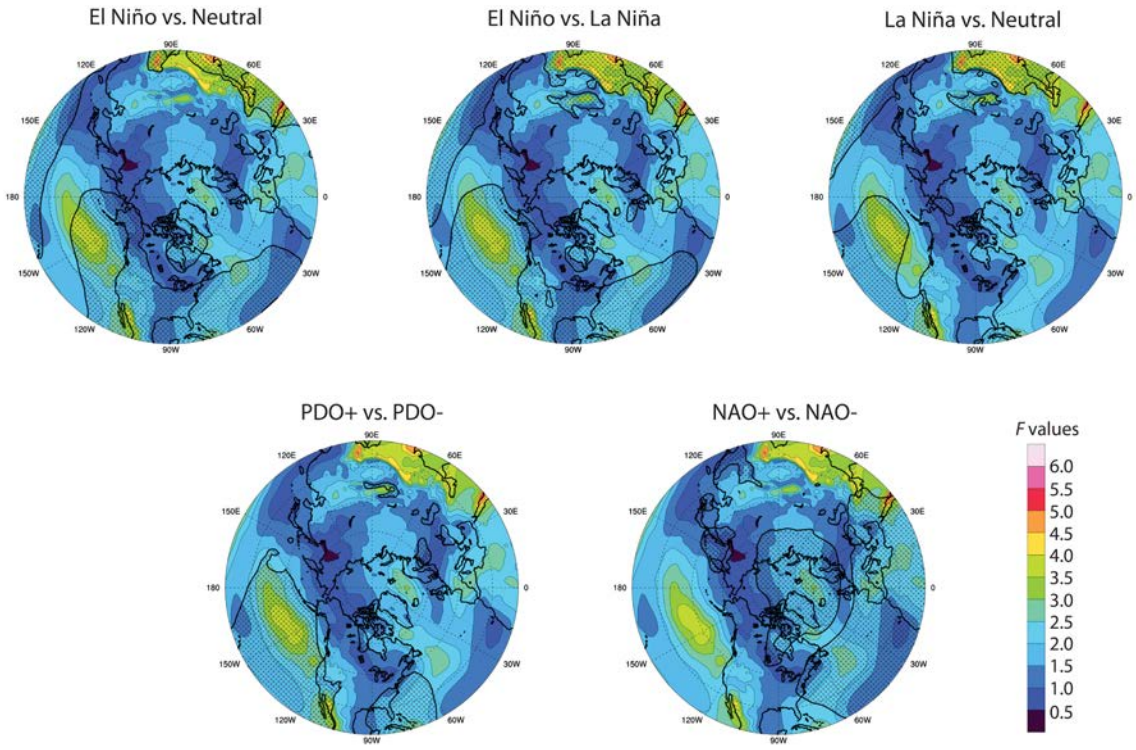

Figure 4.7: MSLP potential predictability and its possible sources for JFM. Colours represent potential predictability (*F*-values above 1.5 are statistically significant at the 0.05 significance level). Shading represents where the teleconnection phase composites differ statistically and, therefore, areas in which the teleconnection is a possible source of the detected potential predictability

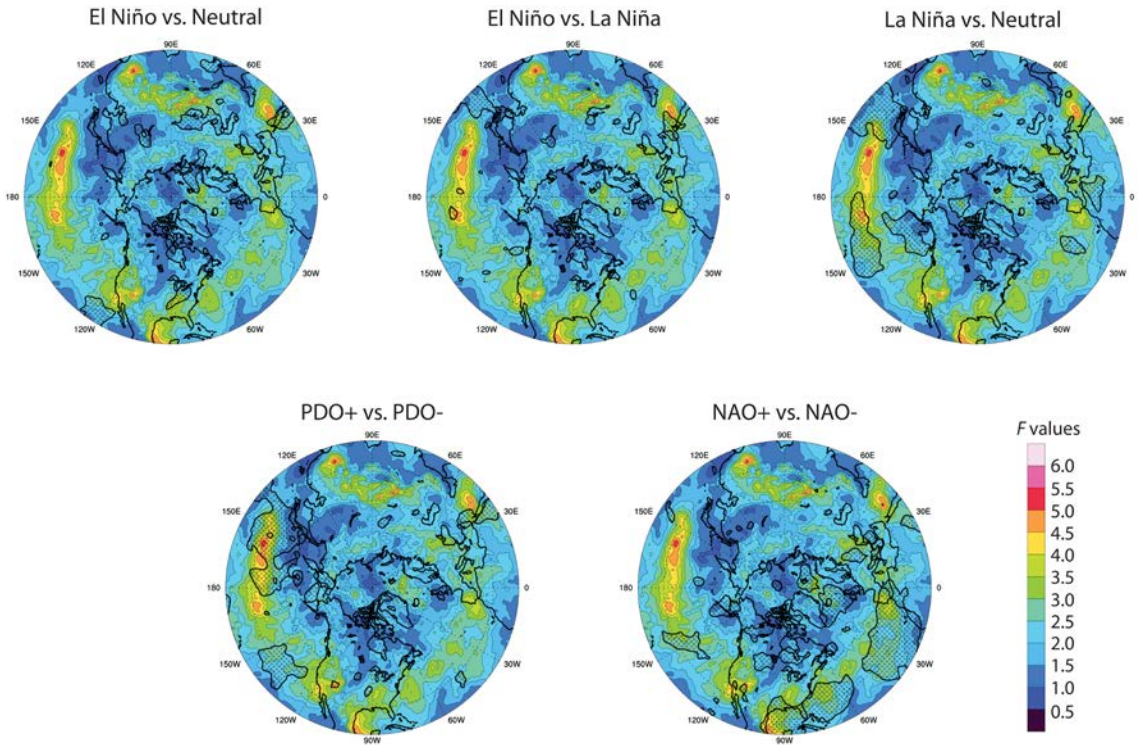

Figure 4.8: As in Fig. 4.7, except for ΔMSLP and OND

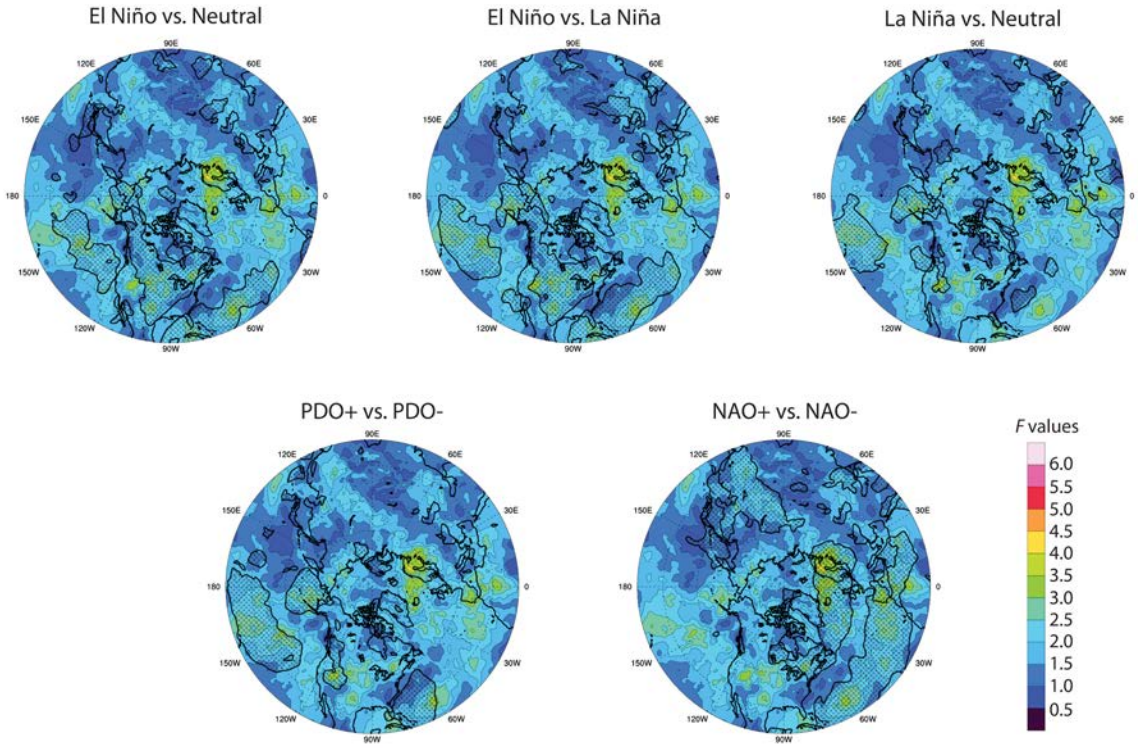

Figure 4.9: As in Fig. 4.7, except for ΔMSLP and JFM

4.10 Supplement to Cold Season Extratropical Storm Activity Potential Predictability and its Sources in the Northern Hemisphere with Focus on the North American Coastal Regions

This section is supplemental to Pingree-Shippee et al. "Cold Season Extratropical Storm Activity Potential Predictability and its Sources in the Northern Hemisphere with Focus on the North American Coastal Regions." Section 4.10.1 provides a detailed mathematical explanation of analysis of variance (ANOVA) in the time domain. Section 4.10.2, "Characteristic Time Between Independent Values", presents information on the autocorrelation present in the ERA-Interim mean sea level pressure (MSLP), 24-hr absolute pressure tendency (ΔMSLP), and 10-m wind speeds time series (1979-2015). Results from the 10-m wind speed-based analysis of variance and composite analysis investigations are presented in Section 4.10.3.

4.10.1 Analysis of Variance (ANOVA) in the Time Domain

When analysis of variance (ANOVA) is performed in the time domain, the data remain in the observed form (i.e., time series) and are decomposed to extract the observed interannual variance and estimate the weather noise variability (Shukla and Gutzler 1983; Trenberth 1984b, 1985b; DelSole and Feng 2013) and, ultimately, calculate potential predictability.

To undertake ANOVA in the time domain, the annual cycle was first removed from the time series using daily climatological means, therefore removing a key aspect of seasonal non-stationarity. The residual time series (composed of the resulting anomalies) were then broken into the seasons of interest (OND, NDJ, DJF, JFM), which, by construction, have comprehensive (all years inclusive) mean seasonal anomalies of zero.

For each season with available data (37 seasons for OND and JFM, 36 seasons for NDJ and DJF), the seasonal mean anomaly was calculated:

$$\overline{x}_j = \frac{1}{N}\sum_{i=1}^{N} x_{i,j} \qquad \text{(Eq. S4.1)}$$

where *N* is the number of daily values in the season (92 days for OND and NDJ, 90/91 days for non-leap/leap year DJF and JFM), *J* is the number of seasons (e.g., 37 OND seasons), and $x_{i,j}$ represents the individual daily value for day *i* in season *j*. From these individual season means (e.g., 1979 OND), the interannual variance (i.e., observed variability) can then be computed for each respective season (e.g., OND):

$$\hat{\sigma}_m{}^2 = \frac{1}{J-1}\sum_{j=1}^{J} \overline{x}_j{}^2 \qquad \text{(Eq. S4.2)}$$

The weather noise variability is then estimated. From the daily data, the intra-segmental variance is calculated for each individual season (e.g., 1979 OND) with data available:

$$s_j{}^2 = \frac{1}{N}\sum_{i=1}^{N}(x_{i,j} - \overline{x}_j)^2 \qquad \text{(Eq. S4.3)}$$

From these intra-segment variances, the mean intra-segmental variance (i.e., average climatic noise over the time series) can then be computed for each respective season (e.g., OND):

$$s^2 = \frac{1}{J}\sum_{j=1}^{J} s_j{}^2 \qquad \text{(Eq. S4.4)}$$

In addition to the mean intra-segmental variance, the calculation of weather noise variability also takes into account autocorrelation present in the time series via the characteristic time between independent values (also referred to as the effective time between independent samples), T_0:

$$\hat{\sigma}_N{}^2 = \frac{T_0}{N-T_0} s^2 \qquad \text{(Eq. S4.5)}$$

Autocorrelation at lag L is calculated:

$$\hat{r}_L = \frac{c_L}{c_0} \quad \text{(Eq. S4.6)}$$

where c_L is the autocovariances at lag L

$$c_L = \frac{1}{N}\sum_{i=L+1}^{N}(x_{i-L,j} - \overline{x_j})(x_{i,j} - \overline{x_j}) \quad \text{(Eq. S4.7)}$$

and c_0, the sample variance, is equal to the mean intra-segmental variance, s^2, for each respective season (e.g., OND). The autocorrelation is then used to calculate the characteristic time between independent values (Leith 1973; Madden 1976; Trenberth 1984a, b, 1985b):

$$T_0 = 1 + 2\sum_{L=1}^{N}(1 - \frac{L}{N})\, r_L \quad \text{(Eq. S4.8)}$$

At large lags, such as those included when working on the seasonal timescale (e.g., 89-day lag), the autocorrelation calculated becomes unreliable (Trenberth 1985a). Therefore, a first order auto-regressive process was applied, as meteorological time series are often characterized by red noise. Autocorrelations for a lag of one day are calculated using the ERA-Interim data (Eq. S4.6). From the 1-day lag autocorrelation, the remaining lags are estimated as:

$$r_L = r_1^L \quad \text{(Eq. S4.9)}$$

The 1-day calculated autocorrelation and estimated autocorrelations for the remaining lags are subsequently used to calculate characteristic time between independent values:

$$T_0 = 1 + 2\sum_{L=1}^{N}(1 - \frac{L}{N})\, r_1^L \quad \text{(Eq. S4.10)}$$

Once the observed interannual variance (Eq. S4.2) and estimated weather noise variability (Eq. S4.5) have been calculated, the potential predictability can be evaluated

by comparing these values using the F ratio and the null hypothesis that there is no potentially predictable variability present (i.e., observed variability equals weather noise variability) for each respective season (e.g., OND):

$$F = \frac{\hat{\sigma}_m{}^2}{\hat{\sigma}_N{}^2} \qquad \text{(Eq. S4.11)}$$

4.10.2 Characteristic Time Between Independent Values

The characteristic time between independent values (T_o, Eq. S4.1) is representative of the overall persistence of a variable's anomalies in the atmospheric circulation and provides insight into the high frequency variability present within the climate system. For all three storm activity proxies, similar geographic patterns are found throughout the four seasons evaluated. In general, as the seasons progress (and extratropical storm activity increases), T_o increases in areas where high persistence and low storm activity are observed and vice versa (Figure B.1 in Appendix B and Figure S4.1).

High persistence (8+ days) of MSLP anomalies is found in subtropical areas (Sahara Desert, subtropical highs in the southern North Atlantic and North Pacific), with the highest values (11+ days) corresponding to the Azores High (Figure S4.1a). High persistence is also observed in the Arctic (8+ days). Alternatively, lower persistence (2-4 days) is found in the mid-latitudes (latitude band of 40°N-60°N and over the North American continent), corresponding to areas of active extratropical storm activity (e.g., oceanic storm tracks). The lowest persistence (1-2 days) is found in the Kuroshio Current region, lee of the Rocky Mountains, and along the North American east coast. These areas of lowest persistence are associated with areas of climatological cyclogenesis, which result in relatively quick changes in MSLP. The Kuroshio Current region, in

particular, is an area of frequent cyclogenesis, often including rapid intensification of storms, therefore causing persistence values to be lowest.

While the ΔMSLP persistence time scale is considerable shorter than that of MSLP persistence (maximum of ~2 days vs. up to ~12+ days, respectively), some similar patterns are observed. High persistence of ΔMSLP anomalies (1.25-2 days) is again found in northern subtropical to mid-latitudes areas (subtropical highs in the North Atlantic and North Pacific) and in the Arctic (Figure S4.1b). Lower persistence values of ΔMSLP (1-1.25 days), however, are not strongly confined to the mid-latitudes as is observed for MSLP. Nevertheless, the lowest ΔMSLP persistence values (0.75-1 days) are found in the Kuroshio Current region, where ΔMSLP is strongly influenced by the rapid changes in pressure associated with cyclogenesis, and close to the region with lowest MSLP persistence values. While the oceanic storm tracks are not as well defined in the ΔMSLP persistence values as with MSLP, their general location is still highlighted (ΔMSLP persistence values of 1-1.25 days).

10-m wind speed persistence values are noticeably different between the subtropics and the mid- and high-latitudes (poleward of ~40°N) (Figure S4.1c). In the subtropics, persistence values of 3-5 days are observed in the North Pacific, particularly in the eastern North Pacific, and 5-7 days across much of the North Atlantic. In the mid- to high-latitudes (40°N-60°N) where extratropical storm activity is most frequent, however, persistence values are limited to 1-2 days, with the lowest persistence (less than 1 day) found in the western North Pacific near the Kuroshio Current region, associated with climatological cyclogenesis. In the Arctic, 10-m wind speed persistence values are 2-3 days.

For all the storm activity proxies, areas with high persistence are found in areas dominated by semi-permanent high pressure cells (e.g., subtropical highs in the North Atlantic and North Pacific basins). Alternatively, low persistence is found in areas of climatologically unstable atmospheric conditions and are influenced by extratropical storm activity (e.g., the North Pacific and North Atlantic storm tracks), with the least persistence observed in areas of cyclogenesis (e.g., Kuroshio Current and along the North American east coast). The T_o values and geographical patterns observed in this research are consistent with previous studies (Madden, 1976; Shukla and Gutzler, 1983).

4.10.3 Seasonal Extratropical Storm Activity Potential Predictability and its Sources: 10-m Wind Speed-based Investigation

Seasonal extratropical storm activity potential predictability and its sources were also investigated using 10-m wind speeds. In both the analysis of variance and composite analysis investigations using 10-m wind speeds, however, the ERA-Interim land mask was applied; *u*- and *v*-wind components at 10-m are classified as "Class B" variables by Kalnay et al. (1996) and, while influenced by observational data, they are also strongly influenced by model physics within the reanalysis. 10-m winds over land are particularly influenced by parameterized sub-grid scale surface properties, such as surface roughness, and the representation of surface topography and are, therefore, less reliable than 10-m winds over the oceans. Subsequently, while the land portions of the North American coastal study domains are not evaluated, the results of the 10-m wind speed-based analysis of variance investigation over ocean areas do provide additional support that extratropical storm activity along the immediate North American coastlines and over the adjacent waters is potentially predictable. The 10-m wind speed-based composite analysis

results also provide additional insight into the sources of this detected potential predictability. Furthermore, the 10-m wind speed results from both investigations provide a more spatially coherent signal than the ΔMSLP results, allowing for more discernible patterns of the potential predictability and its possible sources of storm activity over the oceans to be observed.

4.10.3.1 Analysis of Variance

As with the MSLP- and ΔMSLP-based analysis of variance, a critical *F*-value of 1.5 was utilized in the 10-m wind speed investigation (Tables S4.4, S4.5, and S4.6, respectively). Similar geographical patterns of statistically significant *F*-values are found in the 10-m wind speed analyses throughout the four seasons evaluated, though the spatial extent and strength vary as the seasons progress. The results are also considered field significant for all seasons evaluated, with the percent of the domain over which local *F*-tests are significant being 50% or greater (Table 4.1). Despite the use of the ERA-Interim land mask, the percent of the domain with significant local *F*-values and, subsequently, field significance were evaluated for the complete Northern Hemisphere (20°N-90°N) domain. Nevertheless, the calculated values in Table 4.1 provide a basic estimate for the 10-m wind speed potential predictability results for considering field significance.

The highest *F*-values (3-4.5) are found over the North Pacific and North Atlantic, corresponding with the major oceanic storm tracks (Figure S4.2 and Figure B.4 in Appendix B). High *F*-values are also found in the region between Iceland and Europe. These *F*-values are highest in OND (Figure S4.2) and, in general, decrease as the seasons progress (Figure B.4). *F*-values over the eastern North Pacific, however, do increase noticeably again in JFM (not shown). Statistically significant *F*-values along the North

American west and east coasts also peak during OND (Figure S4.2) and subsequently decline as the seasons progress (not shown). During OND, along the North American west coast, statistically significant *F*-values are observed along the coast of British Columbia and the USA Pacific Northwest (*F*-values of 2 to 3.5). Peak *F*-values (3-3.5) are found off the coast of Vancouver Island, British Columbia, a common secondary exit region for storms tracking across the North Pacific and a region also influenced by atmospheric river events. An area of weak but still statistically significant *F*-values (1.5 to 2) is also detected along the coast of California, an area that is also frequently impacted by atmospheric river events. Along the North American east coast, statistically significant *F*-values extend through the study domain from the Virginia, USA region northward (*F*-values of 2 to 4). Peak east coast *F*-values are found off the coast of the New England region of the USA (*F*-values of 3.5 to 4), corresponding to an area of climatological cyclogenesis, including rapid intensification. The results of the 10-m wind speed-based analysis of variance, therefore, further indicates the potential predictability of storm activity along the North American coasts, supporting the results of the MSLP- and ΔMSLP-based investigations.

4.10.3.2 Composite Analysis

Similar to the ΔMSLP analyses, the anomalous 10-m wind speed conditions observed in the composite analyses of the Southern Oscillation (SO), Pacific Decadal Oscillation (PDO), and North Atlantic Oscillation (NAO) highlight, in particular, the differing strengths of the centres of action and related shifts in extratropical storm activity between the teleconnection phases through dipole and tripole patterns (Figures S4.3-S4.5 and Figures B.5-B.13, bottom, in Appendix B). As with the composite analyses using MSLP

and ΔMSLP, similar geographical patterns of statistically significant differences between the 10-m wind speed composites were found throughout the four seasons evaluated for each teleconnection investigated. Nevertheless, the spatial extents of the regions where the composites differ with statistical significance do vary throughout the seasons. Within the North American coastal study domains, the spatial extent of statistically significant differences increases as the seasons progress, with the greatest spatial extents observed in JFM for all three teleconnections.

The SO composites using 10-m wind speeds highlight, in particular, the differences in the Aleutian Low observed between El Niño and La Niña conditions through dipole patterns in the composite anomalies (Figure S4.3). Within the eastern North Pacific, anomalies of +/-0.6 m s^{-1} or greater are observed between the El Niño and La Niña composites. Anomalies are also observed extending into the eastern North Pacific subtropics from the equatorial Pacific in association with changes in the Walker Circulation. Within the North American west coast domain, statistically significant differences are found off the USA west coast, primarily off the Pacific Northwest region, when comparing El Niño vs. La Niña and El Niño vs. neutral conditions. Within the east coast domain, for all three composite comparisons, statistically significant differences are confined to the waters adjacent to the southeast USA.

Similar to the SO composites, the PDO composites highlight differences in the Aleutian Low between the positive and negative phases (PDO+ and PDO-, respectively) through a dipole pattern with anomalies of +/-0.4 m s^{-1} (Figure S4.4). Furthermore, changes in the subtropical eastern Pacific wind speeds are also featured in the composites, with anomalies of +/-0.4 m s^{-1} (and greater during the PDO- phase), resulting in a tripole

pattern. In concert with the anomaly patterns observed, a tripole pattern of regions with statistically significant differences between the PDO phase composites is observed in the North Pacific; The anomalous conditions and spatial coverage of statistically significant differences are strongly zonal and extend through the Aleutian Low region, mid-latitudes (centered around ~45°N), and subtropics (centered around 25°N). While there are large regions of statistically significant differences over the Pacific Ocean, no areas of statistically significant differences are found within the North American west coast study domain. Within the east coast domain, statistically significant differences are observed over the waters adjacent to the southern half of the USA east coast.

The NAO composites reveal a strong dipole pattern related to changes in the teleconnection's centres of action between the positive and negative NAO phases (NAO+ and NAO-, respectively) (Figure S4.5 [the NAO negative phase is strongest in JFM while the positive phase is strongest in DJF, Figure B.13, bottom, in Appendix B]). Anomalies on the order of +/-0.4 m s^{-1} are observed in association with the changing strengths of the Icelandic Low and Azores High, with larger anomalies (+/-0.8 m s^{-1} and greater) seen during the NAO- phase. Furthermore, a band of considerable anomalies (+/-0.4 m s^{-1}) is also observed in the North Atlantic subtropics (centered around ~20°N), creating a tripole pattern over the North Atlantic basin. This tripole pattern is mirrored by the areas of statistically significant differences between the NAO phases. Within the North American east coast domain, areas of statistically significant differences are found off a large portion of the USA Eastern Seaboard and over the waters northeast of Newfoundland and

Labrador, Canada. There are no areas of statistically significant differences observed in the North American west coast domain.

The results of the 10-m wind speed composite analyses, in addition to the potential predictability of the teleconnection indices themselves (Table 4.2), further indicate that all three teleconnections provide a possible source of the detected potential predictability of the storm activity proxies within the North American coastal regions. In the study domains, potential predictability is greatest during OND while the spatial extent of the teleconnections providing possible sources peak during JFM. As a result, the spatial extent of the teleconnections as possible sources of the detected (statistically significant) potential predictability in the study domains is fairly limited (Figures S4.6 and S4.7). Nevertheless, the NAO in particular is found to provide a possible source of the detected potential predictability in the east coast domain (e.g., along the USA Eastern Seaboard) throughout the four seasons.

4.11 Supplement References

DelSole T, Feng X (2013) The "Shukla-Gutzler" Method for Estimating Potential Seasonal Predictability. Mon Weather Rev 141(2): 822-831

Kalnay E, Kanamitsu M, Kistler R, Collins W, Deaven D, Gandin L, Iredell M, Saha S, White G, Woollen J, Zhu Y, Chelliah M, Ebisuzaki W, Higgins W, Janowiak J, Mo KC, Ropelewski C, Wang J, Leetmaa A, Reynolds R, Jenne R, Joseph D (1996) The NCEP/NCAR 40-Year Reanalysis Project. Bull Am Meteor Soc 77(3): 437-471 doi:10.1175/1520-0477(1996)077<0437:TNYRP>2.0.CO;2.

Leith CE (1973) The Standard Error of Time-Average Estimates of Climatic Means. J Appl Meteor 12(9): 1066-1069

Madden RA (1976) Estimates of the Natural Variability of Time-Averaged Sea-Level Pressure. Mon Weather Rev 104(7): 942-952

Shukla J, Gutzler DS (1983) Interannual Variability and Predictability of 500 mb Geopotential Heights over the Northern Hemisphere. Mon Weather Rev 111(6): 1273-1279

Trenberth KE (1984a) Some Effects of Finite Sample Size and Persistence on Meteorological Statistics. Part I: Autocorrelations. Mon Weather Rev 112(12): 2359-2368

Trenberth KE (1984b) Some Effects of Finite Sample Size and Persistence on Meteorological Statistics. Part II: Potential Predictability. Mon Weather Rev 112(12): 2369-2379

Trenberth KE (1985a) Persistence of daily geopotential heights over the Southern Hemisphere. Mon Weather Rev 113(1): 38-53

Trenberth KE (1985b) Potential Predictability of Geopotential Heights over the Southern Hemisphere. Mon Weather Rev 113(1): 54-64

Season	SO Phase	# of Years in Subsample	Years included in Subsample
OND	El Niño	4	1982, 1991, 1994, 1997
	Neutral	25	1979, 1980, 1981, 1983, 1984, 1985, 1986, 1987, 1989, 1990, 1992, 1993, 1995, 1996, 2001, 2002, 2003, 2004, 2005, 2006, 2009, 2012, 2013, 2014, 2015
	La Niña	8	1988, 1998, 1999, 2000, 2007, 2008, 2010, 2011
NDJ	El Niño	4	1982, 1986, 1991, 1997
	Neutral	24	1979, 1980, 1981, 1983, 1984, 1985, 1987, 1989, 1990, 1992, 1993, 1994, 1995, 1996, 2001, 2002, 2003, 2004, 2005, 2006, 2009, 2012, 2013, 2014
	La Niña	8	1988, 1998, 1999, 2000, 2007, 2008, 2010, 2011
DJF	El Niño	6	1982, 1986, 1991, 1997, 2004, 2009
	Neutral	21	1979, 1980, 1981, 1983, 1984, 1985, 1987, 1989, 1990, 1992, 1993, 1994, 1995, 2001, 2002, 2003, 2005, 2006, 2012, 2013, 2014
	La Niña	9	1988, 1996, 1998, 1999, 2000, 2007, 2008, 2010, 2011
JFM	El Niño	5	1983, 1987, 1992, 1998, 2010
	Neutral	24	1979, 1980, 1981, 1882, 1984, 1985, 1986, 1988, 1990, 1991, 1993, 1994, 1995, 1996, 1997, 2002, 2003, 2004, 2005, 2007, 2012, 2013, 2014, 2015
	La Niña	8	1989, 1999, 2000, 2001, 2006, 2008, 2009, 2011

Table S4.1: Subsamples utilized in the Southern Oscillation composite analyses. For seasons spanning across two calendar years (i.e., NDJ and DJF), the year listed corresponds to the beginning month(s) of the season (e.g., '1979 NDJ season' = November 1979-December 1979-January 1980 season)

Season	PDO Phase	# of Years in Subsample	Years included in Subsample
OND	Positive	17	1979, 1980, 1981, 1982, 1983, 1984, 1986, 1987, 1991, 1992, 1993, 1995, 1997, 2002, 2003, 2014, 2015
	Negative	20	1985, 1988, 1989, 1990, 1994, 1996, 1998, 1999, 2000, 2001, 2004, 2005, 2006, 2007, 2008, 2009, 2010, 2011, 2012, 2013
NDJ	Positive	19	1980, 1981, 1982, 1983, 1984, 1985, 1986, 1987, 1991, 1992, 1993, 1995, 1996, 1997, 2000, 2002, 2003, 2009, 2014
	Negative	17	1979, 1988, 1989, 1990, 1994, 1998, 1999, 2001, 2004, 2005, 2006, 2007, 2008, 2010, 2011, 2012, 2013
DJF	Positive	24	1979, 1980, 1981, 1982, 1983, 1984, 1985, 1986, 1987, 1991, 1992, 1993, 1995, 1996, 1997, 2000, 2002, 2003, 2004, 2005, 2006, 2009, 2013, 2014
	Negative	12	1988, 1989, 1990, 1994, 1998, 1999, 2001, 2007, 2008, 2010, 2011, 2012
JFM	Positive	24	1980, 1981, 1982, 1983, 1984, 1985, 1986, 1987, 1988, 1992, 1993, 1994, 1995, 1996, 1997, 1998, 2001, 2003, 2004, 2005, 2006, 2010, 2014, 2015
	Negative	13	1979, 1989, 1990, 1991, 1999, 2000, 2002, 2007, 2008, 2009, 2011, 2012, 2013

Table S4.2: As in Table S4.1, except for the Pacific Decadal Oscillation composite analyses

Season	NAO Phase	# of Years in Subsample	Years included in Subsample
OND	Positive	20	1979, 1982, 1984, 1986, 1990, 1991, 1992, 1993, 1994, 1998, 1999, 2000, 2004, 2006, 2007, 2008, 2011, 2013, 2014, 2015
	Negative	17	1980, 1981, 1983, 1985, 1987, 1988, 1989, 1995, 1996, 1997, 2001, 2002, 2003, 2005, 2009, 2010, 2012
NDJ	Positive	23	1979, 1980, 1982, 1983, 1986, 1988, 1990, 1991, 1992, 1993, 1994, 1998, 1999, 2003, 2004, 2005, 2006, 2007, 2008, 2011, 2012, 2013, 2014
	Negative	13	1981, 1984, 1985, 1987, 1989, 1995, 1996, 1997, 2000, 2001, 2002, 2009, 2010
DJF	Positive	20	1980, 1982, 1983, 1988, 1989, 1990, 1991, 1992, 1993, 1994, 1998, 1999, 2004, 2006, 2007, 2008, 2011, 2012, 2013, 2014
	Negative	15	1981, 1984, 1985, 1986, 1987, 1995, 1996, 1997, 2000, 2001, 2002, 2003, 2005, 2009, 2010
JFM	Positive	26	1981, 1982, 1983, 1984, 1986, 1988, 1989, 1990, 1991, 1992, 1993, 1994, 1995, 1997, 1998, 1999, 2000, 2002, 2003, 2007, 2008, 2009, 2011, 2012, 2014, 2015
	Negative	10	1979, 1980, 1985, 1987, 1996, 2001, 2005, 2006, 2010, 2013

Table S4.3: As in Table S4.1, except for the North Atlantic Oscillation. Note: NAOI = 0 for the 1979 DJF and 2004 JFM seasons and are, therefore, excluded from the DJF and JFM composite analyses, respectively

Mean Sea Level Pressure				
Season	**T_o Min-Max; Mean (days)**	**Numerator Degrees of Freedom**	**Denominator Degrees of Freedom Min-Max; Mean**	**F_c Min-Max; Mean F_c**
OND	1.9-10.3; 5.6	36	296-1739; 571	1.42-1.46; 1.44
NDJ	1.8-12.3; 5.8	35	234-1800; 535	1.43-1.47; 1.45
DJF	1.9-14.7; 6.3	35	180-1656; 478	1.43-1.49; 1.45
JFM	1.8-13.3; 6.4	36	222-1813; 483	1.42-1.47; 1.44

Table S4.4: Characteristic time between independent values (T_o; calculated in Eq. S4.10), degrees of freedom utilized in the critical F-value calculations, and critical F-values (F_c) from the analysis of variance of MSLP. The numerator and denominator degrees of freedom are calculated using $J - 1$ and $J(N_{\text{eff}} - 1)$, respectively, where J is the number of seasons and N_{eff} is the effective number of independent observations (calculated in Eq. 4.4)

24-hr Absolute Pressure Tendency				
Season	**T_o Min-Max; Mean (days)**	**Numerator Degrees of Freedom**	**Denominator Degrees of Freedom Min-Max; Mean**	**F_c Min-Max; Mean F_c**
OND	0.9-1.8; 1.2	36	1854-3745; 2800	1.42-1.42; 1.42
NDJ	0.9-1.6; 1.2	35	2034-3644; 2724	1.43-1.43; 1.43
DJF	0.9-1.7; 1.2	35	1870-3564; 2664	1.43-1.43; 1.43
JFM	0.9-1.6; 1.2	36	2044-3663; 2738	1.42-1.42; 1.42

Table S4.5: As in Table S4.4, except for ΔMSLP

10-m Wind Speeds				
Season	**T_o Min-Max; Mean (days)**	**Numerator Degrees of Freedom**	**Denominator Degrees of Freedom Min-Max; Mean**	**F_c Min-Max; Mean F_c**
OND	0.9-10.7; 2.5	36	281-3737; 1325	1.42-1.46; 1.43
NDJ	0.9-8.2; 2.4	35	368-3636; 1344	1.43-1.45; 1.43
DJF	0.9-7.7; 2.45	35	385-3564; 1286	1.43-1.45; 1.43
JFM	0.8-8.5; 2.4	36	355-4126; 1351	1.42-1.45; 1.43

Table S4.6: As in Table S4.4, except for 10-m wind speeds

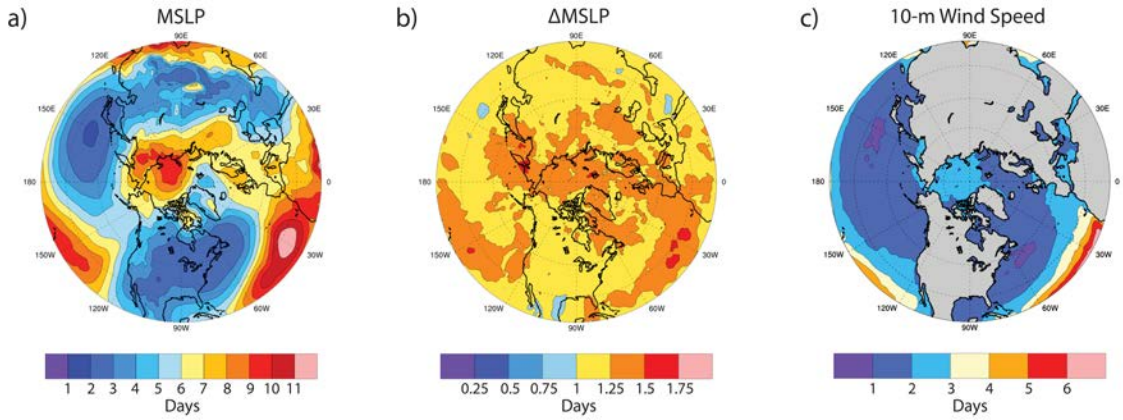

Figure S4.1: Northern Hemisphere (20°N-poleward) characteristic time between independent values for DJF for a) MSLP, b) ΔMSLP, and c) 10-m wind speeds (with ERA-Interim landmass overlay)

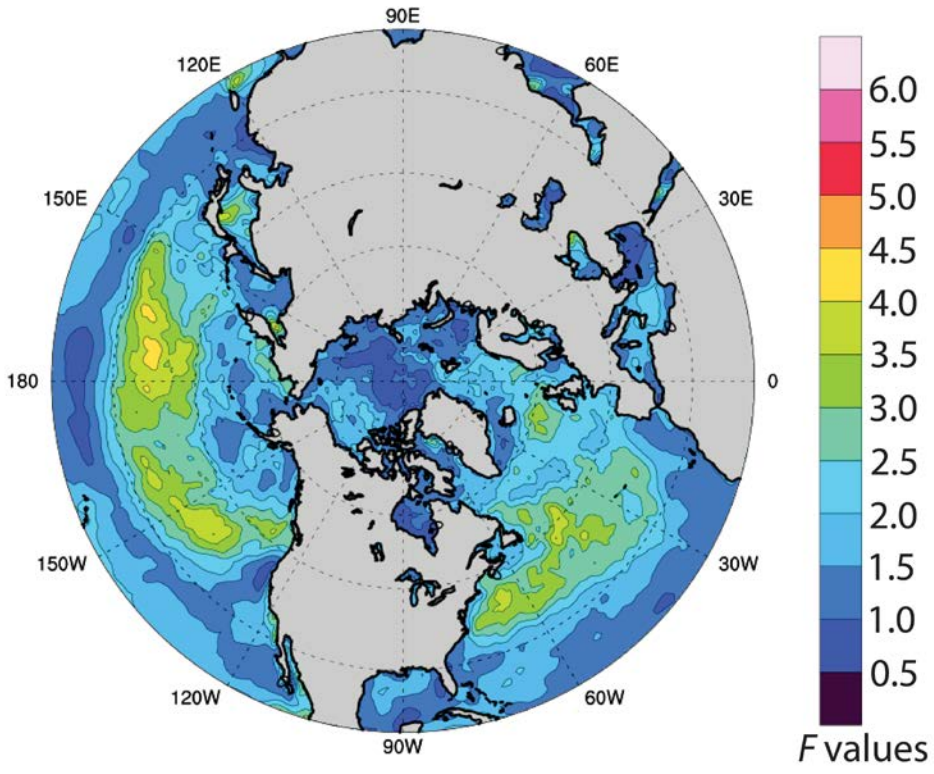

Figure S4.2: Northern Hemisphere (20°N-poleward) 10-m wind speed potential predictability for the OND season with ERA-Interim landmass overlay. *F*-values above 1.5 are statistically significant at the 0.05 significance level

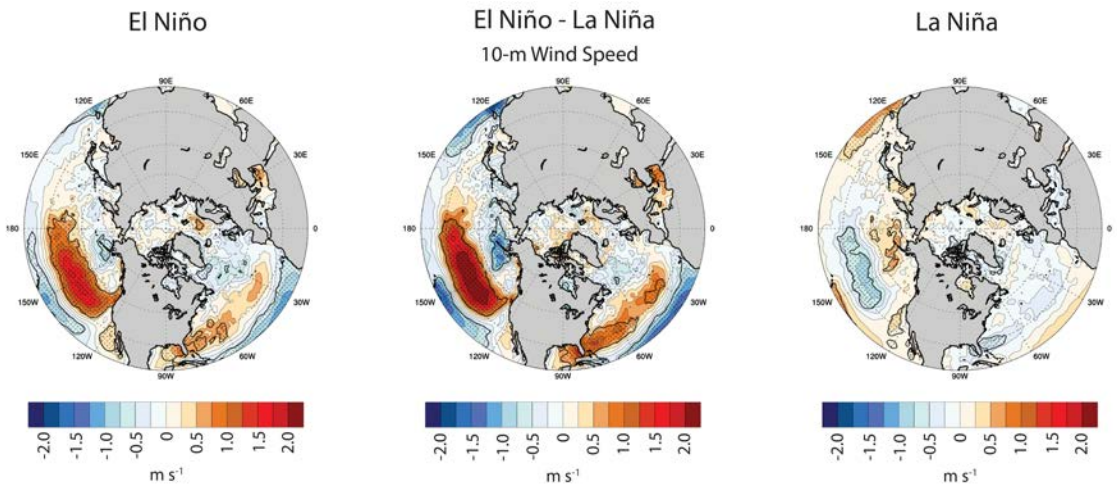

Figure S4.3: Southern Oscillation JFM composite analysis for 10-m wind speed (with ERA-Interim landmass overlay). Colours represent 10-m wind speed anomalies during the El Niño (left) and La Niña (right) phases (composite with the seasonal climatology removed) and differences between the two phases (middle; El Niño composite minus La Niña composite). Shading represents where the composites differ statistically (El Niño vs. neutral conditions [left], El Niño vs. La Niña [middle], La Niña vs. neutral conditions [right])

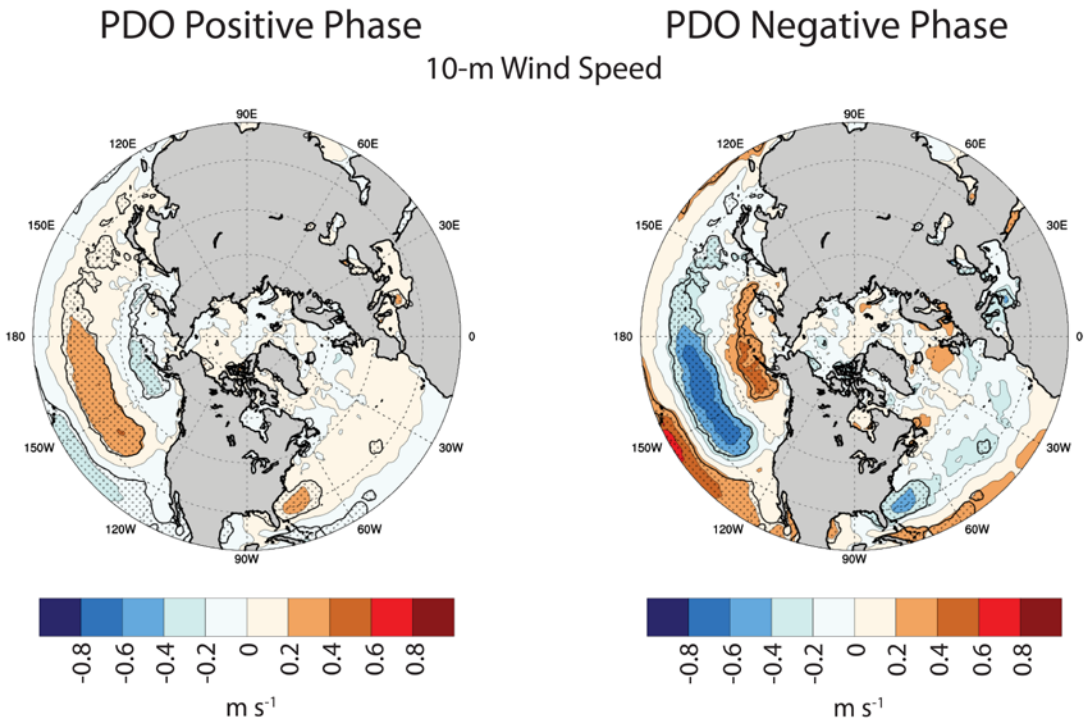

Figure S4.4: Pacific Decadal Oscillation JFM composite analysis for 10-m wind speed (with ERA-Interim landmass overlay). Colours represent 10-m wind speed anomalies during the positive (left) and negative (right) phases (composite with the seasonal climatology removed). Shading represents where the composites differ statistically (positive phase vs. negative phase)

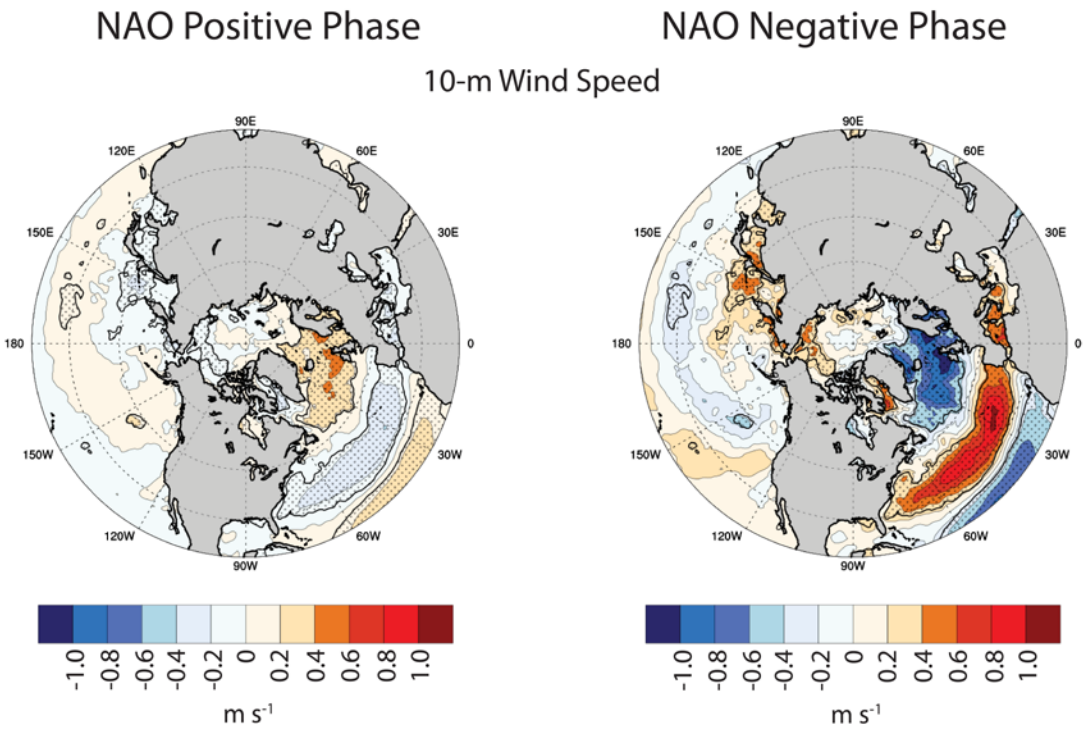

Figure S4.5: As in Fig. S4.4, except for the North Atlantic Oscillation composite analysis

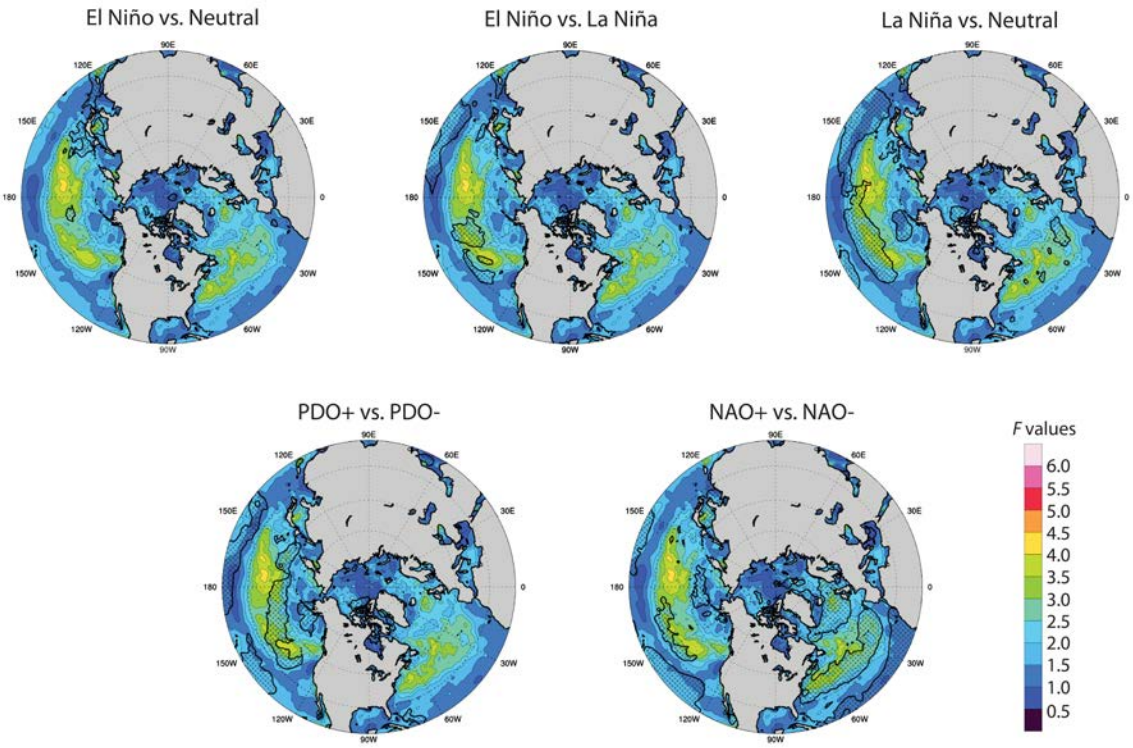

Figure S4.6: 10-m wind speed potential predictability and its possible sources for OND (with ERA-Interim landmass overlay). Colours represent potential predictability (*F*-values above 1.5 are statistically significant at the 0.05 significance level). Shading represents where the teleconnection phase composites differ statistically and, therefore, areas in which the teleconnection is a possible source of the detected potential predictability

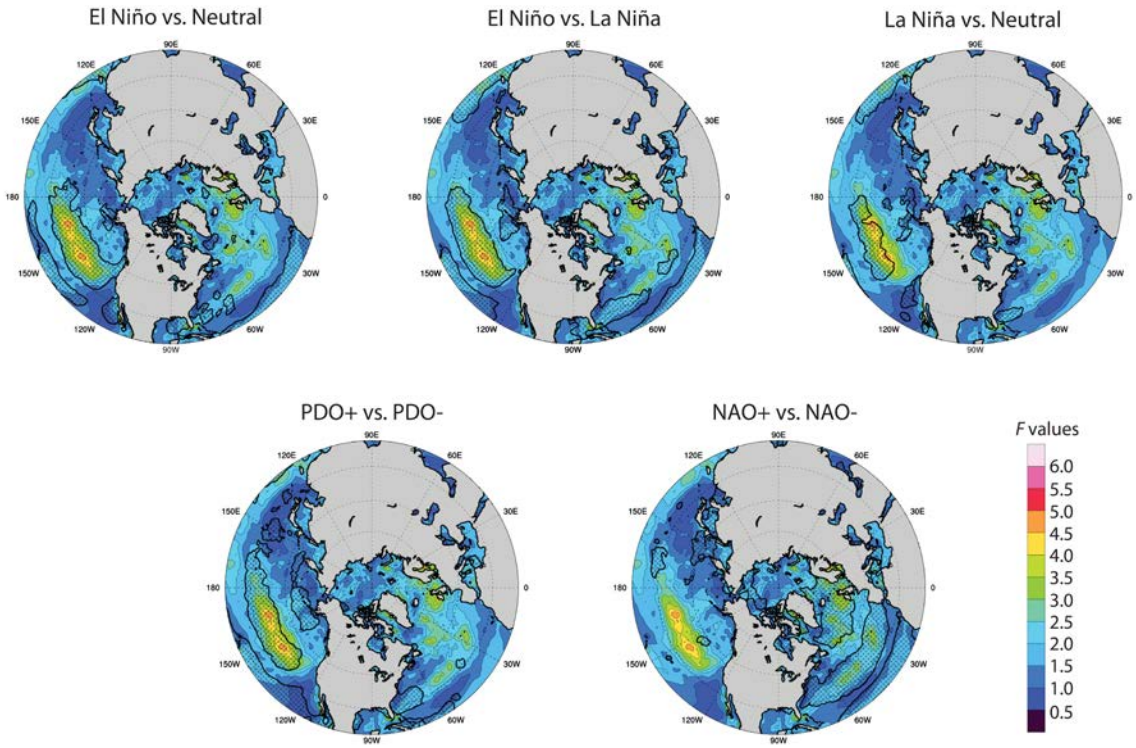

Figure S4.7: As in Fig. S4.6, except for JFM

5.0 Reproduction of Observed North American Coastal Climate Signal-Storm Activity Relationships in CanSIPS

Research Question 3.1 investigates how well the climate signal-storm activity relationships observed in ERA-Interim (Research Question 2.2, Chapter 4) are reproduced in CanSIPS. The climate signal-storm activity relationships are evaluated for the Northern Hemisphere (20°N-90°N) using composite analysis (described in Chapter 4) for the 1981-2010 time period using T42 horizontal resolution (2.79° x 2.79°) data. The climate signal-storm activity relationships are evaluated for CanSIPS-MME and ERA-Interim, respectively, and are then compared for the cold seasons (OND, NDJ, DJF, JFM). The relationships are evaluated for each storm activity proxy (6-hrly MSLP, 6-hrly ΔMSLP, daily mean 10-m wind speeds) and large-scale climate signal investigated in this research project (Southern Oscillation [SO; representative of the El Niño-Southern Oscillation], Pacific Decadal Oscillation [PDO], and North Atlantic Oscillation [NAO]).

Prior to presenting the results of Research Question 3.1, a comparison of seasonal climatologies for CanSIPS-MME and ERA-Interim are presented for each storm activity proxy and season, respectively. Additionally, a comparison of the established (observed) climate indices (which are utilized to create the subsamples used in the composite analysis) and the indices as reproduced in CanSIPS-MME (using the raw, non-calibrated 0-month lead data) are also presented. While the established PDO and NAO indices do not use the base period of 1981-2010 as is used by the SO Index and CanSIPS, the comparisons do provide a general insight into how well CanSIPS reproduces the fluctuations and phase magnitudes of the climate signals.

When considering the 10-m wind speed evaluations it should be noted that the 10-m wind speed results over land, particularly over variable terrain (e.g., the North American Rocky Mountains) could be influenced by parameterized sub-grid scale surface properties, such as the

surface roughness, and the representation of surface topography. In reanalysis datasets, *u*- and *v*-wind components at 10-m are classified as "Class B" variables by Kalnay et al. (1996[1]) and, while influenced by observational data, are also strongly influenced by model physics, particularly over variable terrain. The 10-m wind speed results over land, therefore, are less reliable than the results over the oceans.

5.1 Seasonal Climatologies

Key overall findings from the comparison of seasonal climatologies are the following:

- MSLP: CanSIPS overestimates the seasonal mean MSLP (higher MSLP than observed) in the mid-latitudes (and over Greenland and Svalbard) while underestimating (lower MSLP than observed) in the high-latitudes. In particular, CanSIPS overestimates the average strength of semi-permanent low and high pressure cells, with the Aleutian and Icelandic Lows too deep and the subtropical highs (e.g., Azores Hight) too high. Over North America, CanSIPS is found to overestimate the climatological MSLP in the southern half of the continent, particularly over the variable terrain in the west, while underestimating average MSLP in the northern half.
- ΔMSLP: CanSIPS overestimates the seasonal mean ΔMSLP throughout the majority of the Northern Hemisphere, particularly within the oceanic storm tracks and over land. Over land, average ΔMSLP is noticeably overestimated in areas of high terrain such as the mountainous regions of western North America. In North America, the greatest ΔMSLP overestimation is observed over the US Rocky Mountains.

[1] Kalnay et al. (1996) The NCEP/NCAR 40-Year Reanalysis Project. *Bull. Am. Meteor. Soc.*, 77(3): 437-471.

- 10-m wind speeds: CanSIPS underestimates seasonal mean wind speeds over the mid- and high-latitude oceans, especially in the mid-latitude North Pacific as well as in the higher latitudes of the North Atlantic, Greenland/Norwegian Seas region, and into the Arctic. Over land, though results are relatively noisy, CanSIPS, in general, overestimates climatological wind speeds. In North America, noticeable overestimation is found over the variable terrain in the western half of the continent and in the central US.

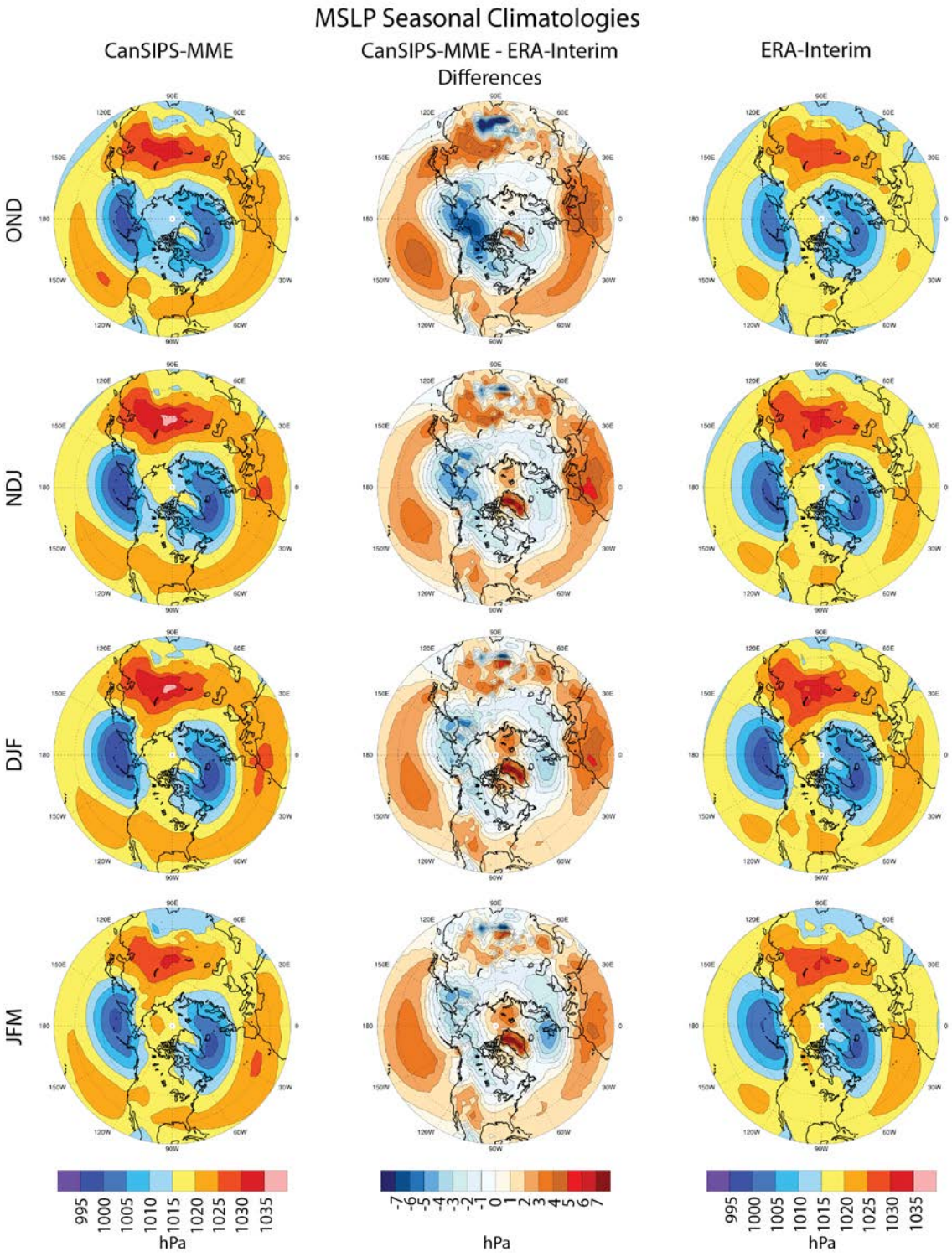

Figure 5.1: MSLP seasonal climatologies for CanSIPS-MME (left) and ERA-Interim (right) and the difference between the two (CanSIPS-MME – ERA-Interim) (middle).

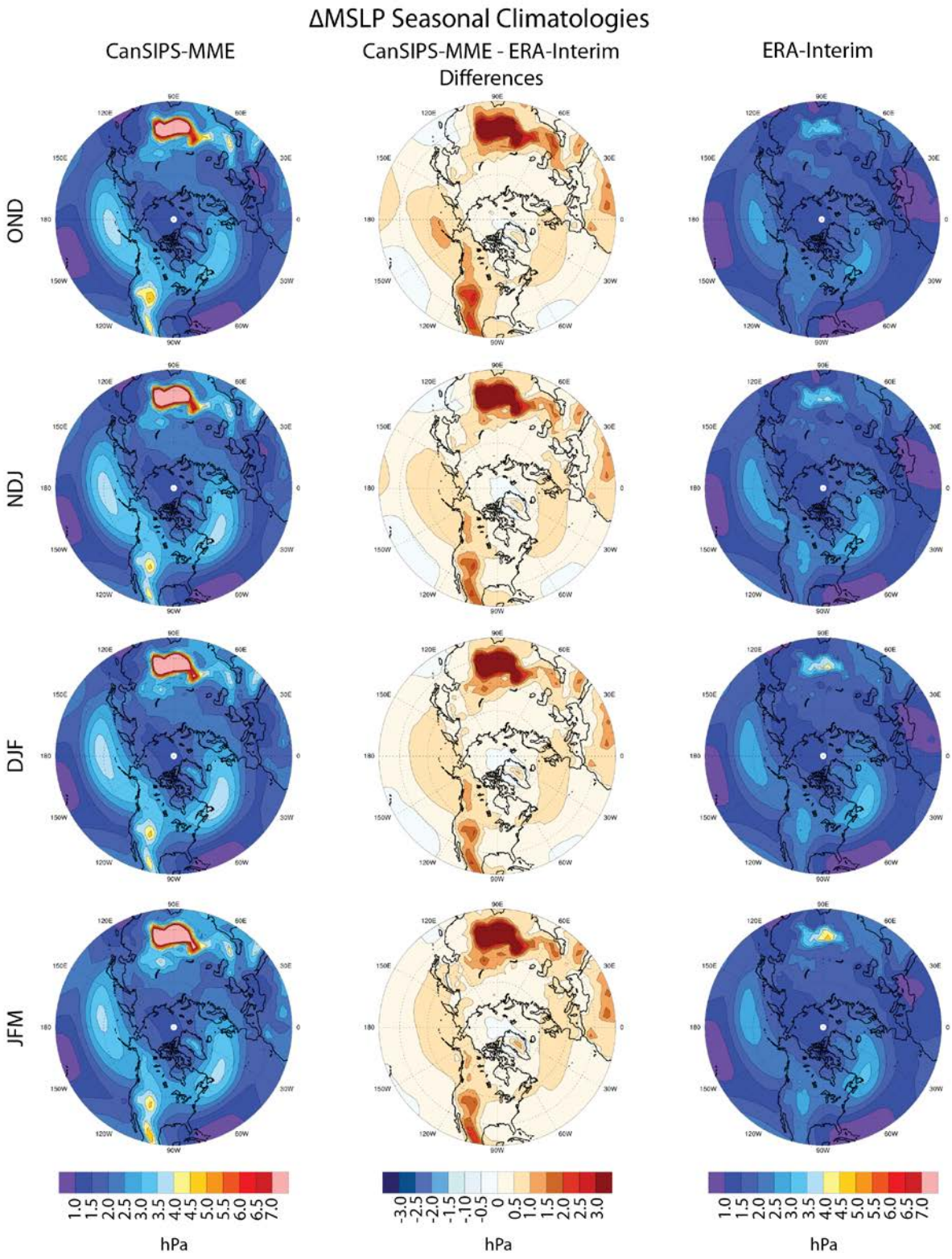

Figure 5.2: 6-hrly ΔMSLP seasonal climatologies for CanSIPS-MME (left) and ERA-Interim (right) and the difference between the two (CanSIPS-MME – ERA-Interim) (middle).

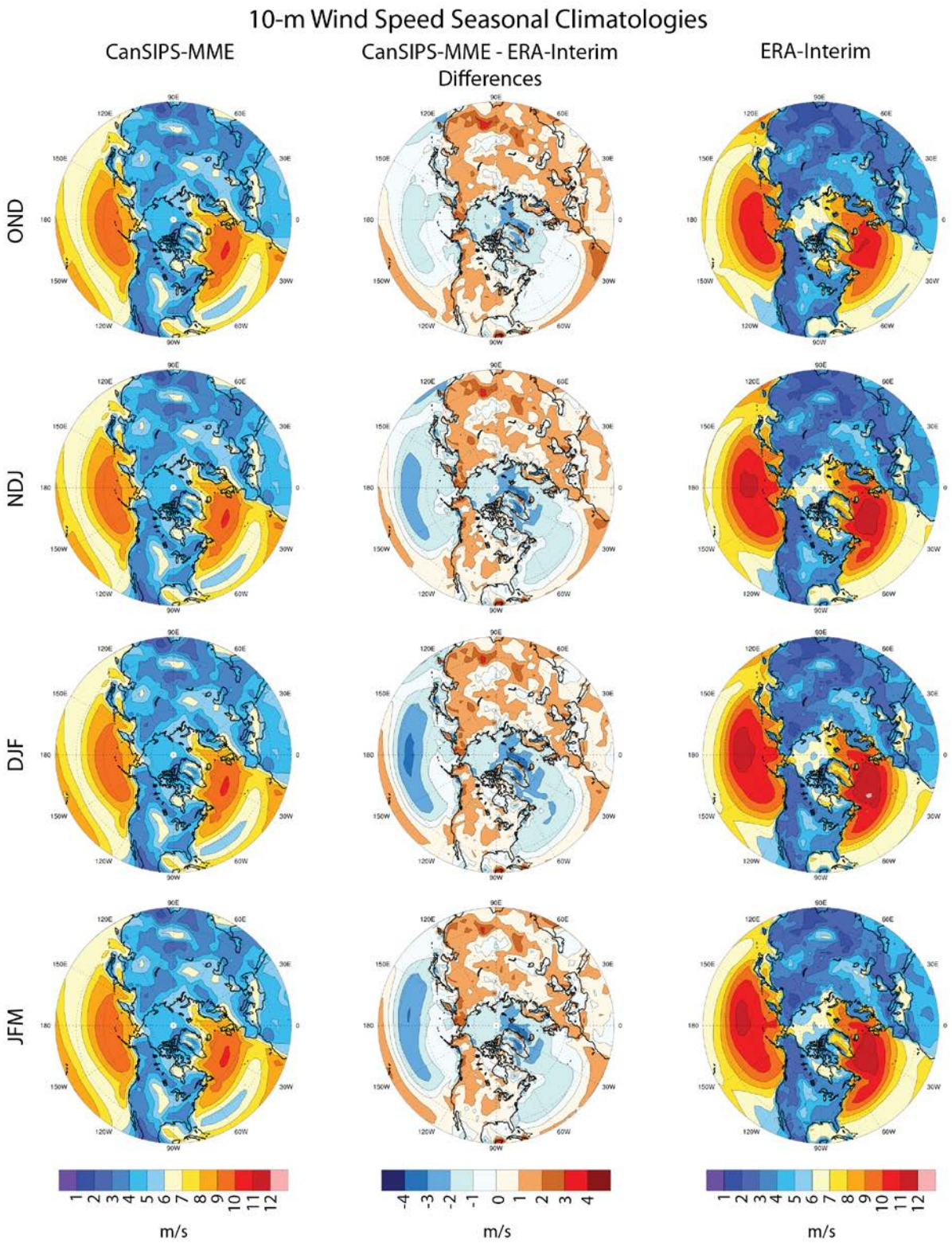

Figure 5.3: 10-m wind speeds seasonal climatologies for CanSIPS-MME (left) and ERA-Interim (right) and the difference between the two (CanSIPS-MME – ERA-Interim) (middle).

5.2 Climate Indices: Established (Observed) vs. CanSIPS-MME

Key overall findings from the comparison of the established climate indices and the indices as reproduced in CanSIPS-MME are the following:

- SOI: CanSIPS does well reproducing the SO Index, reproducing the observed fluctuations in the climate signal and the phase magnitudes (with the occasional underestimating).
- PDOI: In general, CanSIPS does reproduce the PDO Index, reproducing the observed fluctuations in the climate signal but sometimes misrepresenting phase magnitude.
- NAOI: CanSIPS has little success in reproducing the NAO Index, with neither the observed fluctuations in the climate signal nor the phase magnitudes being well represented.

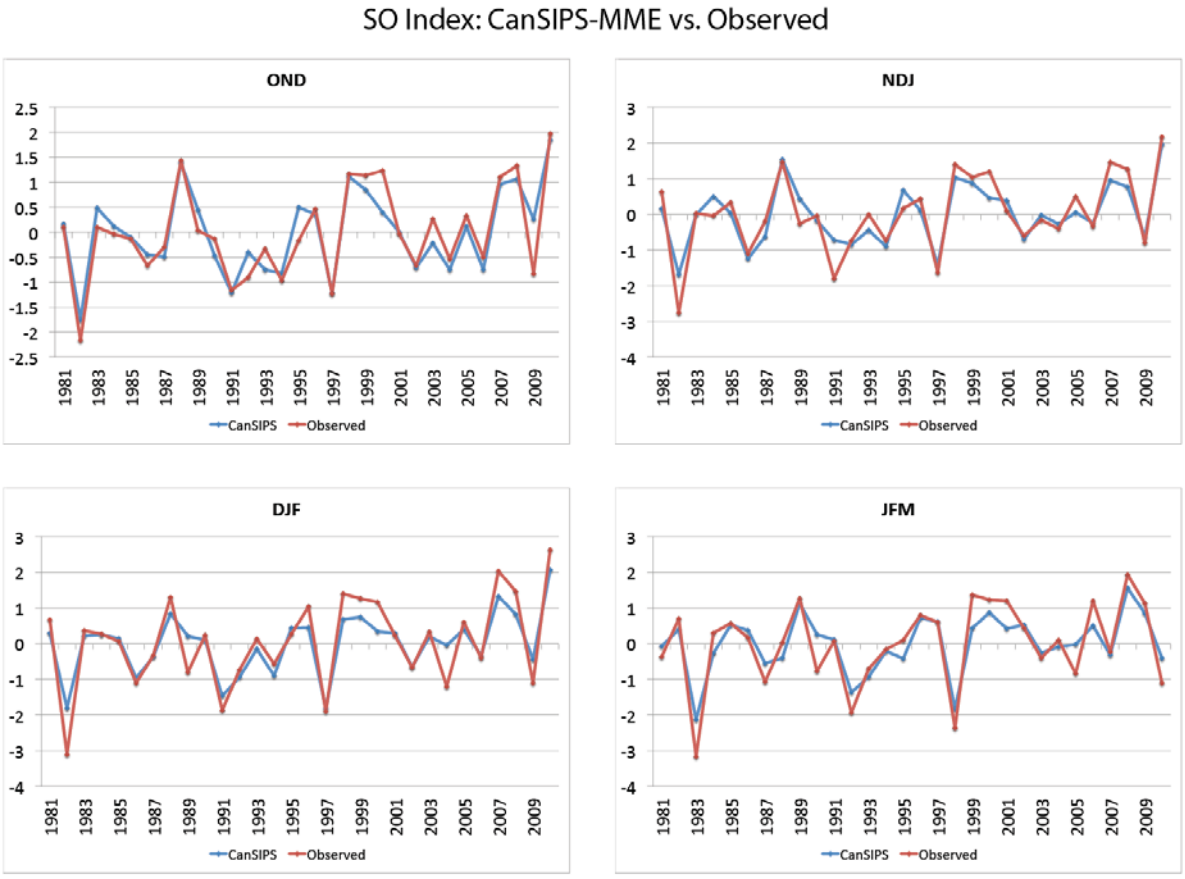

Figure 5.4: The observed Southern Oscillation (SO) Index (red) vs. as reproduced in CanSIPS-MME (blue). The established SO Index is the monthly Standardized Tahiti – Standardized Darwin sea level pressure anomaly (departure from 1981-2010 base period) and was obtained from the NOAA Climate Prediction Center (http://www.cpc.ncep.noaa.gov/data/indices/soi). For seasons spanning across two calendar years (i.e., NDJ and DJF), the year listed corresponds to the beginning month(s) of the season (e.g., '1981 NDJ season' = November 1981-December 1981-January 1982 season).

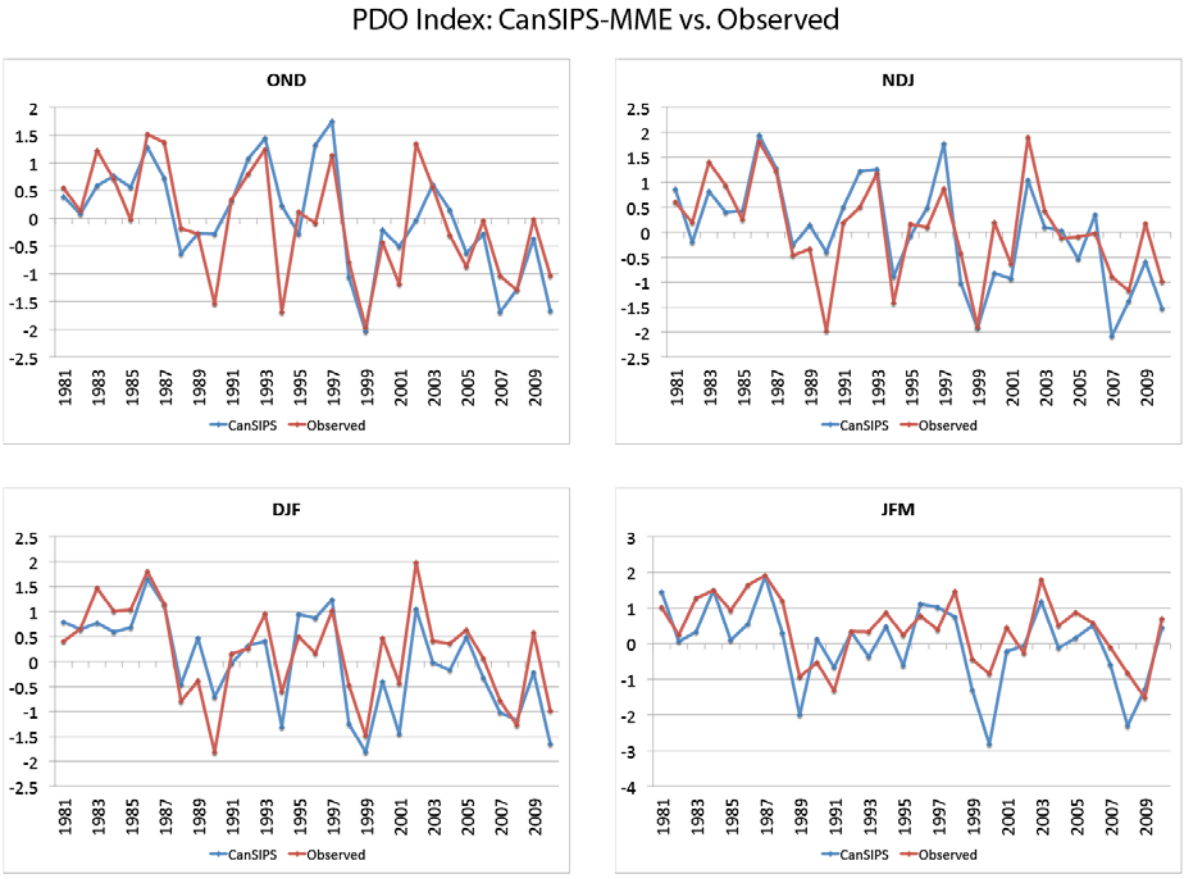

Figure 5.5: The observed Pacific Decadal Oscillation (PDO) Index (red) vs. as reproduced in CanSIPS-MME (blue). The established PDO Index is the leading principle component of monthly mean sea surface temperature anomalies in the North Pacific Ocean poleward of 20°N, maintained by Nathan Mantua at the University of Washington, Joint Institute for the Study of the Atmosphere and Ocean (JISAO), and was obtained through the NCAR UCAR Climate Data Guide (https://climatedataguide.ucar.edu/climate-data/pacific-decadal-oscillation-pdo-definition-and-indices; http://research.jisao.washington.edu/pdo/PDO.latest). For seasons spanning across two calendar years (i.e., NDJ and DJF), the year listed corresponds to the beginning month(s) of the season (e.g., '1981 NDJ season' = November 1981-December 1981-January 1982 season).

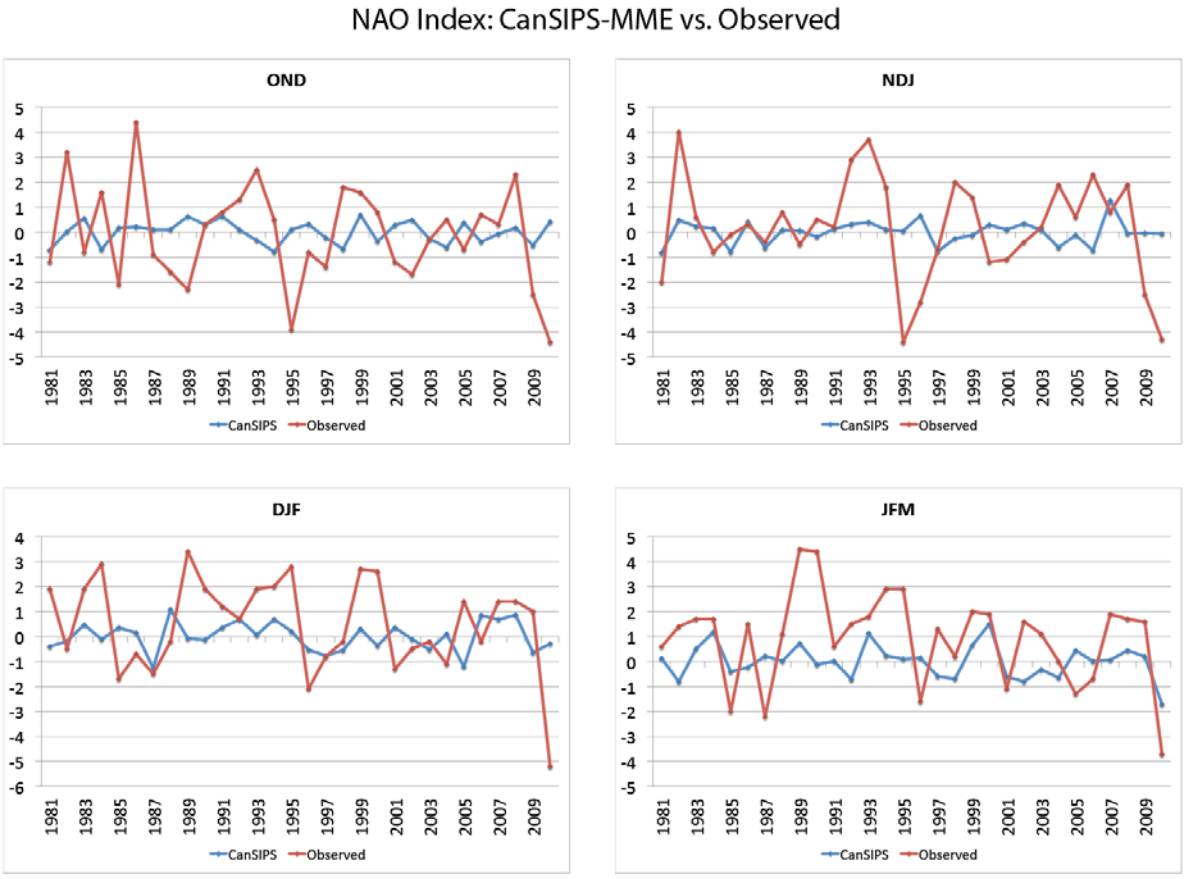

Figure 5.6: The observed North Atlantic Oscillation (NAO) Index (red) vs. as reproduced in CanSIPS-MME (blue). The established NAO Index (the seasonal Hurrell station-based NAO Index is used in this research) is the normalized Lisbon, Portugal – normalized Stykkishólmur/Reykjavík, Iceland sea level pressure anomalies and was obtained from the NCAR UCAR Climate Data Guide (https://climatedataguide.ucar.edu/climate-data/hurrell-north-atlantic-oscillation-nao-index-station-based). For seasons spanning across two calendar years (i.e., NDJ and DJF), the year listed corresponds to the beginning month(s) of the season (e.g., '1981 NDJ season' = November 1981-December 1981-January 1982 season).

5.3 Climate Signal-Storm Activity Relationships in CanSIPS-MME

Key overall findings from the CanSIPS-MME reproduction of observed climate signal-storm activity relationships investigation are similar to those of the seasonal climatology comparisons (Section 5.1) and are presented below:

- MSLP:
    - SO (ENSO): CanSIPS overestimates seasonal mean MSLP in the mid-latitudes, markedly in the eastern Pacific during El Niño and neutral conditions, while underestimating in the high-latitudes, particularly the Bering Sea/eastern Russia region (and the northeast Atlantic/Europe region in later seasons [e.g., DJF and JFM]). In early seasons (e.g., OND), strong underestimation in the Bering Sea/Chukchi Sea/Beaufort Sea region is also seen during La Niña conditions. Over North America, CanSIPS overestimates climatological MSLP in the southern half of the continent, especially over the US Rocky Mountains, and underestimates in the northern half.
    - PDO: Comparable to the SO results. CanSIPS overestimation of climatological MSLP in the eastern North Pacific is particularly strong during the positive PDO phase. The underestimation of average MSLP in the Bering Sea/Chukchi Sea/Beaufort Sea region is noticeably strong in the earlier seasons (e.g., OND).
    - NAO: Similar to the SO and PDO results. CanSIPS overestimation of the NAO's centres of action, as well as the similarly overestimated semi-permanent pressure cells in the North Pacific (including too low MSLP values in Bering Sea/Chukchi Sea/Beaufort Sea region in the earlier seasons [e.g., OND]), is markedly higher during the negative NAO phase.

- ΔMSLP
    - SO (ENSO): CanSIPS overestimation of seasonal mean ΔMSLP in the western Pacific and underestimation in the eastern Pacific are relatively minor. The edge of larger overestimation extending poleward from the tropics is also observed in the subtropics, particularly in the western Pacific. Greater overestimation of climatological ΔMSLP is found over land, with marked overestimation over higher terrain such as in western North America.
    - PDO: Comparable to the SO results. CanSIPS overestimation of average ΔMSLP is increased in the Aleutian Low region during the positive PDO phase and over areas of higher terrain (e.g., western North America).
    - NAO: Similar to the SO and PDO results. While relatively minor disparities are found in a large portion of the North Atlantic, CanSIPS overestimation of the seasonal mean ΔMSLP is consistently observed in association with the North Atlantic storm track, particularly during the positive NAO phase. During the negative NAO phase, noticeable overestimation of average ΔMSLP is confined to the northeast Atlantic/western Europe region.
- 10-m wind speeds:
    - SO (ENSO): CanSIPS underestimates seasonal mean wind speed over the mid-latitude North Pacific, with increased underestimation in the western-central Pacific, particularly in the later seasons (e.g., DJF). Climatological wind speeds in the higher latitudes of the North Atlantic and in the Arctic basin are similarly underestimated, along with in the mid-latitudes of the eastern-central North Atlantic under El Niño conditions during the later seasons (e.g., DJF, JFM). While results over land are noisy,

CanSIPS, in general, overestimates climatological wind speeds, including over western North America.

- PDO: Comparable to the SO results. CanSIPS underestimation of average wind speeds in the North Pacific mid-latitudes is slightly greater during the positive PDO phase. Larger underestimation is also found in the mid-latitude eastern-central North Atlantic during the positive PDO phase in the later seasons (DJF, JFM).
- NAO: Comparable to the SO and PDO results. The largest underestimation of climatological wind speeds in the North Atlantic basin is generally confined to the high-latitudes and the Greenland/Norwegian Seas region – underestimation in these regions is greater during the positive NAO phase. CanSIPS underestimation of average wind speeds in the mid-latitude eastern-central North Atlantic, however, is greater in the negative NAO phase, particularly in the later seasons (DJF, JFM).

Season	SO Phase	# of Years in Subsample	Years included in Subsample
OND	El Niño	4	1982, 1991, 1994, 1997
	Neutral	19	1981, 1983, 1984, 1985, 1986, 1987, 1989, 1990, 1992, 1993, 1995, 1996, 2001, 2002, 2003, 2004, 2005, 2006, 2009
	La Niña	7	1988, 1998, 1999, 2000, 2007, 2008, 2010
NDJ	El Niño	4	1982, 1986, 1991, 1997
	Neutral	19	1981, 1983, 1984, 1985, 1987, 1989, 1990, 1992, 1993, 1994, 1995, 1996, 2001, 2002, 2003, 2004, 2005, 2006, 2009
	La Niña	7	1988, 1998, 1999, 2000, 2007, 2008, 2010
DJF	El Niño	6	1982, 1986, 1991, 1997, 2004, 2009
	Neutral	16	1981, 1983, 1984, 1985, 1987, 1989, 1990, 1992, 1993, 1994, 1995, 2001, 2002, 2003, 2005, 2006
	La Niña	8	1988, 1996, 1998, 1999, 2000, 2007, 2008, 2010
JFM	El Niño	5	1983, 1987, 1992, 1998, 2010
	Neutral	18	1981, 1882, 1984, 1985, 1986, 1988, 1990, 1991, 1993, 1994, 1995, 1996, 1997, 2002, 2003, 2004, 2005, 2007
	La Niña	7	1989, 1999, 2000, 2001, 2006, 2008, 2009

Table 5.1: Subsamples utilized in the Southern Oscillation composite analyses. For seasons spanning across two calendar years (i.e., NDJ and DJF), the year listed corresponds to the beginning month(s) of the season (e.g., '1981 NDJ season' = November 1981-December 1981-January 1982 season).

Season	PDO Phase	# of Years in Subsample	Years included in Subsample
OND	Positive	13	1981, 1982, 1983, 1984, 1986, 1987, 1991, 1992, 1993, 1995, 1997, 2002, 2003
	Negative	17	1985, 1988, 1989, 1990, 1994, 1996, 1998, 1999, 2000, 2001, 2004, 2005, 2006, 2007, 2008, 2009, 2010
NDJ	Positive	17	1981, 1982, 1983, 1984, 1985, 1986, 1987, 1991, 1992, 1993, 1995, 1996, 1997, 2000, 2002, 2003, 2009
	Negative	13	1988, 1989, 1990, 1994, 1998, 1999, 2001, 2004, 2005, 2006, 2007, 2008, 2010
DJF	Positive	20	1981, 1982, 1983, 1984, 1985, 1986, 1987, 1991, 1992, 1993, 1995, 1996, 1997, 2000, 2002, 2003, 2004, 2005, 2006, 2009
	Negative	10	1988, 1989, 1990, 1994, 1998, 1999, 2001, 2007, 2008, 2010
JFM	Positive	21	1981, 1982, 1983, 1984, 1985, 1986, 1987, 1988, 1992, 1993, 1994, 1995, 1996, 1997, 1998, 2001, 2003, 2004, 2005, 2006, 2010
	Negative	9	1989, 1990, 1991, 1999, 2000, 2002, 2007, 2008, 2009

Table 5.2: As in Table 5.1, except for the Pacific Decadal Oscillation composite analyses.

Season	NAO Phase	# of Years in Subsample	Years included in Subsample
OND	Positive	15	1982, 1984, 1986, 1990, 1991, 1992, 1993, 1994, 1998, 1999, 2000, 2004, 2006, 2007, 2008
	Negative	15	1981, 1983, 1985, 1987, 1988, 1989, 1995, 1996, 1997, 2001, 2002, 2003, 2005, 2009, 2010
NDJ	Positive	17	1982, 1983, 1986, 1988, 1990, 1991, 1992, 1993, 1994, 1998, 1999, 2003, 2004, 2005, 2006, 2007, 2008
	Negative	13	1981, 1984, 1985, 1987, 1989, 1995, 1996, 1997, 2000, 2001, 2002, 2009, 2010
DJF	Positive	15	1982, 1983, 1988, 1989, 1990, 1991, 1992, 1993, 1994, 1998, 1999, 2004, 2006, 2007, 2008
	Negative	15	1981, 1984, 1985, 1986, 1987, 1995, 1996, 1997, 2000, 2001, 2002, 2003, 2005, 2009, 2010
JFM	Positive	22	1981, 1982, 1983, 1984, 1986, 1988, 1989, 1990, 1991, 1992, 1993, 1994, 1995, 1997, 1998, 1999, 2000, 2002, 2003, 2007, 2008, 2009
	Negative	7	1985, 1987, 1996, 2001, 2005, 2006, 2010

Table 5.3: As in Table 5.1, except for the North Atlantic Oscillation. Note: NAOI = 0 for the 2004 JFM season and is, therefore, excluded from the JFM composite analyses.

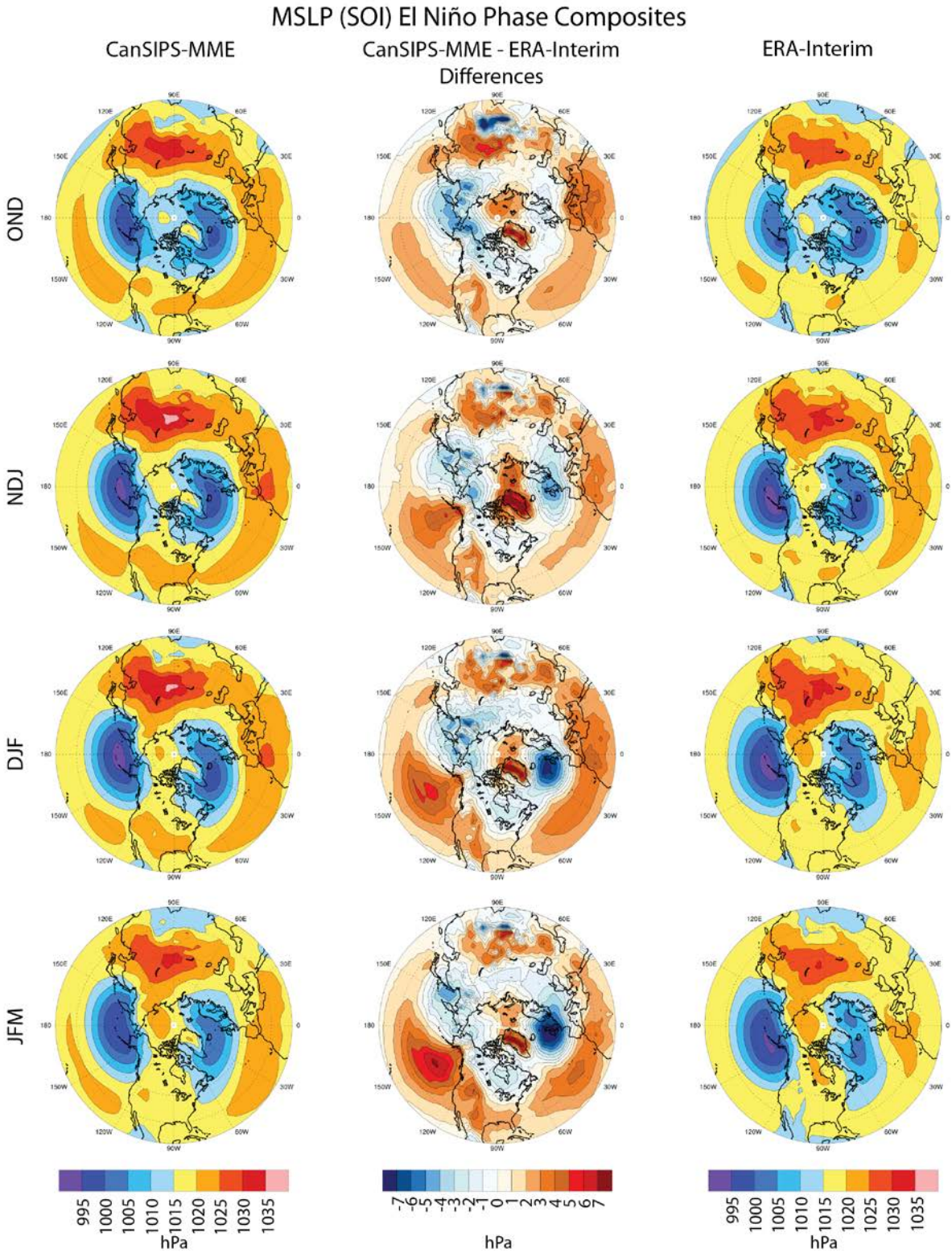

Figure 5.7: MSLP El Niño phase (based on SOI) composites for CanSIPS-MME (left) and ERA-Interim (right) and the difference between the two (CanSIPS-MME – ERA-Interim) (middle).

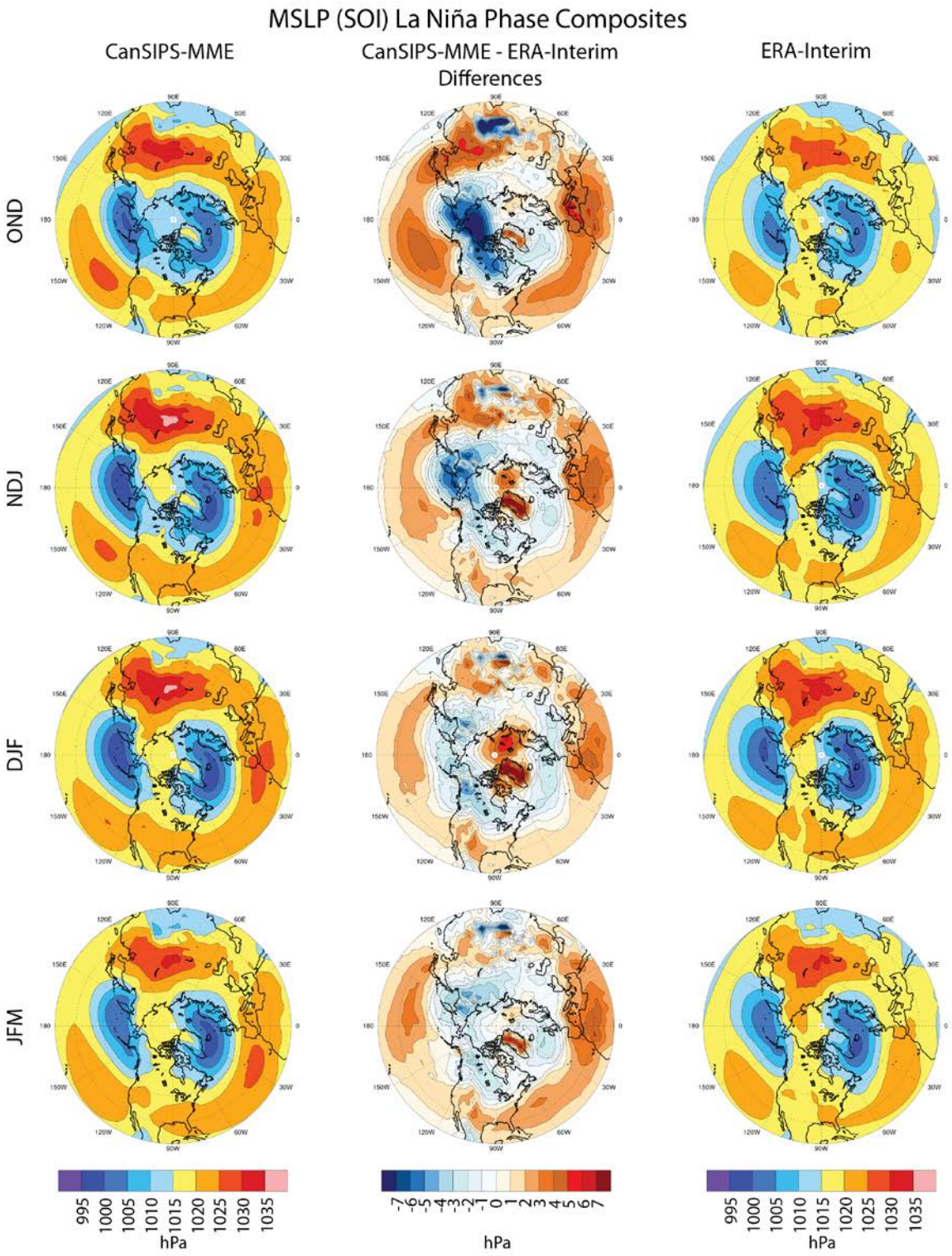

Figure 5.8: MSLP La Niña phase (based on SOI) composites for CanSIPS-MME (left) and ERA-Interim (right) and the difference between the two (CanSIPS-MME – ERA-Interim) (middle).

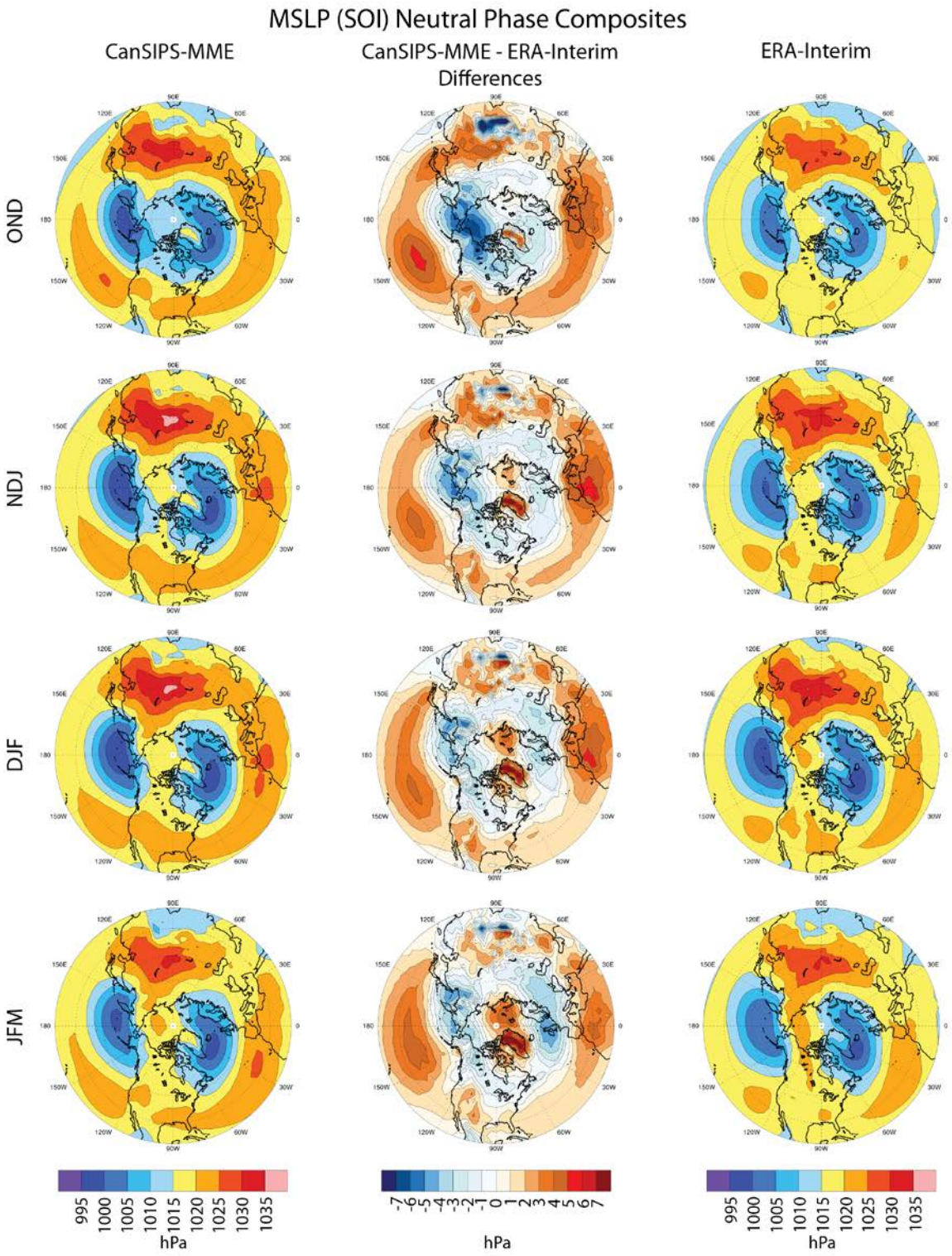

Figure 5.9: MSLP SOI-based neutral conditions phase composites for CanSIPS-MME (left) and ERA-Interim (right) and the difference between the two (CanSIPS-MME – ERA-Interim) (middle).

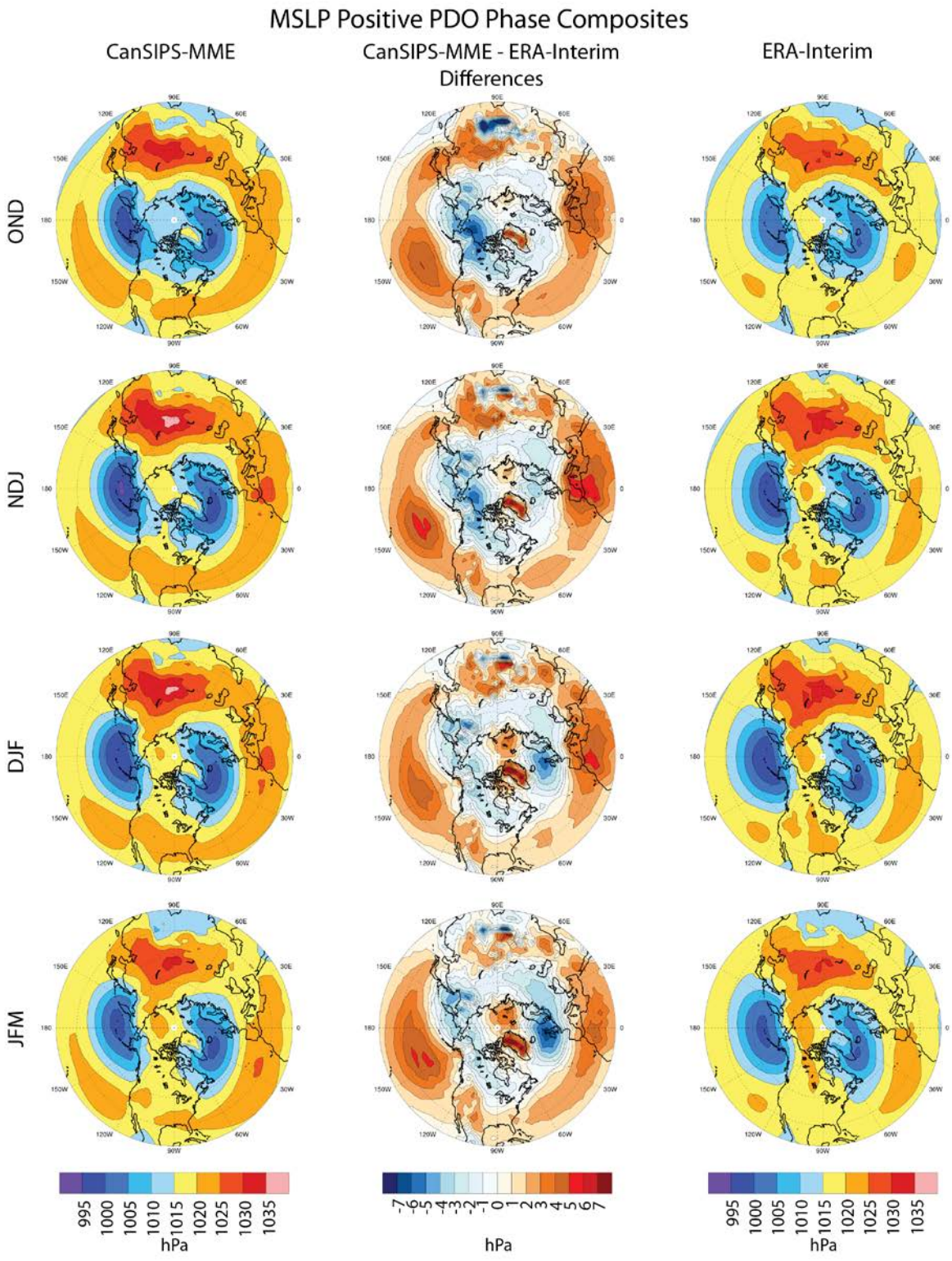

Figure 5.10: MSLP positive PDO phase composites for CanSIPS-MME (left) and ERA-Interim (right) and the difference between the two (CanSIPS-MME – ERA-Interim) (middle).

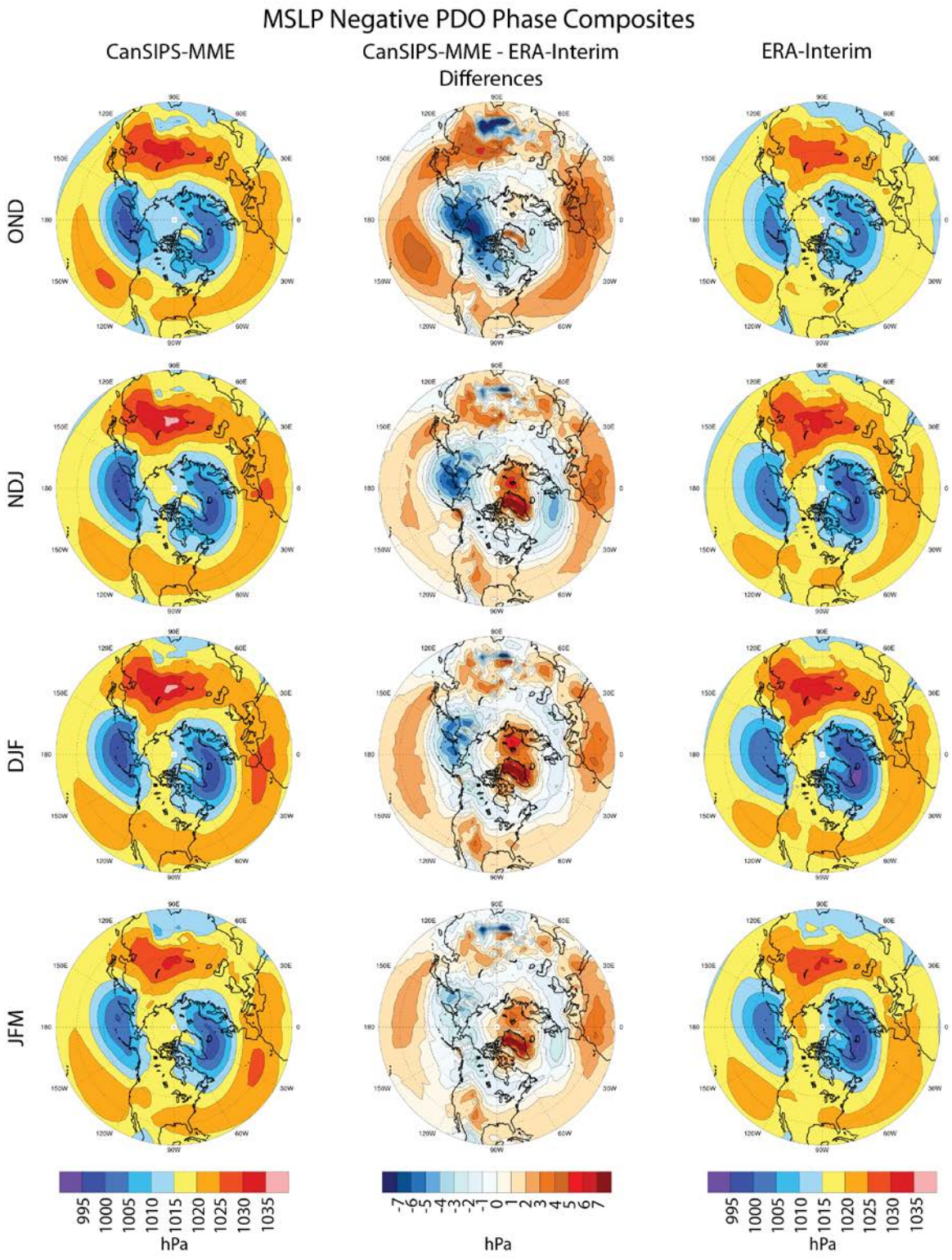

Figure 5.11: MSLP negative PDO phase composites for CanSIPS-MME (left) and ERA-Interim (right) and the difference between the two (CanSIPS-MME – ERA-Interim) (middle).

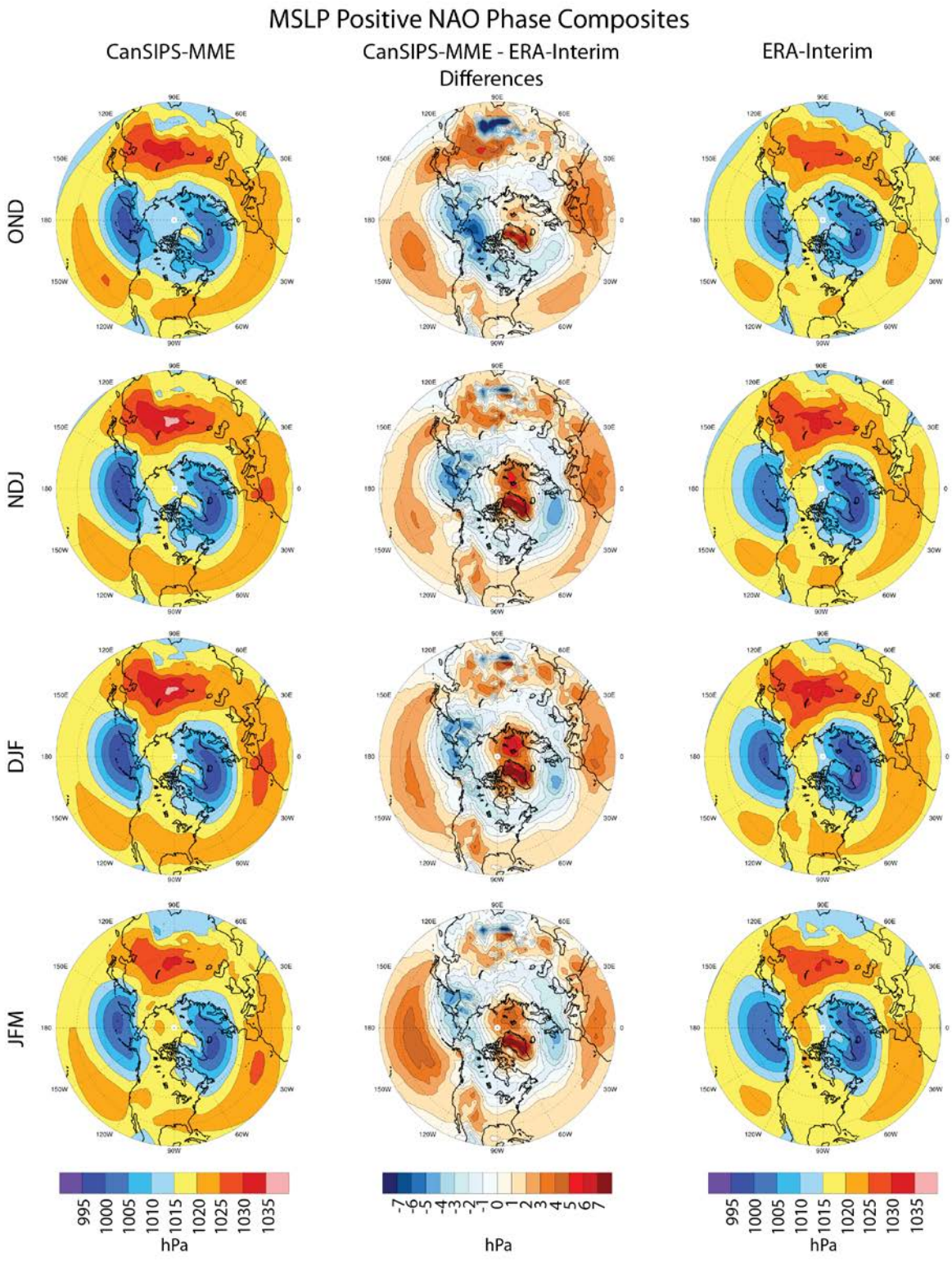

Figure 5.12: MSLP positive NAO phase composites for CanSIPS-MME (left) and ERA-Interim (right) and the difference between the two (CanSIPS-MME – ERA-Interim) (middle).

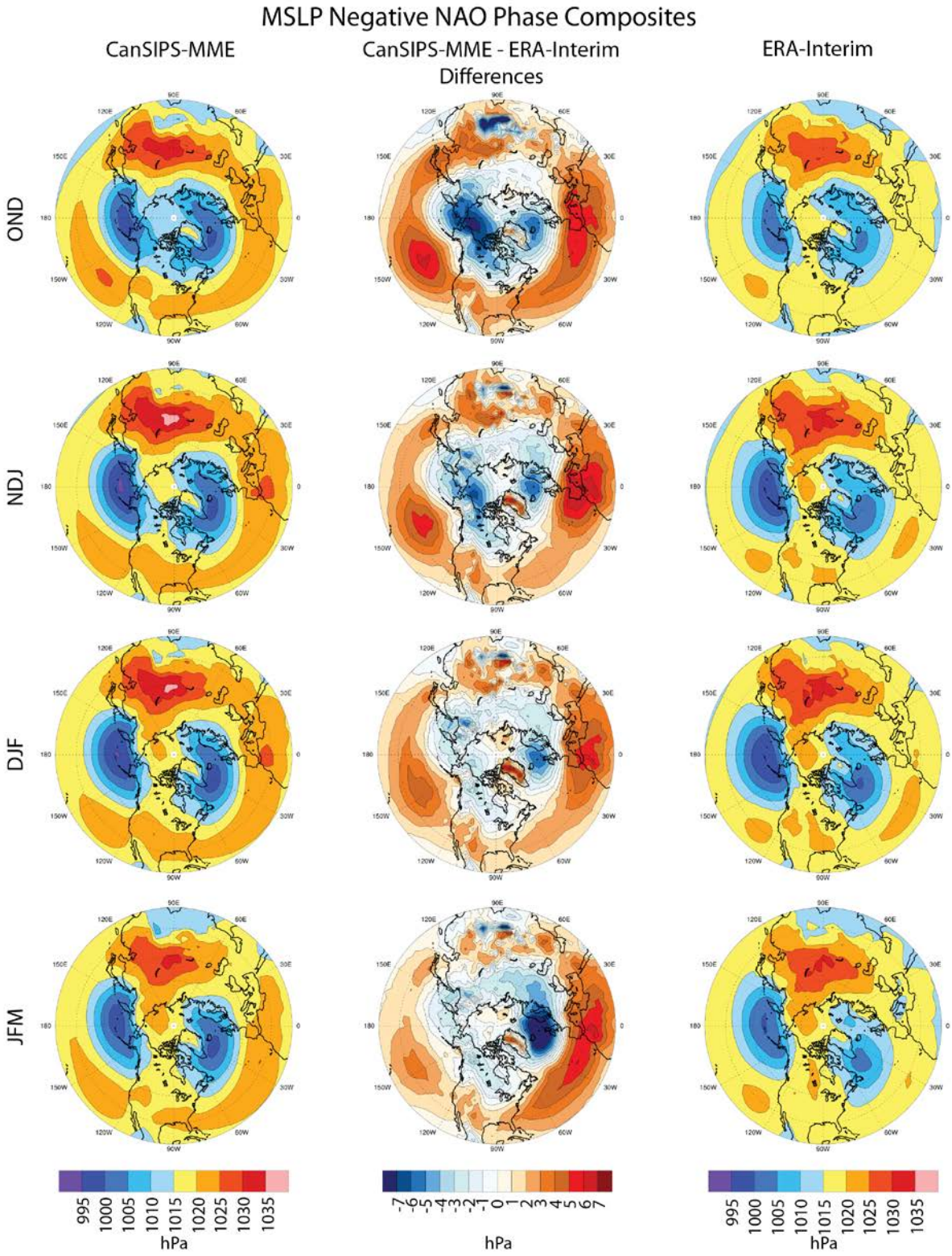

Figure 5.13: MSLP negative NAO phase composites for CanSIPS-MME (left) and ERA-Interim (right) and the difference between the two (CanSIPS-MME – ERA-Interim) (middle).

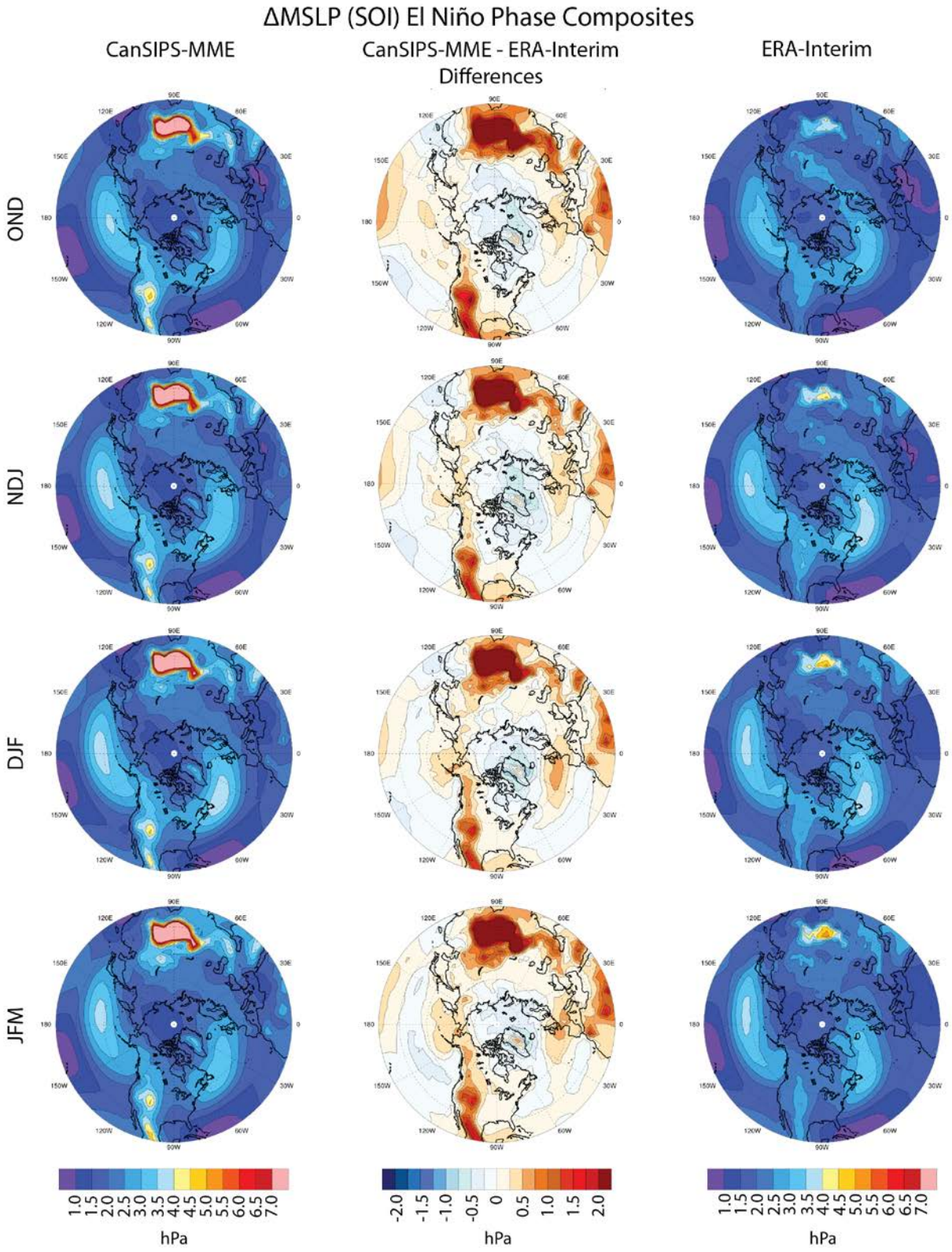

Figure 5.14: As in Figure 5.7, except for 6-hrly ΔMSLP.

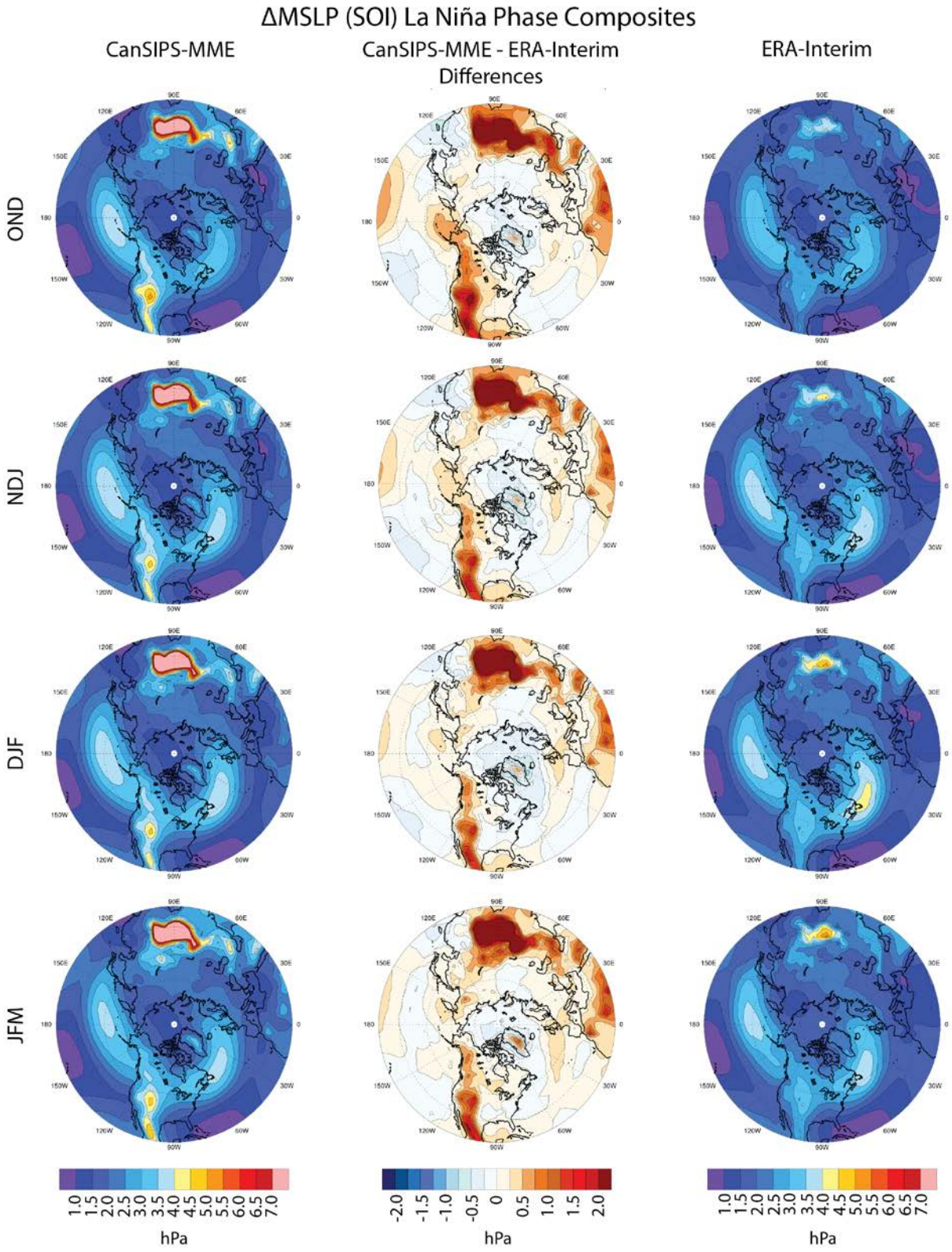

Figure 5.15: As in Figure 5.8, except for 6-hrly ΔMSLP.

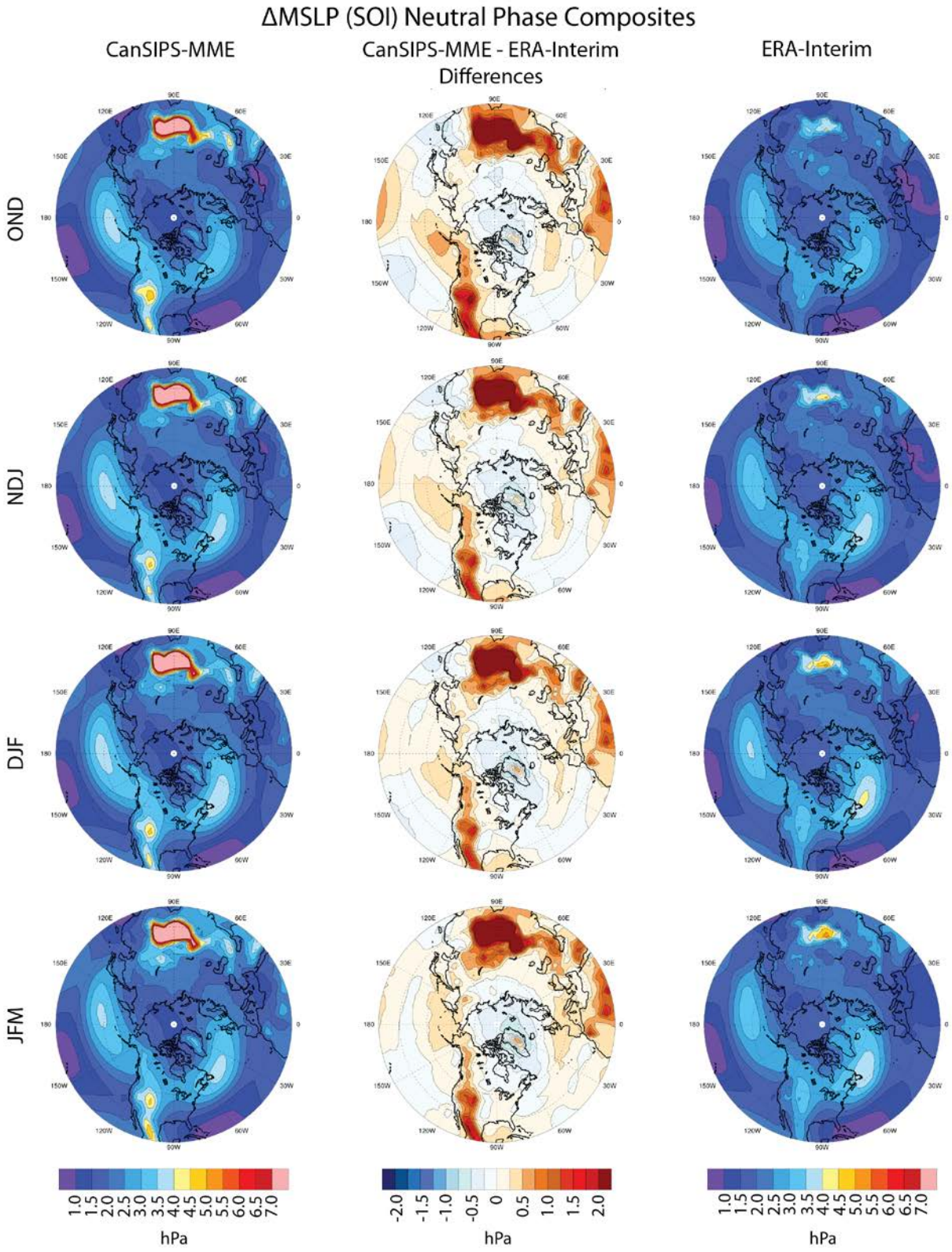

Figure 5.16: As in Figure 5.9, except for 6-hrly ΔMSLP.

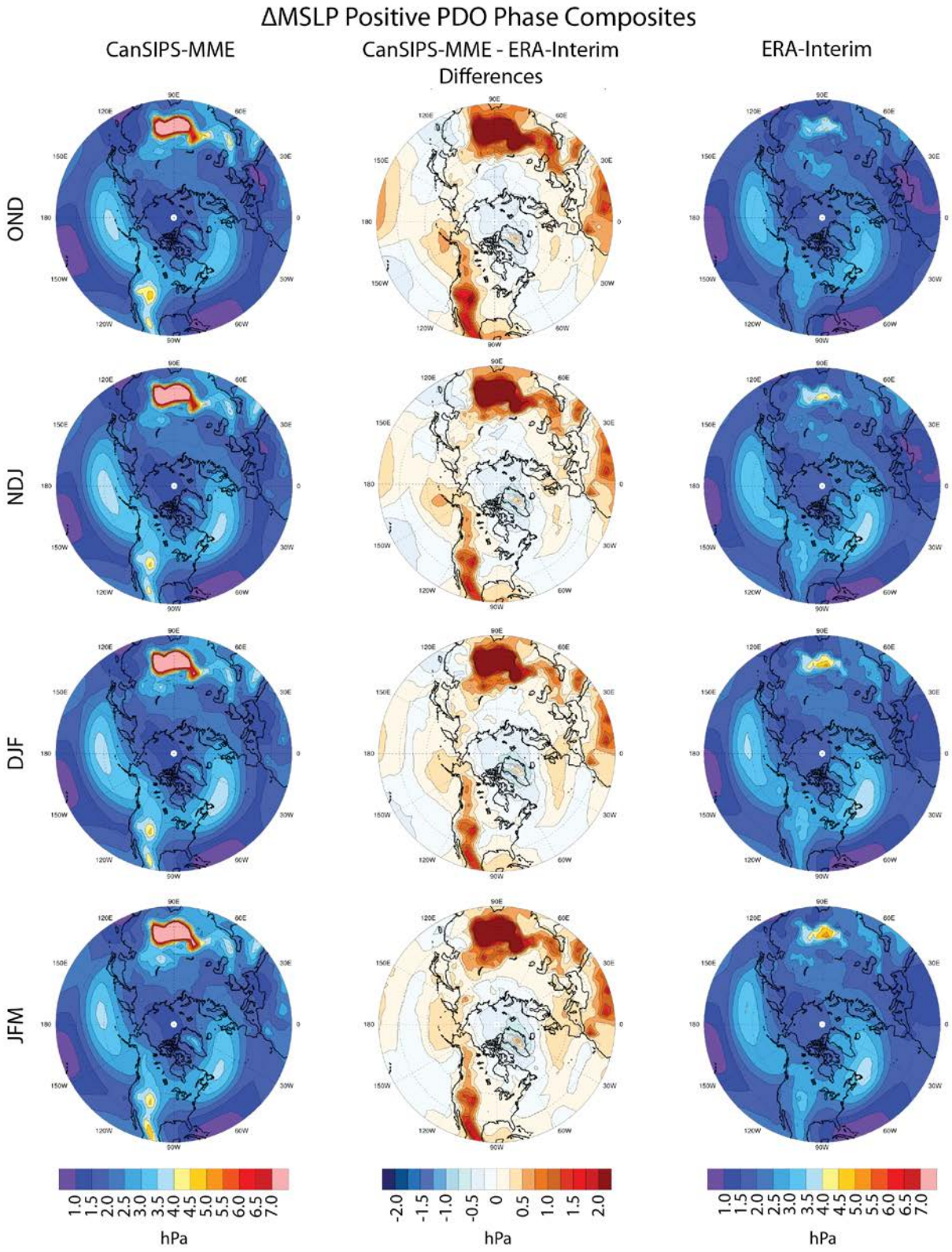

Figure 5.17: As in Figure 5.10, except for 6-hrly ΔMSLP.

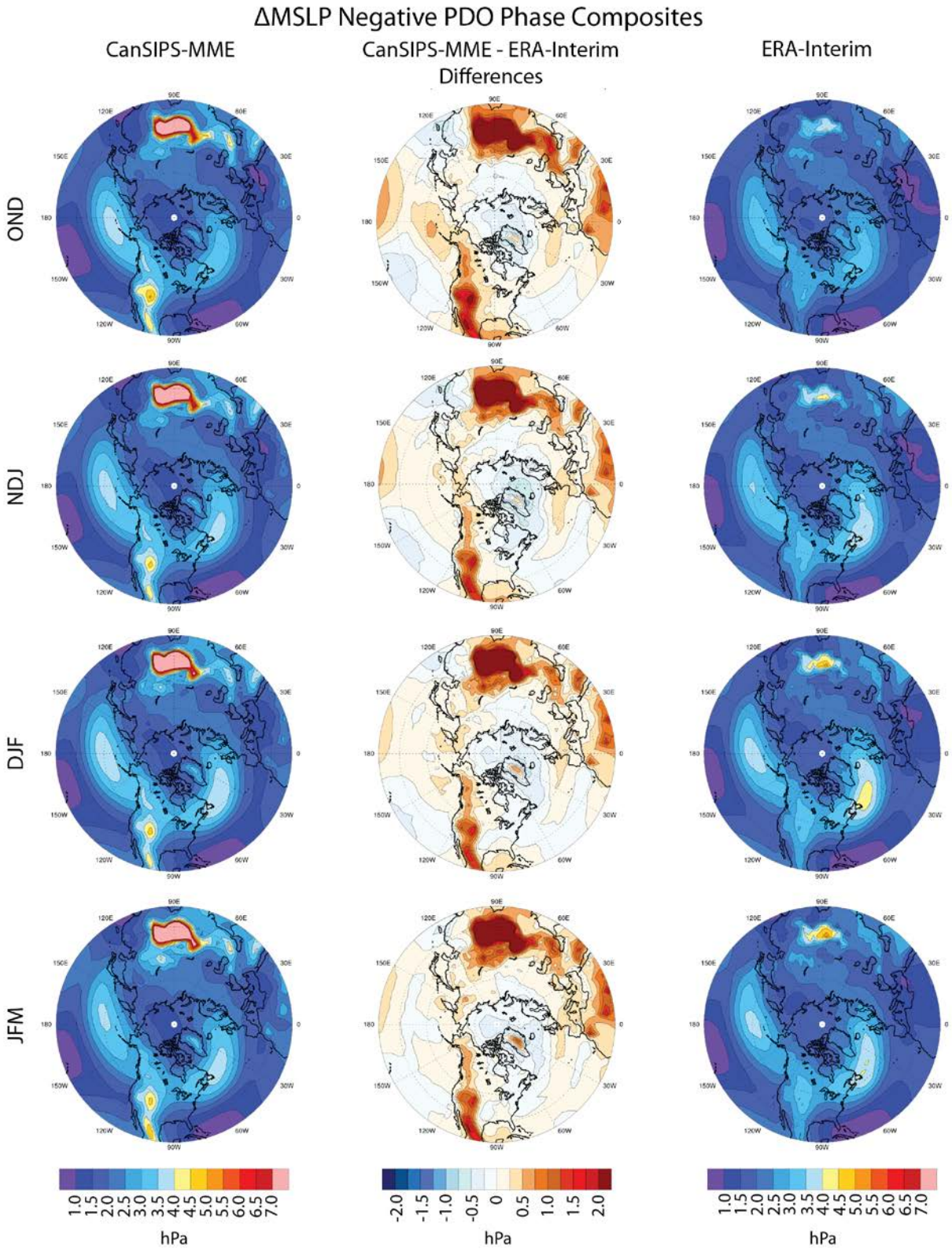

Figure 5.18: As in Figure 5.11, except for 6-hrly ΔMSLP.

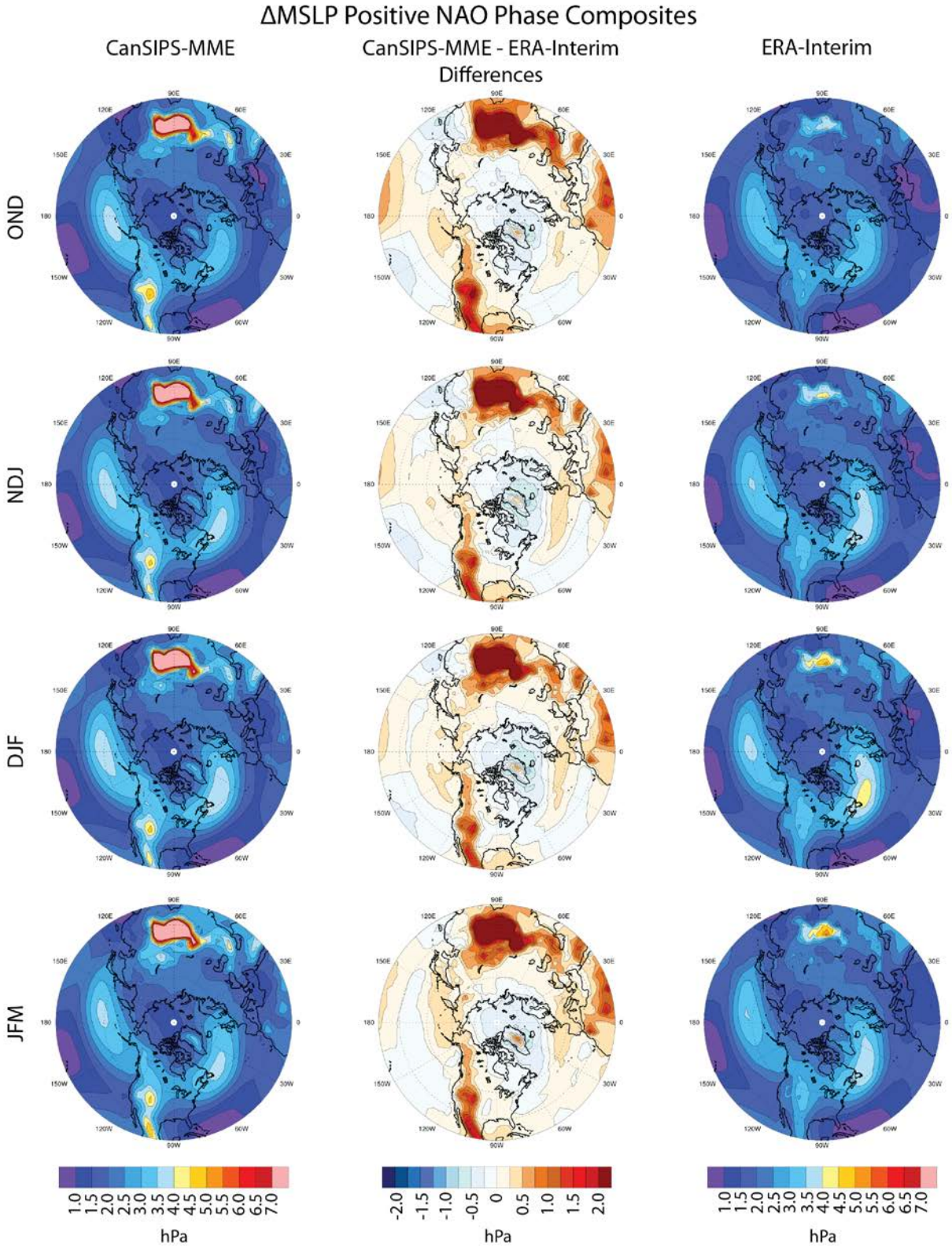

Figure 5.19: As in Figure 5.12, except for 6-hrly ΔMSLP.

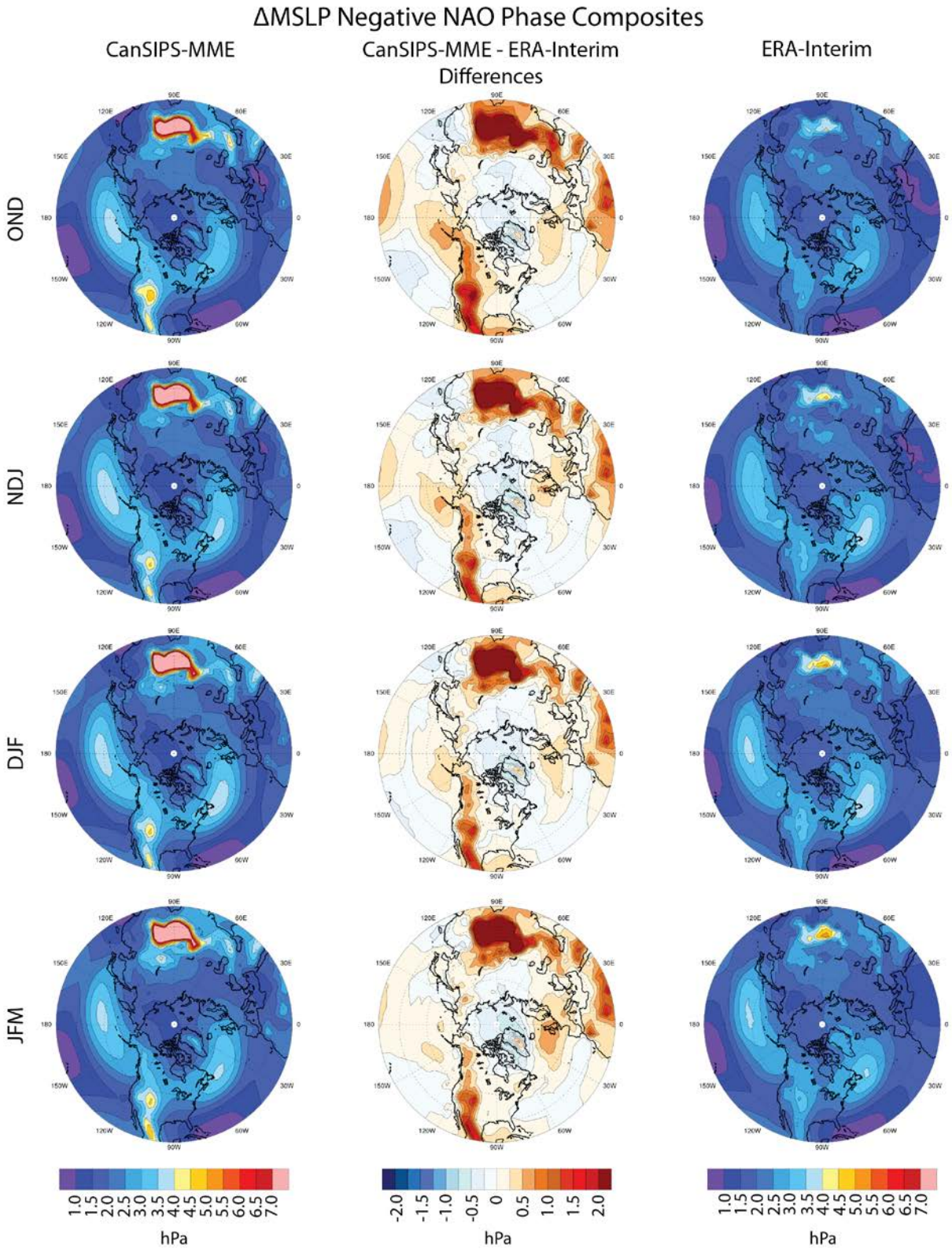

Figure 5.20: As in Figure 5.13, except for 6-hrly ΔMSLP.

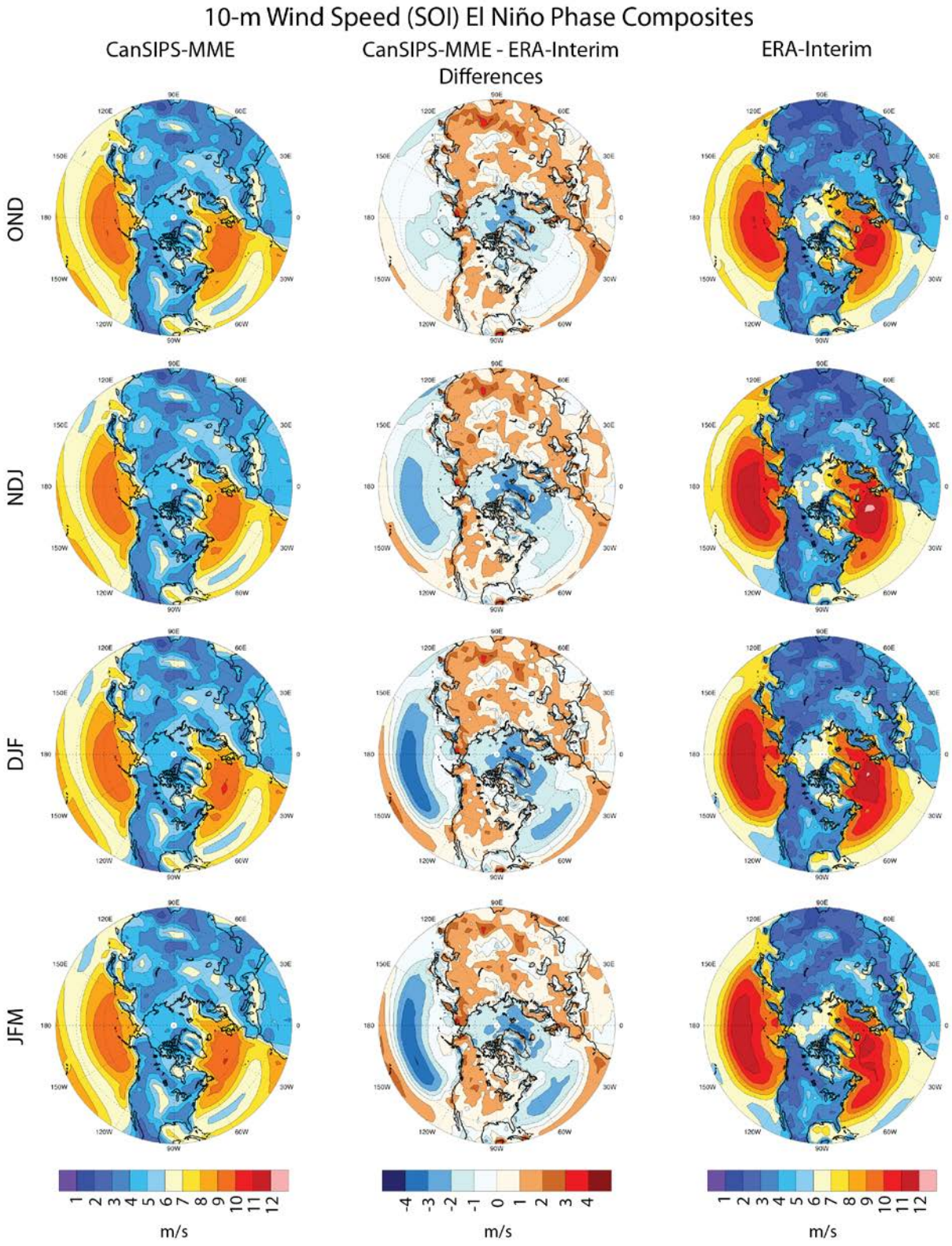

Figure 5.21: As in Figure 5.7, except for 10-m wind speeds.

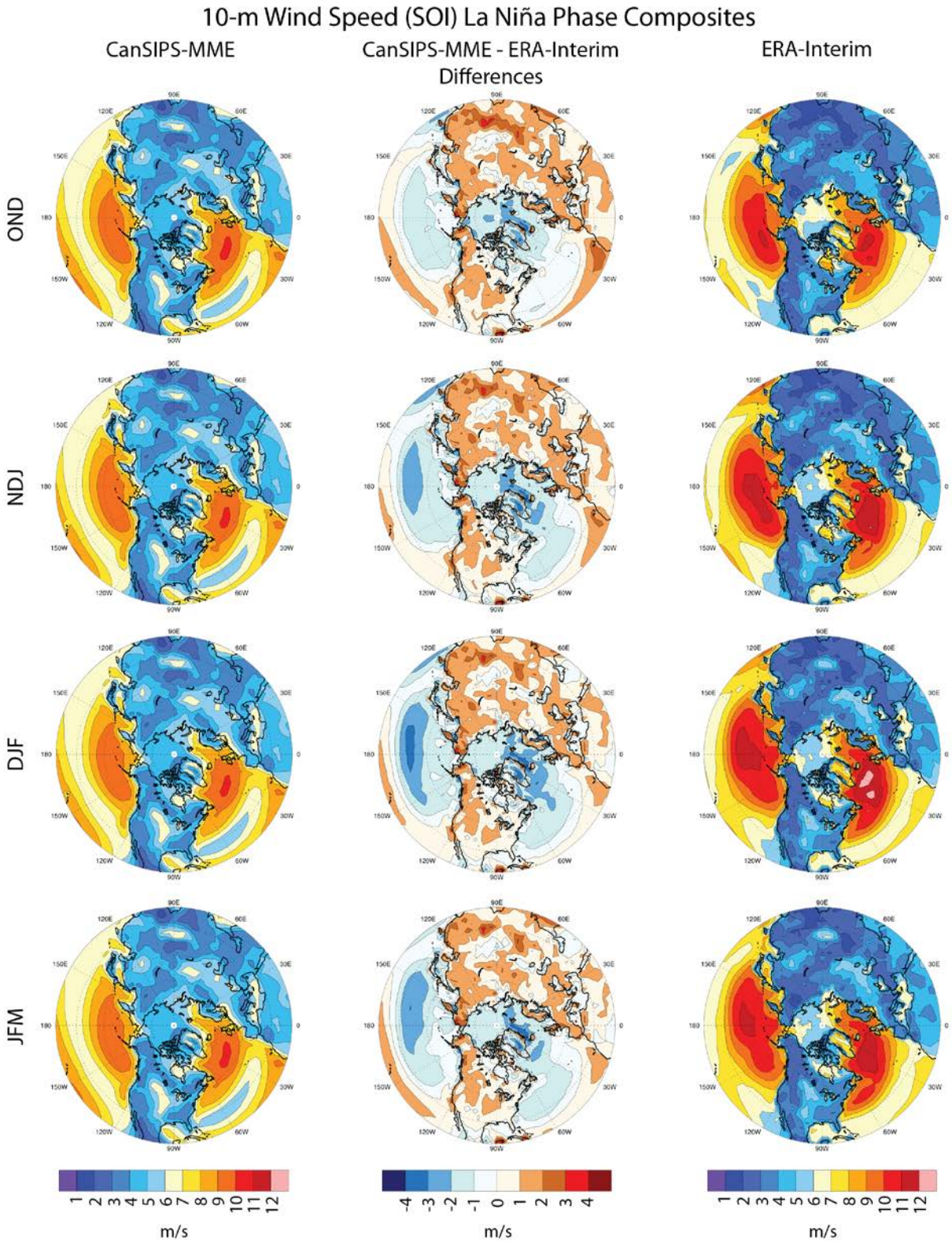

Figure 5.22: As in Figure 5.8, except for 10-m wind speeds.

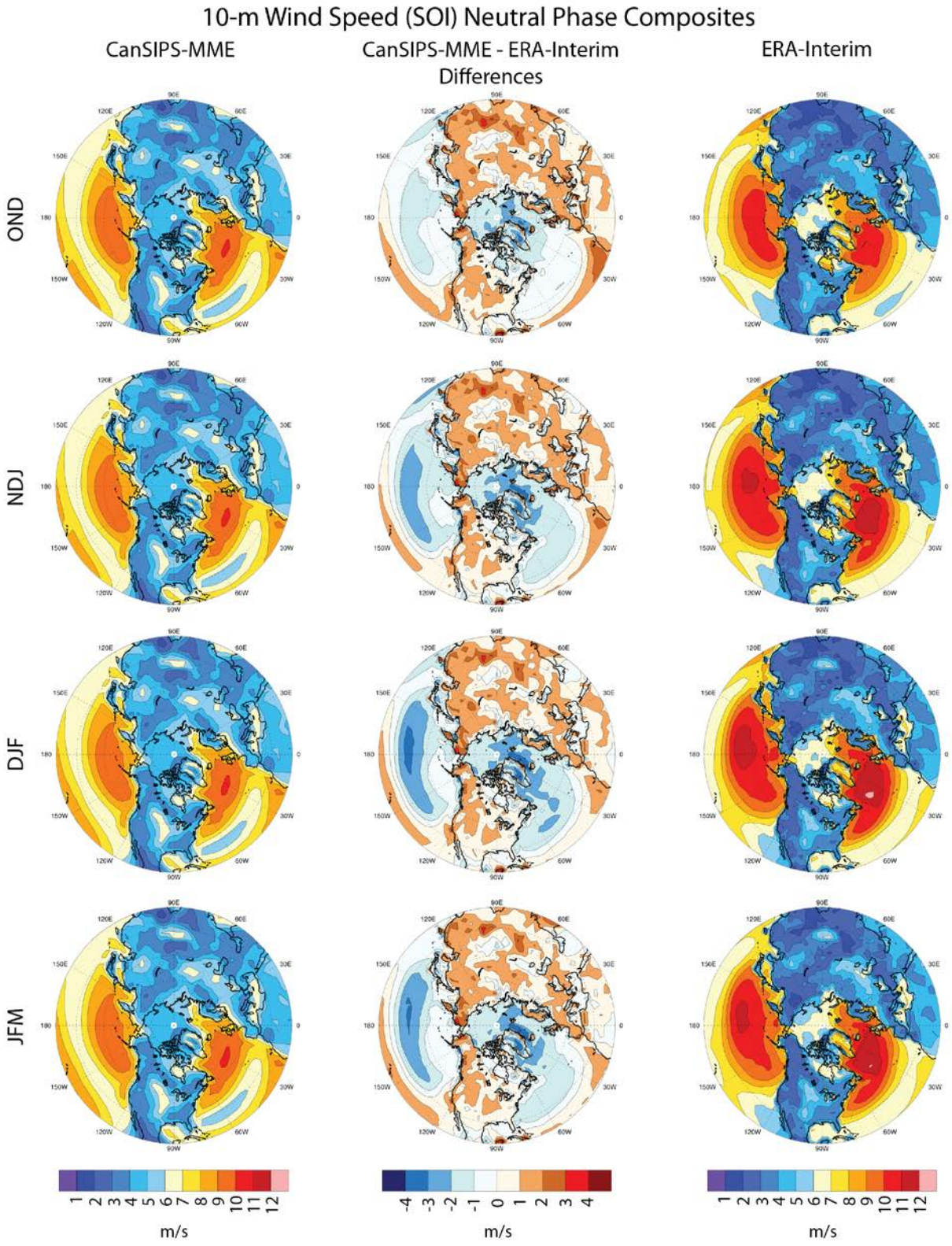

Figure 5.23: As in Figure 5.9, except for 10-m wind speeds.

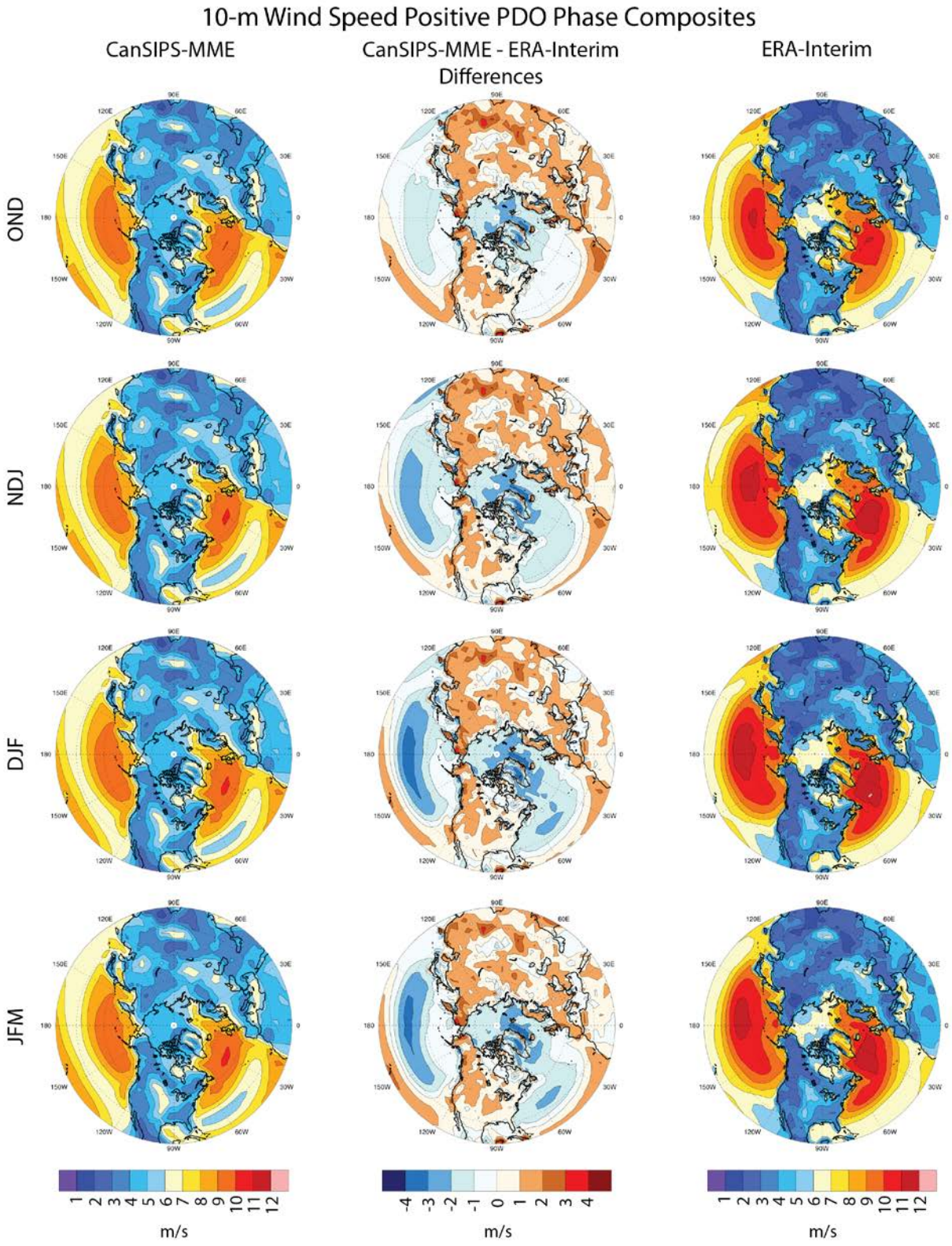

Figure 5.24: As in Figure 5.10, except for 10-m wind speeds.

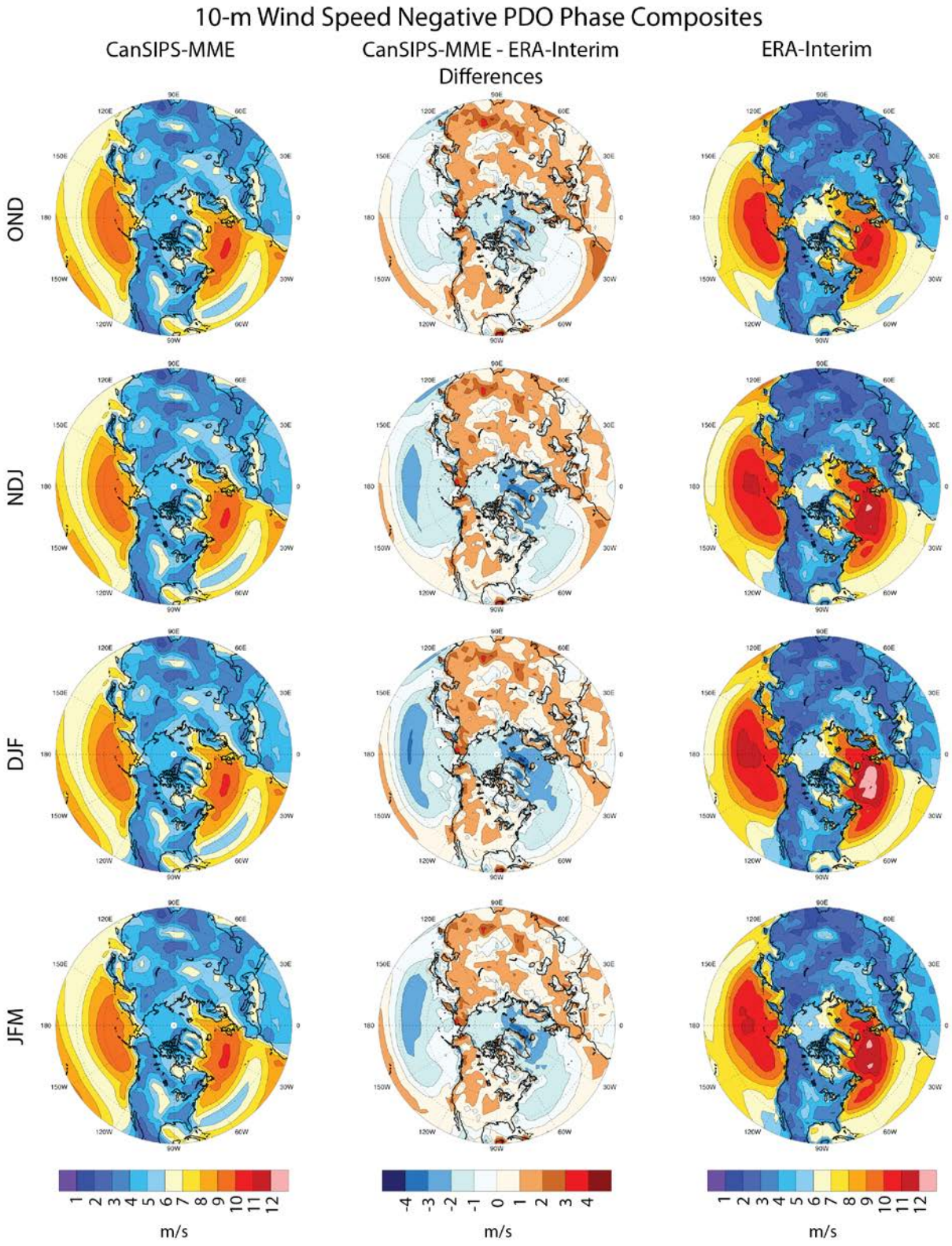

Figure 5.25: As in Figure 5.11, except for 10-m wind speeds.

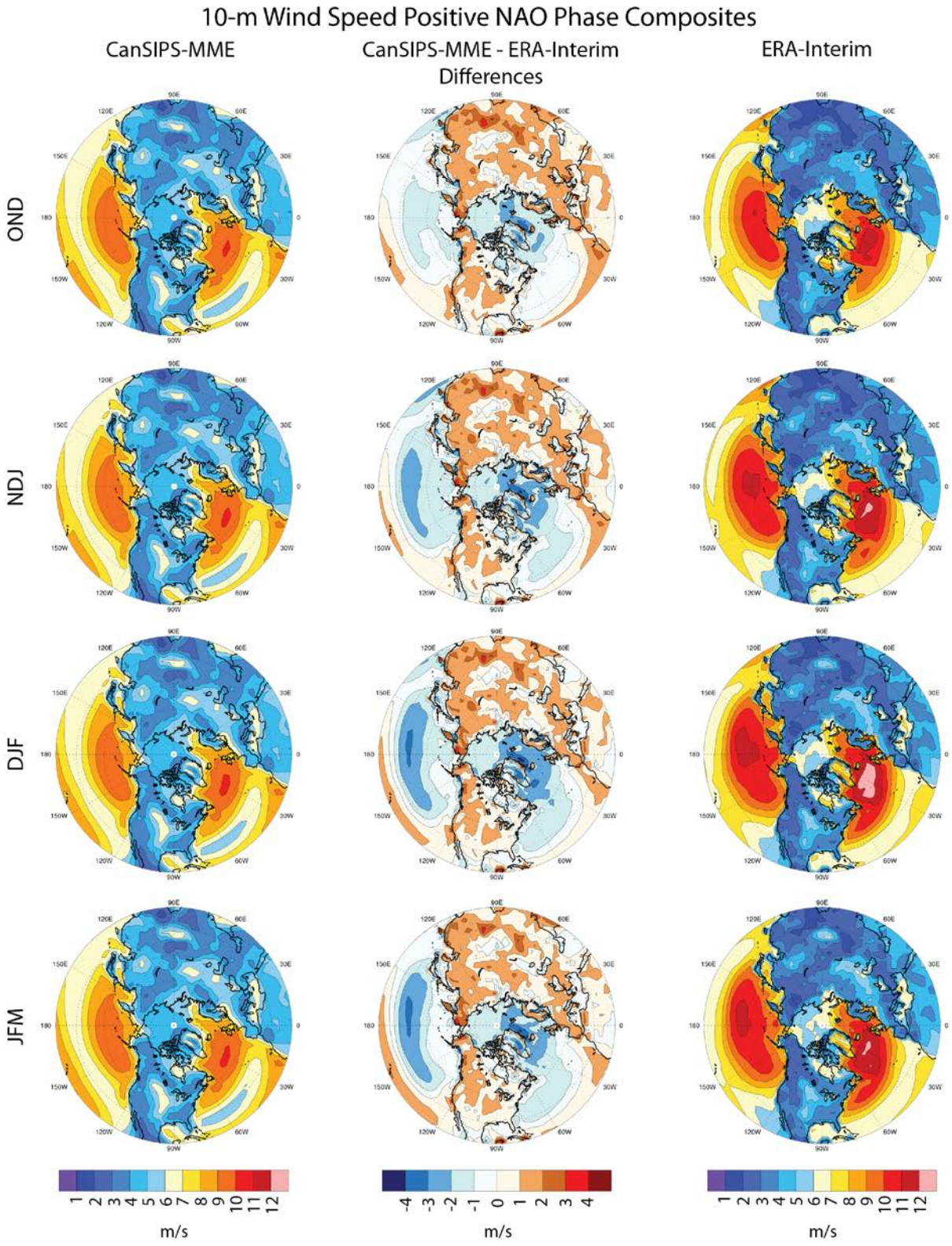

Figure 5.26: As in Figure 5.12, except for 10-m wind speeds.

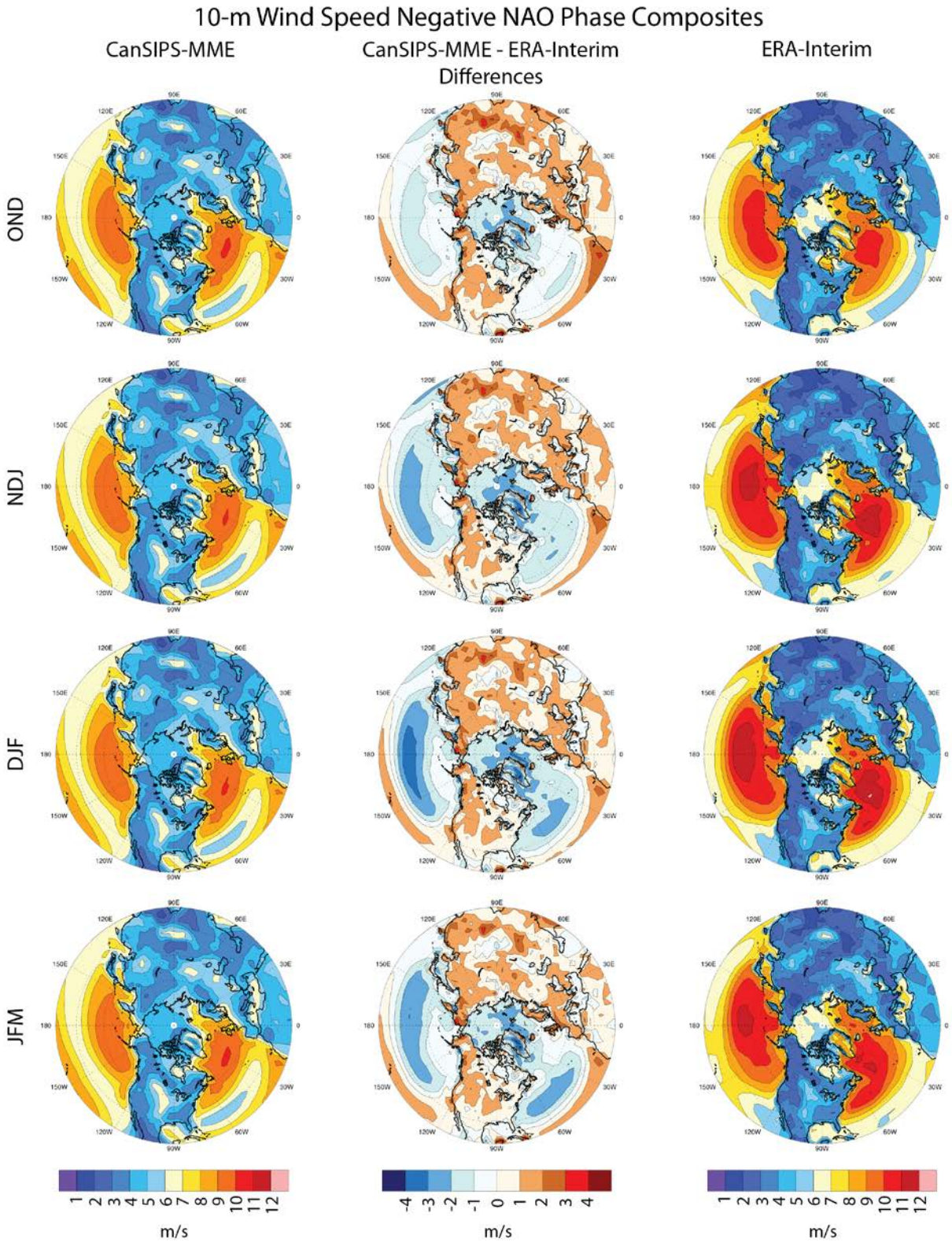

Figure 5.27: As in Figure 5.13, except for 10-m wind speeds.

6.0 Seasonal Prediction Skill of North American Coastal Storm Activity during the Cold Months of the Canadian Seasonal to Interannual Prediction System (CanSIPS)

6.1 Manuscript Information

This manuscript presents research completed in Research Theme 3 (Research Questions 3.2 and 3.3) and is being prepared for submission to the journal Climate Dynamics:

Pingree-Shippee KA, Zwiers FA, Atkinson DA (in prep) Seasonal Prediction Skill of North American Coastal Storm Activity during the Cold Months of the Canadian Seasonal to Interannual Prediction System (CanSIPS).

Results from Research Question 3.1 (reproduction of observed North American coastal climate signal-storm activity relationships in CanSIPS) were presented previously in the Chapter 5.

Additional Research Theme 3 figures not included in this manuscript are provided in Appendix C of this dissertation (including individual evaluation of CanCM3 and CanCM4).

6.2 Abstract

The North American coastal regions are strongly influenced by extratropical cyclones (ETCs), which often produce hazardous conditions such as high winds and heavy precipitation. As a result, land-based, coastal, and maritime economic sectors in Canada

and the USA can all experience strong adverse impacts from extratropical storm activity. Society would benefit if variations in ETC storm activity could be predicted skilfully for the upcoming season. Skilful prediction would enable affected sectors to better anticipate, prepare for, manage, and respond to ETC storm activity and the associated risks. In this study, the seasonal prediction skill of North American coastal storm activity during the cold months is investigated using Environment and Climate Change Canada's Canadian Seasonal to Interannual Prediction System (CanSIPS). Categorical deterministic and probabilistic seasonal forecasts are constructed from the CanSIPS multi-model ensemble mean hindcasts (1981-2010) using the three equiprobable category framework (below-, near-, and above-normal conditions) and the parametric Gaussian method for determining probabilities. The CanSIPS forecasts are evaluated against the ERA-Interim reanalysis using the correlation skill score, percent correct score, and Brier skill score to determine forecast skill and whether that skill is sufficiently high to be useful to end-users. Seasonal prediction skill is investigated for the rolling 3-month cold seasons (OND, NDJ, DJF, JFM), using mean sea level pressure, absolute pressure tendency, and 10-m wind speed as proxies for extratropical storm activity.

6.3 Introduction

Extratropical cyclones (ETCs) are major drivers of the weather in the mid- and high-latitudes, often dictating regional patterns of cloud coverage, precipitation, and winds. While distinct from tropical cyclones (e.g., hurricanes), these mid-latitude cyclones can be as hazardous and damaging. ETCs are frequently associated with extreme weather conditions such as high winds, blizzard conditions, heavy precipitation, and flooding.

Additionally, storm interaction with the ocean often results in high waves and storm surge, which can cause severe coastal damage and major local impacts, such as inundation and erosion. All these various hazardous conditions and associated impacts can have detrimental socio-economic results. The North American east and west coasts are both strongly influenced by ETC storm activity; the east coast is particularly influenced by winter storms following two favoured tracks, the St. Lawrence Valley and the Eastern Seaboard, while the west coast is influenced by the North Pacific storm track and atmospheric river events. The North American coastal regions are also host to many land-based, coastal, and maritime socio-economic sectors, all of which can experience strong adverse impacts from ETC storm activity.

Society would benefit substantially if the risks associated with seasonal variations in ETC storm activity could be skilfully predicted well in advance. Skilful prediction on the seasonal (or longer) timescale would enable affected sectors to better anticipate, prepare for, manage, and respond to ETC storm activity variability (e.g., through improved contingency planning that accounts for the predicted changes in risk). However, the lead-time required for such planning does not currently match the timescales over which skilful forecasts of severe weather can be made. The useful skill of deterministic day-to-day atmospheric variation forecasts (i.e., daily weather and the occurrence of individual storms) is limited to approximately two weeks due to the chaotic nature of the atmosphere. It may be possible, though, to create categorical deterministic and probabilistic forecasts of storm activity variability on longer time scales since storm characteristics (e.g., storm track location and storm intensity) and extreme events are known to be affected by slowly varying large-scale climate signals, such as the El Niño-

Southern Oscillation (ENSO) and the North Atlantic Oscillation (NAO) (Eichler and Higgins 2006; Wang et al. 2006; Gan and Wu 2013; Grise et al. 2013; Gómara et al. 2016; Kim et al. 2017). A growing body of research further indicates that several of these teleconnection patterns are themselves predictable on the seasonal or longer timescales (Chen and Cane 2008; Barnston et al. 2012; Merryfield et al. 2013; Scaife et al. 2014; Athanasiadis et al. 2017). At present, ENSO is the most predictable teleconnection and serves as the primary source of seasonal to interannual predictability in operational seasonal forecasting (Stockdale et al. 2010; Doblas-Reyes et al. 2013).

Current operational seasonal forecasting is primarily focused on near surface temperature and total precipitation, producing categorical deterministic and probabilistic forecasts of the likelihood of below-, near-, and above-normal conditions for the upcoming seasons (Stockdale et al. 2010; Doblas-Reyes et al. 2013). The purpose of this study is to determine if seasonal forecasting could be extended to include the skilful prediction of ETC storm activity variability, specifically for the North American coastal regions and the cold months (October-March), during which ETC storm activity is most frequent and intense. This study investigates seasonal predictability of storm activity in Environment and Climate Change Canada's Canadian Seasonal to Interannual Prediction System (CanSIPS; Merryfield et al., 2013). CanSIPS is used by the Canadian Meteorological Centre to produce seasonal forecasts of temperature and precipitation for Canada and also contributes to the North American Multimodel Ensemble seasonal forecasting system (Kirtman et al. 2014) and the Climate-system Historical Forecast Project (Tompkins et al. 2017).

Research performed to date supports the premise that there is the potential to predict seasonal to interannual variations in ETC storm activity. Compo and Sardeshmukh (2004) investigated the predictability of wintertime (JFM) sea surface temperature (SST) forced Northern Hemisphere extratropical storm tracks, with specific focus on the Pacific-North American and North Atlantic-European regions. They used a multiple linear regression-based 'storm track model' trained on atmospheric general circulation model (AGCM)-generated storm track data (consisting of 540 integrations) to predict the storm track characteristics associated with the variations in SSTs related to ENSO. Storm tracks in the 500-hPa geopotential height field were defined using the 500-hPa omega (vertical velocity) variance with a 2-7 day bandpass filter. The impact of SST changes on the atmospheric circulation were characterized by the resulting anomalous 200-hPa geopotential height mean flow. Evaluating two winters with modest ENSO SST-forcing, 1987 (El Niño) and 1989 (La Niña), a correlation of 0.9 was obtained between the storm track signal predicted by the linear model and the AGCM-generated 60-member ensemble mean storm track anomalies, indicating success of the empirical storm track model. Additionally, reasonable correlations (0.4-0.7+) were noted for the 1950-1999 time period in the eastern Pacific, North American, and western Atlantic regions, with a predictable SST-forced storm track signal (on average, "modest" in strength) found for many winters. Years with stronger ENSO signals (i.e., strong El Niño or La Niña events) possessed greater correlation. Compo and Sardeshmukh concluded that the prediction skill of storm track variations is high enough in the Pacific-North American region to be of practical use.

More recently, Yang et al. (2015) investigated the seasonal predictability of extratropical storm tracks in the Geophysical Fluid Dynamics Laboratory (GFDL) high-resolution climate prediction model. Yang et al. defined storm tracks using the seasonal standard deviation of the 24-hr sea level pressure tendency. The average predictability time (APT) optimization method (DelSole and Tippett 2009a, b) (similar to Empirical Orthogonal Function analysis but patterns are optimized to maximize a predictability metric rather than variance) was applied to a 12-member ensemble seasonal hindcast covering 1982-2014 to identify the predictable patterns of storm tracks. The leading predictable pattern, observable up to 9 months ahead, is found to be strongly related to the ENSO signal, consistent with the results of Compo and Sardeshmukh (2004). Yang et al. also investigated the predictability of extremes (1^{st} and 99^{th} percentiles) by examining how the width of the statistical distribution for selected meteorological variables (wintertime [DJF] sea level pressure, temperature, wind, and precipitation) over North America changes in concert with the ENSO pattern; this also yielded positive results.

Pingree-Shippee et al. (in prep) investigated the potential predictability of Northern Hemisphere cold season (overlapping 3-month seasons of OND, NDJ, DJF, and JFM) extratropical storm activity, with specific focus on the North American coastal regions. Potential predictability was evaluated for the 1979-2015 time period using analysis of variance (ANOVA) in the time domain, the ERA-Interim reanalysis dataset, and proxies at and near the surface to represent extratropical storm activity (mean sea level pressure, 24-hr absolute pressure tendency, and 10-m wind speed). Pingree-Shippee et al. found potential predictability in areas where extratropical storm activity is prevalent, with the highest signals often found in areas of climatological cyclogenesis (e.g.,

Kuroshio Current and along the North American east coast). Within the North American coastal regions, the potentially predictable signals extend throughout much of the regions during peak seasons. Additionally, by applying a composite analysis conditioned on different phases of major teleconnection patterns, a strong association is found between the Southern Oscillation (representative of ENSO), the Pacific Decadal Oscillation, and the NAO and North American ETC storm activity. These results strongly indicate that variations in extratropical storm activity are potentially predictable on the seasonal timescale and, therefore, provides additional support for the premise that skilful prediction may be possible, in particular, along the North American coastal regions.

The remainder of this manuscript is outlined as follows: Descriptions of the study areas, storm activity proxies, datasets, seasonal forecast development, and skill scores used to evaluate the forecasts are provided in Section 6.4. Results are presented in Section 6.5, including example seasonal forecasts in addition to the forecast evaluations. Discussion and conclusions are presented in Section 6.6.

6.4 Data and Methods

6.4.1 Study Areas

The investigation of seasonal predictability of extratropical storm activity variability is focused on the North American west and east coastal regions (Figure 6.1). The North American study domains cover the non-Arctic USA and Canadian coastal regions. The west coast domain extends from 30°N to 60°N and 115°W to 140°W, encompassing the coastal regional from northern Baja California (Mexico), through the contiguous USA west coast and British Columbia (Canada), and into southeast Alaska (USA). The east

coast domain spans 25°N-65°N and 50°W-85°W, encompassing the coastal region from the southern tip of Florida (USA), extending up the Eastern Seaboard and through eastern Canada, to southern Baffin Island, Nunavut, Canada and includes Newfoundland, Canada. Subregions of the coastal domains (Figure 6.1; Table 6.1) are also utilized to provide a more detailed evaluation of probabilistic forecast skill. Extratropical storm activity varies throughout the North American coastal regions (e.g., frequency of storm conditions, cyclone life cycle stage, preferred areas of rapid intensification), therefore subregions were chosen to represent smaller geographical areas within the coastal domains with different climatological synoptic storm activity.

6.4.2 Storm Activity Proxies

Since ETCs are complex features and cannot be summarized in a single parameter, three variables that are continuous in space and time – 6-hrly mean sea level pressure (MSLP), 6-hrly absolute pressure tendency (ΔMSLP), and daily mean 10-m wind speed – are utilized as proxies to represent extratropical storm activity. Information on storm activity characteristics such as frequency and intensity can be derived from these proxies and, thus, would provide valuable information on ETC variability on the seasonal timescale at or near the surface, where the impacts of storm activity are primarily felt by end-users. Variations in MSLP provide information on the frequency (and/or persistence) of storm activity, since a stormier season with more storms (and/or longer-lasting storms) would be expected to have a lower seasonal mean MSLP. Alternatively, variations in ΔMSLP and 10-m wind speed within a season provide information on the intensity of storm activity since higher seasonal mean ΔMSLP and wind speed would be expected to

correspond to increased storminess (e.g., enhanced cyclogenesis and/or stronger pressure gradients).

The three equiprobable categorical framework and parametric Gaussian method for calculating probabilities utilized in this study to develop seasonal forecasts (discussed below) assume the variables used are approximately normally distributed. We therefore use the square root of the 6-hr absolute pressure tendencies in the development and evaluation of the ΔMSLP seasonal forecasts. The distribution of the raw absolute pressure tendencies is strongly right skewed, while the square root of the absolute pressure tendencies has a more symmetric distribution (Figure 6.2). MSLP and 10-m wind speed data are not transformed.

Modeled 10-m wind speed over land, particularly over variable terrain (e.g., the North American Western Cordillera) could be influenced by parameterized sub-grid scale surface properties, such as the surface roughness, and the representation of surface topography. In reanalysis datasets, *u*- and *v*-wind components at 10-m are classified as "Class B" variables by Kalnay et al. (1996) and, while influenced by observational data, are also strongly influenced by model physics, particularly over variable terrain. The 10-m wind speed results over land, therefore, are less reliable than the results over the oceans. Nevertheless, the 10-m wind speed results over land could still provide valuable insight into the seasonal predictability of extratropical storm activity and is, therefore, evaluated.

6.4.3 Datasets

The seasonal predictability of extratropical storm activity is investigated using Environment and Climate Change Canada's operational Canadian Seasonal to

Interannual Prediction System (CanSIPS). CanSIPS is an advanced, multi-model seasonal forecasting system that simultaneously forecasts the evolution of the atmosphere and the ocean (Merryfield et al. 2013). CanSIPS combines the 10 ensemble member forecasts from the Canadian Centre for Climate Modeling and Analysis (CCCma) Coupled Climate Model versions 3 (CanCM3) and 4 (CanCM4), respectively, to create multi-model forecasts. The forecasting system is used operationally at the Canadian Meteorological Centre (CMC) to produce an ensemble of seasonal forecasts that, in turn, are used to make categorical deterministic and probabilistic predictions of the likelihood of below-, near-, and above-normal seasonal mean temperature and precipitation conditions during the coming seasons (seasonal forecasts at 0-, 1-, 3-, 6-, and 9-month leads). The historical forecast skill of CanSIPS is commensurate with that of its peers (Merryfield et al. 2013). This study utilizes the 6-hrly MSLP and daily mean 10-m wind (10-m *u*- and *v*-component) data from the 1981-2010 hindcasts available from CanSIPS (T42 horizontal resolution, equivalent to approximately 2.79° x 2.79°) to construct zero-month lead seasonal forecasts.

The CanSIPS zero-month lead seasonal forecasts of extratropical storm activity are verified against the ERA-Interim reanalysis, distributed by the European Centre for Medium-Range Weather Forecasts (ECMWF), to evaluate forecast skill. ERA-Interim (Dee et al. 2011) is a 3rd-generation reanalysis that extends from 1979 to present, with T255 horizontal resolution (0.75° x 0.75°) and 60 vertical levels, and provides 6-hrly output. ERA-Interim was previously determined to have the best representation of mid-latitude North American coastal extratropical storm activity compared to other commonly used global reanalyses (Pingree-Shippee et al. 2017) and, therefore, was chosen for this

study. ERA-Interim was also used to study the potential predictability of seasonal variations in storm activity over North America's coastal regions (Pingree-Shippee et al., in prep). T42 horizontal resolution data from ERA-Interim are utilized for this study to provide a comparable verification dataset for the CanSIPS forecasts. Daily mean 10-m wind speeds are calculated using the 6-hrly 10-m *u*- and *v*-component data for evaluation of the CanSIPS wind data.

6.4.4 Seasonal Forecast Development

In this study, three types of seasonal forecasts are constructed using the CanSIPS multi-model ensemble mean and the three equiprobable category framework (i.e., below-, near-, and above-normal conditions):

1.) *Quantitative deterministic*: a single value forecast (the forecast seasonal anomaly, with respect to the climatological seasonal average calculated from the CanSIPS 30-yr hindcast) (e.g., the seasonal mean MSLP will be 5 hPa above normal).

2.) *Categorical deterministic*: a qualitative forecast based on whether the forecast anomaly will be below, near, or above normal conditions (e.g., the seasonal mean MSLP will be above normal).

3.) *Categorical probabilistic*: a categorical deterministic forecast which also includes forecast probabilities that the forecast anomaly will fall into each of the categories (e.g, a 70% probability that the seasonal mean MSLP will be above normal, a 20% probability it will be near normal, and a 10% probability it will be below normal). Including probabilities provides an indicator of the strength of the individual forecasts categories (i.e., the likelihood that the forecast anomaly will fall into each category).

Zero-month lead seasonal forecasts of the storm activity proxies (MSLP, ΔMSLP, and 10-m wind speeds) are constructed for 3-month rolling seasons during the cold months – OND, NDJ, DJF, JFM – during which storm activity is most frequent and intense. ΔMSLP and 10-m wind speeds are calculated from the CanSIPS data prior to developing the seasonal forecasts.

The *quantitative deterministic* forecasts are the CanSIPS multi-model ensemble mean seasonal anomaly forecasts and are constructed using the unweighted multi-model ensemble mean forecast method (Kharin et al. 2009). This method is considered to be the simplest way to develop multi-model ensemble forecasts as it simply averages the ensemble mean anomaly forecasts from all models into a single multi-model ensemble forecast:

$$X_U = \frac{1}{M}\sum_{m=1}^{M}\{X\}_m \qquad \text{(Eq. 6.1)}$$

where X_U is the unweighted multi-model ensemble mean foreasts (the quantitative deterministic forecast), M is the number of models, and $\{X\}_m$ is the ensemble mean anomaly forecast of the *m*th model (curly brackets denote individual model ensemble averaging). In this study, $\{X\}_m$ is the ensemble mean MSLP, ΔMSLP, or 10-m wind speed seasonal mean anomaly forecast from CanCM3 and CanCM4.

Various methods for developing *categorical deterministic* and *categorical probabilistic* seasonal forecasts using multi-model ensemble forecast systems have been evaluated for the predecessors of CanSIPS and applied to fields such as 500-hPa geopotential heights and near surface and 700-hPa temperatures (Kharin and Zwiers 2003; Kharin et al. 2009). In this study, seasonal forecasts of storm activity variability are

constructed using the method found to produce the highest forecast skill and which is also implemented in the current operational system utilized by the CMC – the parametric Gaussian method (Kharin and Zwiers 2003; Kharin et al. 2009). Within the parametric Gaussian method, the multi-model ensemble 30-year hindcast and seasonal mean anomaly forecasts are assumed to have Gaussian distributions. The forecast categories (below-, near-, and above-normal conditions) and probabilities are therefore derived using only the ensemble mean anomaly of the individual season being forecast and the historical climatological standard deviation of seasonal mean anomalies (calculated from the 20 ensemble member [CanCM3 + CanCM4] 30-year hindcast). When using the traditional three equiprobable categories (which are mutually exclusive and collectively exhaustive), the categorical boundaries, x_a (the boundary between the near- and above-normal categories) and x_b (the boundary between the near- and below-normal categories), are derived using terciles of the multi-model 30-year normal distribution of seasonal mean anomalies:

$$x_a = -x_b = x_{1/3}\sigma_x \qquad \text{(Eq. 6.2)}$$

where σ_x is the standard deviation of the historical climatology distribution of seasonal mean anomalies (MSLP, ΔMSLP, or 10-m wind speed anomalies in this study), representative of the climatic noise present in the system, and $x_{1/3} \equiv \mathcal{F}_{\mathcal{N}}{}^{-1}(1/3) \approx 0.43$; thus the categorical boundaries are +/- $0.43\sigma_x$ (Figure 6.3a).

The *categorical deterministic* forecasts are determined by comparing the multi-model ensemble mean seasonal anomaly forecast, X_U (Eq. 6.1), against the categorical boundaries (Eq. 6.2) (e.g., a forecast anomaly greater than x_a will result in a forecast for

above-normal conditions). The associated *categorical probabilistic* forecasts are calculated using the Gaussian probability estimator, with the predicted probabilities of below-, above-, and near-normal conditions, respectively, as follows (Kharin and Zwiers 2003):

$$\hat{P}(B) = \mathcal{F}_{\mathcal{N}}\left(\frac{-\hat{\beta}-x_a}{\hat{\sigma}_\epsilon}\right) \quad \text{(Eq. 6.3a)}$$

$$\hat{P}(A) = \mathcal{F}_{\mathcal{N}}\left(\frac{\hat{\beta}-x_a}{\hat{\sigma}_\epsilon}\right) \quad \text{(Eq. 6.3b)}$$

$$\hat{P}(N) = 1 - \hat{P}(B) - \hat{P}(A) \quad \text{(Eq. 6.3c)}$$

where $\mathcal{F}_{\mathcal{N}}$ is the distribution function of the standard normal distribution, $\hat{\beta}$ is the forecast multi-model ensemble mean seasonal anomaly (X_U), and $\hat{\sigma}_\epsilon$ is the standard deviation estimated from the historical climatology. Subsequently, seasonal shifts in $\hat{\beta}$ result in lateral shifts in the Gaussian distribution in relation to the climatological distribution and categorical boundaries, and therefore changes in the probabilities that the forecast anomaly will fall into each category (Figure 6.3b,c).

Further details on CanSIPS multi-model ensemble seasonal forecast development are provided in the Appendix A of this chapter [Section 6.8].

6.4.5 Forecast Evaluation

CanSIPS forecasts are verified against the ERA-Interim reanalysis, representative of the true state of the atmosphere, to determine forecast skill and whether that skill is sufficiently high (i.e., exceeding the climatological forecast) to be useful to end-users. When using the traditional three equiprobable category framework, the climatological probability forecast threshold associated with each category is 33.3% (i.e., a purely random "chance" forecast would be, on average, 33.3% correct). Quantitative

deterministic forecasts are evaluated using the correlation skill score, categorical deterministic forecasts are evaluated using the percent correct score, and the categorical probabilistic forecasts are evaluated using the Brier skill score. These scores are described below.

6.4.5.1 Correlation Skill Score

The correlation skill score calculates the linear correlation coefficient of the forecast and observed mean seasonal anomalies over the time series for each grid point (producing a map of correlations in time):

$$\rho = \frac{\frac{1}{N}\sum_i^N (f_i - \bar{f})(o_i - \bar{o})}{\sigma_f \sigma_o} \qquad \text{(Eq. 6.4)}$$

where f is the forecasted anomaly and o is the observed anomaly (overbar denotes averaging over all values), N is the total number of seasons (i.e., 30 for the CanSIPS hindcast), and σ is the standard deviation of the forecast and observed anomalies, respectively. ρ ranges from -1 to 1 with ρ = 1 representing the best score. Although insensitive to biases and errors in variance, the correlation skill score does provide a measure of the strength of the relationship (i.e., year-to-year time correspondence) between the forecast and observed anomalies and, therefore, a measure of forecast skill. Correlations exceeding 0.361 are statistically significant at the 5% level when based on a 30-year hindcast.

6.4.5.2 Percent Correct Score

The percent correct score is the percentage of correctly predicted categories and is calculated for past performance of the forecast system (i.e., the CanSIPS 30-year hindcast) for each grid point using, for the three equiprobable categories framework, a

3x3 contingency table (Table 6.2) (producing a map of the percent correct over the 30-year time series). The percent correct score is obtained from the sum of the diagonal (i.e., the number of verified forecasts) over the total (i.e., the total number of forecasts made) in the contingency table, multiplied by 100:

$$\text{Percent correct} = 100*(A+F+K)/P \qquad \text{(Eq. 6.5)}$$

where A is the number of verified below-normal forecasts, F is the number of verified near-normal forecasts, K is the number of verified above-normal forecasts, and P is the total number of forecasts produced.

6.4.5.3 Brier Skill Score

The Brier skill score is calculated from the Brier score (BR), which measures the accuracy of a forecast by relating the forecast probability to event occurrence and calculating the mean squared difference between the values:

$$BR = \overline{(P-O)^2} \qquad \text{(Eq. 6.6)}$$

where P is the forecast probability, O is the binary observed event variable that takes the value 1 when a forecast event occurs and 0 otherwise, and the overbar denotes averaging over all forecasts. Smaller BR values are indicative of a better forecast, with BR = 0 indicating a perfect forecast. The BR is calculated for each category (i.e., below-, near-, and above-normal). The corresponding Brier skill score (BSS) for each category compares the BR of the forecast to the BR of a reference forecast (typically climatology and calculated using a forecast probability of 33.3% in the three equiprobable category framework):

$$BSS = 1 - BR/BR_{ref} \qquad \text{(Eq. 6.7)}$$

BSS = 1 indicates a perfect forecast, BSS = 0 indicates a forecast with the same skill as climatology, and BSS < 0 indicates a forecast with larger BR values than of the reference forecast (i.e., a forecast less skilful than the random chance, climatological forecast).

6.5 Results

6.5.1 Seasonal Forecast Interpretation and Example Categorical Forecasts

Quantitative deterministic, categorical deterministic, and categorical probabilistic seasonal forecasts were developed for each cold season (OND, NDJ, DJF, JFM) in the 1981-2010 CanSIPS hindcast. Forecast interpretation for the ΔMSLP and 10-m wind speed forecasts is straightforward – a forecast for above-normal conditions suggests an increase in storm activity during the coming season and vice versa for below-normal conditions. Forecast interpretation for the MSLP forecasts, however, is slightly counterintuitive, as a forecast for below-normal conditions would suggest an increase in storm activity during the coming season and vice versa for above-normal conditions. Since extratropical cyclone activity cannot be summarized in a single proxy, the forecasts for all three proxies should be considered together when determining the predicted level of storm activity for the coming season.

Examples of the categorical deterministic and probabilistic forecasts produced by CanSIPS for the three storm activity proxies (MSLP, ΔMSLP, and 10-m wind speed) are provide for JFM 1983, representing a season with high forecast probabilities (Figure 6.4). JFM 1983 is influenced by a strong El Niño event and the expected changes in storm activity under these ENSO conditions for the North American coastal regions can be seen to be predicted. For JFM 1983, more confidence can be placed in a forecast of increased

storm activity in areas where a below-normal MSLP forecast coincides with above-normal forecasts for ΔMSLP and 10-m wind speed (e.g., along the California, USA and Baja California, Mexico coasts and in the southeast region of the USA).

6.5.2 Correlation Skill Score

Using the correlation skill score to evaluate the quantitative deterministic (mean seasonal anomaly) forecasts, CanSIPS is found to have skill forecasting the three extratropical storm activity proxies within at least parts of the North American coastal regions when compared against the critical correlation of 0.361. MSLP forecasts have high skill throughout the majority of the North American coastal domains while, for ΔMSLP and 10-m wind speed forecasts, higher skill is confined primarily to over land and the waters adjacent to the southeast (e.g., Florida region). Peak correlations within the study domains are observed during DJF for ΔMSLP and 10-m wind speed forecasts (Figure 6.5) and JFM for MSLP forecasts (Figure C.1 in Appendix C). Amongst the three proxies, MSLP forecasts are most skilful (highest correlation values and spatial extent of skill) followed by the ΔMSLP and 10-m wind speed forecasts, respectively. In DJF, skilful correlations are observed throughout the study domain for the MSLP forecasts, with peak correlations (~0.7 to 0.9) observed in the southeastern and southwestern regions of North America. For the ΔMSLP forecasts, skill is observed throughout much of the North American east coast domain, with peak correlations (~0.6) found over land in the Great Lakes region (and extension of the higher correlations observed over the North American interior) and over the southeast USA. Within the North American west coast domain, skilful correlations for the ΔMSLP forecasts are found over British Columbia, Canada, and over the waters adjacent to the central USA west coast (e.g., the northern half of

California). While similar correlation values to the ΔMSLP forecasts are also observed for the 10-m wind speed forecasts, the spatial extent of skill for the 10-m wind speed forecasts within the study domains is, in general, reduced. Nevertheless, peak correlations for the 10-m wind speed forecasts in the North American east coast domain are again found over the Great Lakes and Florida, USA regions; an additional peak is also observed over the Atlantic Canada. In the North American west coastal domain, skilful correlations for the 10-m wind speed forecasts are essentially confined to over the Sierra Nevada mountains region and the southern tip of the study domain (e.g., Baja California, Mexico).

6.5.3 Percent Correct Score

Evaluating the categorical deterministic forecasts using the percent correct score (PCS), CanSIPS is seen to have skill forecasting all three extratopical storm activity proxies when compared to the climatological forecast (33.3%). For all three proxies, the spatial extent and strength of the skill within the North American coastal regions increases as the seasons progress (Figure C.2 in Appendix C) and peak in JFM for MSLP and ΔMSLP forecasts (Figure 6.6) and in DJF for 10-m wind speed forecasts. Similar to the correlation skill score, within the North American study domains, the MSLP forecasts are most skilful (highest PCS), followed by ΔMSLP, and with 10-m wind speed forecasts having the lowest skill (lowest PCS). In JFM, high PCS (50% or greater) for the MSLP forecasts are found throughout the majority of both study domains, particularly the west coast domain, with notably high scores (66.6% or greater) observed along the coastal regions of California, USA and Baja California, Mexico. For the ΔMSLP forecasts, peak levels of skill (PCS 41.7% or greater) are confined to land areas in the east coast domain.

While outside the coastal study domains, the highest PCS (66.7% or greater) are found for the ΔMSLP forecasts over the interior of North America in association with the continental storm tracks originating in the lee of the Rocky Mountains (USA and Canadian). Relatively low levels of skill (PCS up to 41.7%) are observed throughout the study domains for the 10-m wind speed forecasts. Higher PCS (up to 58.3%) for the 10-m wind speed forecasts are found in the North American interior and over the waters adjacent to the mid- and high-latitude North American west coast (e.g., the Pacific Northwest and British Columbia).

6.5.4 Brier Skill Score

Brier skill scores (BSS) are calculated for each forecast category and season (OND, NDJ, DJF, JFM), respectively. The BSS of the categorical seasonal probabilistic forecasts is assessed in two ways: 1.) at each grid point, performance over time is assessed, producing plots of BSS for 30-season periods and 2.) for each season, performance over the Northern Hemisphere geographical domain is assessed, producing a time series of BSS, one value for each of the 30 seasons. CanSIPS is considered to have skill when BSS > 0.

BSS values assessed over the 30-year seasonal hindcast sequences for each grid point in the Northern Hemisphere (20°N-poleward) provide insight into the overall skill of the CanSIPS probabilistic forecasts (Figures 6.7 and 6.8). Similar to the correlation skill and percent correct scores, BSS plots indicate the MSLP forecasts are, in general, the most skilful (highest BSS values), followed by the ΔMSLP and 10-m wind speed forecasts, respectively. CanSIPS is most skilful in producing below- and above-normal categorical probabilistic forecasts, with 30-season BSS values as high as 0.5 in the North

American region (coastal domains or continental interior). Due to the insensitivity of the near-normal category probabilistic forecasts to changes in the climatic signal (e.g., the teleconnections; $\hat{\beta}$ in Eq. 6.3; Kharin and Zwiers 2003), the 30-season BSS values for the near-normal category are confined to -0.1 to 0.1 and, therefore, similar skill to that of the climatological forecast. Similar patterns of skill are observed in the BSS plots for the below- and above-normal categories as those seen in the correlation skill and percent correct scores. Higher skill (BSS values up to 0.5) are observed throughout the North American coastal study domains for the MSLP forecasts, with skill peaking in the southeast and southwest USA, and higher skill over the North American interior for ΔMSLP (BSS values up to 0.5) and 10-m wind speeds (BSS values up to 0.4). Higher skill (BSS values up to 0.4) is also observed in the mid-latitudes over the North Pacific for the 10-m wind speed forecasts.

The temporal variation in performance as measured by the BSS is next assessed for the North American coastal study domains (Figure 6.9 and Figures C.5-C.7 in Appendix C). It is again evident that the MSLP forecasts are most skilful, having the highest BSS values (as high as 0.9 in some years), followed by the ΔMSLP forecasts (BSS as high as 0.8), and then the 10-m wind speed forecasts (BSS as high as 0.4). For each proxy respectively, the peak BSS values observed are comparable between the two coastal study domains. For well-forecast seasons (the forecast category with high probabilities verifying), such as the JFM 1989 MSLP forecast for both study domains (Figure 6.10), high BSS values are observed for all three forecast categories. Conversely, for poorly-forecast seasons (the forecast category with low probabilities verifying), such as the JFM 2002 MSLP forecast for the east coast domain (Figure 6.11), poor BSS values

(BSS < 0) are observed for the below- and above-normal forecast categories, including a notably poor BSS value for the category with high probabilities forecast (e.g., the below-normal category for JFM 2002 MSLP). Occasionally, a skilful BSS value is observed for either the below- or above-normal category while a notably poorer BSS value is observed for the opposing category, such as the JFM 2000 MSLP forecast for the west coast domain (Figure 6.12). These opposing BSS values are due to CanSIPS forecasting high probabilities for the below- or above-normal category (and consequently low probabilities for the opposing category) and having near-normal conditions observed. A hypothetical example of each of these forecast results and the associated Brier score (BR), reference Brier score (BR calculated using the climatological threshold of 33.3%), and BSS values are presented in Table 6.3. Well-forecast and opposing BSS values forecast seasons comprise the majority of the 30-year hindcast with limited poorly-forecast seasons, suggesting minimal overall underperformance by CanSIPS when assessing the all the individual seasonal BSS values within the complete study domains.

The temporal variation in performances, as measured by the BSS, across subregions of the coastal study domains is also assessed (Figures 6.13-6.15) to gain insight into how well CanSIPS produces probabilistic forecasts for smaller geographical areas along the North American coastal regions, which represent different climatological synoptic storm activity (Figure 6.1, Table 6.1). As with the complete study domain assessments, well-forecast seasons, poorly-forecast seasons, and those with opposing BSS values are all observed for the subregions. By assessing subregionally, however, it is found that a single forecast result may not be observed throughout the whole coastal domain. For example, JFM 2002 mean MSLP anomalies were found to be poorly forecast

when BSS is assessed over the complete east coast domain but, while this forecast result is also found for the US_E_Seaboard and NE_CM_Nfl subregions, opposing BSS values are observed for the QC_Lab subregion and mean MSLP anomalies are found to be well-forecast for the Great_Lakes subregion. Additionally, the subregional assessments reveal that the notably poor BSS values associated with the poorly-forecast and opposing BSS values seasons are often considerably more negative compared to those of the complete study domain assessments. When used in conjunction with the BSS plots (Figures 6.7 and 6.8), the subregional BSS assessments can provide more detail into CanSIPS' geographical skill in producing probabilistic forecasts, including identifying seasons with noticeably well or noticeably poor forecasts.

6.6 Discussion and Conclusions

Seasonal prediction skill of North American extratropical coastal storm activity is investigated using the Canadian Seasonal to Interannual Prediction System (CanSIPS) 1981-2010 hindcast. CanSIPS multi-model ensemble mean quantitative deterministic, categorical deterministic, and categorical probabilistic seasonal forecasts of storm activity proxies – MSLP, absolute pressure tendency (ΔMSLP), and 10-m wind speed – are developed for the cold seasons (OND, NDJ, DJF, JFM). The categorical deterministic and probabilistic seasonal forecasts are constructed using the three equiprobable category framework (below-, near-, and above-normal conditions) and the parametric Gaussian method for determining probabilities. Forecasts are then evaluated against the ERA-Interim reanalysis dataset, representative of the true state of the atmosphere, using the

correlation skill score, percent correct score (PCS), and Brier skill score (BSS) to determine forecast skill.

Interpretation of the ΔMSLP and 10-m wind speed forecasts is similar to the that of the current operational temperature and precipitation forecasts – an above-normal forecast represents an increased seasonal mean absolute pressure tendency and wind speed value and, therefore, suggests an increase in storm activity and the reverse for below-normal conditions. Interpretation of the MSLP forecasts, however, is slightly contrary as a below-normal forecast represents a lower seasonal mean pressure value, which suggests an increase in storm activity and vice versa for above-normal conditions. Forecasts for all three storm activity proxies should be considered together when determining the predicted storm activity conditions for the coming season as storm activity cannot be summarized in a single proxy. Furthermore, changes in a single proxy's conditions may not be directly associated with a change in storm activity; for example a change in seasonal mean MSLP could be representative of a change in the large-scale circulation patterns. Therefore, greater confidence can be placed on a forecast when the anomalies of the three proxies behave in concert; i.e., more confidence can be place on a forecast of increased storm activity when forecasted below-normal MSLP conditions coincide with forecasted above-normal ΔMSLP and 10-m wind speed conditions and the reverse for a forecast of decreased storm activity.

CanSIPS is found to have skill producing seasonal forecasts of North American coastal storm activity when compared to the climatological forecast (33.3% forecast threshold). For all three proxies, the quantitative deterministic forecasts (evaluated using correlation skill score) and the categorical deterministic forecasts (evaluated using

percent correct score) are most skilful in DJF and JFM. The MSLP forecasts are found to be most skilful (highest correlation and PCS values) within the North American study domains, followed by the ΔMSLP forecasts, and then by the 10-m wind speed forecasts. Within both North American study domains, peak correlation skill and percent correct scores are found to correspond to areas strongly influenced by extratropical storm activity. While MSLP forecasts have high skill over land and ocean, ΔMSLP forecasts have considerably higher skill over the North American continent than over the oceans and 10-m wind speed forecasts have notably high skill in the mid-latitudes over the North Pacific.

The higher skill of MSLP forecasts in the west coast domain and ΔMSLP forecasts in the east coast domain may be associated with the different synoptic situations on the two coasts (such that cyclolysis and cyclogenesis dominate, respectively). Within the west coast domain, peak correlation skill scores and PCS for the MSLP forecasts strongly highlight the Aleutian Low and the exit region of the North Pacific storm track, with cyclones decaying climatologically as they impact the Gulf of Alaska and British Columbia, Canada. With consistent cyclolysis impacting the west coast domain (i.e., the decaying phase of the storm life cycle), changes in the seasonal mean MSLP signal may be more predictable in CanSIPS compared to the east coast, which is impacted by cyclones in various life stages (e.g., developing and maturing cyclones along the Eastern Seaboard including rapidly intensifying cyclones in the Atlantic Canada region, reintensifying cyclones in the Great Lakes region, and decaying cyclones tracking into the Hudson Bay region from the continental interior). On the other hand, the relatively high frequency of cyclogenesis, including rapid intensification, and reintensification of cyclones within the east coast domain may create a stronger ΔMSLP signal compared to

the west coast domain, therefore allowing changes in the seasonal mean ΔMSLP signal along the east coast to be more predictable in CanSIPS.

Nevertheless, high correlation skill scores and PCS are found within the east coast domain for all three proxies, often highlighting components of the Eastern Seaboard storm track. For example, peaks in PCS for the MSLP forecasts and the higher correlation values for the 10-m wind speed forecasts highlight the region of climatological cyclogenesis, including rapid intensification, near Atlantic Canada. Furthermore, the North American interior storm tracks, which extend into the Great Lakes region and St. Lawrence Valley, are also highlighted in the high correlation and PCS values for the ΔMSLP forecasts along with the higher correlation values for the 10-m wind speed forecasts. In addition to the exit region of the North Pacific storm track, the influence of atmospheric river events within the west coast domain (frequently impacting the California, USA region) is also highlighted by peaks in the correlation skill scores and PCS for the MSLP forecasts and high correlation values for the 10-m wind speed forecasts.

Brier skill scores were evaluated for each forecast category and each season (OND, NDJ, DJF, JFM), respectively. CanSIPS is found to have skill producing probabilistic forecasts throughout the North American coastal regions for all three proxies. Highest skill is observed for the below- and above-normal categorical forecasts while similar skill to that of the climatological forecast is found for the near-normal forecast category. The BSS results further indicate that, in general, MSLP forecasts are most skilful, followed by ΔMSLP and 10-m wind speed forecasts, respectively. The plots of the 30-season BSS have similar patterns of skill as those observed in the correlation

skill and percent correct scores. BSS assessed for each study domain reveals three forecast results: well-forecast seasons (the forecast category with high probabilities verifies, resulting in high BSS values for all categories), poorly-forecast seasons (the forecast category with low probabilities verifies, resulting in poor BSS values), and opposing BSS values seasons (seasons when near-normal conditions are observed, resulting in a skilful BSS value for the forecast category with low probabilities but a poor BSS value for the forecast category with high probabilities). Well-forecast and opposing BSS values seasons are found to comprise the majority of the 30-year hindcast, therefore suggesting minimal overall underperformance by CanSIPS.

BSS assessed for the subregions provide further insight into CanSIPS' performance, evaluating smaller geographical areas within the coastal domains that represent different climatological synoptic storm activity and, arguably, geographical domains more relevant to potential end-users and socio-economic needs (e.g., fishing grounds). Due to the smaller geographical areas being evaluated, notably poor BSS values are often found in association with poorly-forecast and opposing BSS values seasons in the subregional results. These poor BSS values are more commonly found subregionally because the smaller evaluation areas are typically dominated by a single forecast category and, if that category does not verify, a noticeably poor BSS value for the domain will result and will be particularly poor when CanSIPS has high probabilities forecast. Nevertheless, valuable information can still be gained from the probabilistic forecasts. Since well-forecast and opposing BSS values seasons make up the majority of the CanSIPS hindcast, the forecast category with high probabilities or the near-normal category commonly verifies and, therefore, provides at least some guidance to end-users

– arguably, being able to remove one extreme (increased or decreased storm activity) would be beneficial to end-users when planning for the coming season.

While subregional assessments of BSS could provide further insight into CanSIPS' performance and would be beneficial to end-users, additional investigation is needed to determine the extent to which smaller domains can be utilized. The spatial limit of seasonal predictability on the zero-month lead timescale needs to be investigated to determine the minimum domain size applicable for forecast evaluation and interpretation. Additionally, how the size of the domain evaluated influences the uncertainty of the BSS results should also be investigated. Using the JFM 2002 MSLP forecast example (Figure 6.11), while the mean MSLP anomalies are found to be poorly forecast when BSS is assessed over the complete east coast domain (and for the US_E_Seaboard and NE_CM_Nfl subregions), mean MSLP anomalies are found to be well-forecast when BSS is assessed for the Great_Lakes subregion. How much certainty can be placed on the BSS results from the Great_Lakes subregion when the subregion is 10°x10° and differing from the results of the much larger, complete east coast domain? Different regional synoptic conditions and storm tracks could explain the differing results between the complete coastal domain and a subregion (or between subregions). For the JFM 2002 example, differences in the BSS results between the Great_Lakes subregion and the US_E_Seaboard and NE_CM_Nfl subregions could be due to the different storm tracks influencing the regions (continental and coastal, respectively). As such, further investigation into the use of smaller domains in seasonal probabilistic forecast evaluation is needed.

The skill levels observed in this study for the CanSIPS seasonal forecasts of the North American coastal storm activity proxies should be considered representative of baseline skill. For this study, the seasonal forecasts were constructed from the raw CanSIPS data using the unweighted multi-model ensemble mean forecast method and then evaluated as is. Operationally, however, during the development of the temperature and precipitation seasonal forecasts, a calibration coefficient is also calculated from the 30-year hindcast and used to optimally rescale the multi-model ensemble mean anomaly and ensemble spread (https://weather.gc.ca/saisons/info_prev_proba_e.html). The inclusion of a calibration coefficient in the construction of the storm activity seasonal forecasts could improve the subsequent skill scores. Additionally, other statistical adjustments based on observed relationships could potentially be applied during post-processing of the forecasts to help improve skill levels (Kharin and Zwiers 2003; Kharin et al. 2009), although the potential for meaningful improvement is limited by the length of the CanSIPS hindcast. Due to the exclusion of a calibration coefficient and post-processing statistical adjustment in this study, the skill reported in this paper is representative of the baseline skill achievable in CanSIPS. Thus, baseline forecast skill is found for the seasonal forecasts of all three extratropical storm activity proxies evaluated, with MSLP forecasts found to be most skilful and, in general, 10-m wind speed forecasts the least skilful for the North American coastal regions. Skilful seasonal forecasting of North American coastal extratropical storm activity is, therefore, possible in CanSIPS and should be further pursued.

6.7 Acknowledgements

Funding for this research was provided by the Marine Environmental Observation Prediction and Response (MEOPAR) Network of the Centres of Excellence of Canada, subproject 2.1.2 “Coastal Storm Activity”, PI Francis Zwiers, under Project 2.1 “Climate Change and Extreme Events in the Marine Environment”, PIs Greg Flato, Gordon McBean, Bill Merryfield, Barbara Neis, Ronald Pelot, Jinyu Sheng, and Francis Zwiers. This research was also supported by the University of Victoria’s Department of Geography and the Pacific Climate Impacts Consortium.

Thank you to William (Bill) Merryfield at the Canadian Centre for Climate Modelling and Analysis (CCCma) for providing the CanSIPS data utilized in this research. Thank you to Bill Merryfield and Viatcheslav (Slava) Kharin at CCCma for their guidance in the development and evaluation of the seasonal forecasts.

6.8 Appendix A: Further Details on Seasonal Forecast Development

The raw seasonal forecasts produced by CanSIPS consist of ~90 days of 6-hrly values for MSLP (and, subsequently, for the calculated ΔMSLP) and ~90 days of daily mean values for 10-m winds (10-m *u*- and *v*-component data) from each of the 10 ensembles members from both CanCM3 and CanCM4. For each ensemble member and for each year, the seasonal mean is computed (e.g., the OND seasonal average for the year 1981); the corresponding model’s 30-year hindcast average (climatological seasonal mean) for the same season (e.g., OND) is removed, resulting in the ensemble member’s seasonal anomaly forecast. Removing the model’s climatological seasonal mean and constructing forecasts using the resulting anomalies reduces the influence of ensemble member-

specific systematic biases on the seasonal forecasts. The ensemble mean seasonal anomaly forecast is then calculated for each model and subsequently combined using the unweighted multi-model ensemble mean forecast method (Eq. 6.1). The multi-model ensemble mean seasonal anomaly forecast is then compared against the categorical boundaries (Eq. 6.2) to designate the deterministic categorical forecast. The corresponding forecast probabilities are calculated for the three categories using the parametric Gaussian method, in which the multi-model ensemble 30-year hindcast and forecasts of seasonal mean anomalies are assumed to have Gaussian distributions. The seasonal forecast (Gaussian-fitted) distributions are estimated to have the same standard deviation as the climatological (Gaussian-fitted) distribution; that is, climatic noise present in the system is presumed to be unaffected by boundary conditions (e.g., teleconnection activity), and is therefore assumed to be constant from one season to the next. That is, it is assumed that only the mean of the deterministic forecasts change from season to season in response to the boundary conditions. As such, the Gaussian probability estimator utilizes only the ensemble mean anomaly of the individual season being forecast and the historical climatological standard deviation of seasonal mean anomalies (and the predetermined categorical boundaries) to calculate the corresponding probabilities (Eq. 6.3). An estimate of the standard deviation of the collective interannual variability is calculated by fitting a Gaussian distribution to the combined 30-year distribution of seasonal mean anomalies (comprised of the seasonal mean anomalies from each individual ensemble member of CanCM3 and CanCM4). Basing the seasonal probability forecast on an individual quantity – the predicted seasonal mean anomaly – is important because strategies that require the estimation of additional parameters from an

ensemble of seasonal hindcasts of limited size tend to have lower skill (Kharin and Zwiers 2003).

6.9 References

Athanasiadis PJ, Bellucci A, Scaife AA, Hermanson L, Materia S, Sanna A, Borrelli A, MacLachlan C, Gualdi S (2017) A Multisystem View of Wintertime NAO Seasonal Predictions. J Clim 30(4): 1461-1475

Barnston AG, Tippett MK, L'Heureux ML, Li S, DeWitt DG (2012) Skill of real-time seasonal ENSO model predictions during 2002-11: Is Out Capability Increasing? Bull Am Meteorol Soc 93(5): 631-651

Chen D, Cane MA (2008) El Niño prediction and predictability. J Comput Phys 227(7): 3625-3640

Compo GP, Sardeshmukh PD (2004) Storm Track Predictability on Seasonal and Decadal Scales. J Clim 17(19): 3701-3720

Dee DP, Uppala SM, Simmons AJ, Berrisford P, Poli P, Kobayashi S, Andrae U, Balmaseda MA, Balsamo G, Bauer P, Bechtold P, Beljaars ACM, van de Berg L, Bidlot J, Bormann N, Delsol C, Dragani R, Fuentes M, Geer AJ, Haimberger L, Healy SB, Hersbach H, Holm EV, Isaksen L, Kallberg P, Kohler M, Matricardi M, McNally AP, Monge-Sanz BM, Morcrette JJ, Park BK, Peubey C, de Rosnay P, Tavolato C, Thepaut JN, Vitart F (2011) The ERA-Interim reanalysis: configuration and performance of the data assimilation system. Q J R Meteorol Soc 137(656): 553-597

DelSole T, Tippett MK (2009a) Average Predictability Time. Part I: Theory. J Atmos Sci 66(5): 1172-1187

DelSole T, Tippett MK (2009b) Average Predictability Time. Part II: Seamless Diagnoses of Predictability on Multiple Time Scales. J Atmos Sci 66(5): 1188-1204

Doblas-Reyes FJ, García-Serrano J, Lienert F, Biescas AP, Rodrigues LRL (2013) Seasonal climate predictability and forecasting: status and prospects. WIREs Clim Change 4(4): 245-268

Eichler T, Higgins W (2006) Climatology and ENSO-Related Variability of North American Extratropical Cyclone Activity. J Clim 19(10): 2076-2093

Gan B, Wu L (2013) Seasonal and Long-Term Coupling between Wintertime Storm Tracks and Sea Surface Temperature in the North Pacific. J Clim 26(16): 6123-6136

Gómara I, Rodríguez-Fonseca B, Zurita-Gotor P, Ulbrich S, Pinto JG (2016) Abrupt transitions in the NAO control of explosive North Atlantic cyclone development. Clim Dyn 47(9-10): 3091-3111

Grise KM, Son S, Gyakum JR (2013) Intraseasonal and Interannual Variability in North American Storm Tracks and Its Relationship to Equatorial Pacific Variability. Mon Weather Rev 141(10): 3610-3625

Kalnay E, Kanamitsu M, Kistler R, Collins W, Deaven D, Gandin L, Iredell M, Saha S, White G, Woollen J, Zhu Y, Chelliah M, Ebisuzaki W, Higgins W, Janowiak J, Mo KC, Ropelewski C, Wang J, Leetmaa A, Reynolds R, Jenne R, Joseph D (1996) The NCEP/NCAR 40-Year Reanalysis Project. Bull Am Meteor Soc 77(3): 437-471 https://doi.org/10.1175/1520-0477(1996)077<0437:TNYRP>2.0.CO;2.

Kharin VV, Zwiers FW (2003) Improved Seasonal Probability Forecasts. J Clim 16(11): 1684-1701

Kharin VV, Teng Q, Zwiers FW, Boer GJ, Derome J, Fontecilla JS (2009) Skill assessment of seasonal hindcasts from the Canadian historical forecast project. Atmos-Ocean 47(3): 204-223

Kim H-M, Zhou Y, Alexander MA (2017) Changes in atmospheric rivers and moisture transport over the Northeast Pacific and western North America in response to ENSO diversity. Clim Dyn. https://doi.org/10.1007/s00382-017-3598-9

Kirtman BP, Min D, Infanti JM, Kinter III JL, Paolino DA, Zhang Q, van den Dool H, Saha S, Pena Mendez M, Becker E, Peng P, Tripp P, Huang J, DeWitt DG, Tippett MK, Barnston AG, Li S, Rosati A, Schubert SD, Rienecker M, Suarez M, Li ZE, Marshak J, Lim Y-K, Tribbia J, Pegion K, Merryfield WJ, Denis B, Wood EF (2014) The North American Multimodel Ensemble: Phase-I Seasonal-to-Interannual Prediction; Phase-2 toward Developing Intraseasonal Prediction. Bull Am Meteorol Soc 95(4): 585-601

Livezey RE, Chen WY (1983) Statistical Field Significance and its Determination by Monte Carlo Techniques. Mon Weather Rev 111(1): 46-59

Merryfield WJ, Lee W-S, Boer GJ, Kharin VV, Scinocca JF, Flato GM, Ajayamohan RS, Fyfe JC, Tang Y, Polavarapu S (2013) The Canadian Seasonal to Interannual Prediction System. Part I: Models and Initialization. Mon Weather Rev 141(8): 2910-2945

Pingree-Shippee KA, Zwiers FW, Atkinson DE (2017) Representation of Mid-latitude North American Coastal Storm Activity by Six Global Reanalyses. Int J Climatol 38(2): 1041-1059. https://doi.org/10.1002/joc.5235

Pingree-Shippee KA, Zwiers FW, Atkinson DE (in prep) Cold Season Extratropical Storm Activity Potential Predictability and its Sources in the Northern Hemisphere with Focus on the North American Coastal Regions.

Scaife AA, Arribas A, Blockley E, Brookshaw A, Clark RT, Dunstone N, Eade R, Fereday D, Folland CK, Gordon M, Hermanson L, Knight JR, Lea DJ, MacLachlan C, Maidens A, Martin M, Peterson AK, Smith D, Vellinga M, Wallace E, Waters J, Williams A (2014) Skillful long-range prediction of European and North American winters. Geophys Res Lett 41, 2514-2519. https://doi.org/10.1002/2014GL059637

Stockdale TN, Alves O, Boer G, Deque M, Ding Y, Kumar A, Kumar K, Landman W, Mason S, Nobre P, Scaife A, Tomoaki O, Yun WT (2010) Understanding and Predicting Seasonal-to-Interannual Climate Variability - The Producer Perspective. Procedia Environ Sci 1: 55-80

Tompkins AM, Inés Ortiz de Zárate M, Saurral RI, Vera C, Saulo C, Merryfield WJ, Sigmond M, Lee W-S, Baehr J, Braun A, Butler A, Déqué M, Doblas-Reyes FJ, Gordon M, Scaife AA, Imada Y, Ishii M, Ose T, Kirtman B, Kumar A, Müller WA, Pirani A, Stockdale T, Rixen M, Yasuda T (2017) The Climate-system Historical Forecast Project: providing open access to seasonal forecast ensembles from centers around the globe. Bull Amer Meteor Soc. https://doi.org/10.1175/BAMS-D-16-0209.1

Wang XL, Wan H, Swail VR (2006) Observed Changes in Cyclone Activity in Canada and Their Relationships to Major Circulation Regimes. J Clim 19(6): 896-915

Yang X, Vecchi GA, Gudgel RG, Delworth TL, Zhang S, Rosati A, Jia L, Stern WF, Wittenberg AT, Kapnick S, Msadek R, Underwood SD, Zeng F, Anderson W, Balaji V (2015) Seasonal Predictability of Extratropical Storm Tracks in GFDL's High-Resolution Climate Prediction Model. J Clim 28(9): 3592-3611

Subregion Number	Subregion (Abbreviation)	Latitude, Longitude Range	Climatological Synoptic Storm Activity
West Coast Subregions			
1	NE Gulf of Alaska and SE Alaska (GofA_SE_AK)	50°N-60°N, 130°W-140°W	Exit region of N. Pacific storm track
2	Pacific NW and British Columbia (PNW_BC)	45°N-55°N, 120°W-130°W	Exit region of N. Pacific storm track; E. Pacific ETCs; Atmospheric rivers
3	California and Oregon (CA_OR)	35°N-45°N, 120°W-130°W	Atmospheric rivers
East Coast Subregions			
4	Northern Quebec and Labrador (QC_Lab)	50°N-60°N, 60°W-75°W	Exit region of N. American interior storm tracks
5	Eastern Great Lakes (Great Lakes)	40°N-50°N, 75°W-85°W	Secondary cyclogenesis region (intensify/reintensify of N. American interior ETCs)
6	New England, Canadian Maritimes, and Newfoundland (NE_CM_Nfl)	40°N-50°N, 55°W-75°W	Cyclogenesis region, including rapid intensification
7	US Eastern Seaboard (US_E_Seaboard)	30°N-40°N, 70°W-80°W	Cyclogenesis region

Table 6.1: Domain subregions

		FORECASTS			
		BELOW	**NORMAL**	**ABOVE**	**TOTAL**
OBSERVATIONS	**BELOW**	**A**	**B**	**C**	**D**
	NORMAL	**E**	**F**	**G**	**H**
	ABOVE	**I**	**J**	**K**	**L**
TOTAL		**M**	**N**	**O**	**P**

Table 6.2: 3x3 contingency table (as presented at https://weather.gc.ca/saisons/info_contingency_e.html)

Forecast	70% Probability of Below-Normal Conditions	20% Probability of Near-Normal Conditions	10% Probability of Above-Normal Conditions
a) well-forecast season			
Forecast Verified? (binary for BR calc.)	Yes (1)	No (0)	No (0)
BR	0.09	0.04	0.01
BR_{ref}	0.4449	0.1109	0.1109
BSS	0.7977	0.6393	0.9098
b) poorly-forecast season			
Forecast Verified? (binary for BR calc.)	No (0)	No (0)	Yes (1)
BR	0.49	0.04	0.81
BR_{ref}	0.1109	0.1109	0.4449
BSS	-3.418	0.6393	-0.8206
c) opposing BSS values season			
Forecast Verified? (binary for BR calc.)	No (0)	Yes (1)	No (0)
BR	0.49	0.64	0.01
BR_{ref}	0.1109	0.4449	0.1109
BSS	-3.418	-0.4385	0.9098

Table 6.3: A hypothetical probabilistic seasonal forecast and the resulting Brier scores (BR; Eq. 6.6), reference BR (BR_{ref}; Eq. 6.6, using the climatological forecast probability of 33.3%), and Brier skill scores (BSS; Eq. 6.7) based on which forecast category verifies. The three hypothetical seasons presented represent a) a well-forecast season, in which the forecast category with a high probability verifies, resulting in high (skilful) BSS values for all forecast categories, b) a poorly-forecast season, in which the forecast category with a low probability verifies, resulting in poor (< 0) BSS values for both the below- and above-normal forecast categories, and c) an opposing BSS values season, in which near-normal conditions are observed, resulting in a high BSS value for the forecast category with a low probability forecast and a poor BSS value for the forecast category with a high probabity forecast.

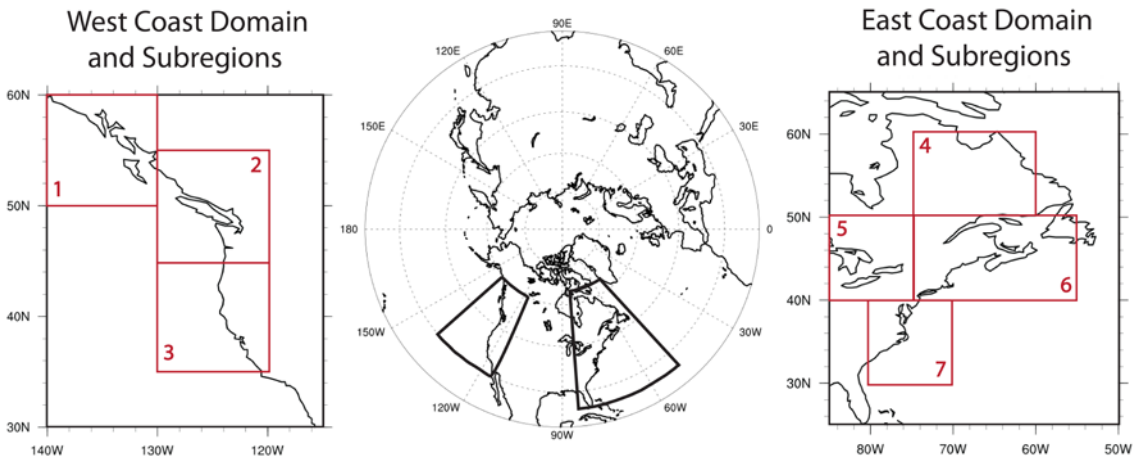

Figure 6.1: The North American (a) west and (b) east coastal study domains and subregions. Subregion information is provided in Table 6.1

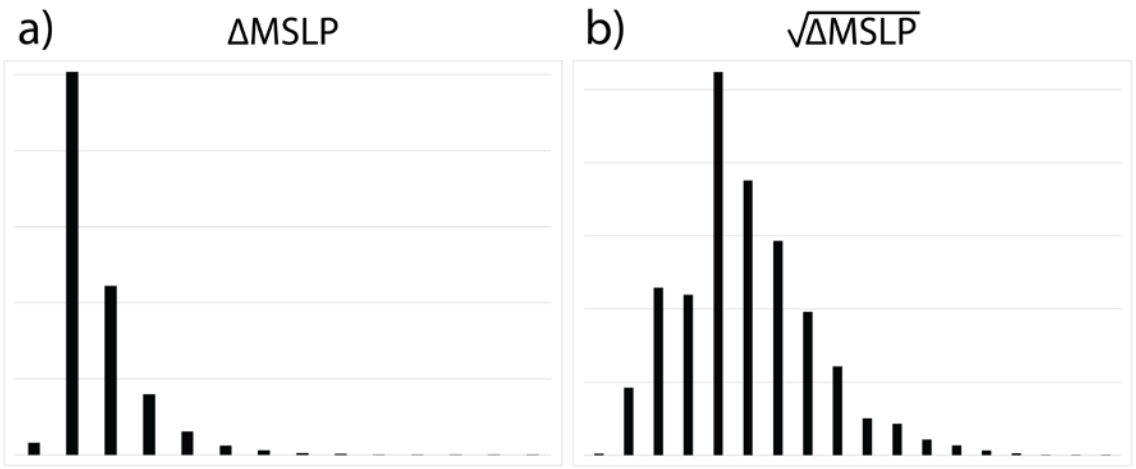

Figure 6.2: Example ΔMSLP distributions exhibiting a) the strongly right skewed distribution of raw absolute pressure tendencies vs. b) the more symmetric distribution of the square root of the absolute pressure tendencies

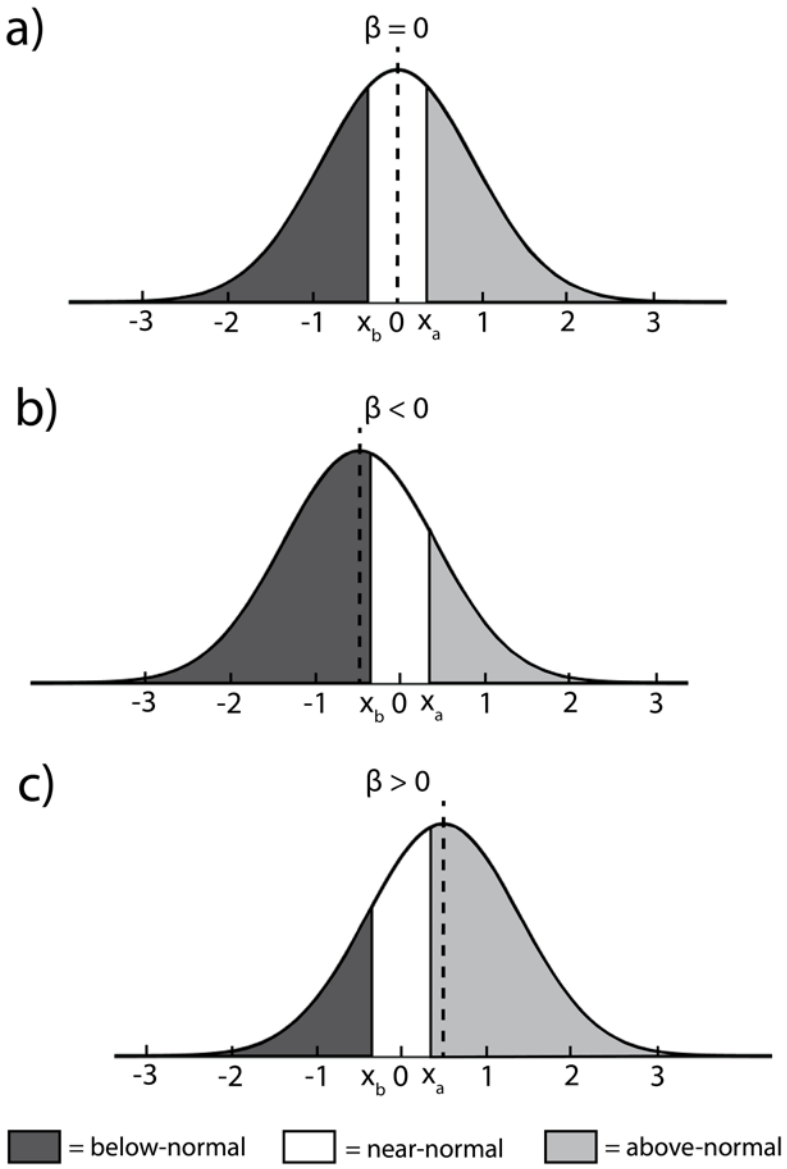

Figure 6.3: Schematic of shifts in the Gaussian distribution, its relation to the categorical boundaries (x_a and x_b; Eq. 6.2), and the resulting changes in forecast probabilities due to changes in the forecast mean seasonal anomaly ($\hat{\beta}$; Eq. 6.3). Distributions represent a) the historical climatological distribution of seasonal mean anomalies with a forecast probability of 33.3% for all categories, b) a forecast with a negative mean seasonal anomaly and therefore a noticeably increased probability forecast for below-normal conditions and decreased probability forecast for above-normal conditions, and c) the opposing forecast

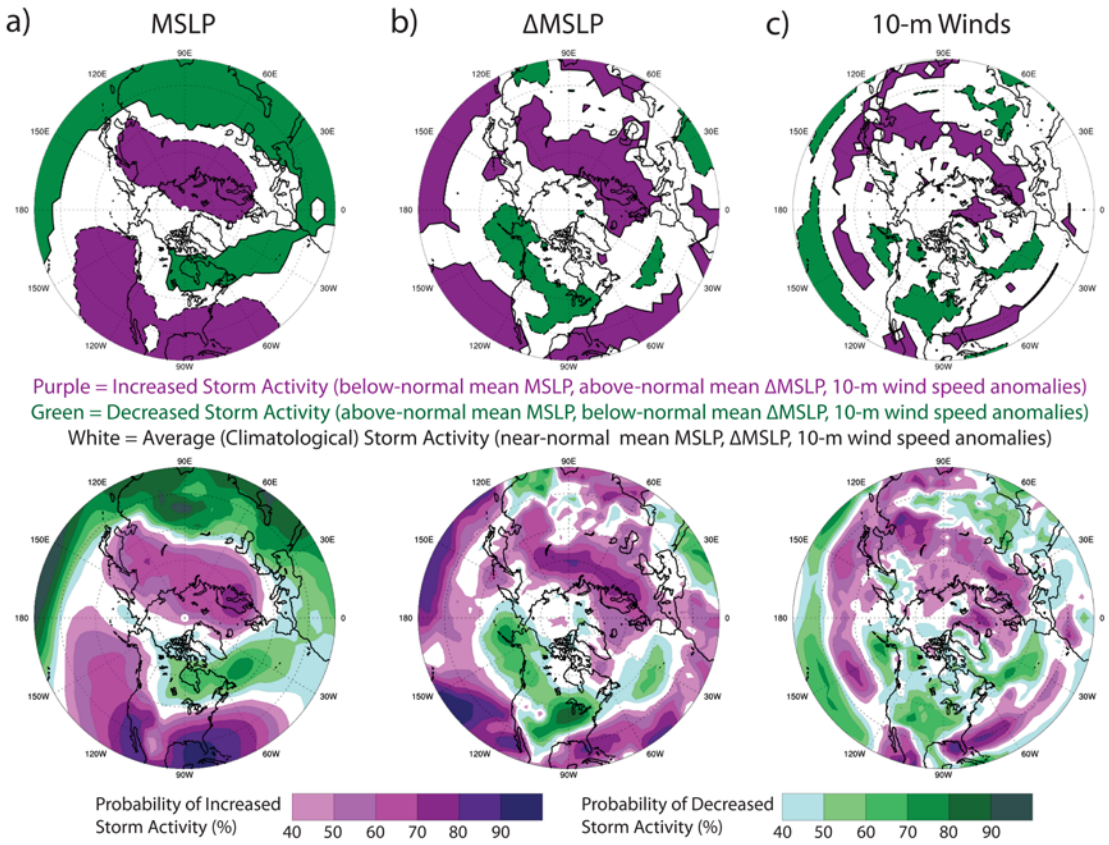

Figure 6.4: CanSIPS categorical deterministic (top) and probabilistic (bottom) forecasts for JFM 1983 storm activity as represented by a) MSLP, b) ΔMSLP, and c) 10-m wind speed

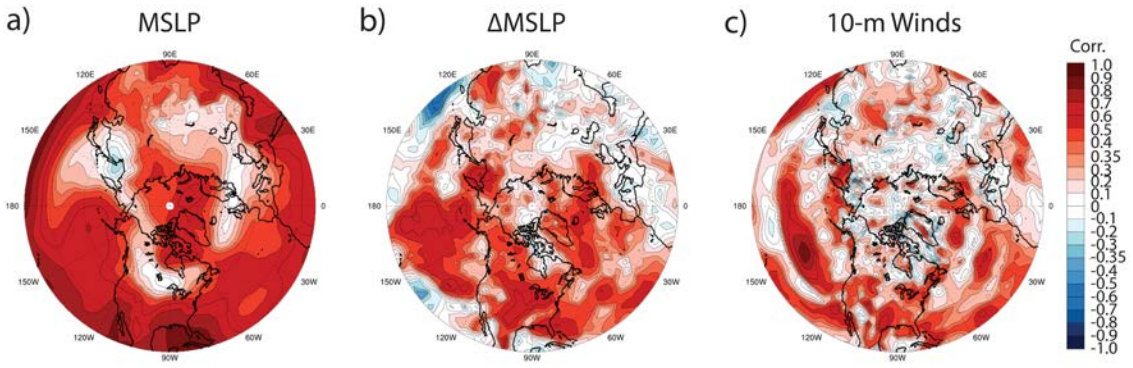

Figure 6.5: Correlation skill scores for DJF for a) MSLP, b) ΔMSLP, and c) 10-m wind speed

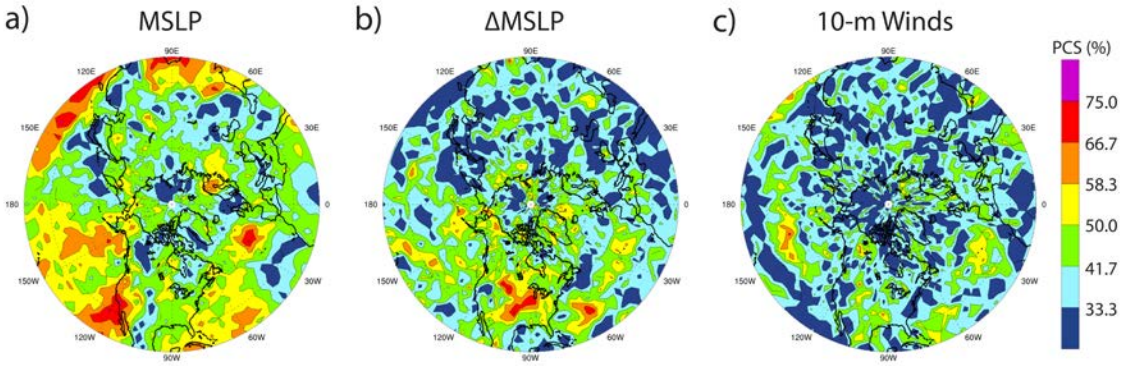

Figure 6.6: Percent correct scores for JFM for a) MSLP, b) ΔMSLP, and c) 10-m wind speed

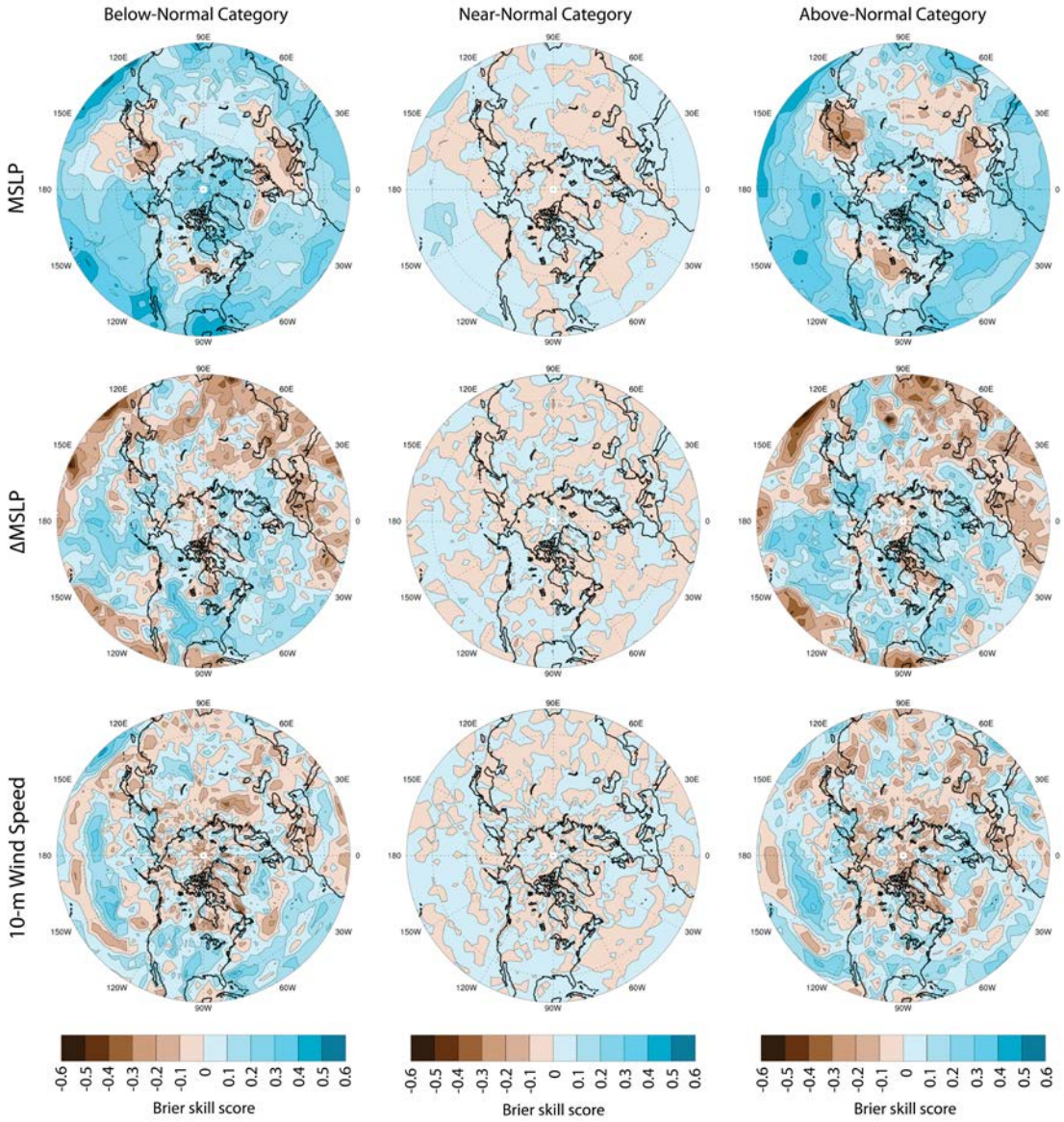

Figure 6.7: Brier skill scores assessed over the 30-year seasonal hindcast sequences for the Northern Hemisphere (20°N-poleward) DJF MSLP (top), ΔMSLP (middle), and 10-m wind speed (bottom) forecasts

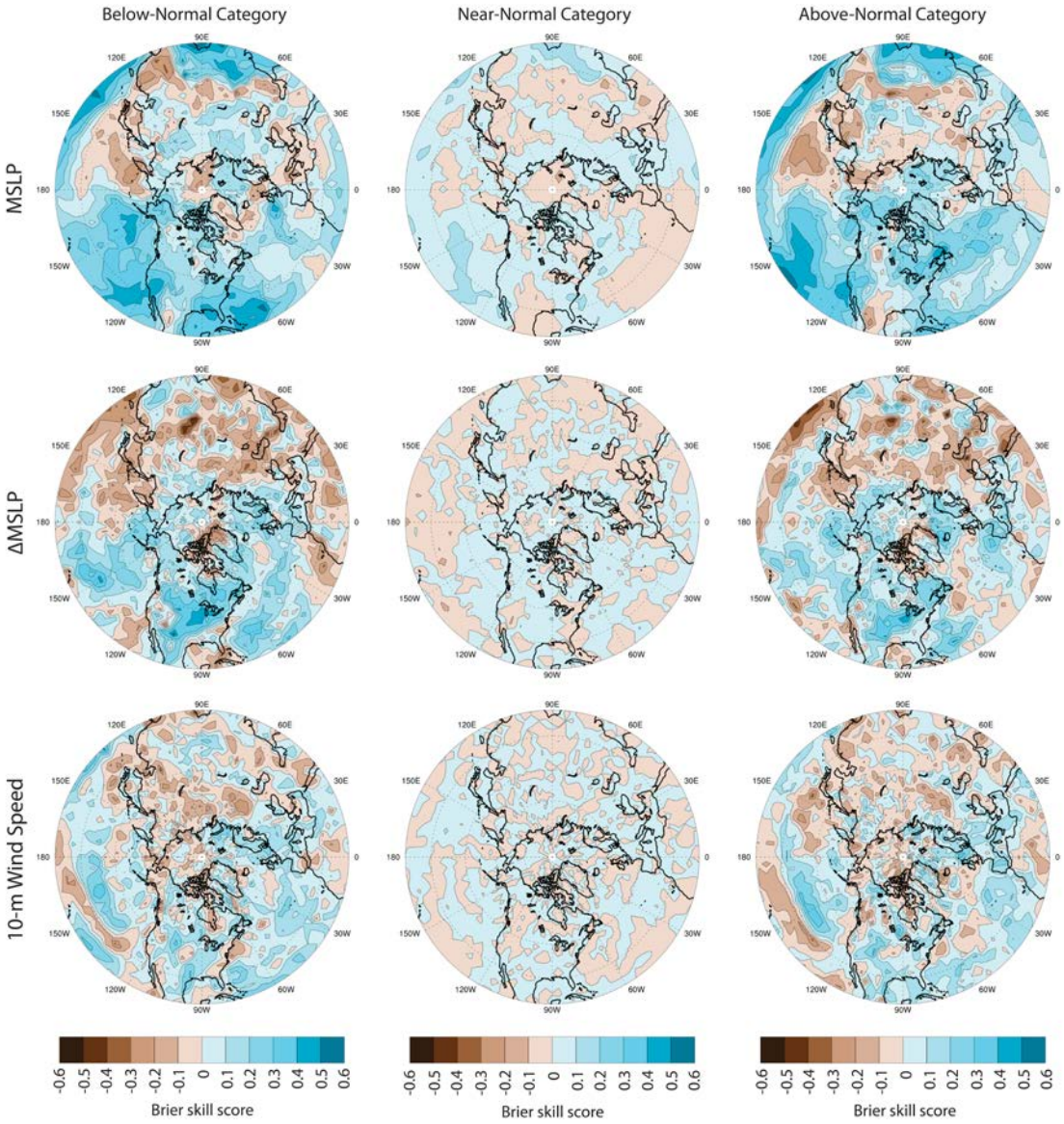

Figure 6.8: As in Fig. 6.7, except for JFM

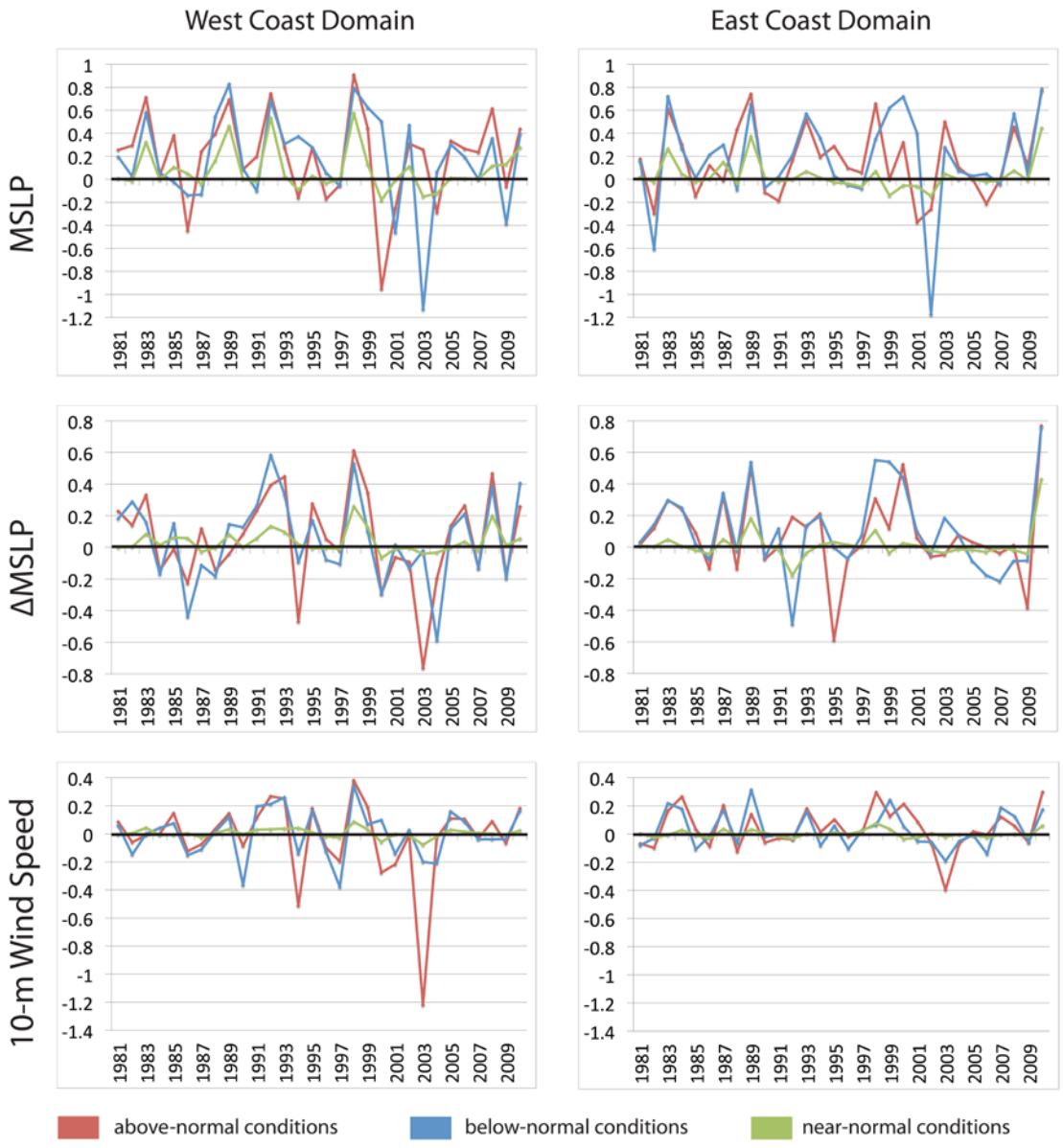

Figure 6.9: Temporal variation in forecast performance as measured by the Brier skill scores assessed for the North American west and east coast study domains (Fig. 6.1) for JFM MSLP (top), ΔMSLP (middle), and 10-m wind speed (bottom) forecasts

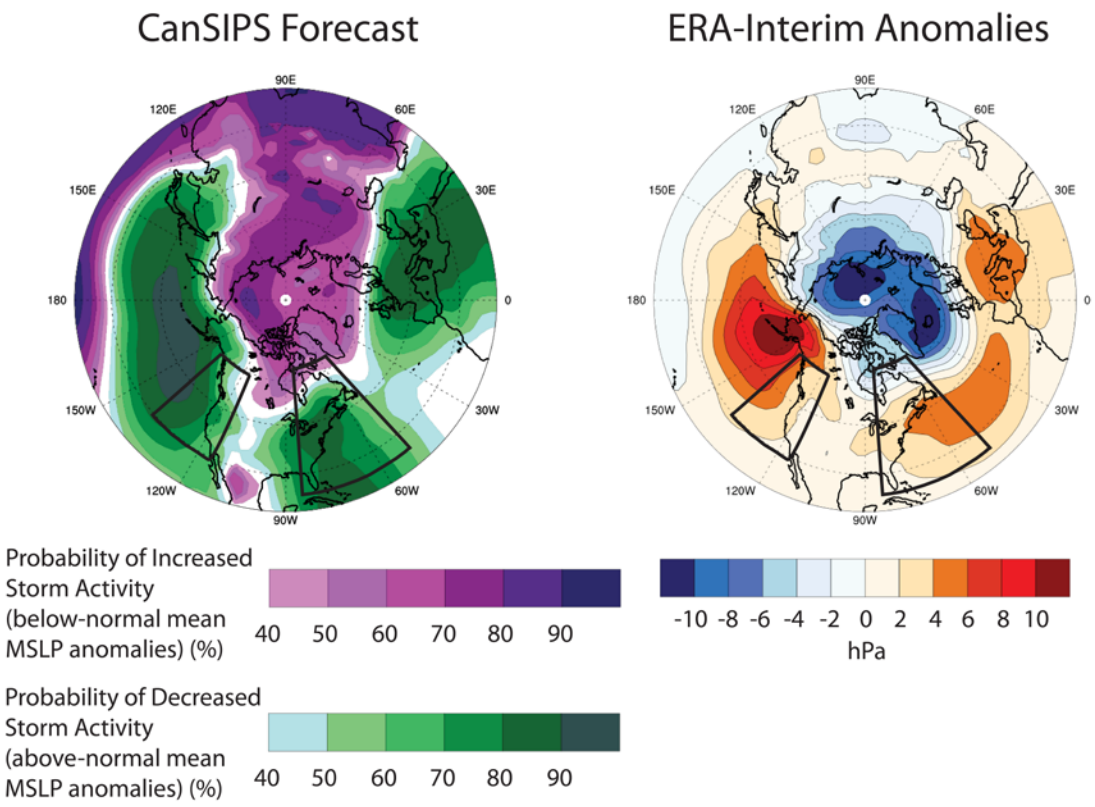

Figure 6.10: CanSIPS probabilistic JFM 1989 MSLP forecast and the "observed" ERA-Interim MSLP anomalies. JFM 1989 mean MSLP anomalies were well forecast by CanSIPS for the North American coastal domains (highlighted), resulting in high Brier skill scores for all three forecast categories (Fig. 6.9)

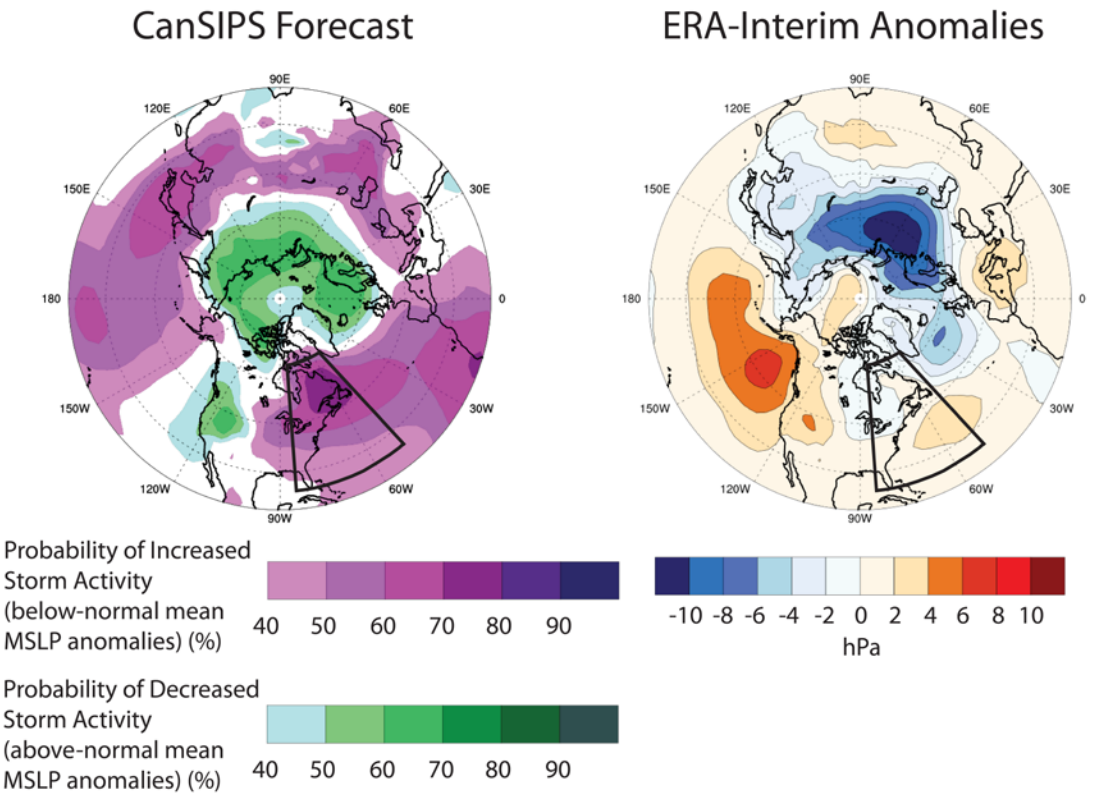

Figure 6.11: CanSIPS probabilistic JFM 2002 MSLP forecast and the "observed" ERA-Interim MSLP anomalies. JFM 2002 mean MSLP anomalies were poorly forecast by CanSIPS for the North American east coast domain (highlighted), resulting in poor Brier skill scores for the below-normal and above-normal forecast categories, including a notably poor BSS for the below-normal conditions category (Fig. 6.9)

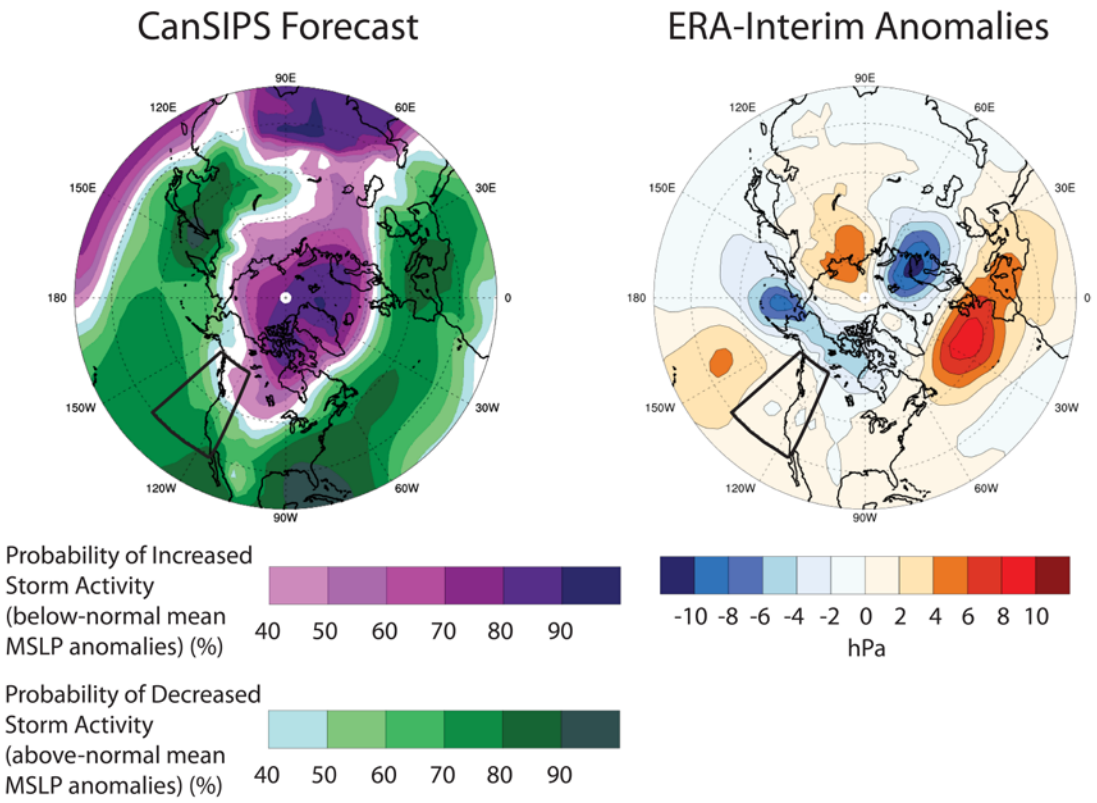

Figure 6.12: CanSIPS probabilistic JFM 2000 MSLP forecast and the "observed" ERA-Interim MSLP anomalies. For the North American west coast domain (highlighted), CanSIPS forecast above-normal seasonal mean MSLP anomalies with high probabilities (up to 70-80%) for the majority of the study domain. Although positive anomalies are observed throughout much of the study domain, these anomalies are small and are considered to be "near-normal" conditions based on the categorical boundaries (Eq. 6.2) and, therefore, the near-normal category verifying. As a result, opposing Brier skill scores are observed, with the above-normal category having a notably poor score (high probabilities that did not verify) and the below-normal category has a relatively high score (low probabilities that did not verify) (Fig. 6.9)

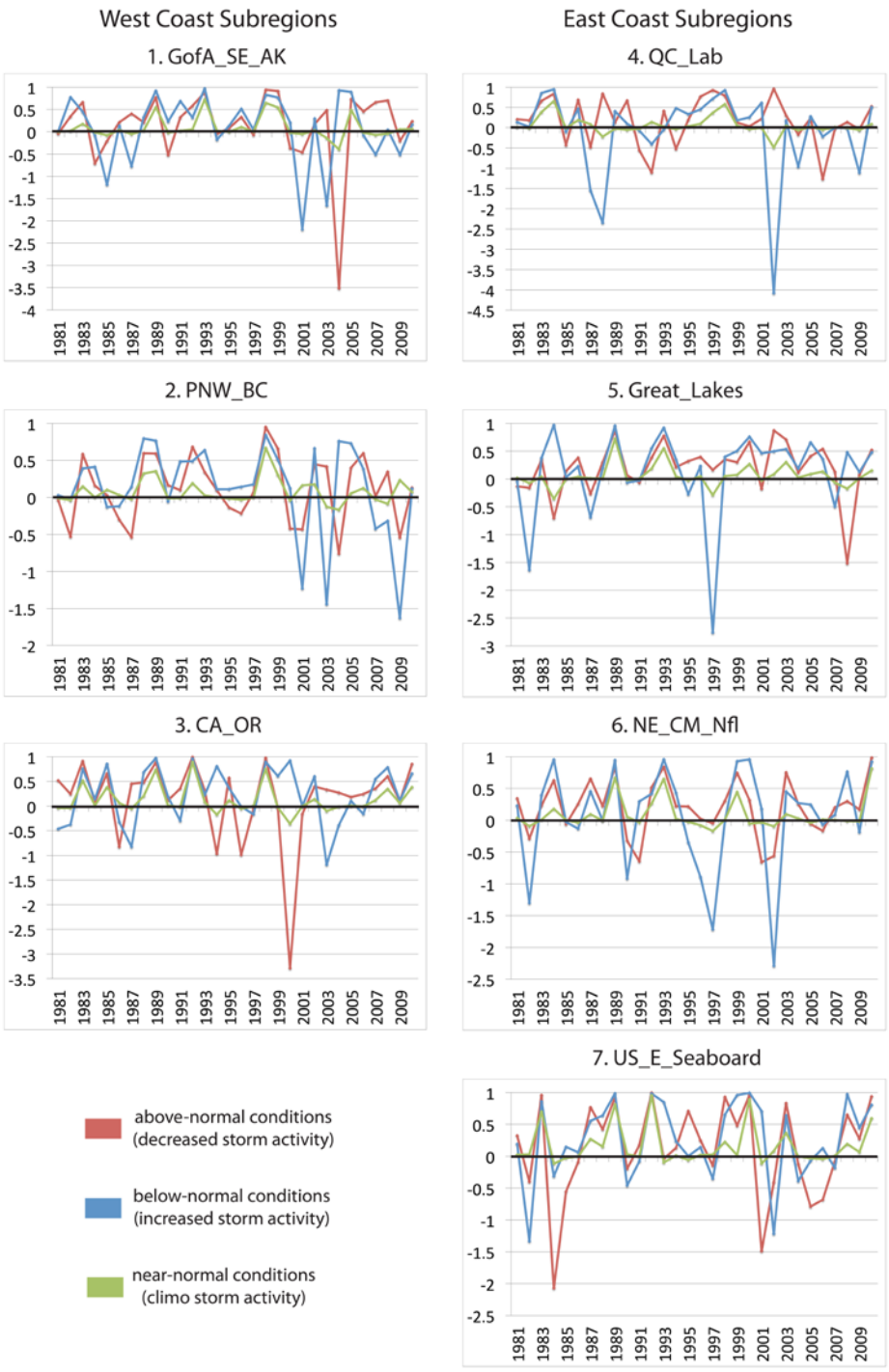

Figure 6.13: Temporal variation in forecast performance as measured by the Brier skill scores assessed for the North American west and east coast study domain subregions (Fig. 6.1; Table 6.1) for the JFM MSLP forecast

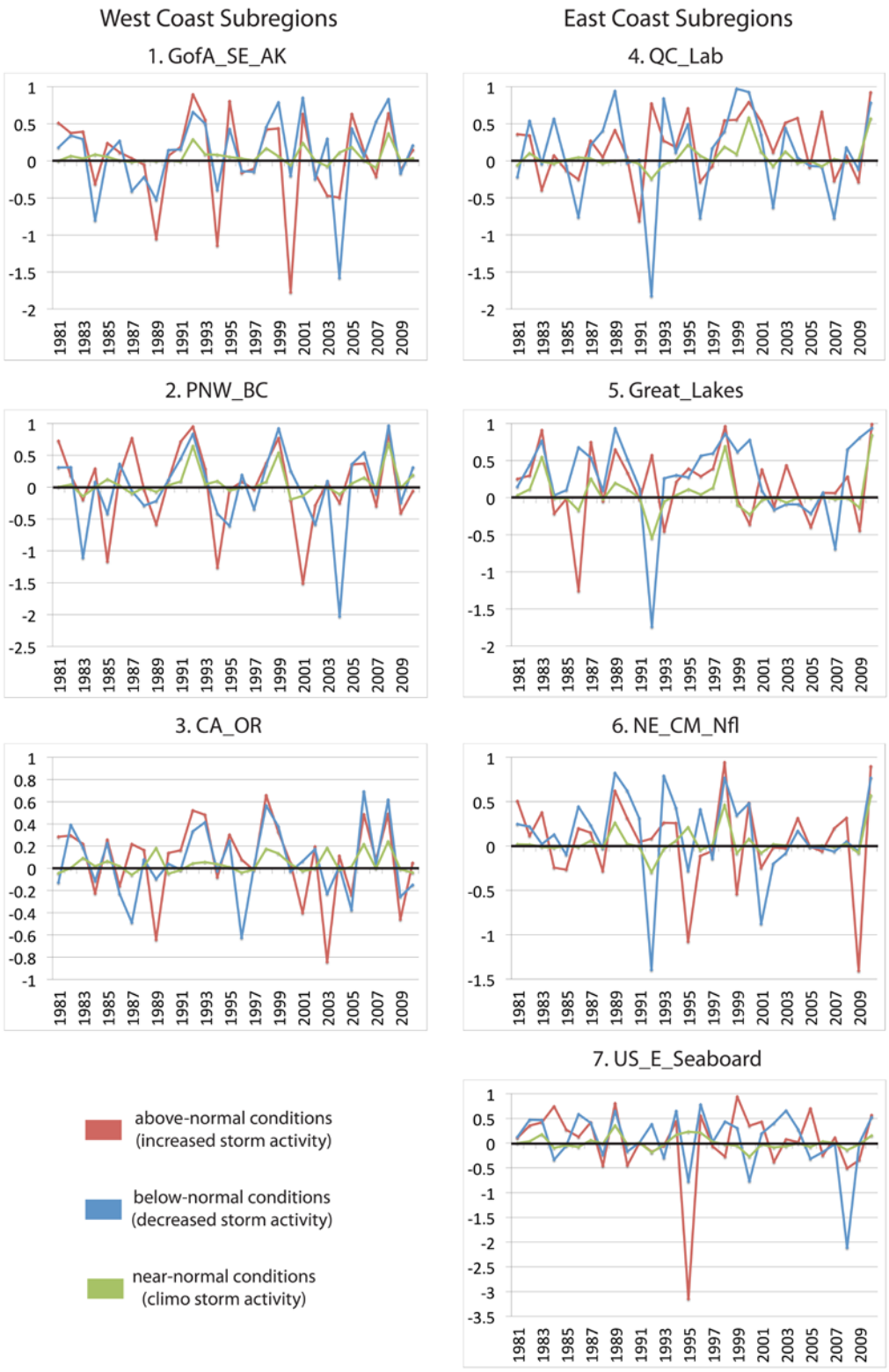

Figure 6.14: As in Fig. 6.13, except for ΔMSLP forecasts

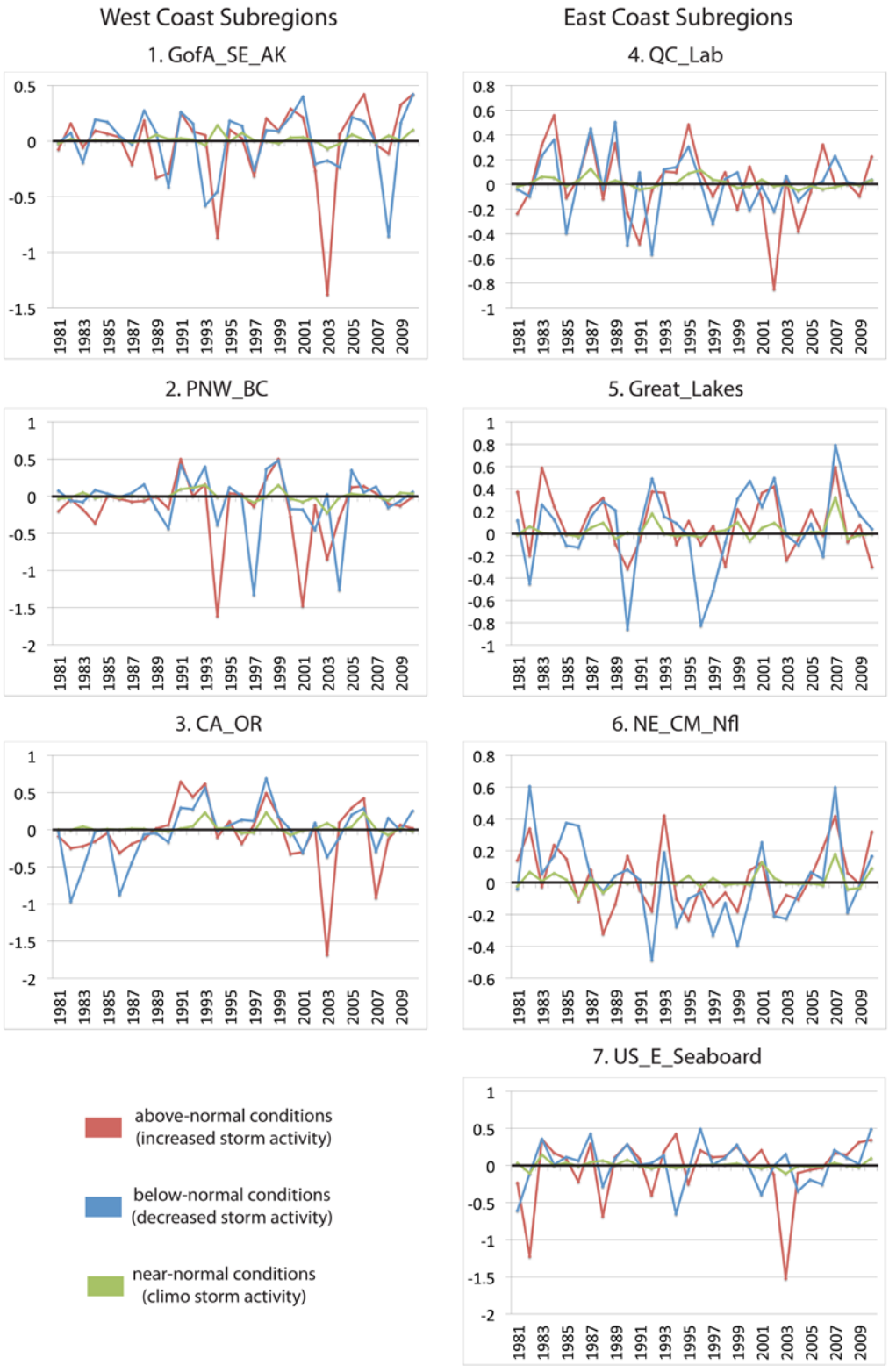

Figure 6.15: As in Fig. 6.13, except for 10-m wind speed forecasts

7.0 Conclusions

The overall objective of this research project was to determine the seasonal predictability of North American coastal extratropical storm activity during the cold months (October-March) using Environment and Climate Change Canada's operational Canadian Seasonal to Interannual Predictions System (CanSIPS), and to develop methods that could be used operationally to produce seasonal storm activity forecasts. To complete this seasonal predictability investigation, the following research questions (grouped into three research themes) were addressed:

1. *Reanalysis Representation of North American Coastal Storm Activity*
    1.1. Which global reanalysis dataset best represents North American coastal storm activity?
2. *Potential Predictability of Storm Activity and Climate Signal-Storm Activity Relationships for the North American Coastal Regions During the Cold Seasons*
    2.1. Is North American coastal storm activity potentially predictable on the seasonal timescale?
    2.2. What are the relationships between large-scale modes of climate variability and North American coastal storm activity on the seasonal timescale?
3. *Seasonal Prediction using the Canadian Seasonal to Interannual Prediction System: Can the potential predictability of North American coastal storm activity during the cold seasons be realized within the CanSIPS dynamical forecasting system?*

3.1. Are observed North American coastal climate signal-storm activity relationships reproduced in CanSIPS?

3.2. How can CanSIPS be used to produce seasonal forecasts of North American coastal storm activity?

3.3. What is the skill of the seasonal forecasts of North American coastal storm activity that can be produced using CanSIPS?

The overall conclusions of this research project are presented in Section 7.1. In Section 7.2, key findings for the Research Themes' respective research question(s) are presented. Recommendations for future work are provided in Section 7.3.

7.1 Overall Conclusions

In Research Theme 1, the ERA-Interim reanalysis was found to provide the best representation of North American coastal extratropical storm activity. ERA-Interim was then used in Research Theme 2 to determine that extratropical storm activity, as represented by mean sea level pressure (MSLP), absolute pressure tendency (ΔMSLP), and 10-m wind speeds, is potentially predictable in the North American coastal regions and that the El Niño-Southern Oscillation (ENSO), Pacific Decadal Oscillation (PDO), and North Atlantic Oscillation (NAO) are three possible sources of this detected potential predictability. Research Theme 2 provided a basis upon which seasonal forecasting of North American coastal extratropical storm activity can be developed. Finally, in Research Theme 3, quantitative deterministic, categorical deterministic, and categorical probabilistic seasonal forecasts of the extratropical storm activity proxies were constructed for the cold seasons (OND, NDJ, DJF, JFM) using the CanSIPS 1981-2010

hindcasts and evaluated against the ERA-Interim reanalysis. Baseline forecast skill was found for the seasonal forecasts of all three proxies, with MSLP forecasts found to be most skilful and, in general, 10-m wind speed forecasts the least skilful for the North American coastal regions. Skilful seasonal forecasting of North American coastal extratropical storm activity is, therefore, possible in CanSIPS and should be further pursued.

7.2 Key Findings from the Research Themes

7.2.1 Research Theme 1: Reanalysis Representation of North American Coastal Storm Activity

Reanalysis provides an invaluable tool for reconstructing historical storm activity and studying the characteristics of storm events that are identified as causing the most severe impacts. The accuracy and reliability of reanalyses differ, however, due to differences in the spatial resolution, model physics, data assimilation system, and observational data that are assimilated.

7.2.1.1 Research Question 1.1: Which global reanalysis dataset best represents North American coastal storm activity?

Research Question 1.1 investigated reanalysis representation of mid-latitude North American coastal storm activity by six global reanalyses – NCEP-1, NCEP-2, ERA-Interim MERRA, CFSR, and 20CR (ensemble mean) – on the annual and seasonal (JFM, AMJ, JAS, OND, and “extended winter” ONDJFM) timescales (Chapter 3 and Appendix A). Key findings are

- All six reanalyses successfully represent most aspects of mid-latitude North American coastal strong storm activity, annually and seasonally.
- Reanalyses using more recent data assimilation systems and model physics, more complete observational data coverage, and higher grid resolutions (i.e., ERA-Interim, MERRA, and CFSR) provide better representations.
- ERA-Interim performs best in most of the cases, particularly during "extended winter" when extratropical storm activity is most frequent and intense.
- Performance among the reanalyses is generally more consistent (i.e., smaller spread) on the west coast than the east coast.

7.2.2 Research Theme 2: Potential Predictability of Storm Activity and Climate Signal-Storm Activity Relationships for the North American Coastal Regions During the Cold Seasons

Prior to investigating seasonal forecasting methods for North American coastal storm activity, potential predictability of extratropical storm activity on the seasonal timescale was evaluated along with sources of the potential predictability using the ERA-Interim reanalysis. The detected potential predictability provides evidence, quantitative and geographical, indicative of whether it may be possible to predict variations in extratropical storm activity on the seasonal timescale. Identified possible sources (climate signal-storm activity relationships) of the detected potential predictability provide a basis upon which storm activity forecasts can be constructed. Mean sea level pressure (MSLP), absolute pressure tendency (ΔMSLP), and 10-m wind speeds are utilized as proxies to represent extratropical storm activity.

7.2.2.1 Research Question 2.1: Is North American coastal storm activity potentially predictable on the seasonal timescale?

Research Question 2.1 investigated the potential predictability of seasonal variations in extratropical storm activity for the cold seasons (OND, NDJ, DJF, JFM), during which extratopical storm activity is most frequent and intense (Chapter 4 and Appendix B). Key findings are

- Within the Northern Hemisphere (20°N-90°N), potential predictability is found in the mid- to high-latitudes in areas where extratropical storm activity is prevalent, with the strongest potentially predictable signals typically found in areas of cyclogenesis.
- Potential predictability in the North American coastal regions is greatest during the DJF and JFM seasons for MSLP and the OND season for ΔMSLP and 10-m wind speeds.
    - During these peak seasons, potentially predictable signals extent throughout the majority, if not all, of the North American coastal regions.

7.2.2.2 Research Question 2.2: What are the relationships between large-scale modes of climate variability and North American coastal storm activity on the seasonal timescale?

Research Question 2.2 investigated three large-scale climate signals (teleconnections), known to be strongly associated with extratropical storm activity, as possible sources of the potential predictability detected during the cold seasons in Research Question 2.1 (Chapter 4 and Appendix B). Composite analyses of the ETC proxies conditioned on the

teleconnection phases of the Southern Oscillation (SO; representative of the El Niño-Southern Oscillation [ENSO] teleconnection), the Pacific Decadal Oscillation (PDO), and the North Atlantic Oscillation (NAO) were evaluated. Key findings are

- The anomalous conditions highlighted in the composite analyses mirror changes in atmospheric circulation (e.g., strengths of climatological low and high pressure cells) and in extratropical storm activity (e.g., shifts in storm track location and intensity) observed between the teleconnections' phases, respectively.
- All three teleconnections are found to provide a possible source of the detected potential predictability.
- The potential predictability of the storm activity proxies originates, in large measure, with the potential predictability of the large-scale climate signals.

7.2.3 Research Theme 3: Seasonal Prediction using the Canadian Seasonal to Interannual Prediction System

Extratropical cyclones (ETCs) often produce hazardous weather conditions, such as high winds, heavy precipitation, and blizzard conditions, all of which can have detrimental socio-economic impacts. The North American coastal regions are strongly influenced by ETCs and, subsequently, land-based, coastal, and maritime economic sectors all experience strong adverse impacts from extratropical storm activity from time to time. Society would therefore benefit if seasonal variations in ETC storm activity could be skilfully predicted for the upcoming season. Skilful prediction would enable affected sectors to better anticipate, prepare for, manage, and respond to ETC storm activity and the associated risks and impacts. Mean sea level pressure (MSLP), absolute pressure

tendency (ΔMSLP), and 10-m wind speeds are utilized as proxies to represent extratropical storm activity.

7.2.3.1 Research Question 3.1: Are observed North American coastal climate signal-storm activity relationships reproduced in CanSIPS?

Research Question 3.1 investigated how well the climate signal-storm activity relationships observed in Research Question 2.2 are reproduced in CanSIPS multi-model ensemble mean during the cold seasons (OND, NDJ, DJF, JFM) (Chapter 5). By using composite analyses, the observed biases can also be attributed to the different teleconnection phases. Key findings are

- Overall, CanSIPS overestimates (higher MSLP than observed) seasonal mean MSLP in the mid-latitudes (and over Greenland and Svalbard) while underestimating (lower MSLP than observed) in the high latitudes, particularly for semi-permanent pressure cells (e.g., Aleutian Low).
    - E.g., during El Niño and neutral SO conditions (eastern Pacific), the positive PDO phase (eastern North Pacific), and the negative NAO phase (semi-permanent pressure cells in the Atlantic and Pacific).
- Seasonal average ΔMSLP is overestimated throughout much of the Northern Hemisphere, noticeably within the oceanic storm tracks and over land (and markedly in areas of high terrain).
    - E.g., during the positive PDO phase (Aleutian Low region) and the positive NAO phase (North Atlantic storm track).

- CanSIPS underestimates seasonal mean 10-m wind speeds over the mid- and high-latitude oceans and especially in the mid-latitude North Pacific and the high-latitude North Atlantic and poleward into the Arctic. Over North America, CanSIPS overestimates wind speeds, particularly in the west and central east regions.
    - E.g., during El Niño (North Atlantic and Arctic basins), the positive PDO phase (eastern-central North Atlantic), and the positive NAO phase (high-latitude North Atlantic and the Greenland/Norwegain Seas region).
- CanSIPS reproduces the SO and PDO indices but fails to reproduce the NAO index.

7.2.3.2 Research Question 3.2: How can CanSIPS be used to produce seasonal forecasts of North American coastal storm activity?

Research Question 3.2 investigated the construction of zero-month lead quantitative deterministic, categorical deterministic, and categorical probabilistic seasonal forecasts of the three storm activity proxies from the 1981-2010 CanSIPS multi-model ensemble mean hindcasts for the cold seasons (OND, NDJ, DJF, JFM; during which extratropical storm activity is most frequent and intense and, arguably, the most hazardous) (Chapter 6). Key findings are

- Forecast interpretation of the ΔMSLP and 10-m wind speed forecasts is straightforward (and similar to that of the current operational temperature and precipitation seasonal forecasts) – an above-normal conditions forecast represents an increased seasonal mean absolute pressure tendency and wind speed,

respectively, and therefore suggests an increase in storm activity during the coming season and vice versa for below-normal conditions.

    - Seasonal mean ΔMSLP and 10-m wind speed forecasts provide information on storm activity intensity (e.g., enhanced cyclogenesis and/or stronger pressure gradients).

- Forecast interpretation of the MSLP forecasts is slightly counterintuitive, as a below-normal conditions forecast represents a lower seasonal mean pressure and therefore would suggest an increase in storm activity during the coming season and vice versa for above-normal conditions.
    - Seasonal mean MSLP forecasts provide information on storm activity frequency and/or duration of stormy conditions
- Forecasts for all three storm activity proxies should be considered together when determining the predicted storm activity conditions for the coming season as storm activity cannot be summarized in a single variable.

7.2.3.3 Research Question 3.3: What is the skill of the seasonal forecasts of North American coastal storm activity that can be produced using CanSIPS?

Research Question 3.3 investigated the skill of the CanSIPS seasonal forecasts constructed in Research Question 3.2 and whether that skill is sufficiently high (i.e., exceeding the climatological reference forecast) to be useful to end-users (Chapter 6 and Appendix C). The CanSIPS seasonal forecasts were evaluated against ERA-Interim, using the correlation skill score to evaluate the quantitative deterministic forecasts, the

percent correct score to evaluate the categorical deterministic forecasts, and the Brier skill score (BSS) to evaluate the probabilistic forecasts. Key findings are

- CanSIPS has skill producing seasonal forecasts of North American coastal extratropical storm activity, represented by MSLP, ΔMSLP, and 10-m wind speed.
- Overall, forecasts are most skilful in the later seasons (DJF and JFM), with the MSLP forecasts generally being most skilful, followed by the ΔMSLP forecasts, and then by the 10-m wind speed forecasts.
    - MSLP forecasts have high skill over land and ocean.
    - ΔMSLP forecasts have considerably higher skill over the North American continent than over the oceans.
    - 10-m wind speed forecasts have notably high skill in the mid-latitudes over the North Pacific.
- CanSIPS is most skilful in producing probabilistic forecasts for the above-normal and below-normal categories and, in general, has similar skill to that of the climatological forecast for the near-normal forecast category.
- Within both North America study domains, peak correlation skill and percent correct scores correspond with areas strongly influenced by extratropical storm activity (e.g., where the exit region of the North Pacific storm track impacts the North American west coast and the Eastern Seaboard storm track). Plots of the BSS assessed over the 30-year seasonal hindcast sequences reveal similar patterns.
- BSS assessed for the North American coastal domains provide insight into the temporal variation in CanSIPS' categorical probabilistic forecast performance:

- Well-forecast seasons and opposing BSS values seasons (seasons in which near-normal conditions were observed therefore resulting in a skilful BSS value for the forecast category with low probabilities but a poor BSS value for the forecast category with high probabilities) comprise the majority of the 30-year hindcast, therefore suggesting minimal overall underperformance by CanSIPS and the ability to provide at least some guidance to end-users. Arguably, being able to remove one extreme (increased or decreased storm activity) would be beneficial to end-users when planning for the coming season.

- The seasonal forecasts were developed without the inclusion of calibration (included operationally) and/or statistical adjustment during post-processing, therefore, forecast skill found is considered baseline skill.

While primary focus was on the CanSIPS multi-model ensemble mean results (Chapter 6), seasonal prediction skill for CanCM3 and CanCM4 was also evaluated (presented in Appendix C). CanCM3 and CanCM4 seasonal forecasts were constructed using the respective model's ensemble mean.

7.3 Recommendations for Future Work

Future work that could be undertaken to further the investigation of seasonal predictability of North American coastal extratropical storm activity using CanSIPS and the development of methods that can used operationally to produce seasonal storm activity forecasts includes the following:

- *Evaluation of additional extratropical storm activity proxies*. Extratropical storm activity cannot be described completely using only the three at or near-surface proxies (mean sea level pressure, absolute pressure tendency, and 10-m wind speeds) evaluated in this research project. The inclusion of additional proxies, including those at upper-air levels, would provide a more comprehensive understanding of the seasonal predictability of North American coastal extratropical storm activity.
- *Evaluation of additional large-scale climate signals (teleconnections) as possible sources of the detected potential predictability*. Not all of the possible sources of potential predictability can be accounted for using only the three climate signals (SO [representative of ENSO], PDO, and NAO) evaluated in this research project. Additional large-scale and more regional-scale teleconnections (e.g., Arctic Oscillation and Pacific/North American pattern) are also known to be strongly associated with North American coastal extratropical storm activity. Identifying additional possible sources of the detected potential predictability would provide a stronger basis upon which seasonal forecasting for the North American coastal regions can be developed.
- *Identify and consult with potential end-users of seasonal storm activity forecasts.* Potential end-users can provide recommendations and guidance for the future direction of the seasonal predictability investigation and continued development of methods for extratropical storm activity seasonal forecasting. Subsequently,

the investigation can also, therefore, be expanded to include forecasting user specific impacts (e.g., flooding) that are the result of extratropical storm activity.

- *Inclusion of a calibration coefficient during the development of seasonal forecasts*. In this research project, seasonal forecasts were constructed from the raw CanSIPS data and then evaluated as is. Operationally, however, during the development of the temperature and precipitation seasonal forecasts, a calibration coefficient is also calculated from the 30-year hindcast and used to optimally rescale the multi-model ensemble mean anomaly and ensemble spread. Inclusion of a calibration coefficient in the development of seasonal forecasts of North American coastal storm activity could, therefore, be expected to improve the subsequent skill scores.
- *Investigation of the application of statistical adjustment during post-processing of seasonal forecasts*. Along with including a calibration coefficient during the development of storm activity seasonal forecasts, statistical adjustments based on observed relationships could potentially be applied during post-processing as well to further help improve skill levels for the North American coastal regions.
- *Expansion of study domains to include all of North America*. This research project focused on the North American coastal regions, which are strongly influenced by extratropical storm activity and are highly populated, socio-economically key, and environmentally sensitive areas. The Canadian Meteorological Centre (CMC), however, issues operational seasonal forecasts of average temperature and total precipitation Canada-wide. Extending the seasonal predictability of extratropical

storm activity investigation to include all of North America would, therefore, be another step toward operational usage consistent with that of CMC while continuing to allow forecast skill for Canada to be placed into context with regard to North America.

- *Expand the investigation of seasonal predictability of North American coastal extratropical storm activity to include additional modelling systems through the North American Multimodel Ensemble prediction experiment*[2]. The inclusion of additional modelling systems in the development of seasonal forecasts should further reduce model-related error, resolve uncertainty, and produce more skilful forecasts of the storm activity proxies. The Canadian Meteorological Centre (CMC) contributes CanCM3 and CanCM4 data to the North American Multimodel Ensemble forecasting project along with various modelling centres in the USA.

[2] Kirtman et al. (2014) The North American Multimodel Ensemble: Phase-I Seasonal-to-Interannual Prediction; Phase-2 toward Developing Intraseasonal Prediction. *Bull. Am. Meteorol. Soc.*, 95(4): 585-601.

Appendix A

Additional Research Theme 1 Figures and Tables

Appendix A provides additional figures and tables from the evaluation of reanalysis representation of mid-latitude North American coastal storm activity (Research Theme 1) not presented in Chapter 3.

A.1 Additional Count/Frequency-Based Proxies (PR980 and APT12) Results

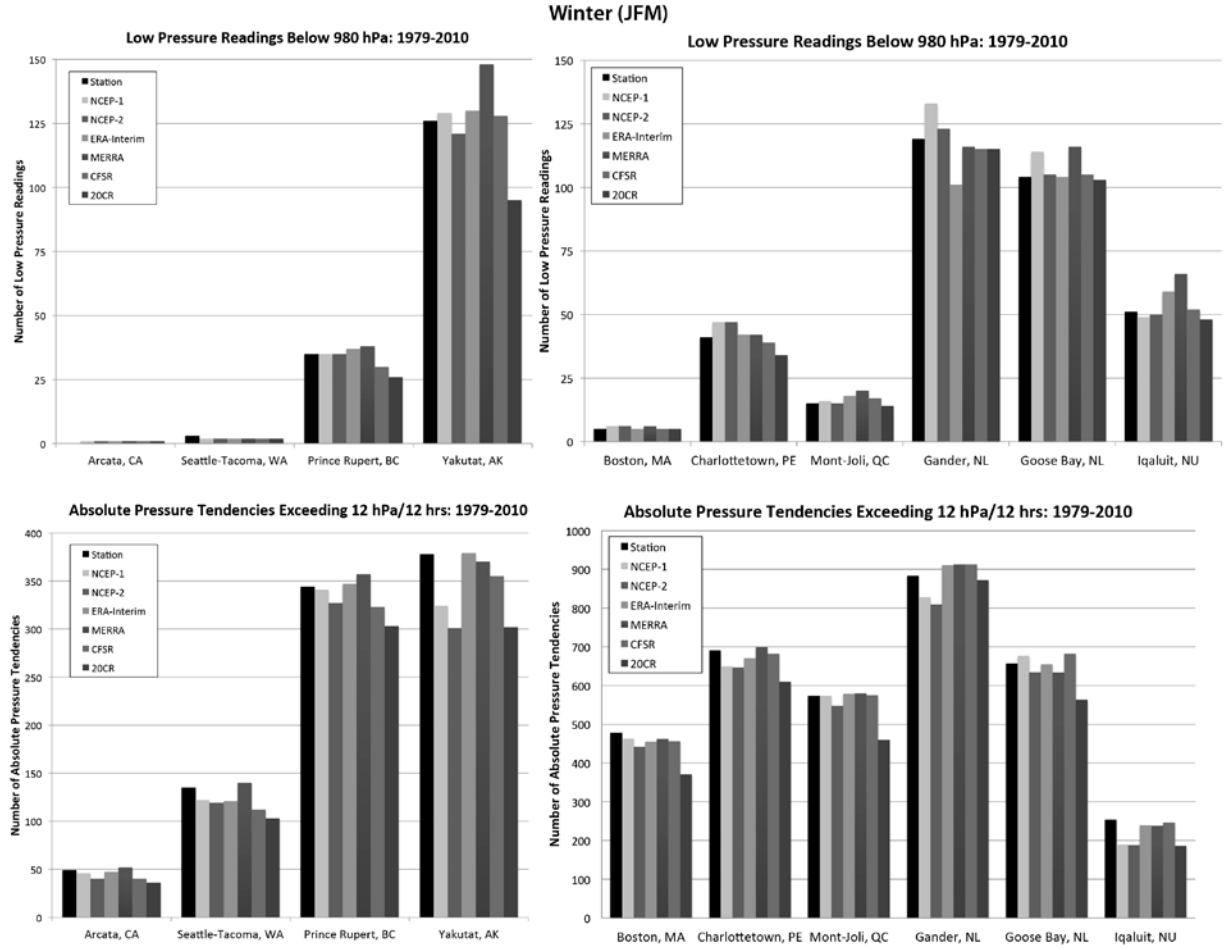

Figure A.1: Comparison of reanalysis detection of winter (JFM) strong storm activity along the mid-latitude North American west (left) and east (right) coasts as represented by the number of low pressure readings below 980 hPa (top) and the frequency of absolute pressure tendencies above 12 hPa/12 h (bottom).

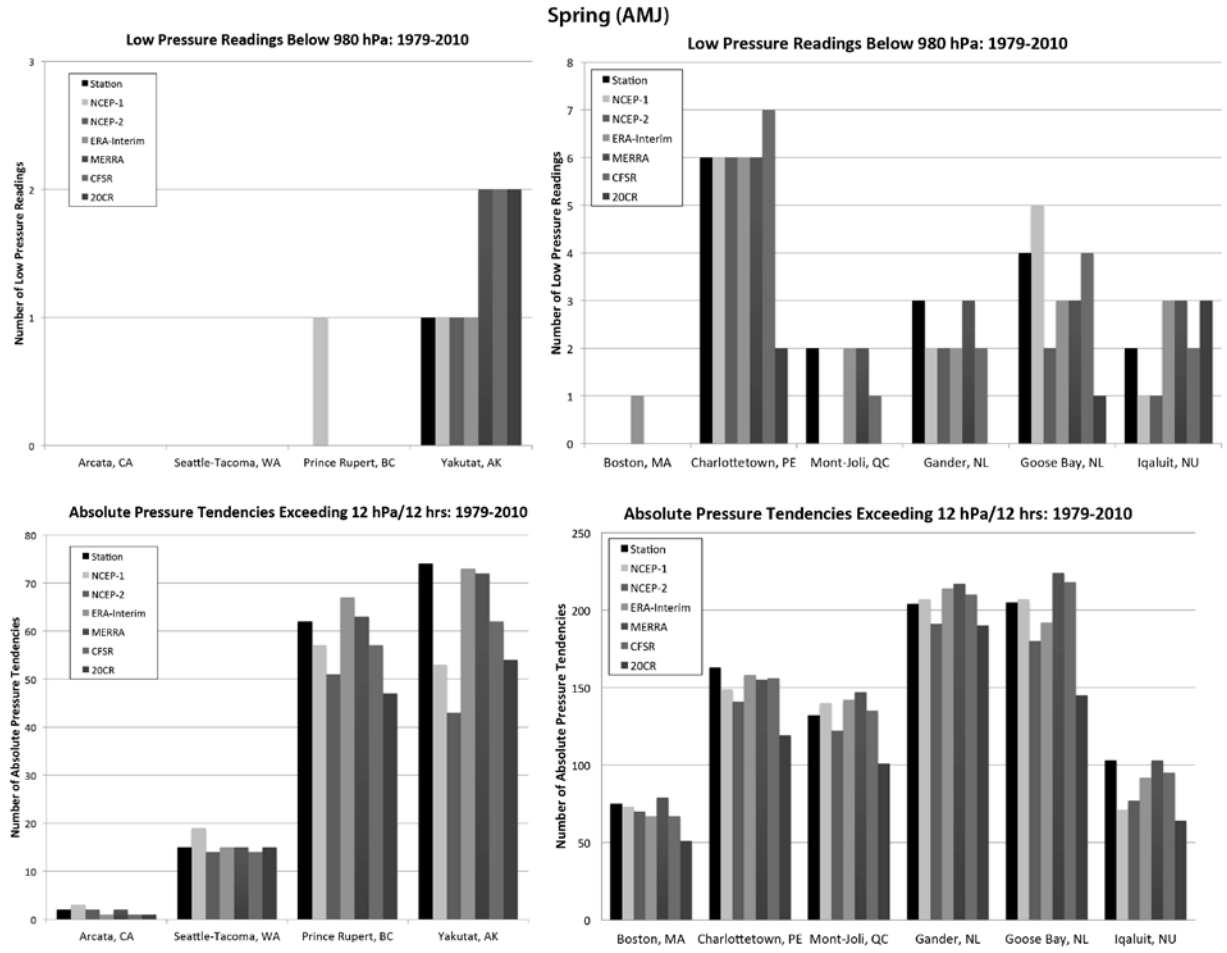

Figure A.2: As in Figure A.1, except for spring (AMJ).

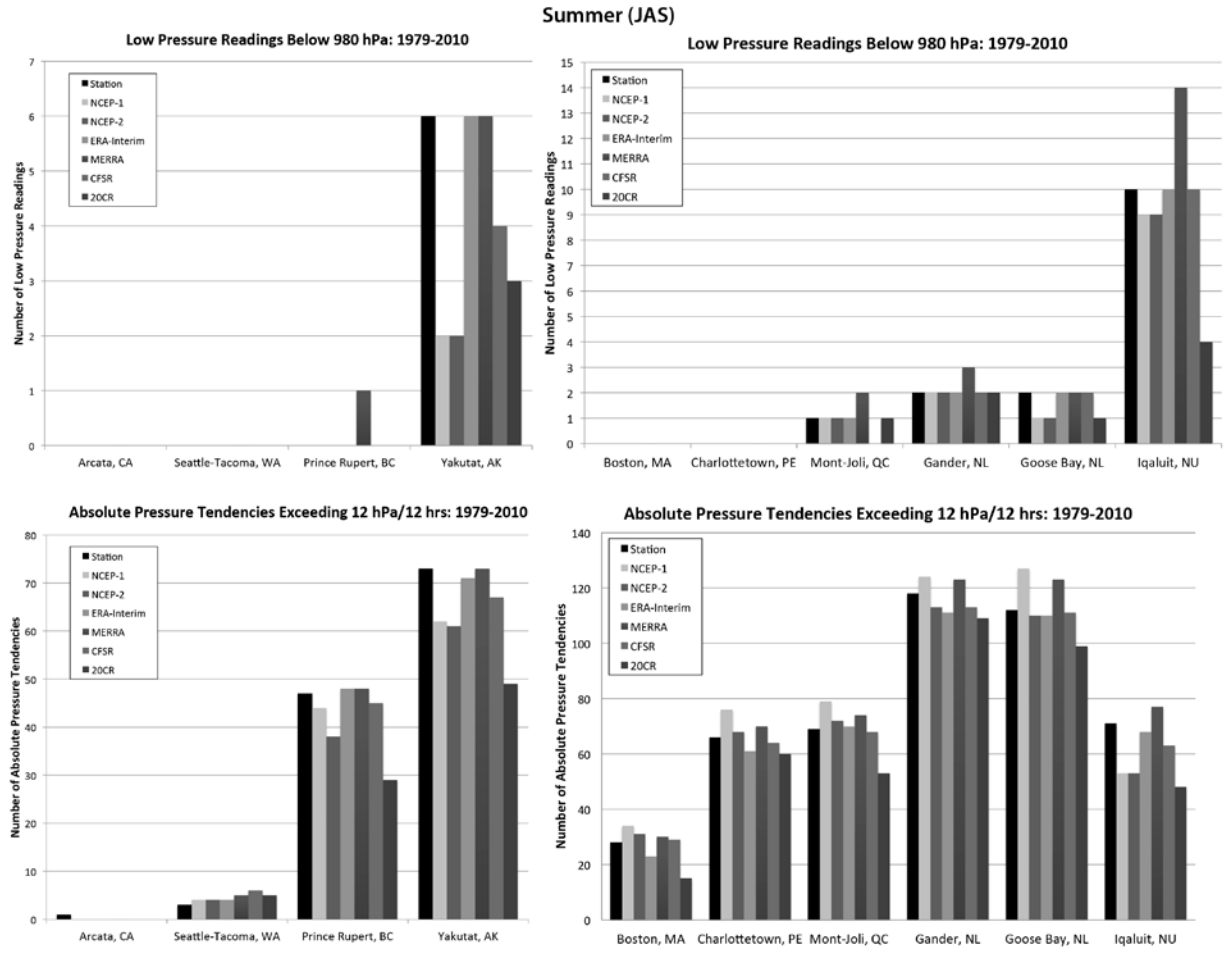

Figure A.3: As in Figure A.1, except for summer (JAS).

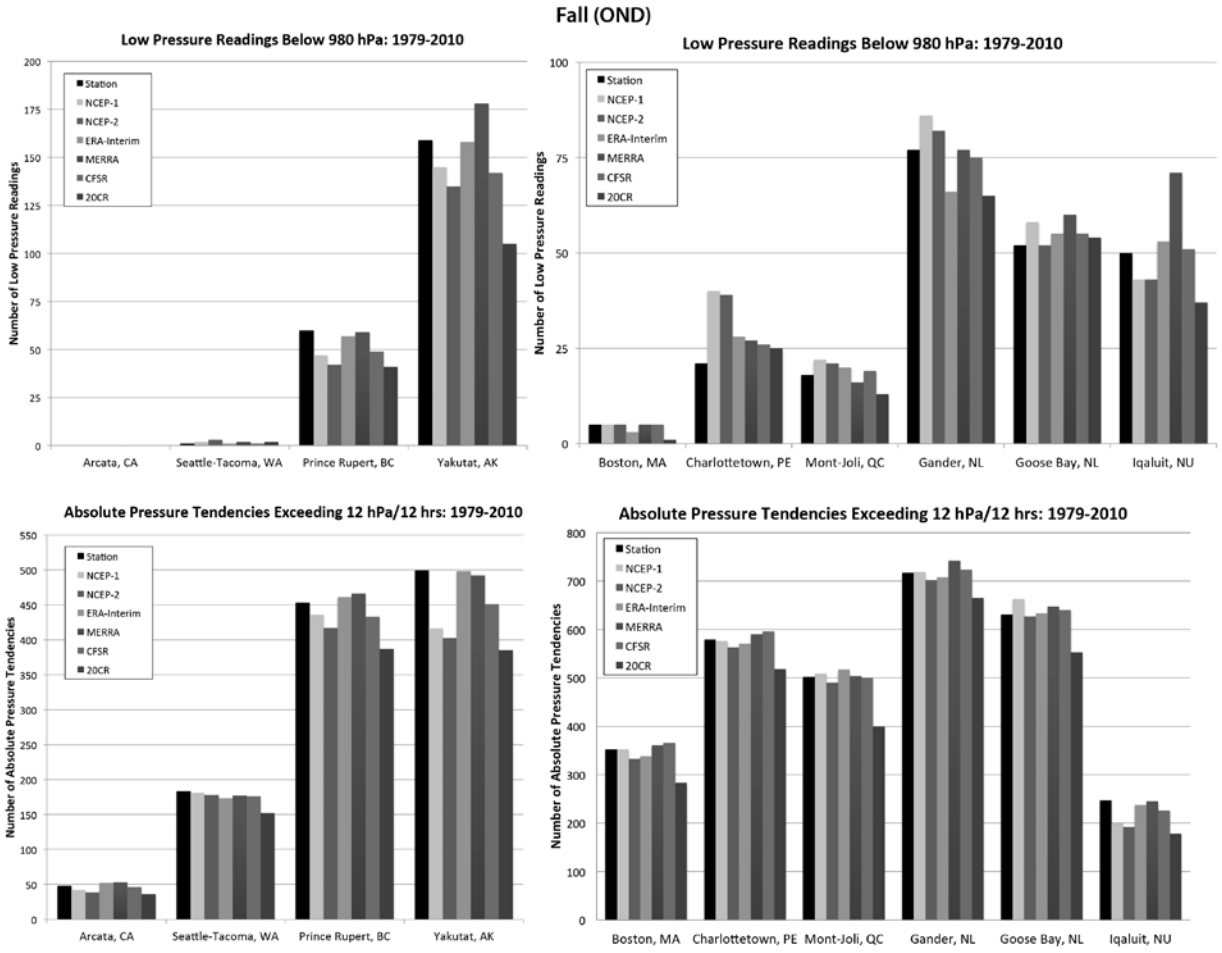

Figure A.4: As in Figure A.1, except for fall (OND).

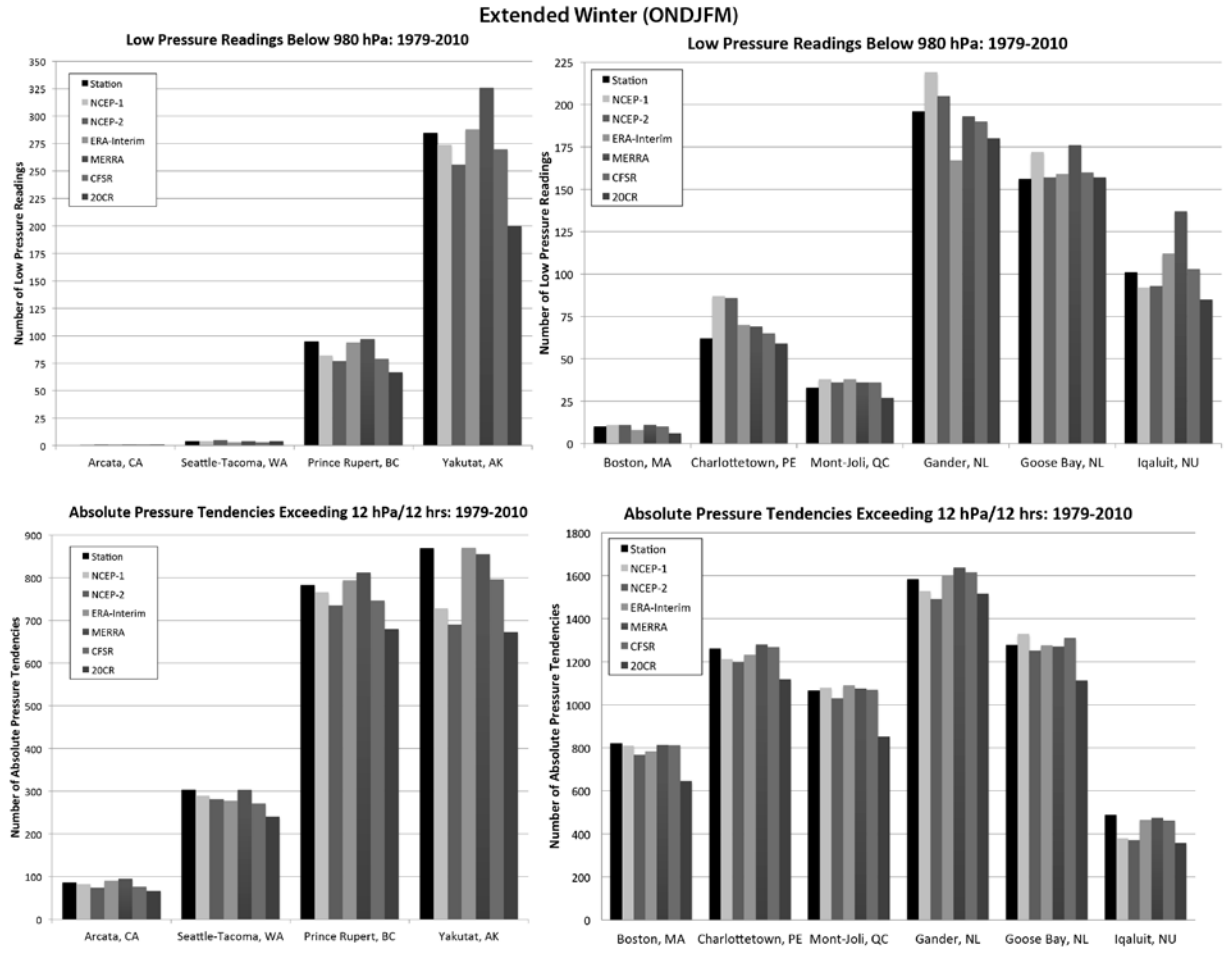

Figure A.5: As in Figure A.1, except for extended winter (ONDJFM).

A.2 Additional Percentile-Based Proxies (1PR and 99APT) Results

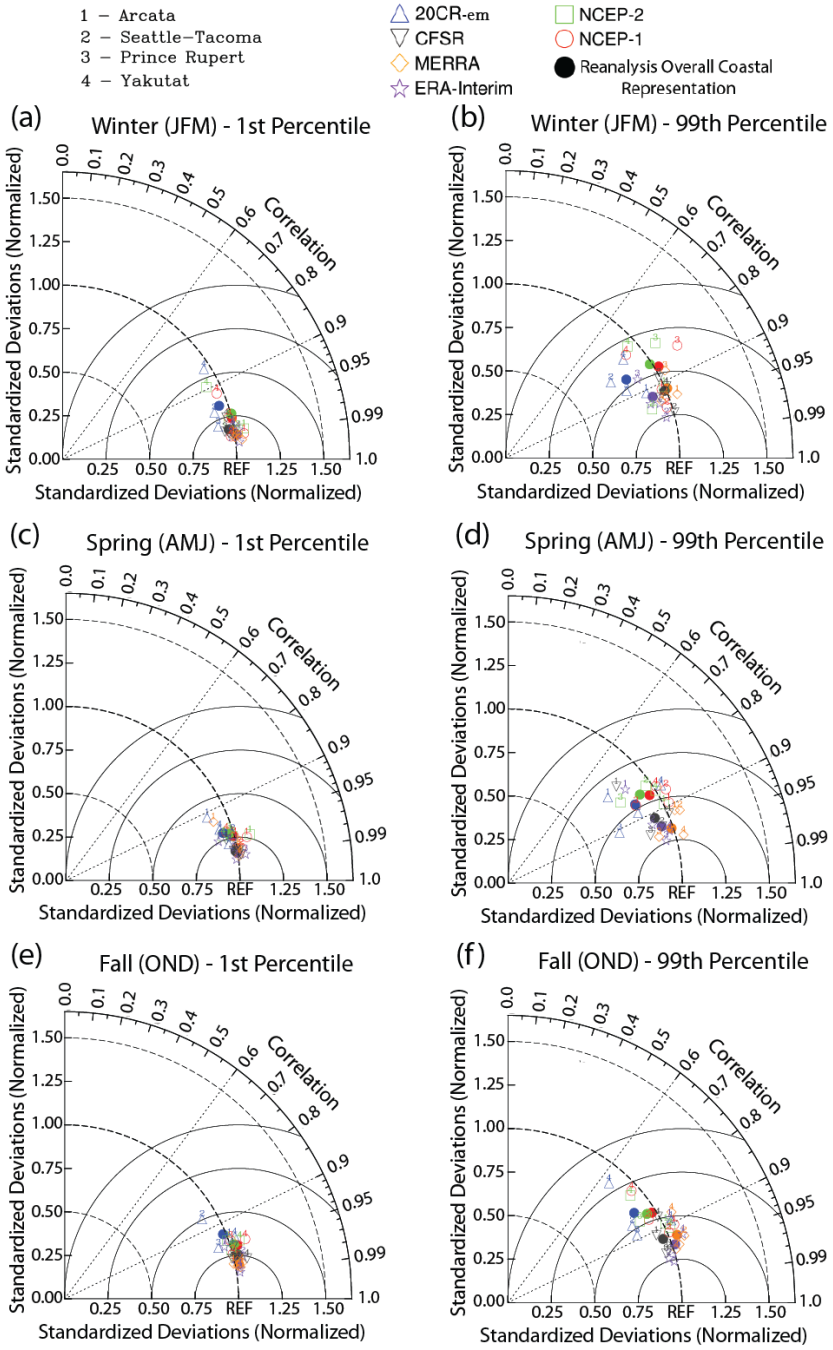

Figure A.6: Taylor diagrams comparing reanalysis representation of strong storm activity along the mid-latitude North American west coast for the winter (JFM; top), spring (AMJ; middle), and fall (OND; bottom) seasons using (a, c, and e) first percentile of pressure readings and (b, d, and f) 99th percentile of absolute pressure tendencies proxies, respectively. Associated reanalysis representation skill scores are presented in Tables A.1-A.3.

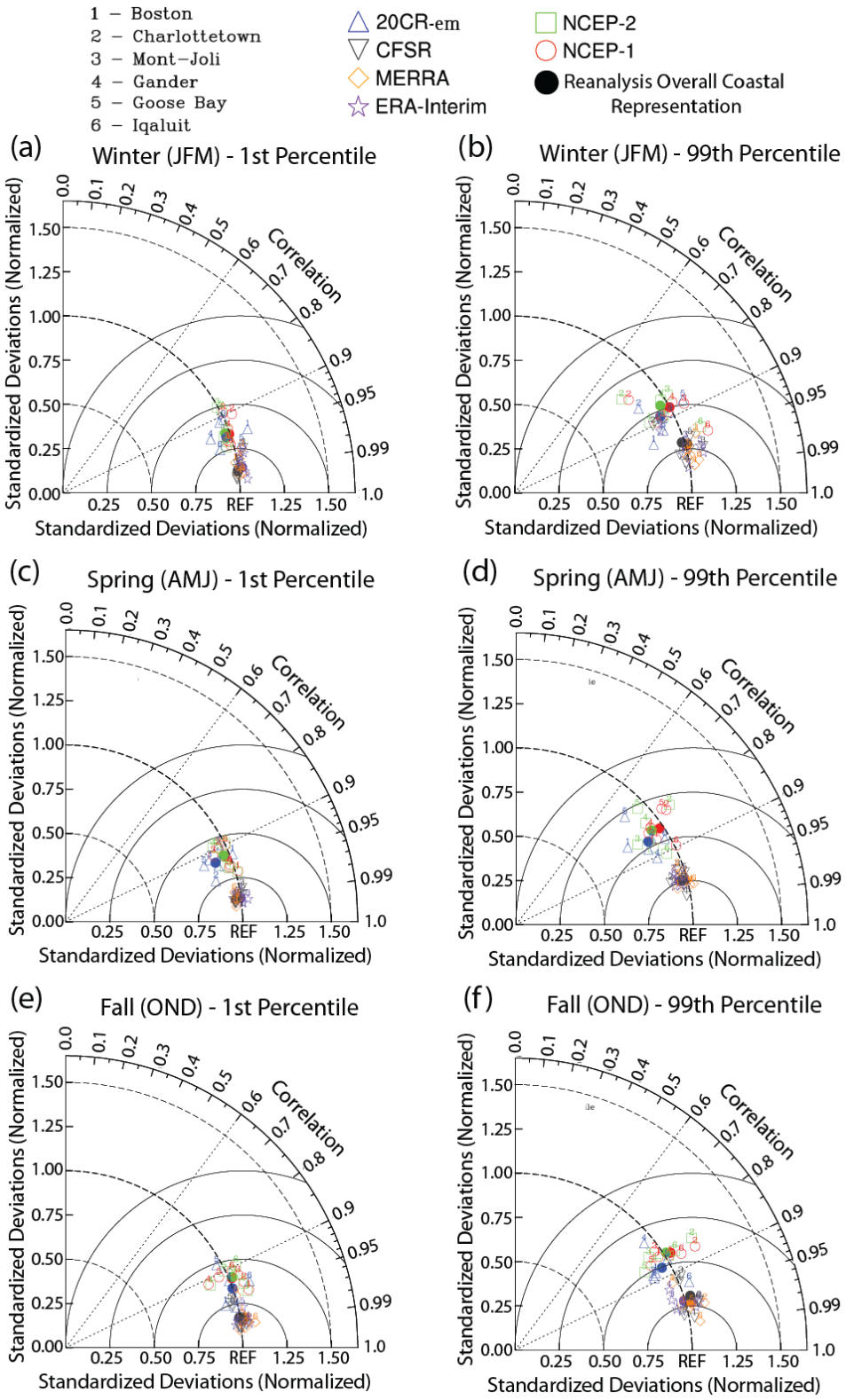

Figure A.7: As in Figure A.6, except for the mid-latitude North American east coast. Associated reanalysis representation skill scores are presented in Tables A.4-A.6.

(a)	***Winter 1st Percentile Skill Scores***					
	NCEP-1	NCEP-2	ERA-Interim	MERRA	CFSR	20CR
Arcata, CA	0.98	0.97	0.98	0.99	0.98	0.96
Seattle-Tacoma, WA	0.98	0.97	0.99	0.98	0.98	0.91
Prince-Rupert, BC	0.94	0.95	0.96	0.98	0.97	0.95
Yakutat, AK	0.85	0.80	0.97	0.96	0.94	0.72
Overall Coastal Representation	0.94	0.93	0.98	0.98	0.97	0.89
(b)	***Winter 99th Percentile Skill Scores***					
	NCEP-1	NCEP-2	ERA-Interim	MERRA	CFSR	20CR
Arcata, CA	0.84	0.83	0.89	0.88	0.87	0.82
Seattle-Tacoma, WA	0.91	0.89	0.94	0.88	0.93	0.62
Prince-Rupert, BC	0.69	0.64	0.73	0.77	0.79	0.73
Yakutat, AK	0.59	0.57	0.87	0.88	0.84	0.60
Overall Coastal Representation	0.74	0.71	0.85	0.85	0.85	0.69

Table A.1: Skill scores (associated with Figure A.6a,b Taylor diagrams) for the winter (JFM) seasonal reanalysis representation of strong storm activity along the mid-latitude North American west coast using the (a) 1st percentile of pressure readings and (b) 99th percentile of absolute pressure tendencies proxies.

(c)	***Spring 1st Percentile Skill Scores***					
	NCEP-1	NCEP-2	ERA-Interim	MERRA	CFSR	20CR
Arcata, CA	0.94	0.94	0.93	0.86	0.94	0.83
Seattle-Tacoma, WA	0.97	0.93	0.96	0.96	0.98	0.93
Prince-Rupert, BC	0.94	0.92	0.98	0.98	0.98	0.95
Yakutat, AK	0.92	0.92	0.98	0.98	0.97	0.90
Overall Coastal Representation	0.93	0.92	0.97	0.96	0.97	0.91
(d)	***Spring 99th Percentile Skill Scores***					
	NCEP-1	NCEP-2	ERA-Interim	MERRA	CFSR	20CR
Arcata, CA	0.80	0.80	0.61	0.84	0.56	0.55
Seattle-Tacoma, WA	0.74	0.68	0.85	0.85	0.88	0.76
Prince-Rupert, BC	0.72	0.64	0.93	0.91	0.88	0.74
Yakutat, AK	0.71	0.73	0.90	0.93	0.84	0.72
Overall Coastal Representation	0.73	0.70	0.88	0.90	0.83	0.72

Table A.2: As in Table A.1, except for the spring (AMJ) seasonal reanalysis representation evaluation (associated with Figure A.6c,d Taylor diagrams).

(e)	***Fall 1st Percentile Skill Scores***					
	NCEP-1	NCEP-2	ERA-Interim	MERRA	CFSR	20CR
Arcata, CA	0.94	0.94	0.90	0.96	0.91	0.88
Seattle-Tacoma, WA	0.93	0.92	0.94	0.96	0.95	0.75
Prince-Rupert, BC	0.89	0.89	0.98	0.97	0.94	0.90
Yakutat, AK	0.90	0.90	0.97	0.96	0.95	0.88
Overall Coastal Representation	0.91	0.91	0.95	0.96	0.94	0.86
(f)	***Fall 99th Percentile Skill Scores***					
	NCEP-1	NCEP-2	ERA-Interim	MERRA	CFSR	20CR
Arcata, CA	0.82	0.80	0.79	0.90	0.83	0.80
Seattle-Tacoma, WA	0.84	0.83	0.93	0.87	0.91	0.71
Prince-Rupert, BC	0.75	0.73	0.94	0.91	0.91	0.77
Yakutat, AK	0.57	0.59	0.86	0.77	0.76	0.46
Overall Coastal Representation	0.73	0.72	0.89	0.86	0.86	0.67

Table A.3: As in Table A.1, except for the fall (OND) seasonal reanalysis representation evaluation (associated with Figure A.6e,f Taylor diagrams).

(a)	***Winter 1st Percentile Skill Scores***					
	NCEP-1	NCEP-2	ERA-Interim	MERRA	CFSR	20CR
Boston, MA	0.91	0.89	0.95	0.97	0.98	0.89
Charlottetown, PE	0.82	0.79	0.97	0.96	0.97	0.83
Mont-Joli, QC	0.80	0.77	0.95	0.94	0.94	0.83
Gander, NL	0.87	0.87	0.98	0.99	0.99	0.87
Goose Bay, NL	0.93	0.93	0.98	0.99	0.99	0.93
Iqaluit, NU	0.92	0.91	0.99	0.99	0.99	0.93
Overall Coastal Representation	0.89	0.88	0.98	0.98	0.98	0.90
(b)	***Winter 99th Percentile Skill Scores***					
	NCEP-1	NCEP-2	ERA-Interim	MERRA	CFSR	20CR
Boston, MA	0.80	0.77	0.95	0.96	0.95	0.86
Charlottetown, PE	0.60	0.56	0.84	0.80	0.80	0.68
Mont-Joli, QC	0.78	0.72	0.91	0.90	0.93	0.79
Gander, NL	0.76	0.72	0.98	0.98	0.97	0.80
Goose Bay, NL	0.79	0.80	0.93	0.96	0.91	0.76
Iqaluit, NU	0.89	0.88	0.95	0.97	0.94	0.84
Overall Coastal Representation	0.77	0.74	0.93	0.93	0.92	0.79

Table A.4: Skill scores (associated with Figure A.7a,b Taylor diagrams) for the winter (JFM) seasonal reanalysis representation of strong storm activity along the mid-latitude North American east coast using the (a) 1st percentile of pressure readings and (b) 99th percentile of absolute pressure tendencies proxies.

(c)	***Spring 1st Percentile Skill Scores***					
	NCEP-1	NCEP-2	ERA-Interim	MERRA	CFSR	20CR
Boston, MA	0.92	0.92	0.97	0.98	0.99	0.86
Charlottetown, PE	0.81	0.81	0.98	0.98	0.98	0.92
Mont-Joli, QC	0.83	0.80	0.98	0.99	0.96	0.83
Gander, NL	0.89	0.89	0.98	0.99	0.99	0.80
Goose Bay, NL	0.90	0.90	0.99	0.98	0.99	0.84
Iqaluit, NU	0.82	0.81	0.99	0.97	0.98	0.88
Overall Coastal Representation	0.86	0.85	0.98	0.98	0.98	0.86
(d)	***Spring 99th Percentile Skill Scores***					
	NCEP-1	NCEP-2	ERA-Interim	MERRA	CFSR	20CR
Boston, MA	0.73	0.76	0.94	0.95	0.97	0.64
Charlottetown, PE	0.65	0.63	0.90	0.89	0.92	0.71
Mont-Joli, QC	0.68	0.68	0.92	0.92	0.90	0.75
Gander, NL	0.67	0.63	0.94	0.95	0.95	0.81
Goose Bay, NL	0.63	0.55	0.92	0.92	0.91	0.52
Iqaluit, NU	0.81	0.82	0.95	0.95	0.93	0.76
Overall Coastal Representation	0.70	0.68	0.93	0.94	0.93	0.72

Table A.5: As in Table A.4, except for the spring (AMJ) seasonal reanalysis representation evaluation (associated with Figure A.7c,d Taylor diagrams).

(e)	***Fall 1st Percentile Skill Scores***					
	NCEP-1	NCEP-2	ERA-Interim	MERRA	CFSR	20CR
Boston, MA	0.90	0.91	0.98	0.96	0.99	0.93
Charlottetown, PE	0.88	0.88	0.98	0.98	0.98	0.92
Mont-Joli, QC	0.85	0.84	0.99	0.99	0.98	0.95
Gander, NL	0.83	0.84	0.98	0.99	0.99	0.86
Goose Bay, NL	0.83	0.81	0.95	0.92	0.93	0.78
Iqaluit, NU	0.83	0.81	0.98	0.98	0.94	0.88
Overall Coastal Representation	0.85	0.85	0.98	0.97	0.97	0.89
(f)	***Fall 99th Percentile Skill Scores***					
	NCEP-1	NCEP-2	ERA-Interim	MERRA	CFSR	20CR
Boston, MA	0.71	0.73	0.94	0.95	0.97	0.77
Charlottetown, PE	0.74	0.70	0.93	0.93	0.93	0.77
Mont-Joli, QC	0.68	0.68	0.90	0.93	0.84	0.78
Gander, NL	0.74	0.74	0.87	0.85	0.86	0.61
Goose Bay, NL	0.72	0.72	0.95	0.94	0.96	0.75
Iqaluit, NU	0.75	0.73	0.94	0.97	0.93	0.87
Overall Coastal Representation	0.73	0.72	0.92	0.93	0.91	0.77

Table A.6: As in Table A.4, except for the fall (OND) seasonal reanalysis representation evaluation (associated with Figure A.7e,f Taylor diagrams).

Appendix B

Additional Research Theme 2 Figures

Appendix B provides additional figures from the Northern Hemisphere extratropical storm activity potential predictability and its sources investigation (Research Theme 2) not presented in Chapter 4.

B.1 Additional Potential Predictability Figures

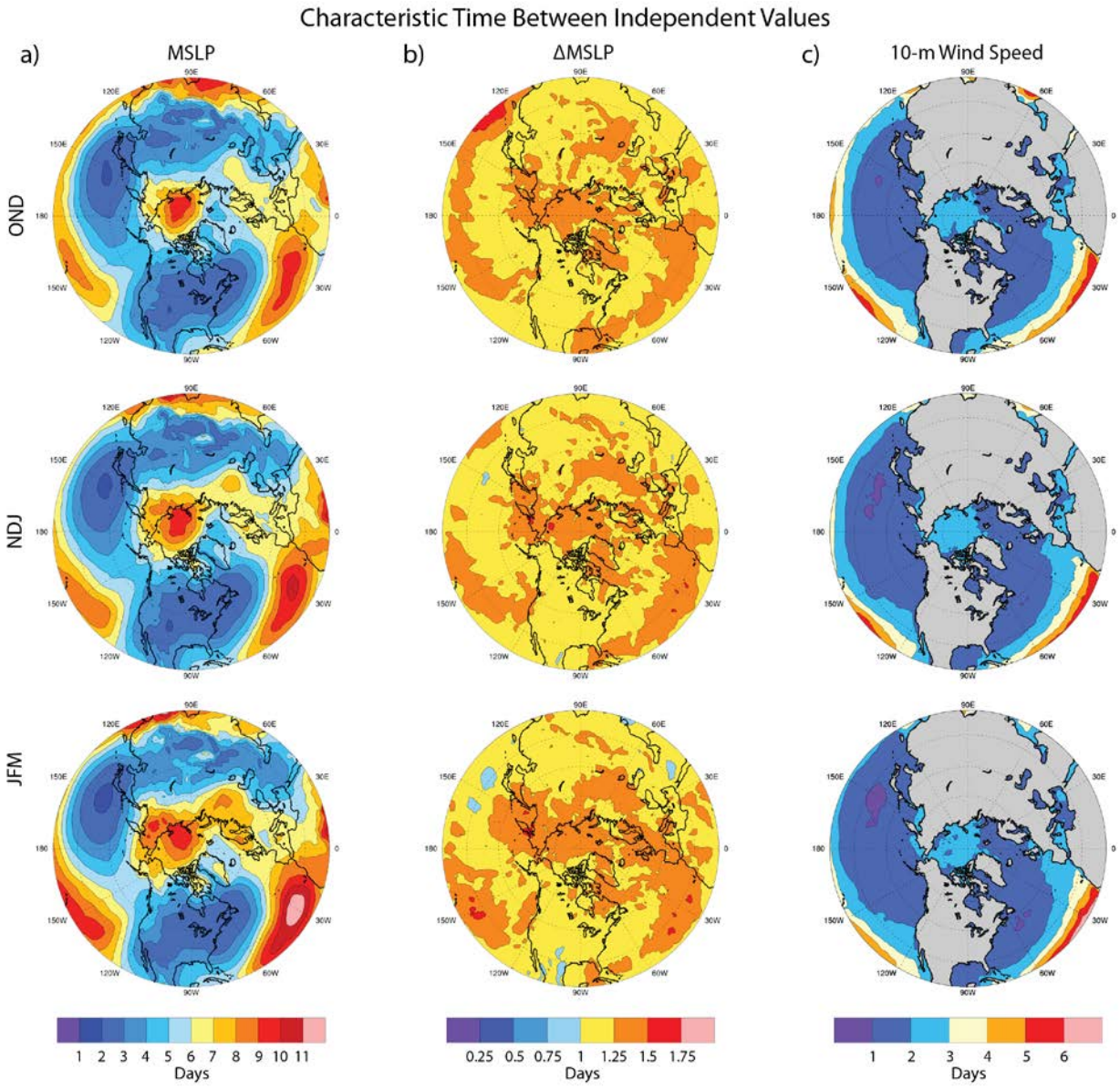

Figure B.1: Northern Hemisphere (20°N-poleward) characteristic time between independent values for OND (top), NDJ (middle), and JFM (bottom) for a) MSLP, b) ΔMSLP, and c) 10-m wind speeds (with ERA-Interim landmass overlay).

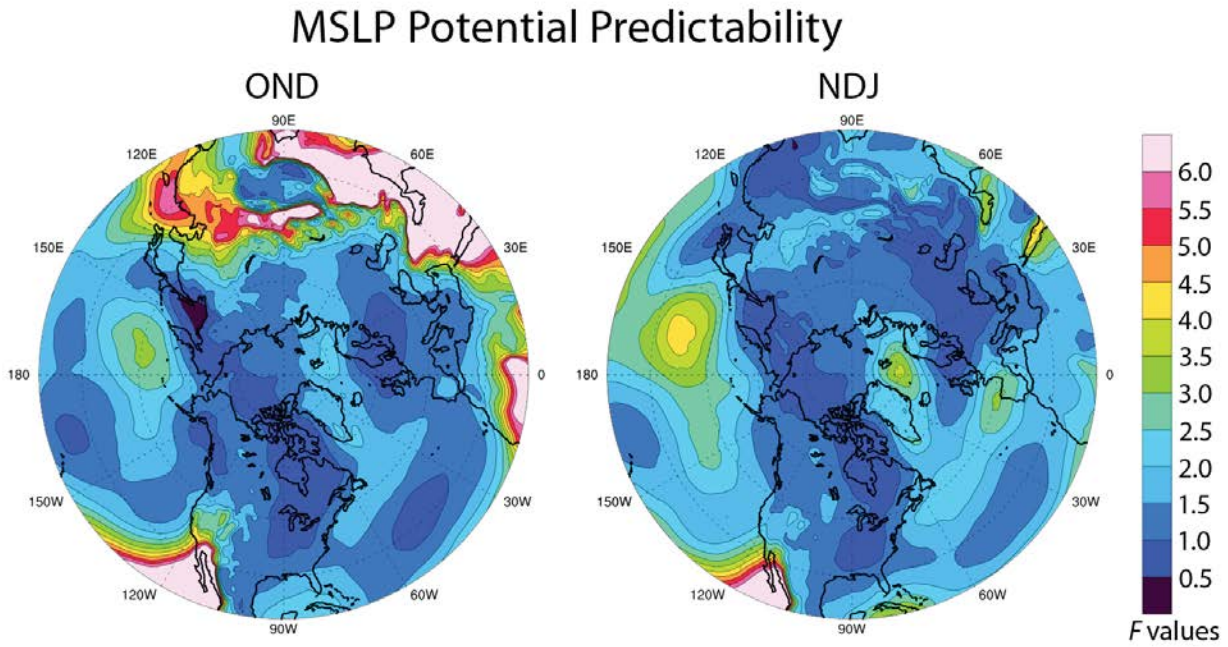

Figure B.2: Northern Hemisphere (20°N-poleward) MSLP potential predictability for OND (left) and NDJ (right). *F*-values above 1.5 are statistically significant at the 0.05 significance level.

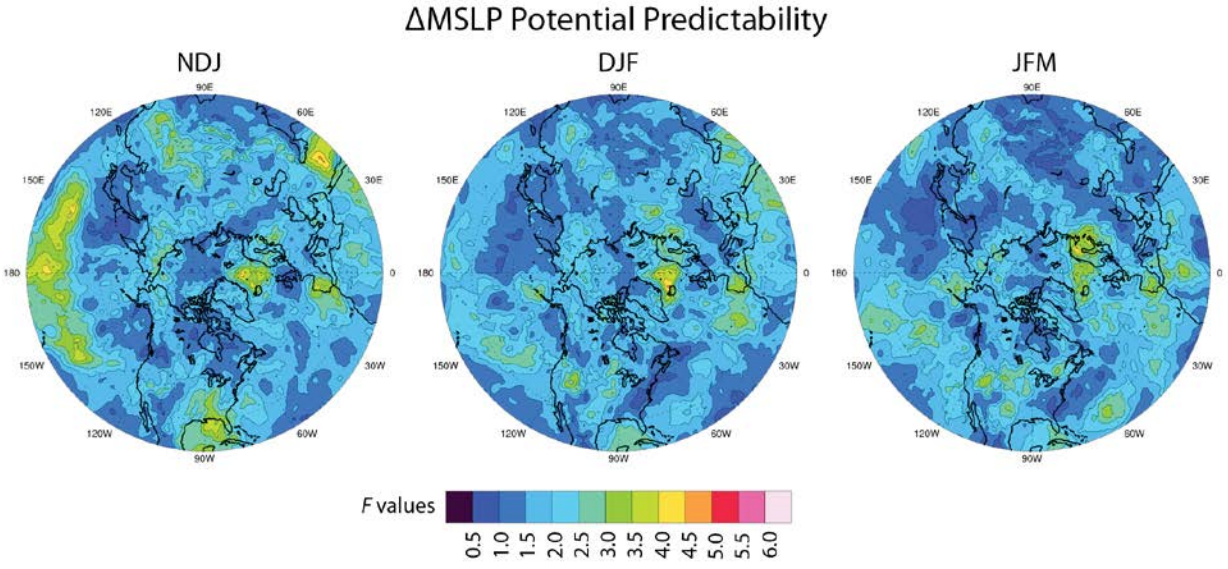

Figure B.3: Northern Hemisphere (20°N-poleward) ΔMSLP potential predictability for NDJ (left), DJF (middle), and JFM (right). *F*-values above 1.5 are statistically significant at the 0.05 significance level.

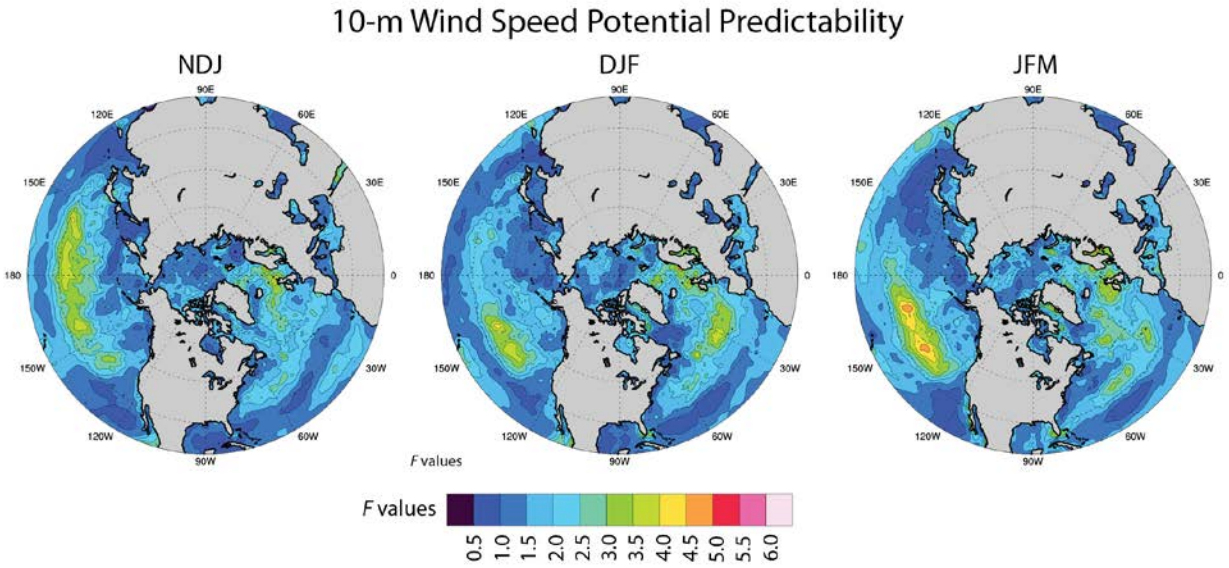

Figure B.4: Northern Hemisphere (20°N-poleward) 10-m wind speed potential predictability for NDJ (left), DJF (middle), and JFM (right) (with ERA-Interim landmass overlay). *F*-values above 1.5 are statistically significant at the 0.05 significance level.

B.2 Additional Composite Analysis Figures

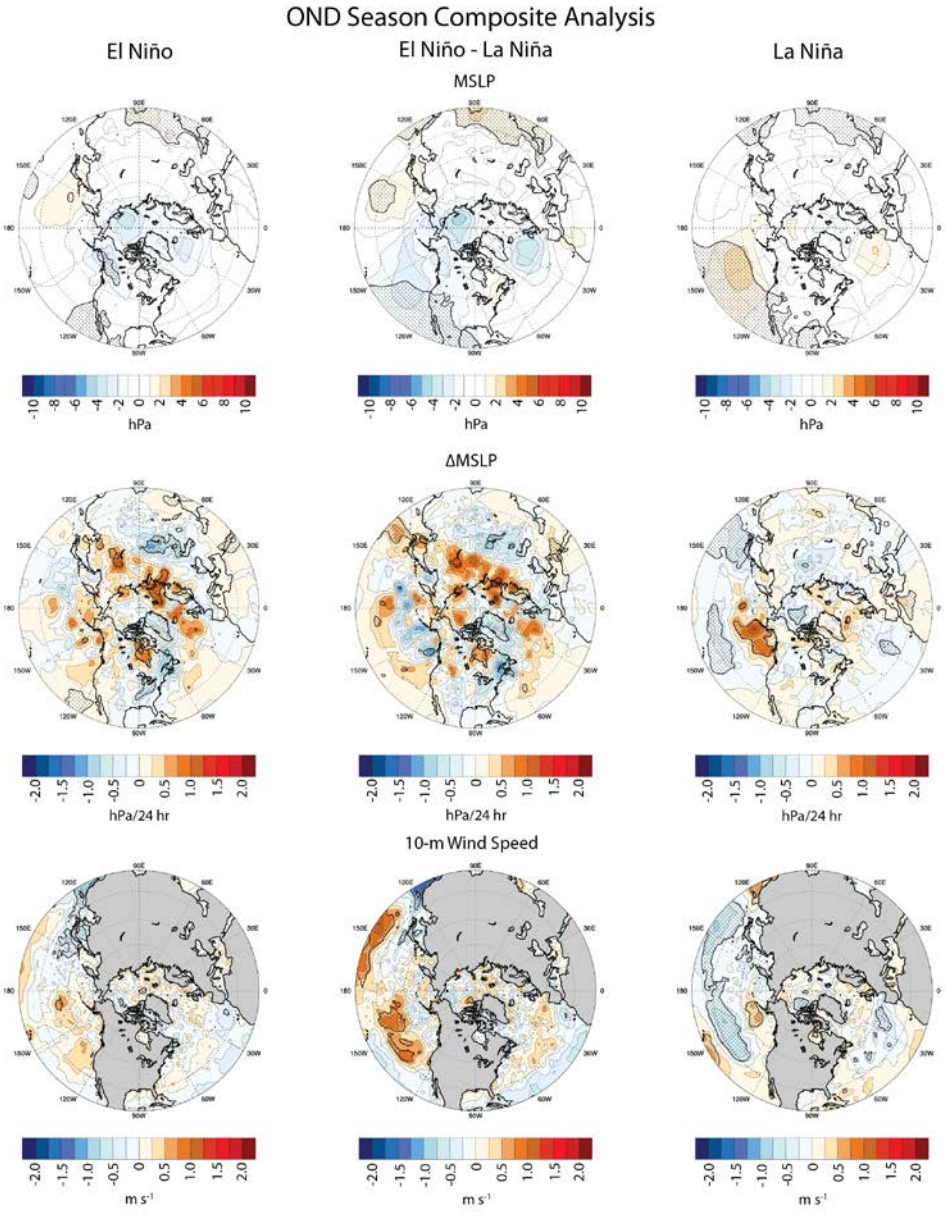

Figure B.5: Southern Oscillation OND composite analysis for MSLP (top), ΔMSLP (middle), and 10-m wind speed (with ERA-Interim landmass overlay; bottom). Colours represent MSLP, ΔMSLP, and 10-m wind speed anomalies during the El Niño (left) and La Niña (right) phases (composite with the seasonal climatology removed) and differences between the two phases (middle; El Niño composite minus La Niña composite). Shading represents where the composites differ statistically (El Niño vs. neutral conditions [left], El Niño vs. La Niña [middle], La Niña vs. neutral conditions [right]).

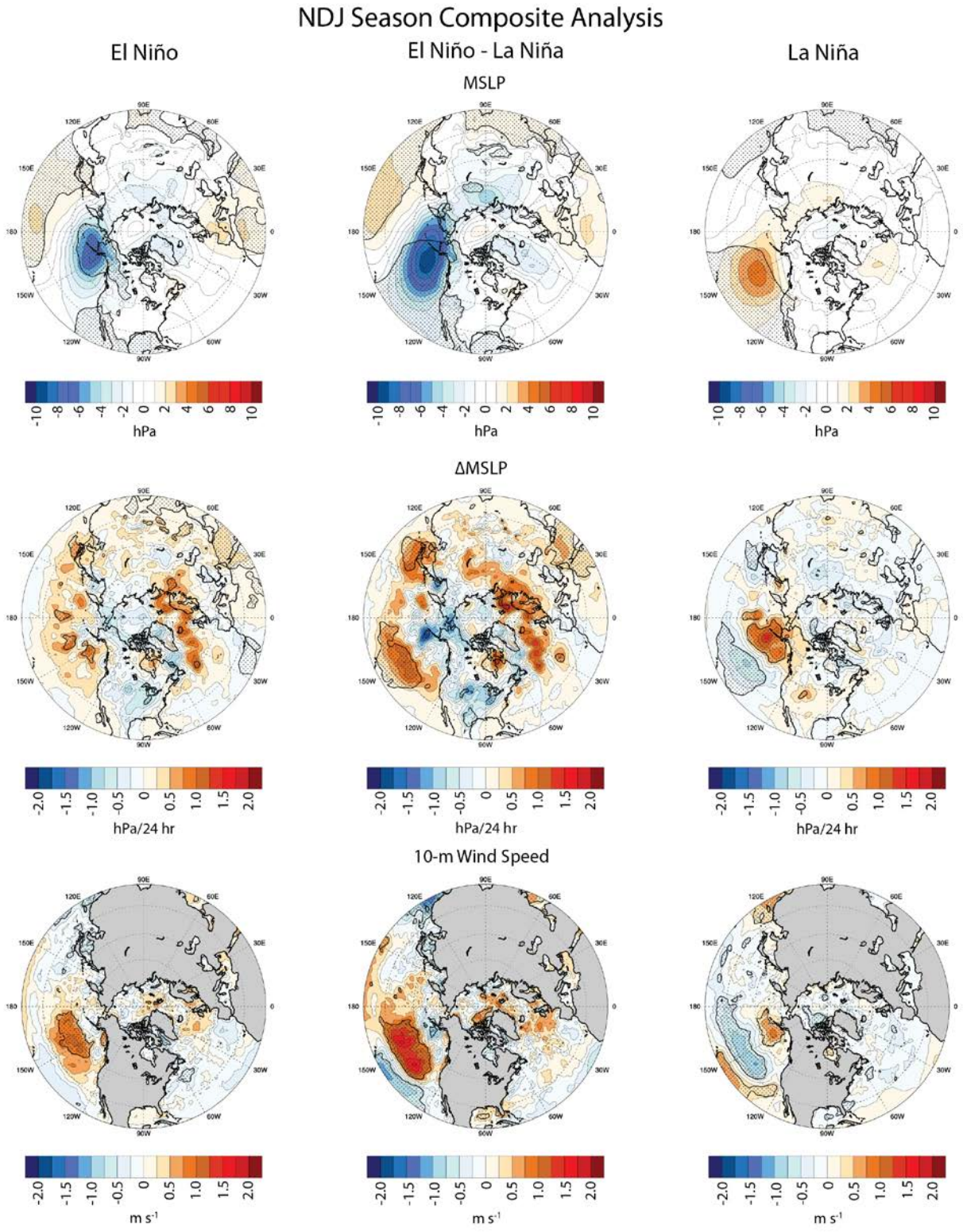

Figure B.6: As in Figure B.5, except for NDJ.

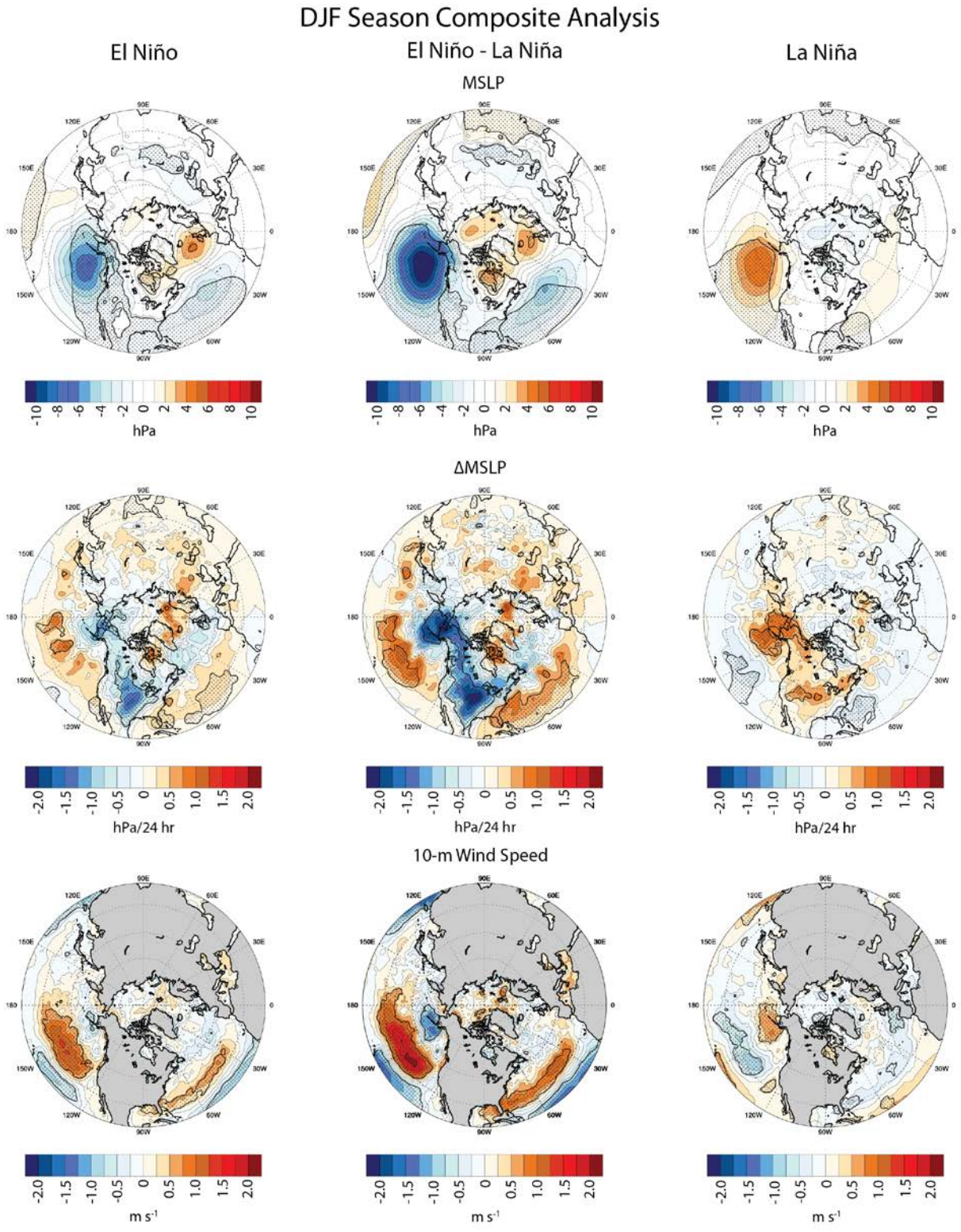

Figure B.7: As in Figure B.5, except for DJF.

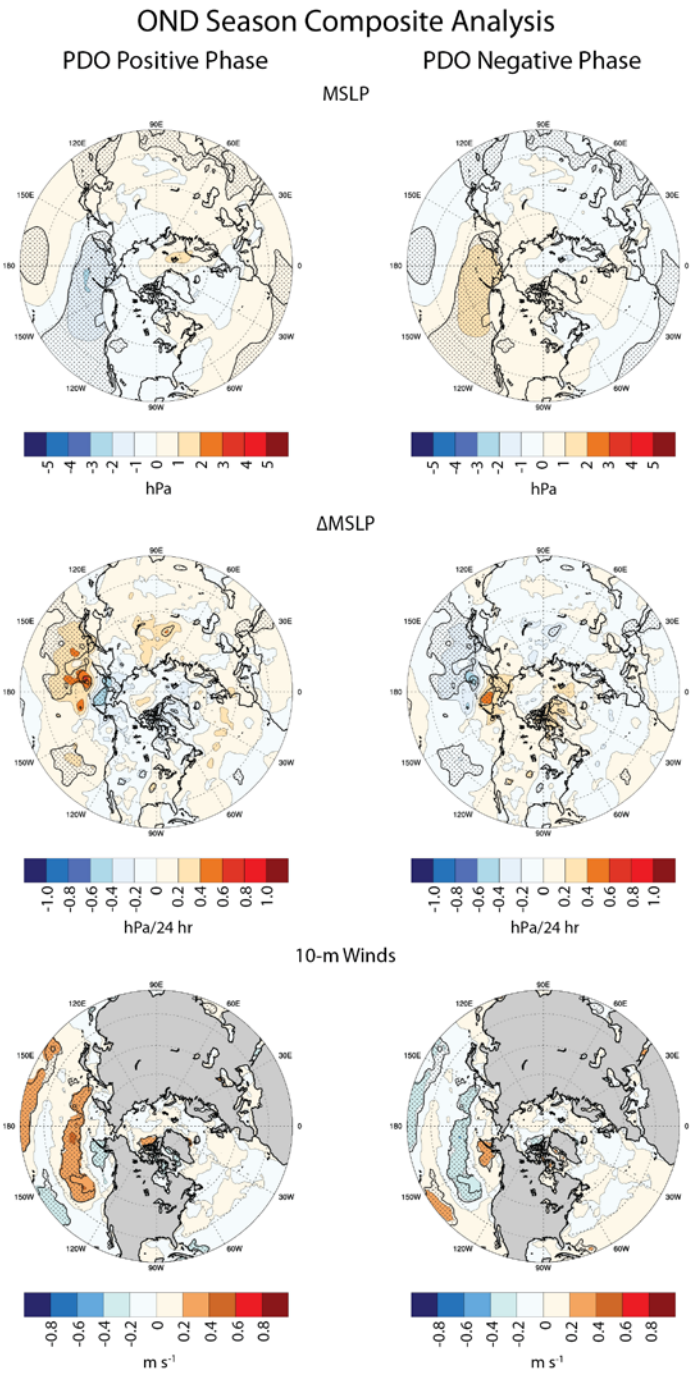

Figure B.8: Pacific Decadal Oscillation OND composite analysis for MSLP (top), ΔMSLP (middle), and 10-m wind speed (with ERA-Interim landmass overlay; bottom). Colours represent MSLP, ΔMSLP, and 10-m wind speed anomalies during the positive (left) and negative (right) phases (composite with the seasonal climatology removed). Shading represents where the composites differ statistically (positive phase vs. negative phase).

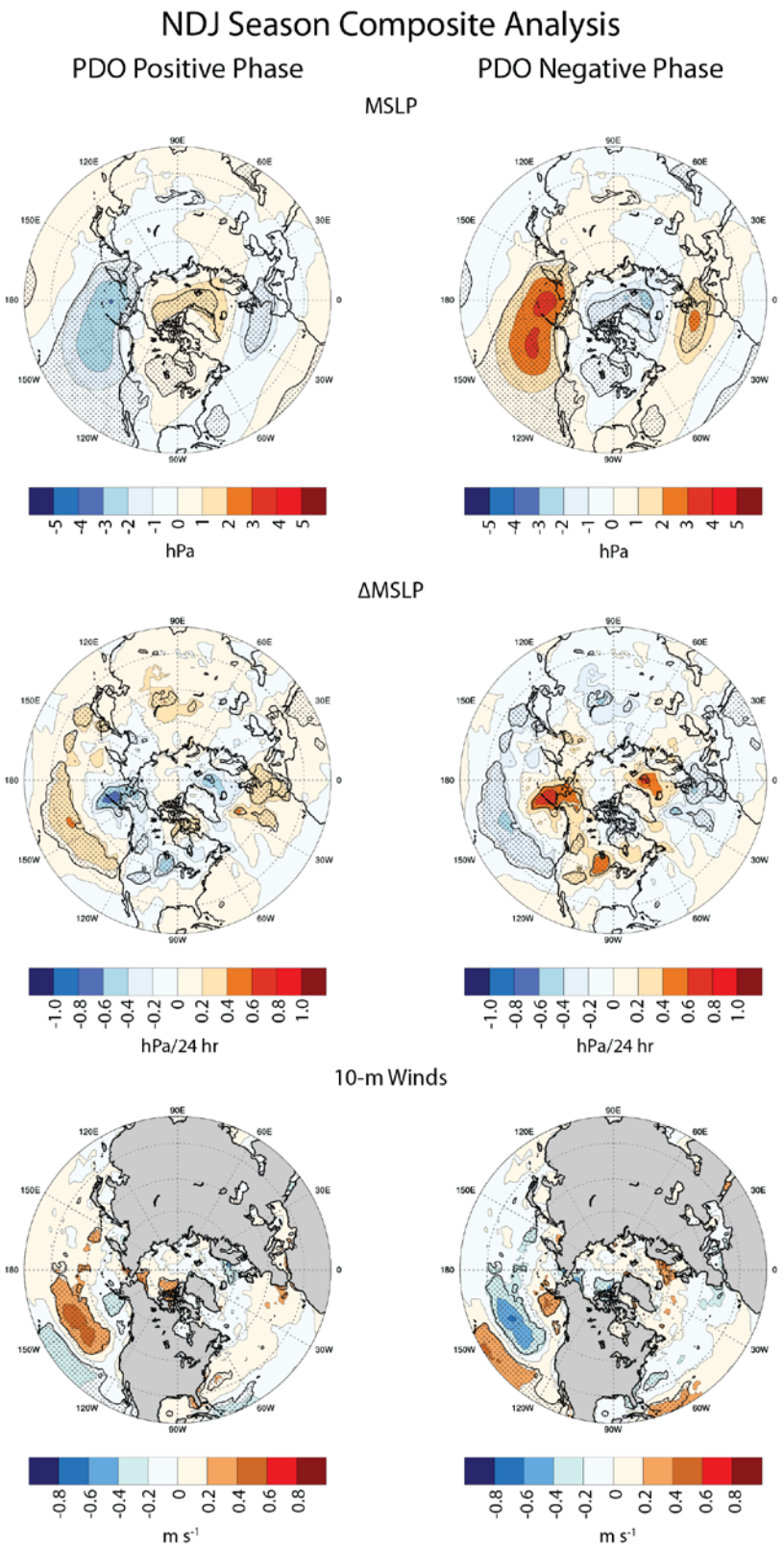

Figure B.9: As in Figure B.8, except for NDJ.

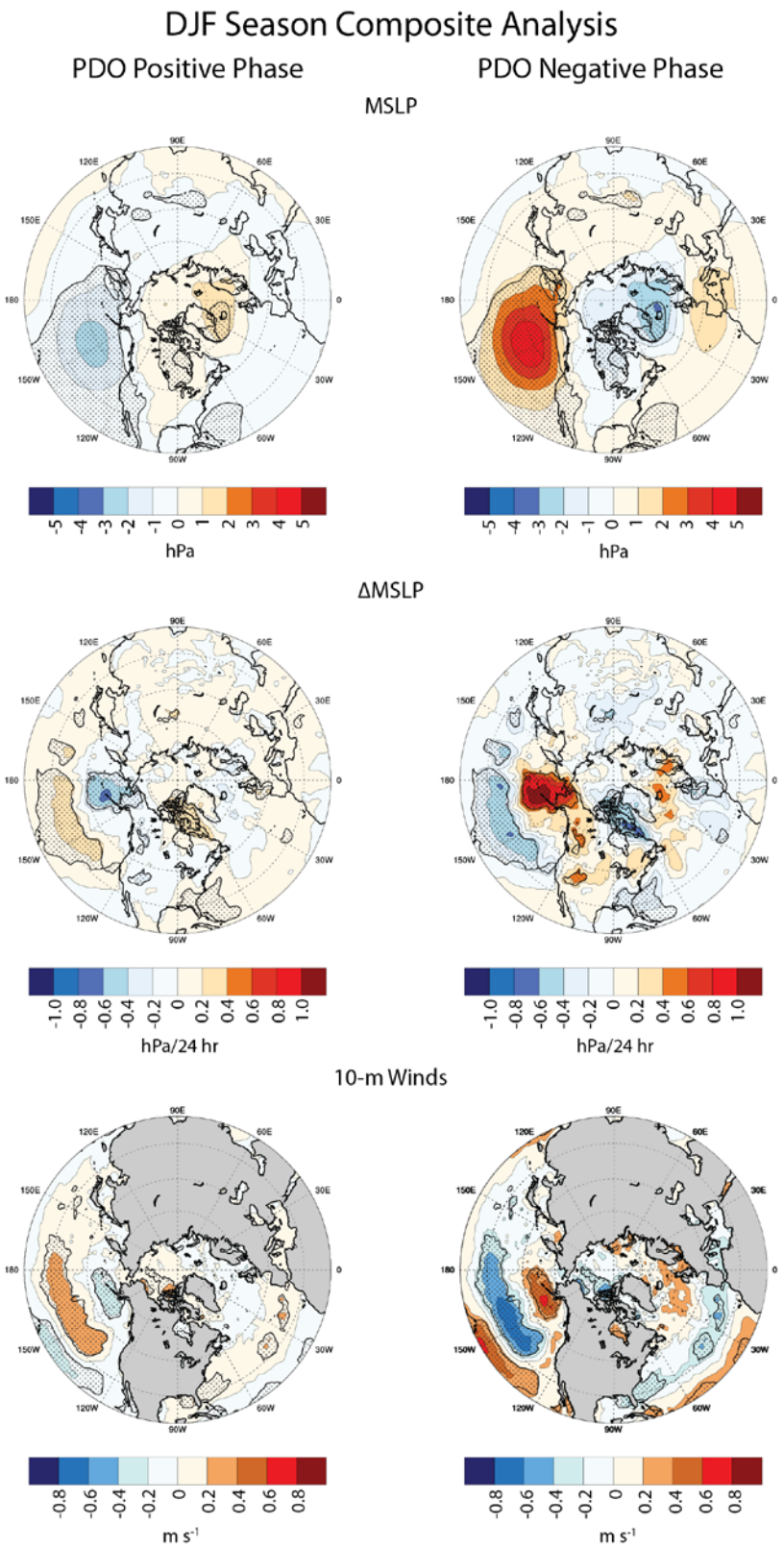

Figure B.10: As in Figure B.8: except for DJF.

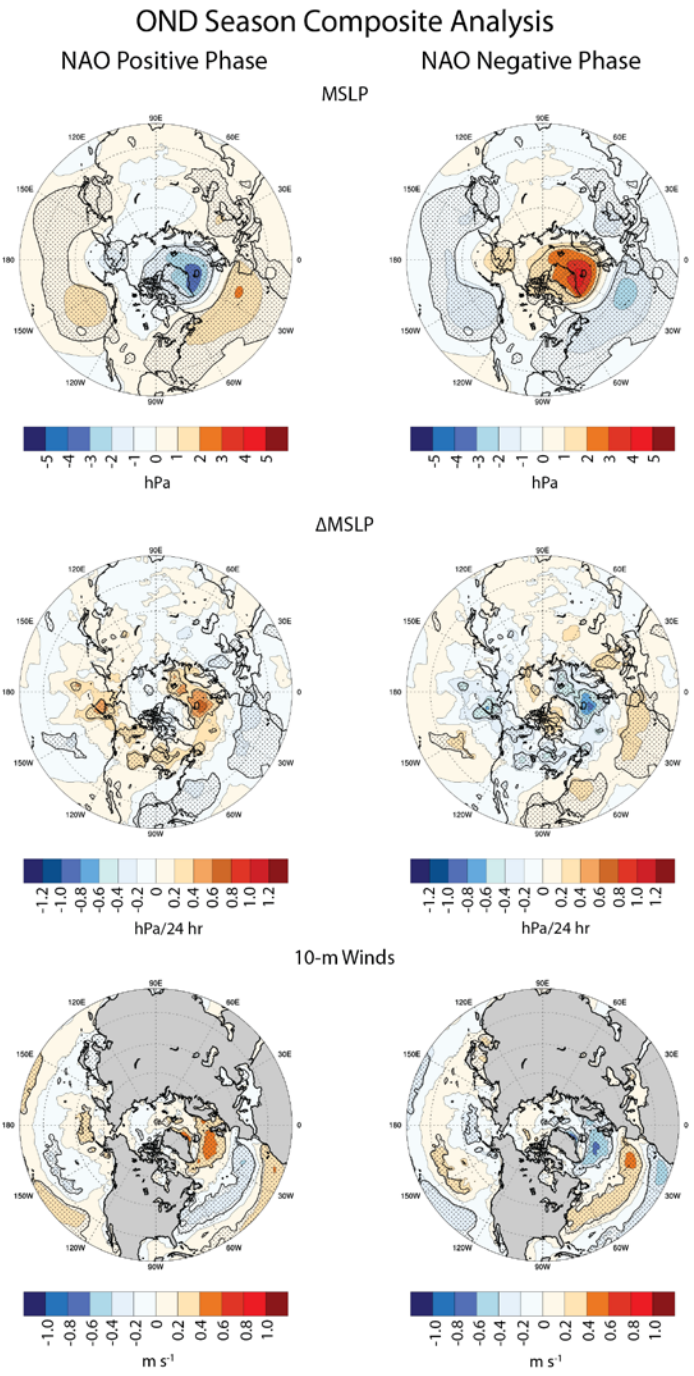

Figure B.11: North Atlantic Oscillation OND composite analysis for MSLP (top), ΔMSLP (middle), and 10-m wind speed (with ERA-Interim landmass overlay; bottom). Colours represent MSLP, ΔMSLP, and 10-m wind speed anomalies during the positive (left) and negative (right) phases (composite with the seasonal climatology removed). Shading represents where the composites differ statistically (positive phase vs. negative phase).

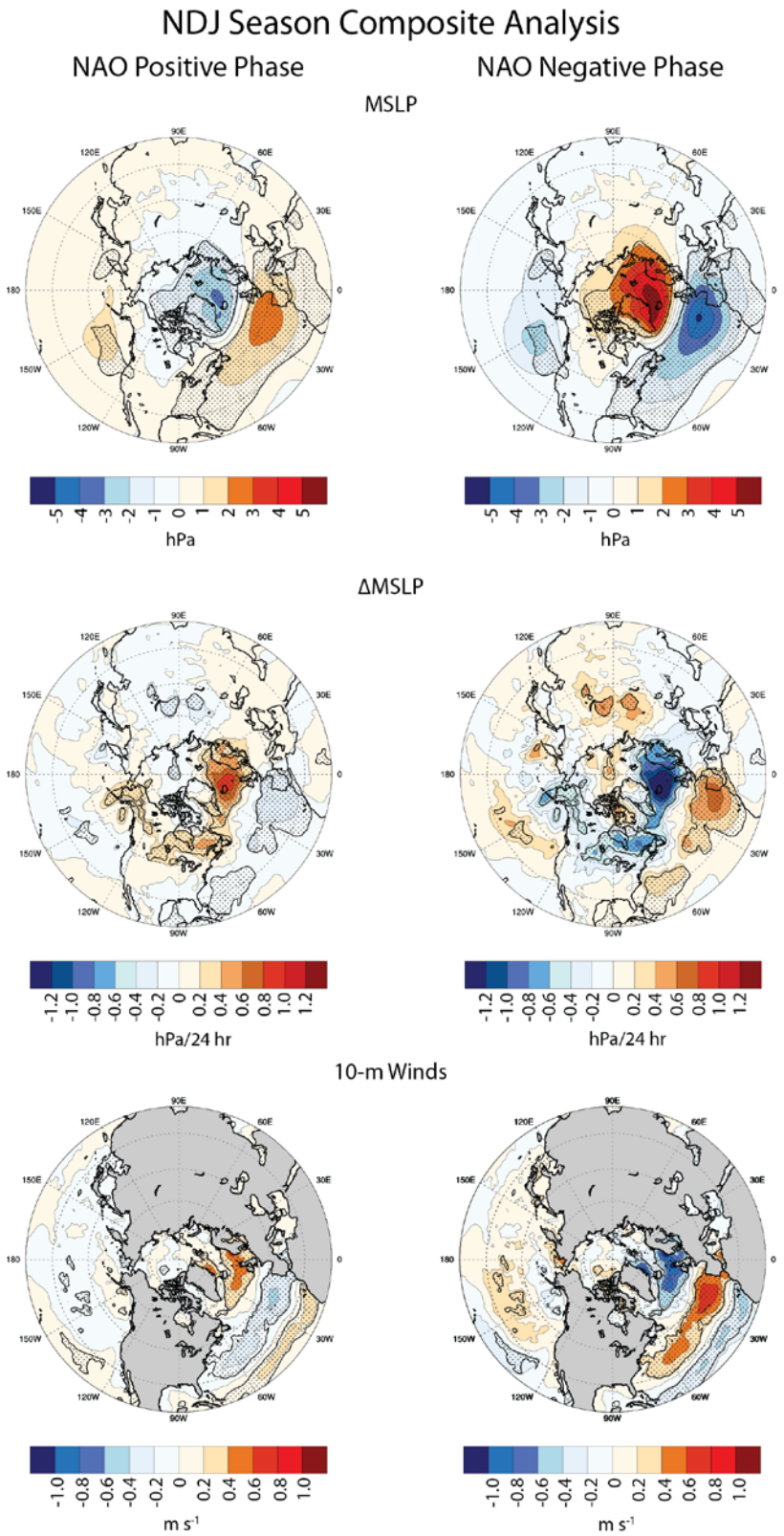

Figure B.12: As in Figure B.11, except for NDJ.

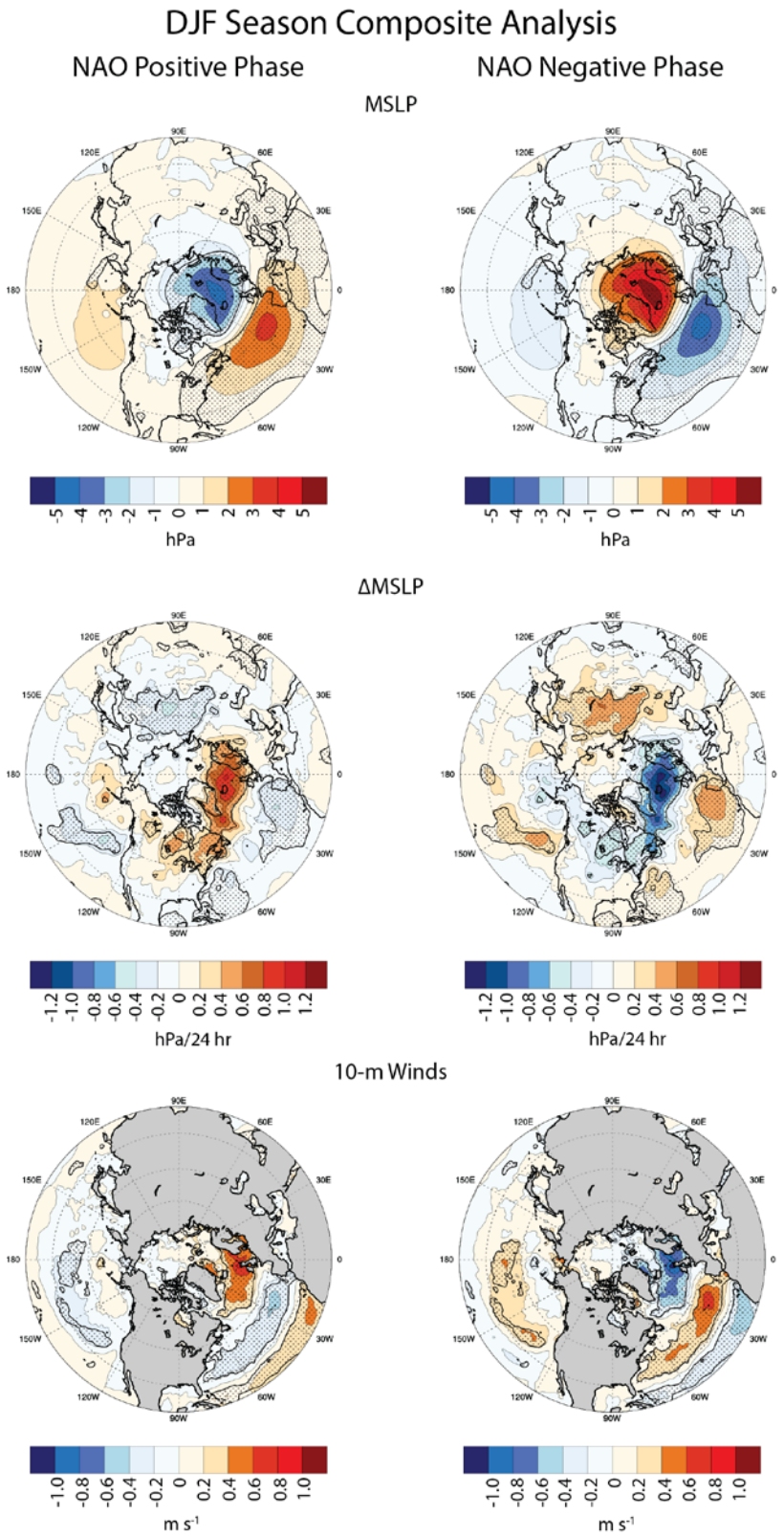

Figure B.13: As in Figure B.11, except for DJF.

B.3 Additional Potential Predictability and its Possible Sources Figures

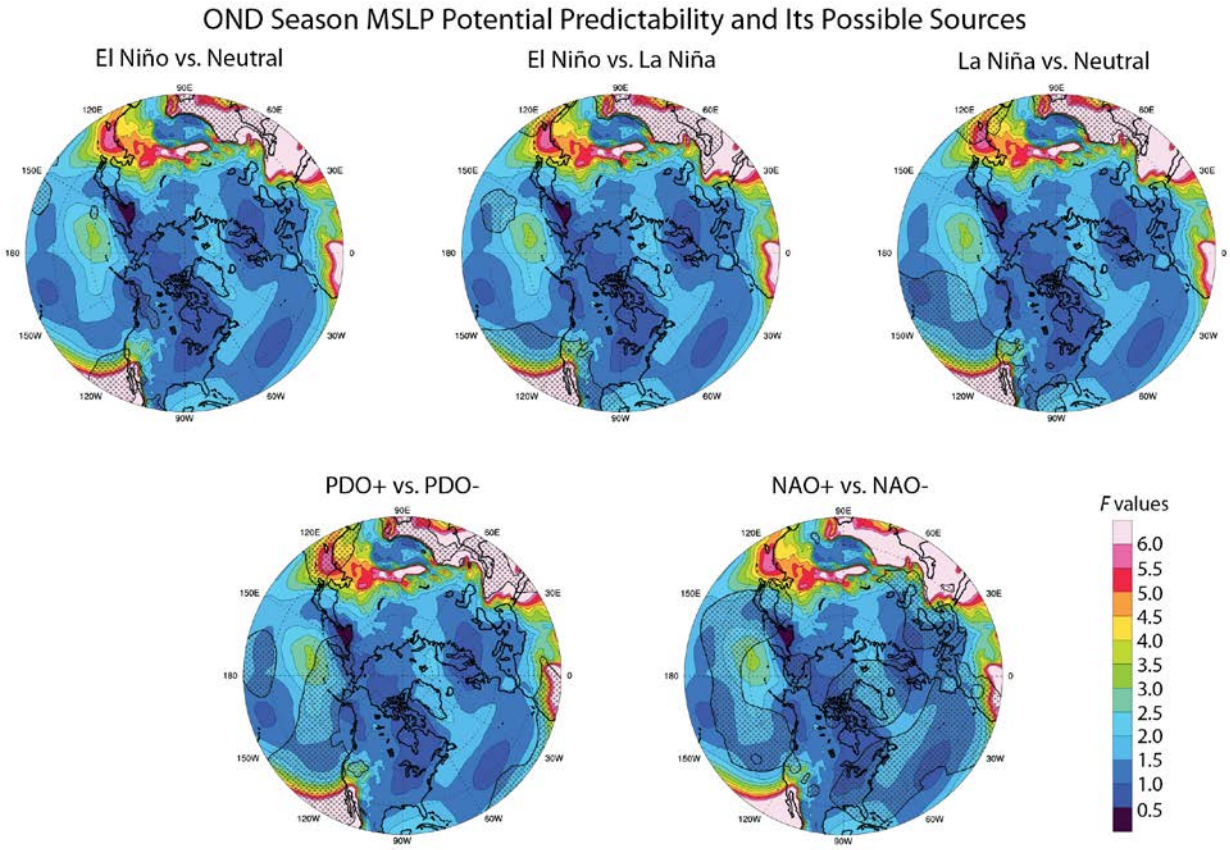

Figure B.14: MSLP potential predictability and its possible sources for OND. Colours represent potential predictability (*F*-values above 1.5 are statistically significant at the 0.05 significance level). Shading represents where the teleconnection phase composites differ statistically and, therefore, areas in which the teleconnection is a possible source of the detected potential predictability.

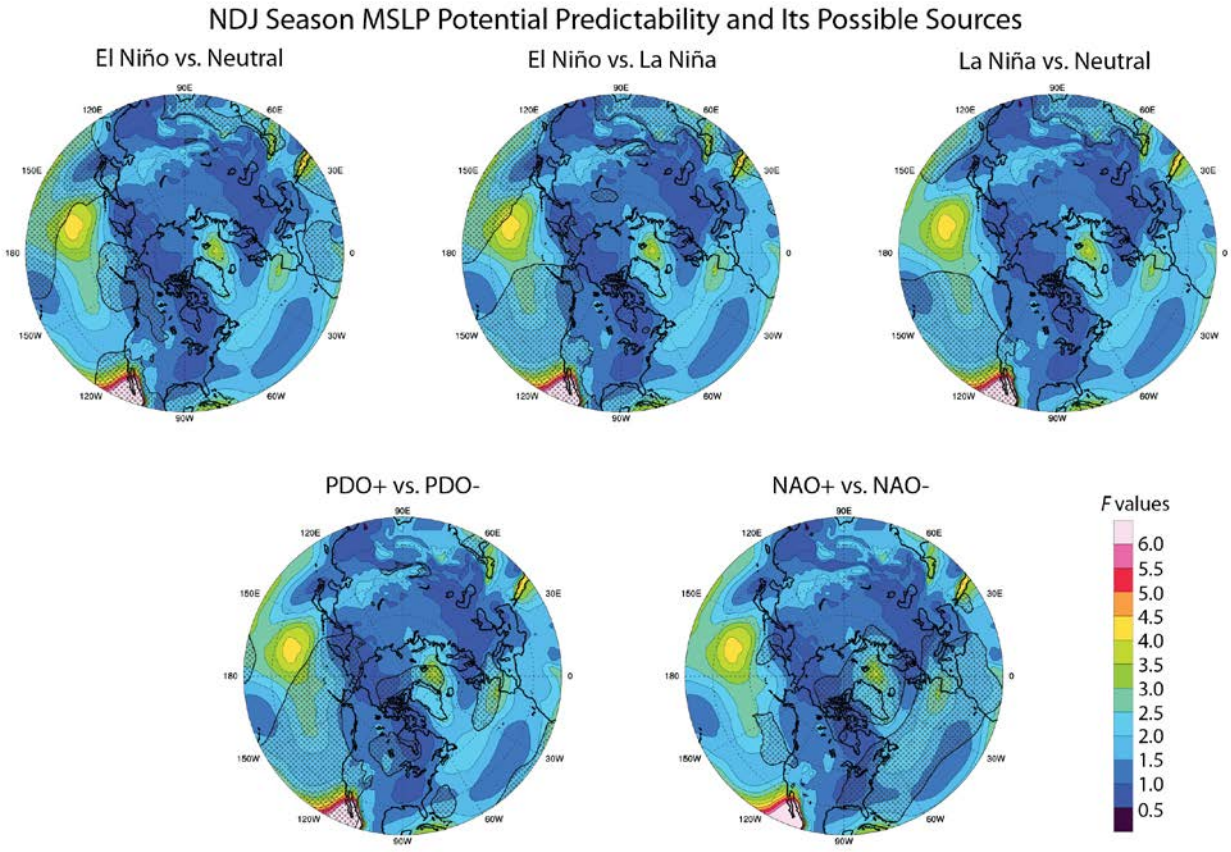

Figure B.15: As in Figure B.14, except for NDJ.

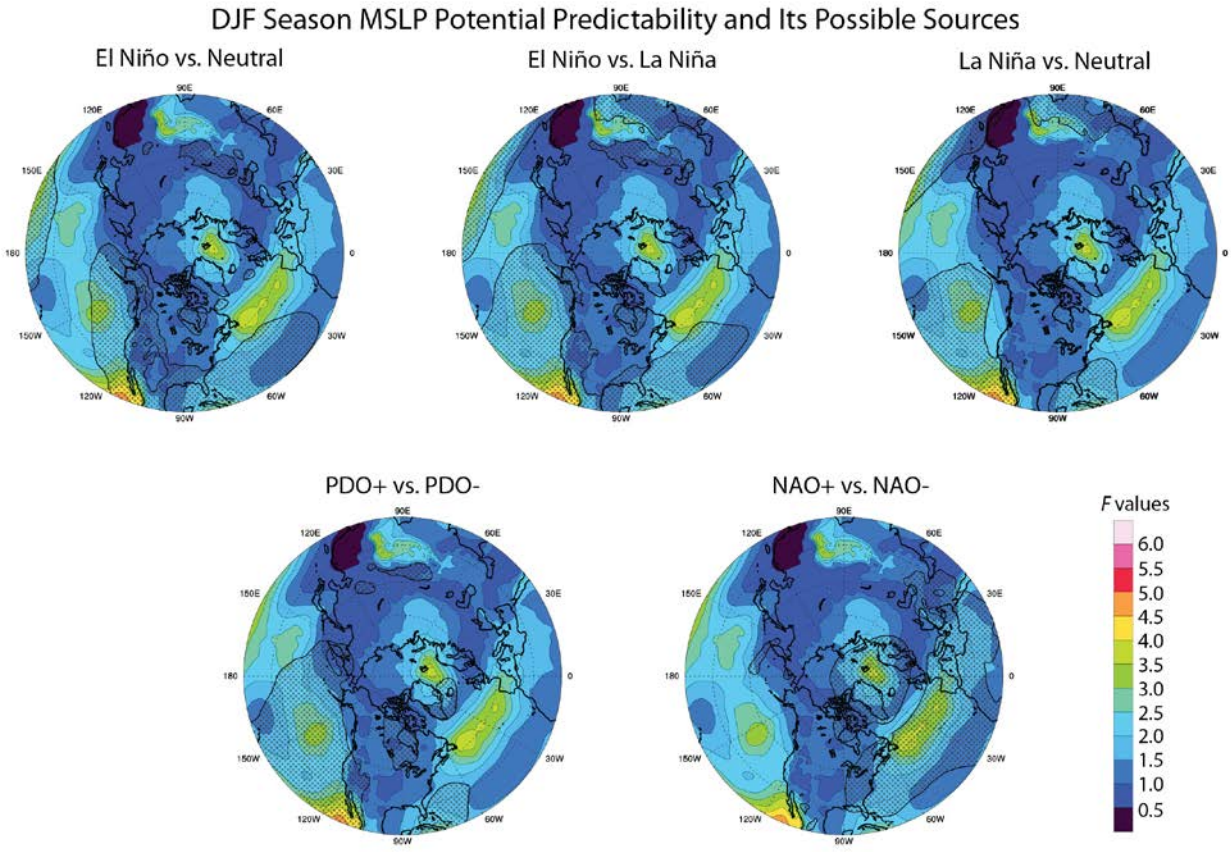

Figure B.16: As in Figure B.14, except for DJF.

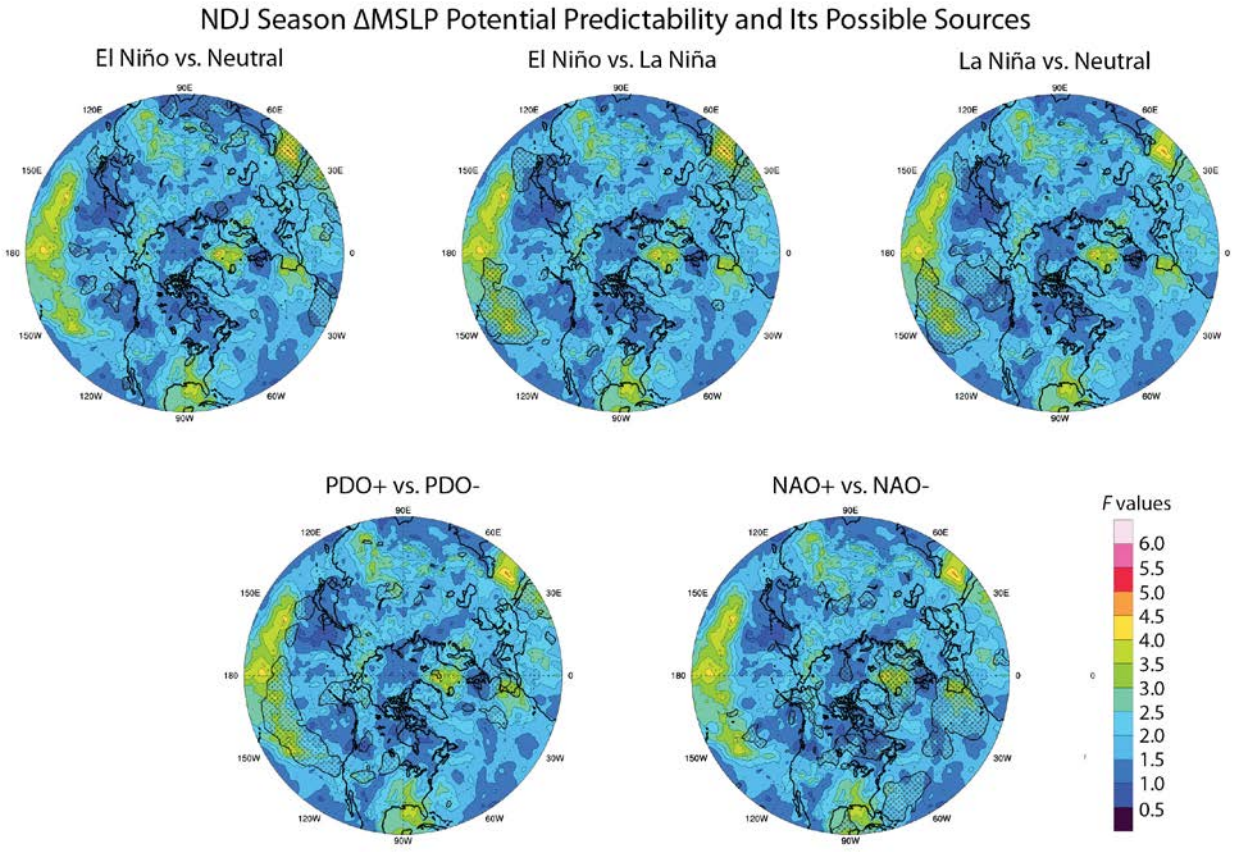

Figure B.17: ΔMSLP potential predictability and its possible sources for NDJ. Colours represent potential predictability (*F*-values above 1.5 are statistically significant at the 0.05 significance level). Shading represents where the teleconnection phase composites differ statistically and, therefore, areas in which the teleconnection is a possible source of the detected potential predictability.

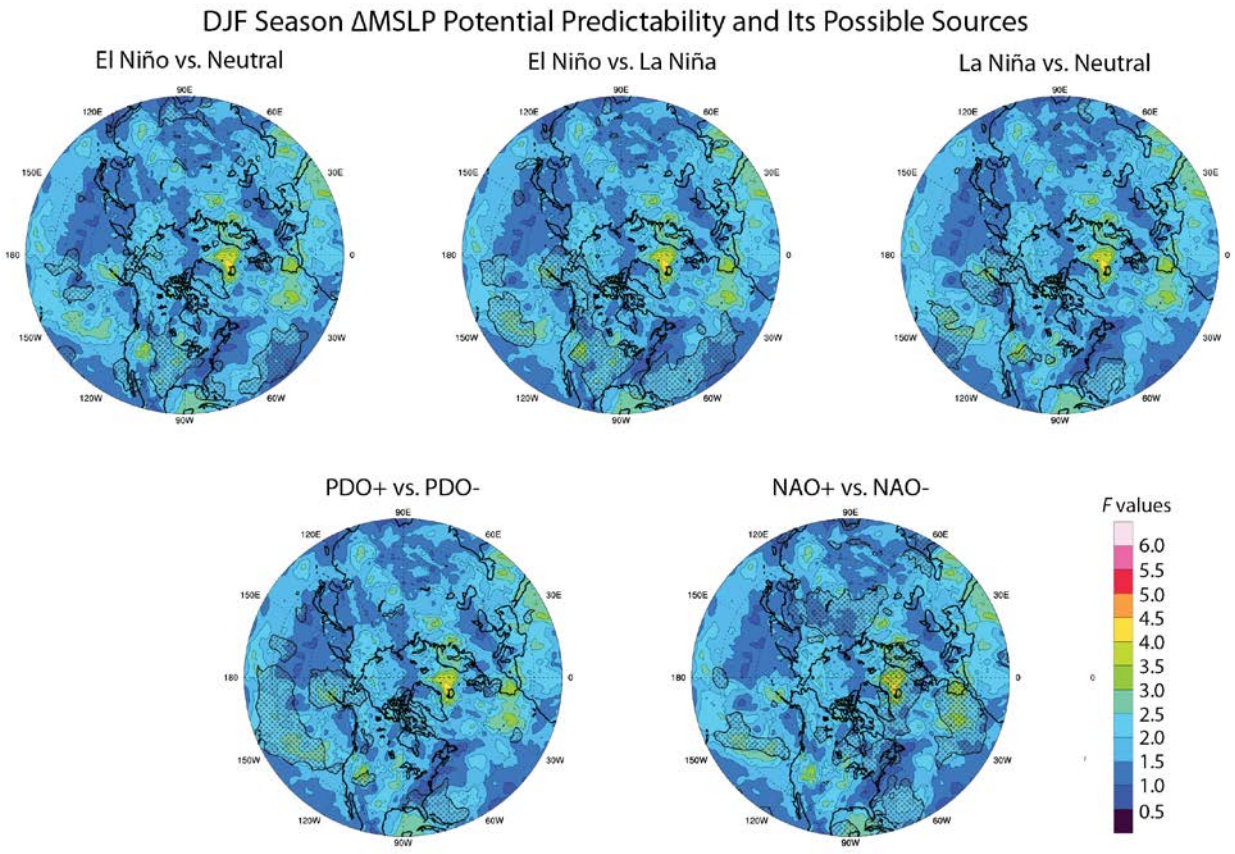

Figure B.18: As in Figure B.17, except for DJF.

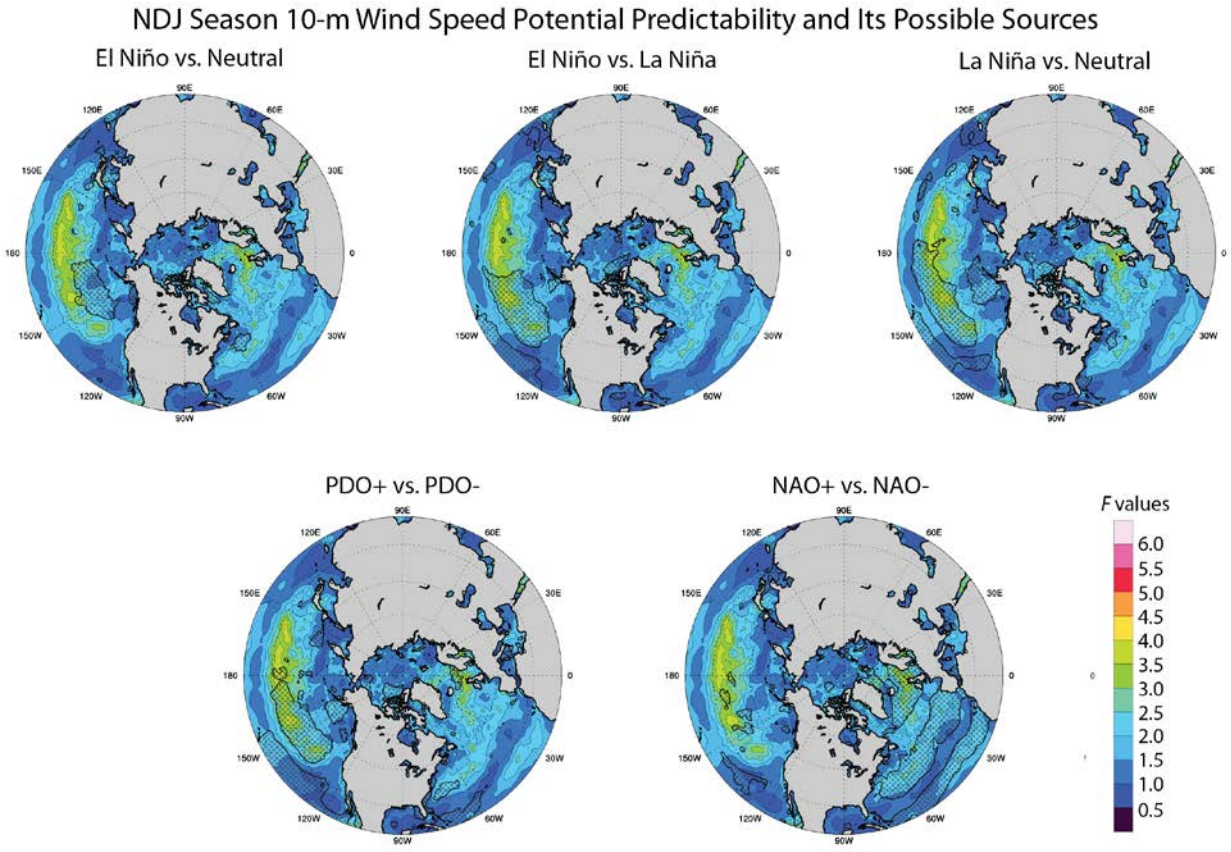

Figure B.19: 10-m wind speed potential predictability and its possible sources for NDJ (with ERA-Interim landmass overlay). Colours represent potential predictability (*F*-values above 1.5 are statistically significant at the 0.05 significance level). Shading represents where the teleconnection phase composites differ statistically and, therefore, areas in which the teleconnection is a possible source of the detected potential predictability.

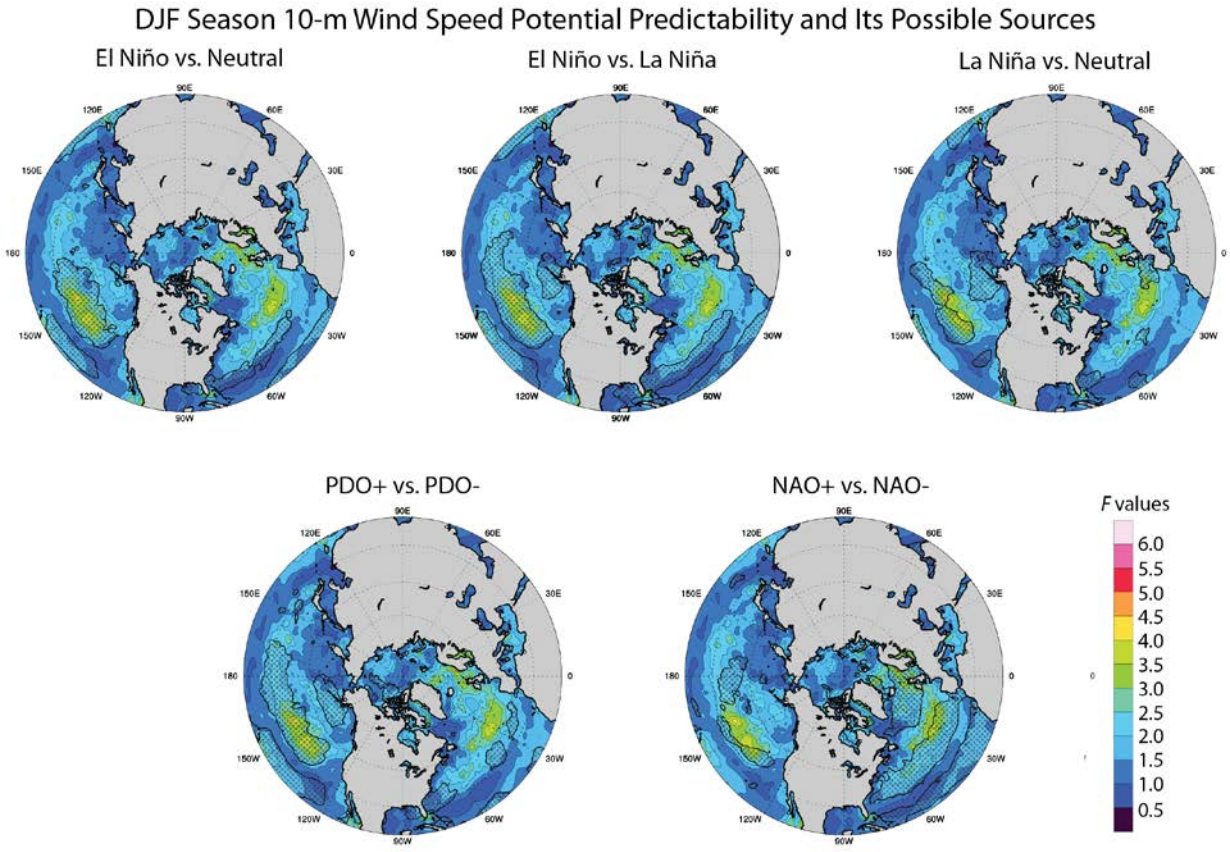

Figure B.20: As in Figure B.19, except for DJF.

Appendix C

Additional Research Theme 3 Figures

and

Seasonal Prediction Skill of CanCM3 and CanCM4

Appendix C provides supplementary material to the investigation of the seasonal prediction skill of North American coastal extratropical storm activity of the Canadian Seasonal to Interannual Prediction System (CanSIPS) (Research Theme 3) not presented in Chapter 6. Accompanying the additional figures from the CanSIPS-MME skill evaluation (Chapter 6), figures evaluating CanCM3 and CanCM4's individual performance producing quantitative deterministic, categorical deterministic, and categorical probabilistic forecasts are also presented. Forecast skill in CanCM3 and CanCM4 is evaluated using the ensemble mean forecasts from each model and the same methods as in the CanSIPS-MME evaluation – verified against ERA-Interim using the correlation skill score, percent correct score, and Brier skill score and the 33.3% threshold. Evaluating the forecast skill for the individual models utilized in CanSIPS provides additional insight into the seasonal predictability within the forecast system. Overall, CanCM3 and CanCM4 perform similarly and reflect the findings from the CanSIPS-MME evaluation, e.g.:

- MSLP forecasts are most skilful, 10-m wind speed forecasts are least skilful,
- ΔMSLP forecasts have higher skill over the North American continent than over the oceans, and
- 10-m wind speed forecasts have notably high skill in the mid-latitudes over the North Pacific.

In general, CanCM4 has higher correlations and percent correct scores but lower Brier skill scores than CanCM3.

C.1 Additional Research Theme 3 Figures: Seasonal Prediction Skill of CanSIPS-MME

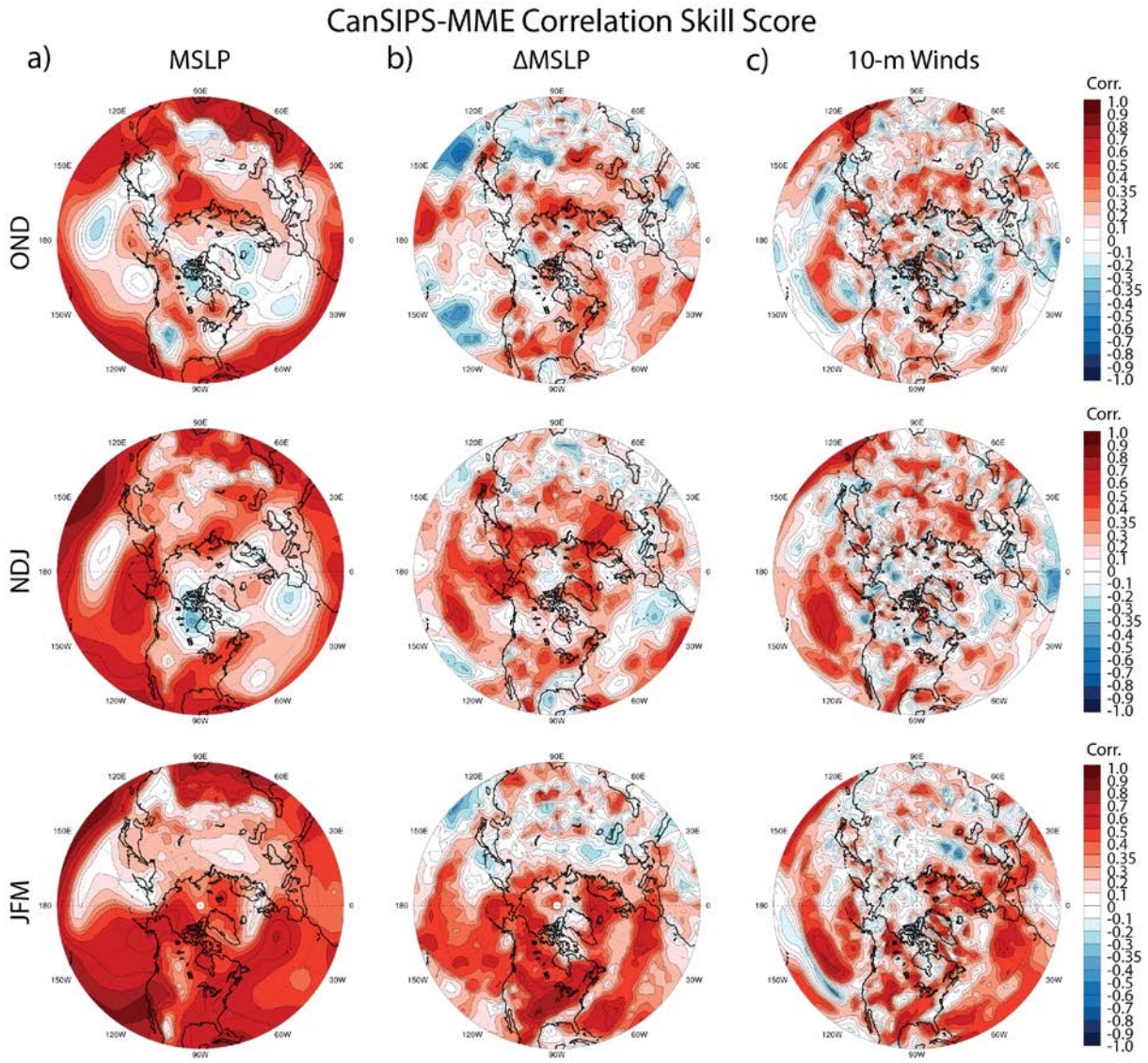

Figure C.1: Correlation skill scores for OND (top), NDJ (middle), and JFM (bottom) for a) MSLP, b) ΔMSLP, and c) 10-m wind speed.

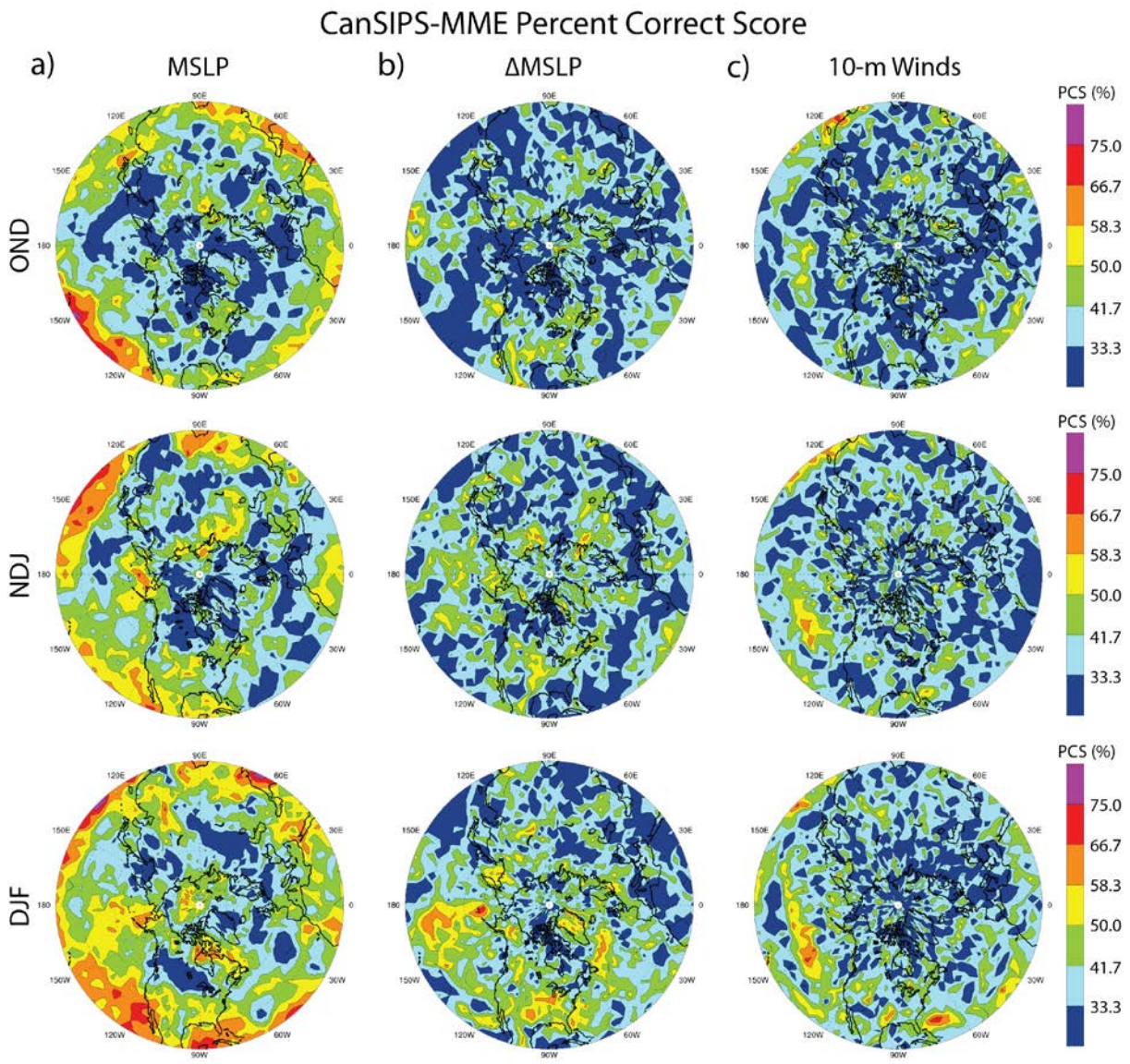

Figure C.2: Percent correct scores for OND (top), NDJ (middle), and DJF (bottom) for a) MSLP, b) ΔMSLP, and c) 10-m wind speed.

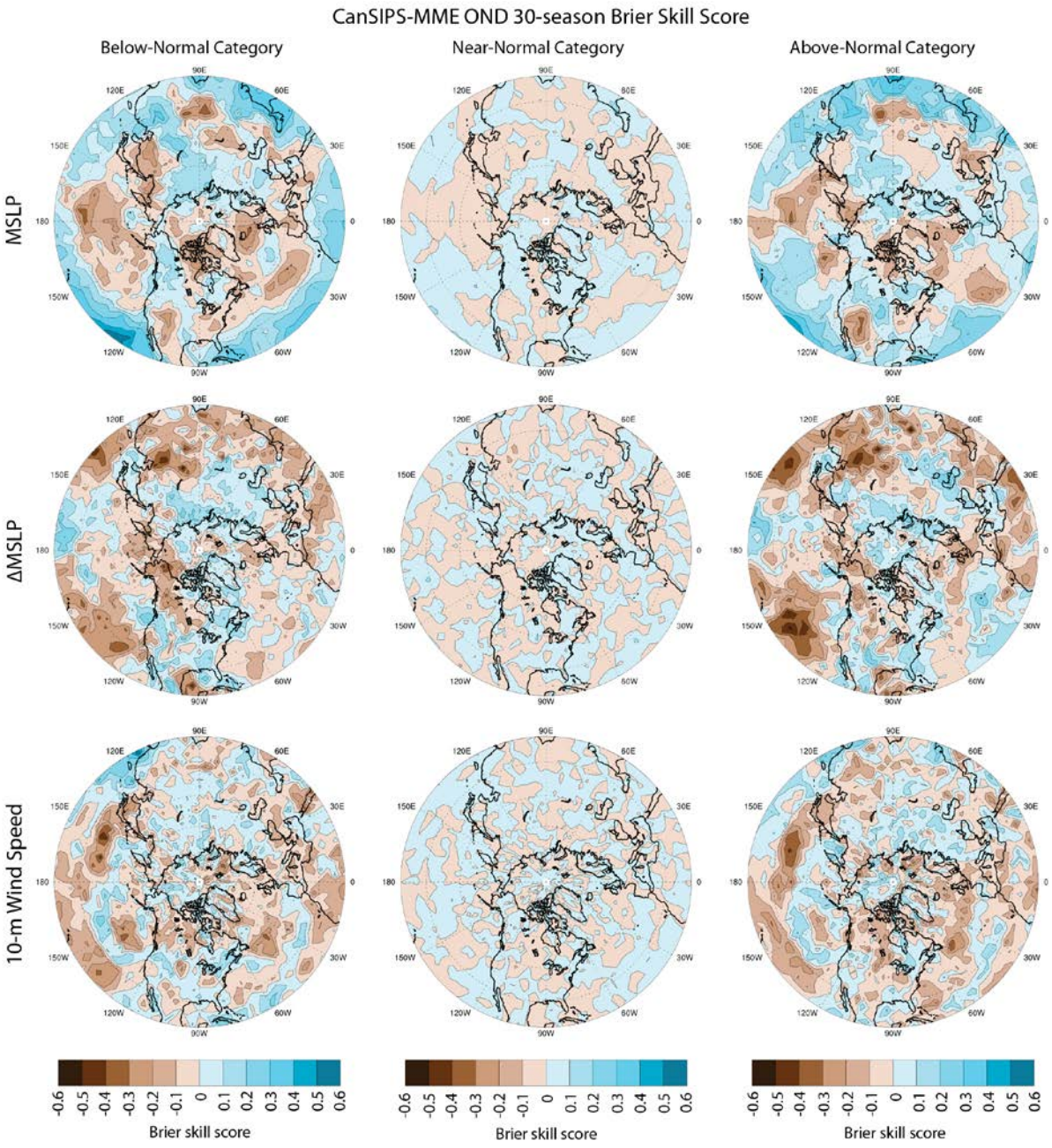

Figure C.3: Brier skill scores assessed over the 30-year seasonal CanSIPS-MME hindcast sequences for the Northern Hemisphere (20°N-poleward) OND MSLP (top), ΔMSLP (middle), and 10-m wind speed (bottom) forecasts.

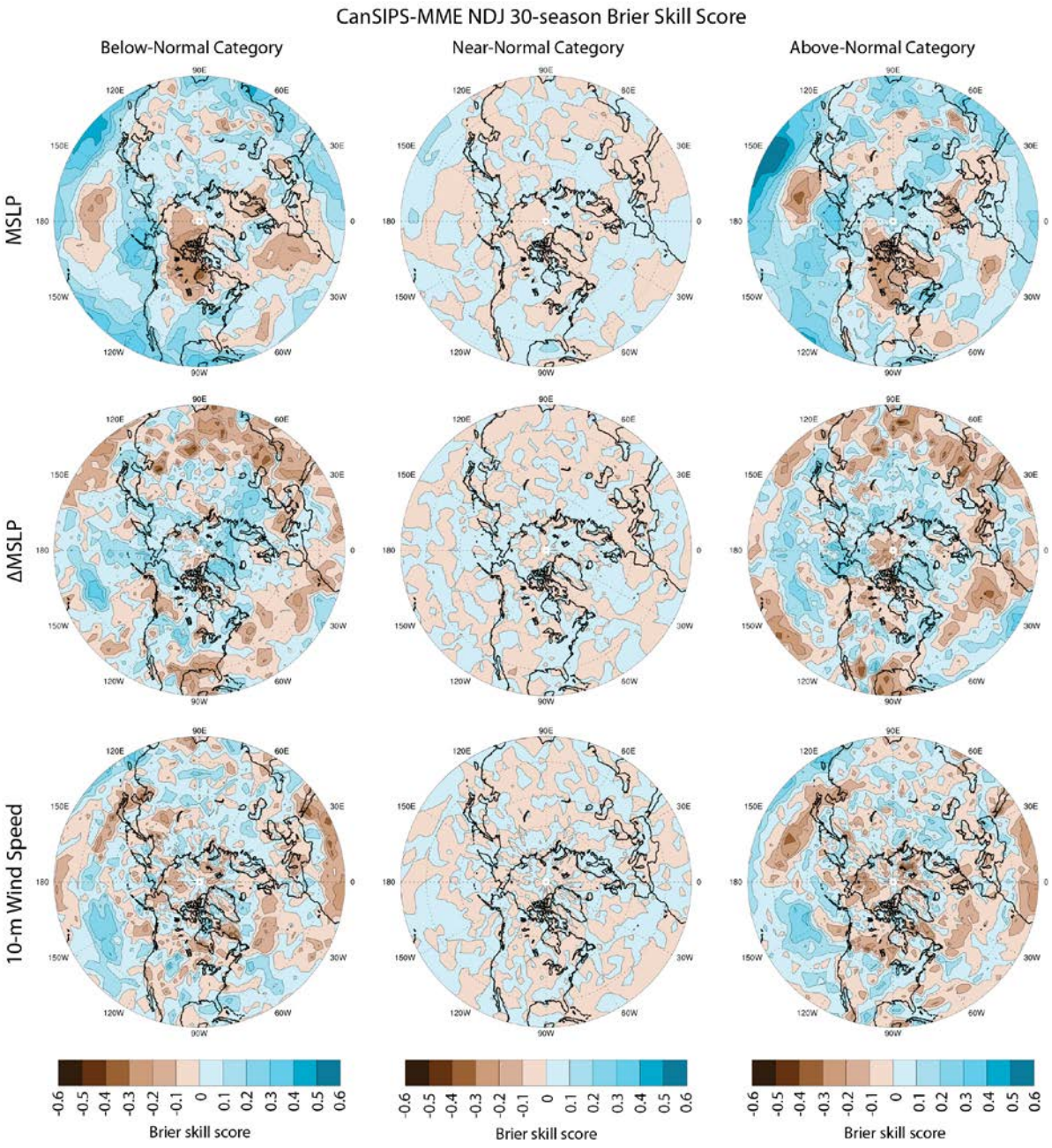

Figure C.4: As in Figure C.3, except for NDJ.

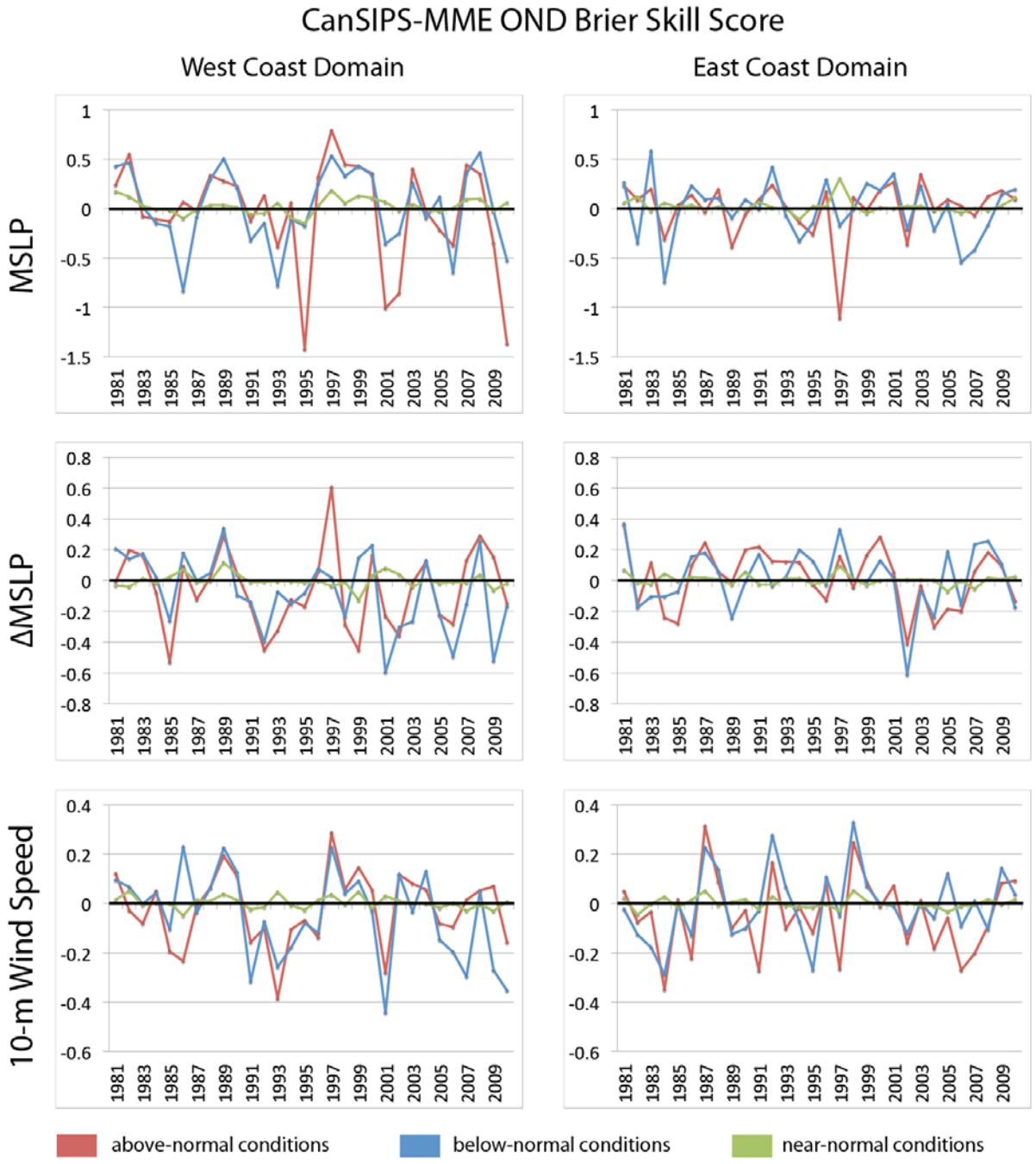

Figure C.5: Temporal variation in CanSIPS-MME forecast performance as measured by the Brier skill scores assessed for the North American west and east coast study domains (Figure 6.1) for OND MSLP (top), ΔMSLP (middle), and 10-m wind speed (bottom) forecasts.

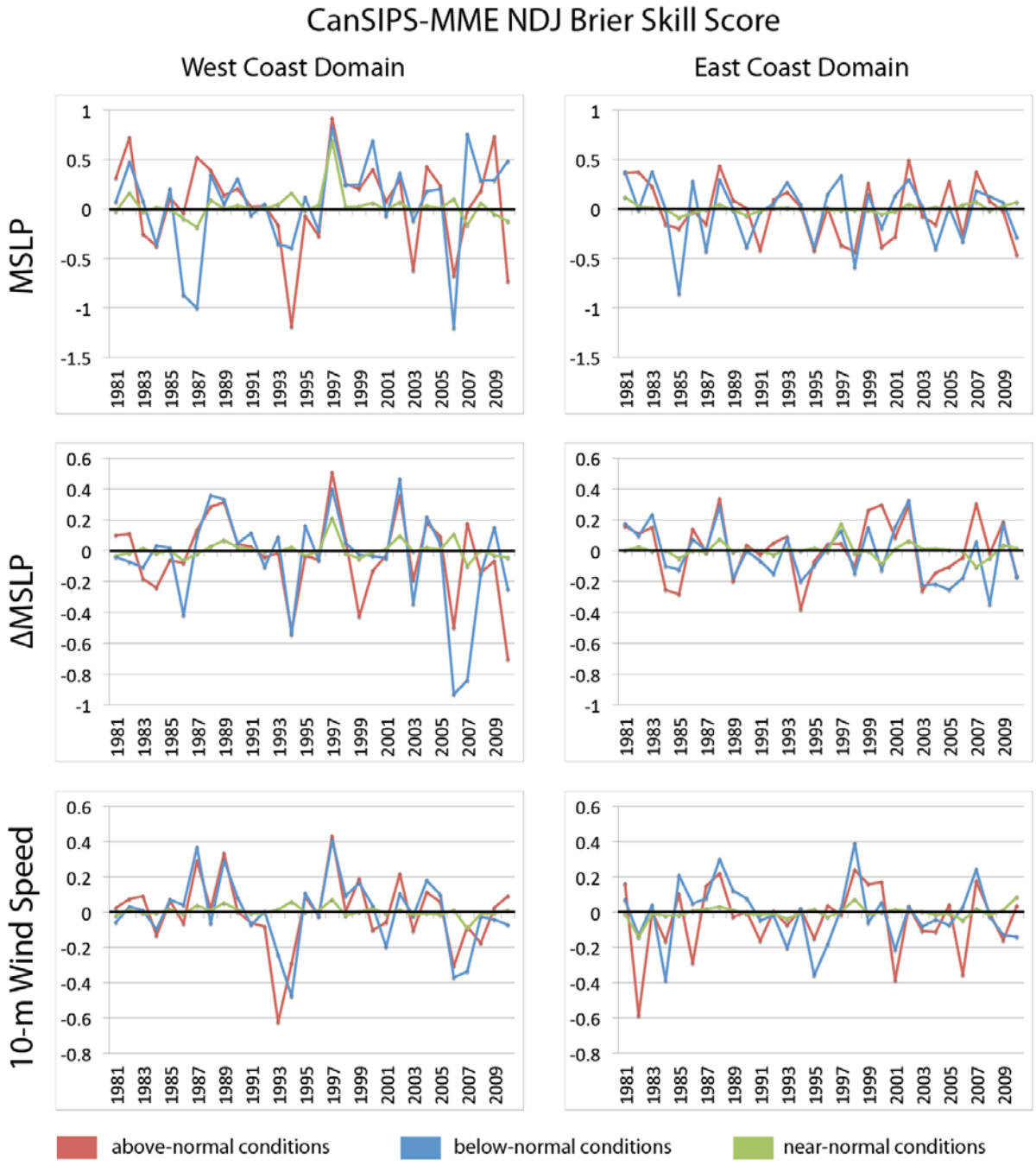

Figure C.6: As in Figure C.5, except for NDJ.

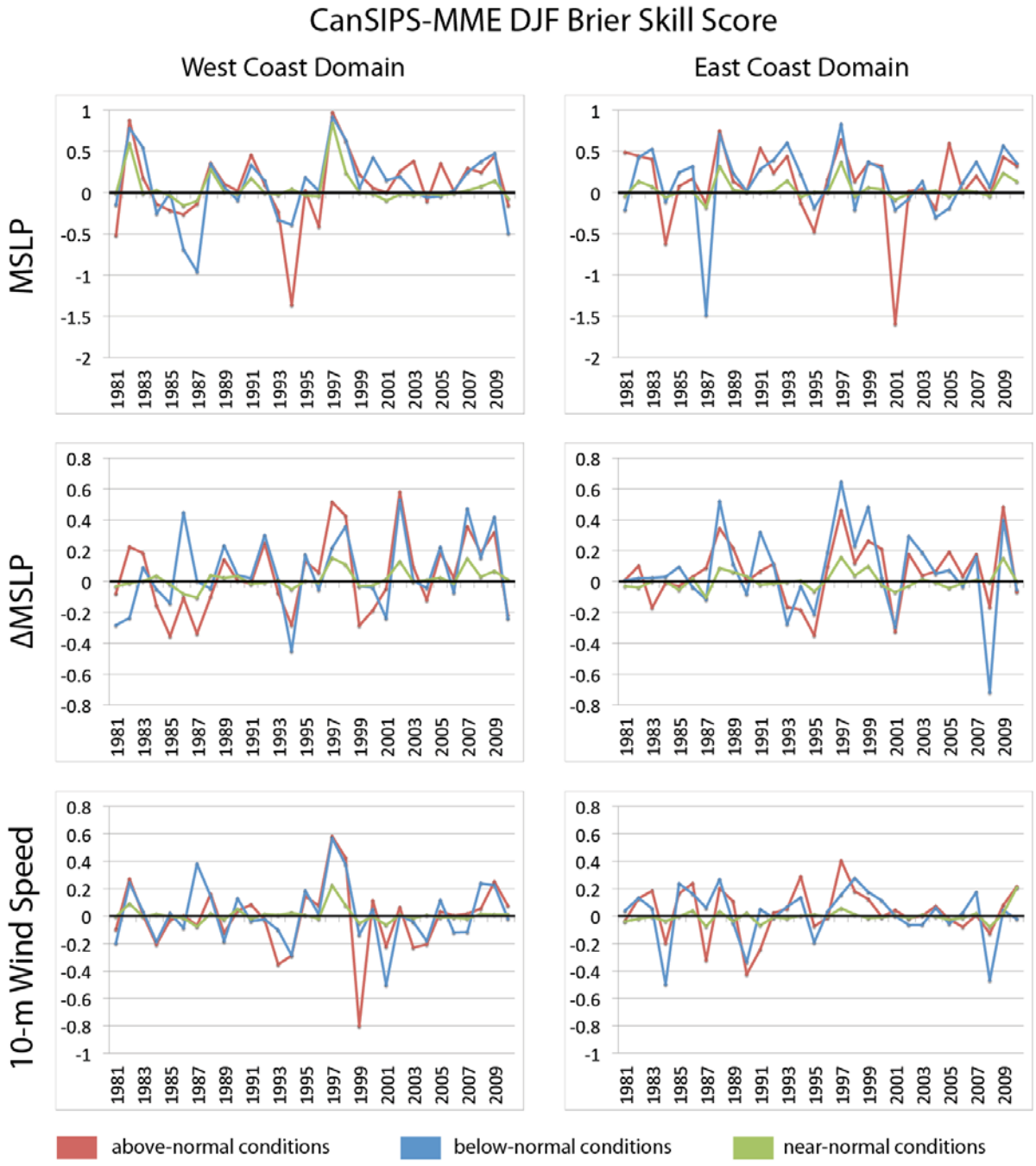

Figure C.7: As in Figure C.5, except for DJF.

C.2 Seasonal Prediction Skill of CanCM3

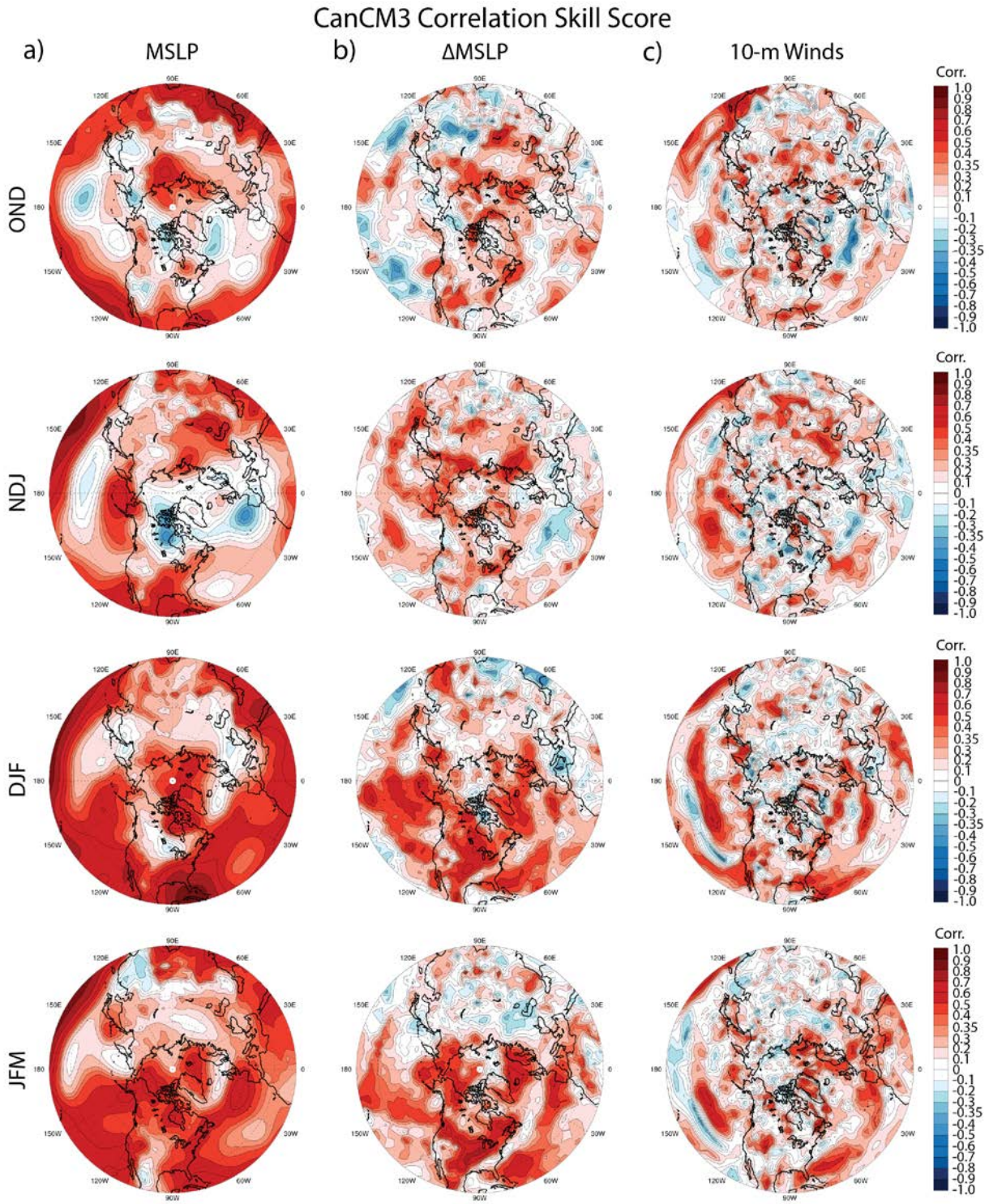

Figure C.8: CanCM3 correlation skill scores for the rolling 3-month cold seasons (OND, NDJ, DJF, JFM; top to bottom) for a) MSLP, b) ΔMSLP, and c) 10-m wind speed.

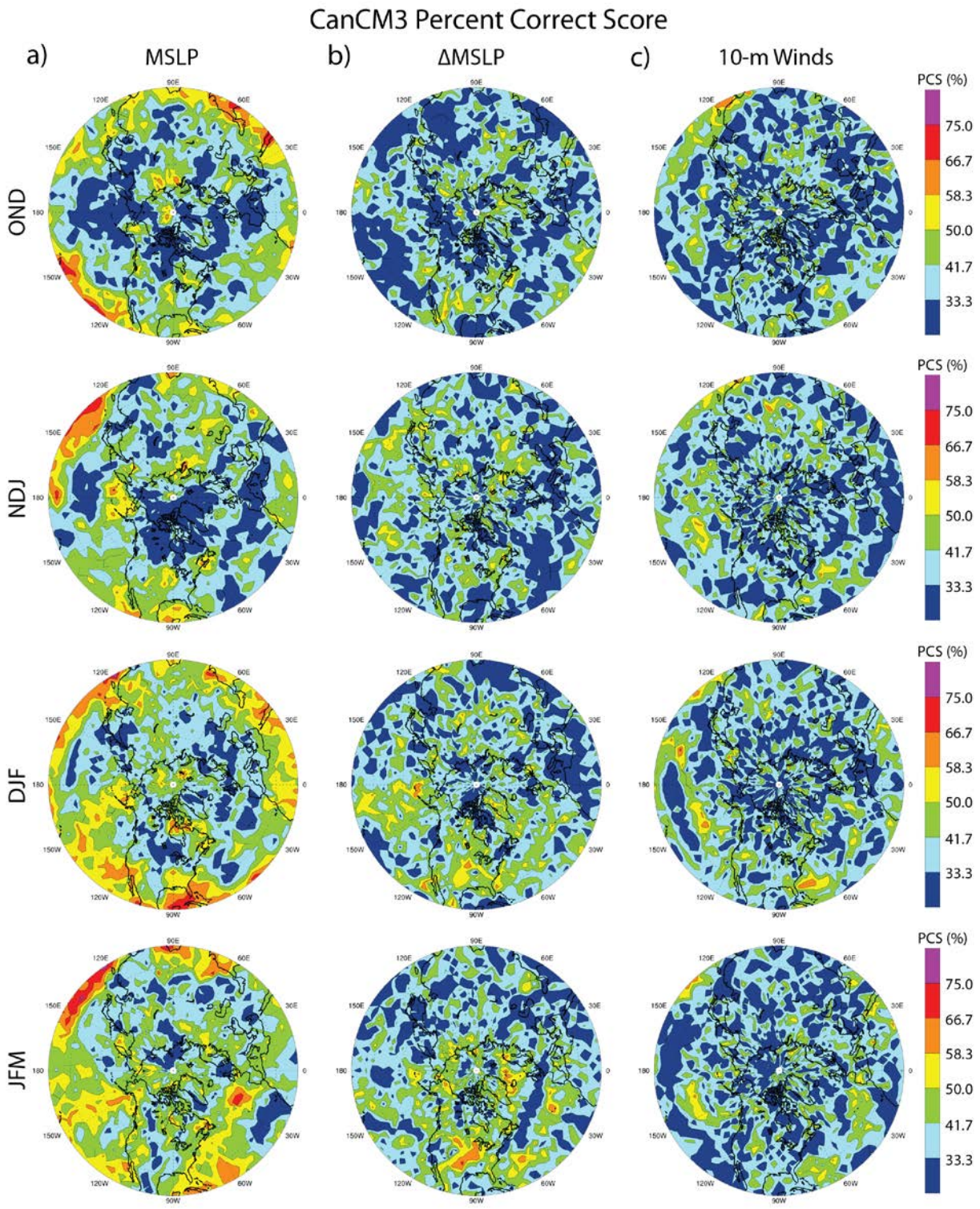

Figure C.9: CanCM3 percent correct scores for the rolling 3-month cold seasons (OND, NDJ, DJF, JFM; top to bottom) for a) MSLP, b) ΔMSLP, and c) 10-m wind speed.

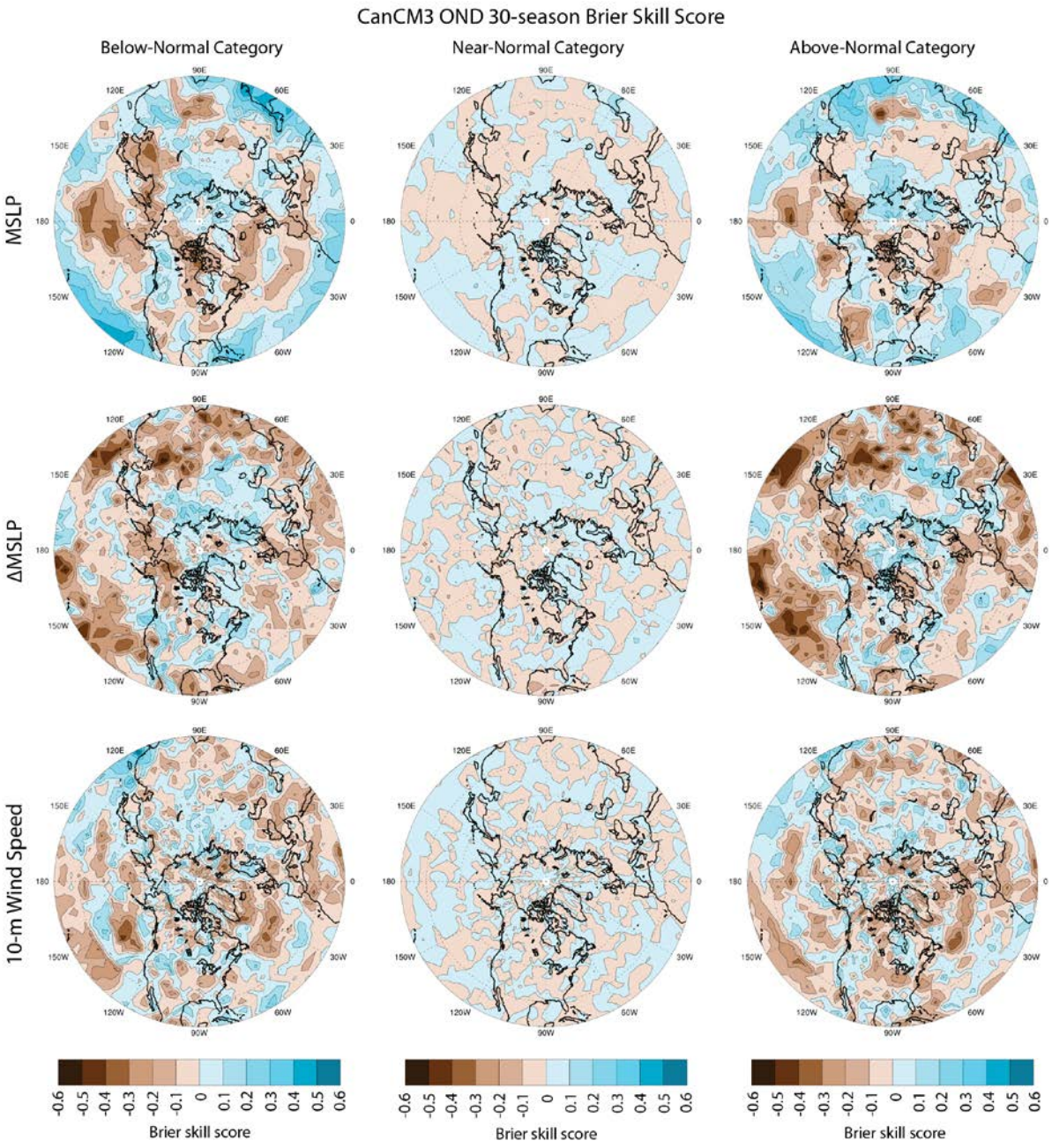

Figure C.10: Brier skill scores assessed over the 30-year seasonal CanCM3 hindcast sequences for the Northern Hemisphere (20°N-poleward) OND MSLP (top), ΔMSLP (middle), and 10-m wind speed (bottom) forecasts.

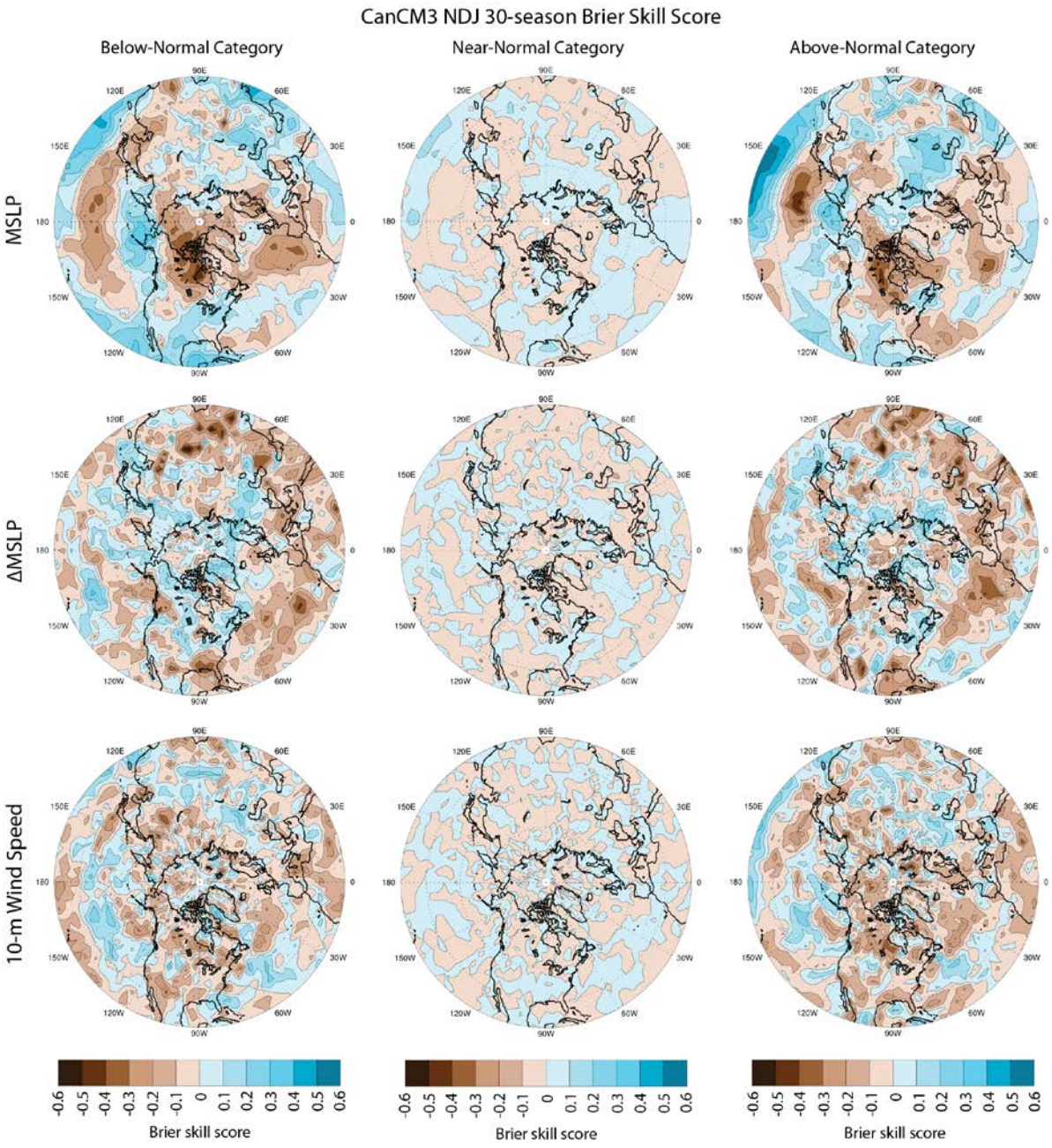

Figure C.11: As in Figure C.10, except for NDJ.

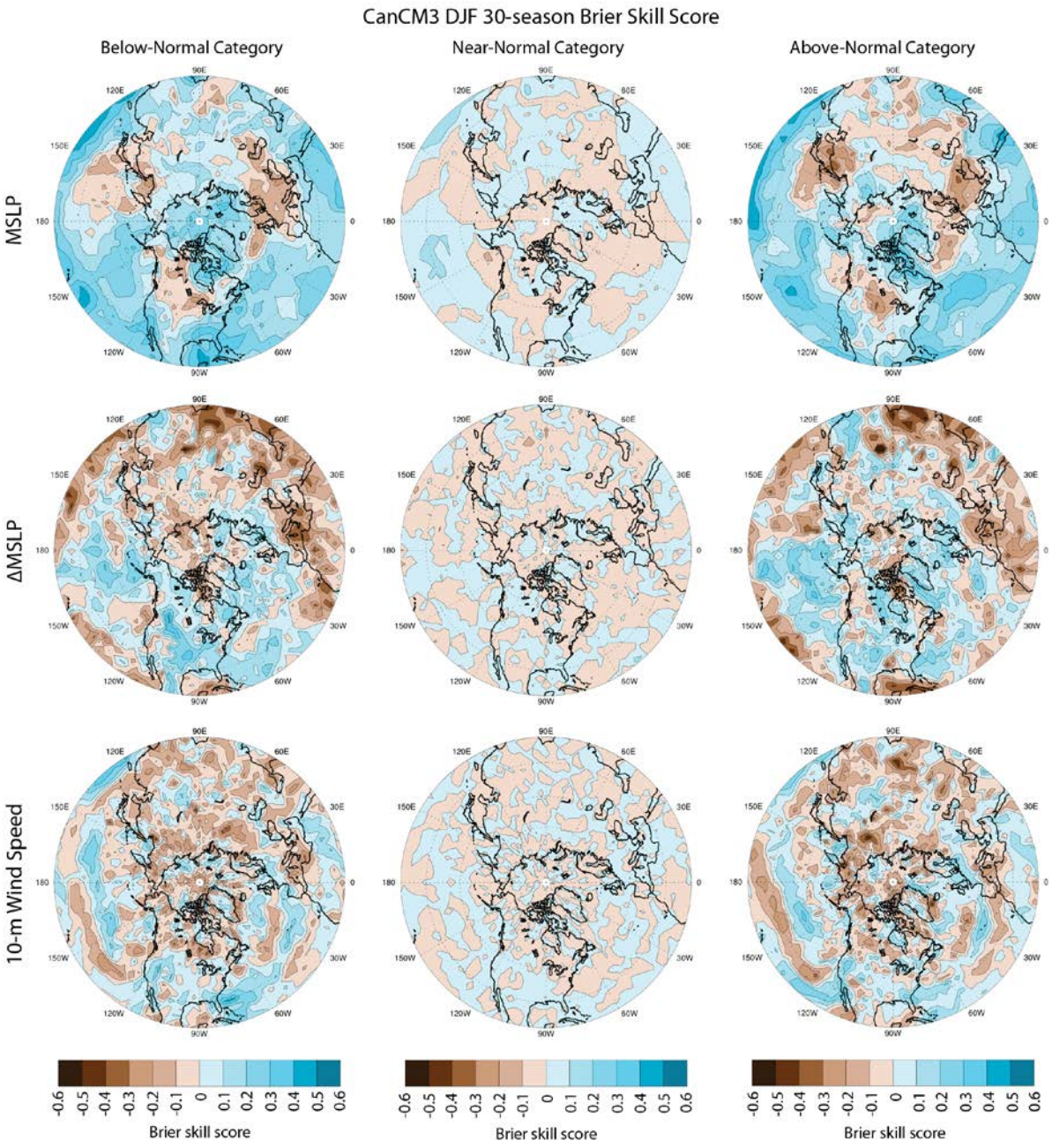

Figure C.12: As in Figure C.10, except for DJF.

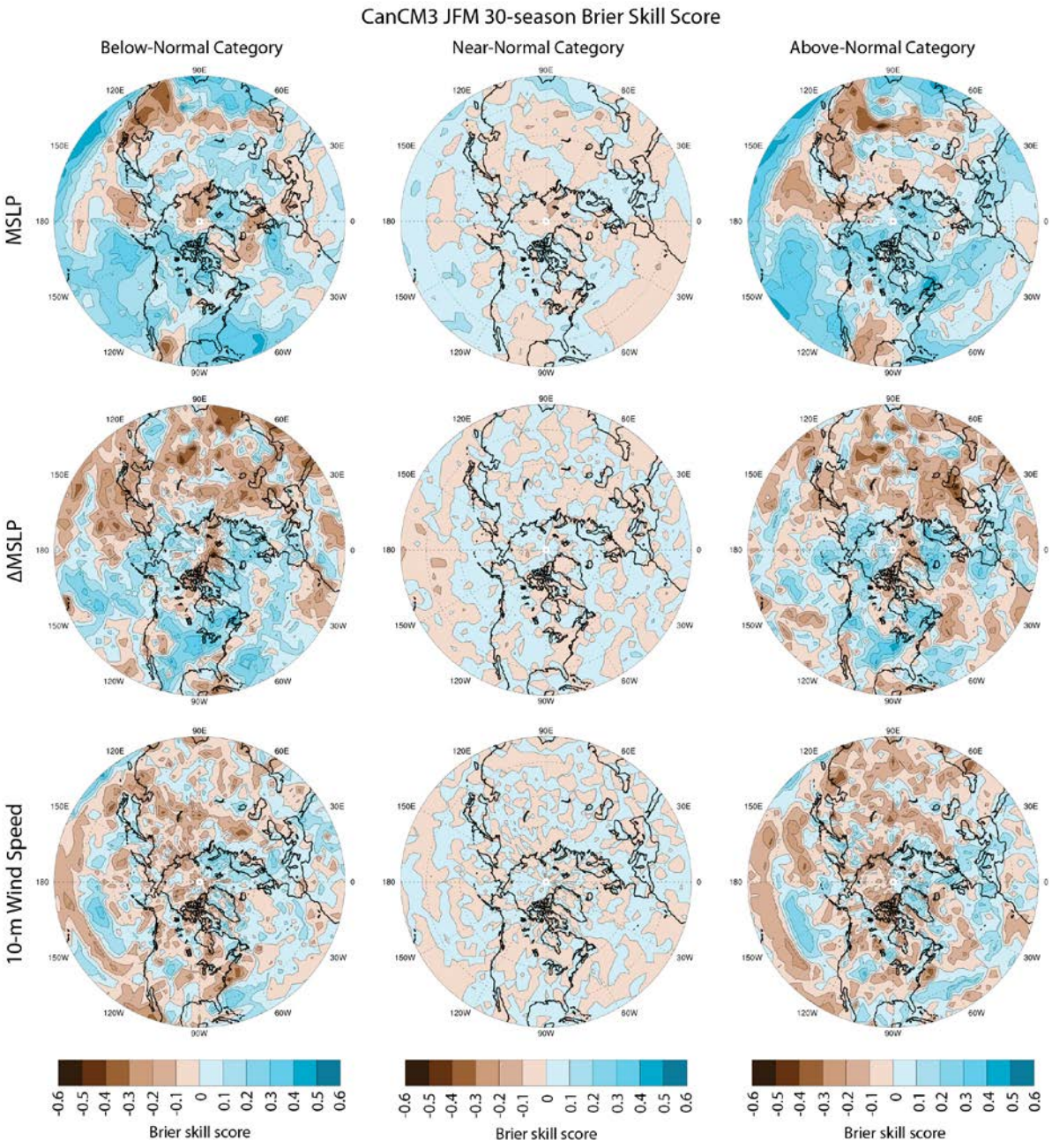

Figure C.13: As in Figure C.10, except for JFM.

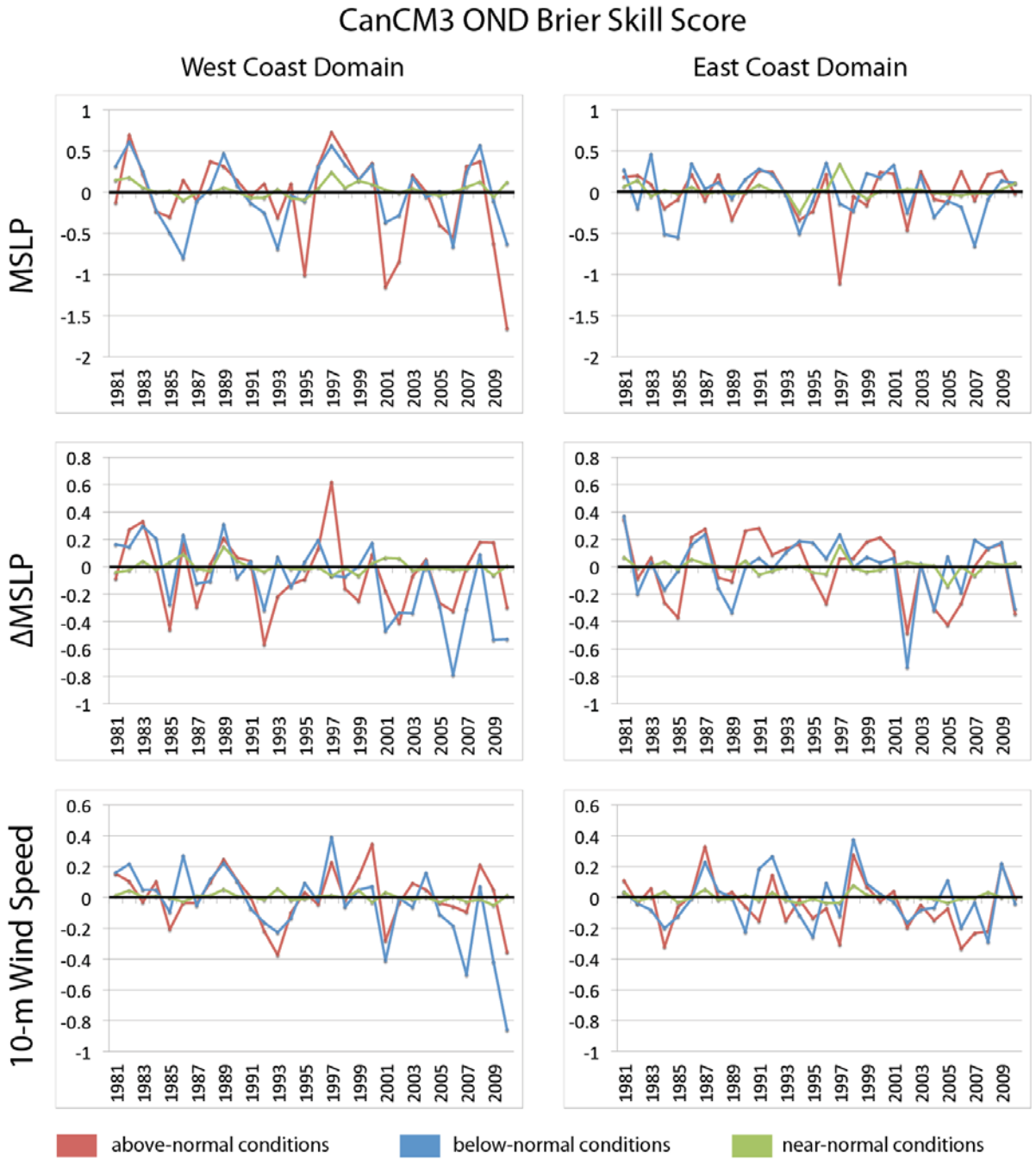

Figure C.14: Temporal variation in CanCM3 forecast performance as measured by the Brier skill scores assessed for the North American west and east coast study domains (Figure 6.1) for OND MSLP (top), ΔMSLP (middle), and 10-m wind speed (bottom) forecasts.

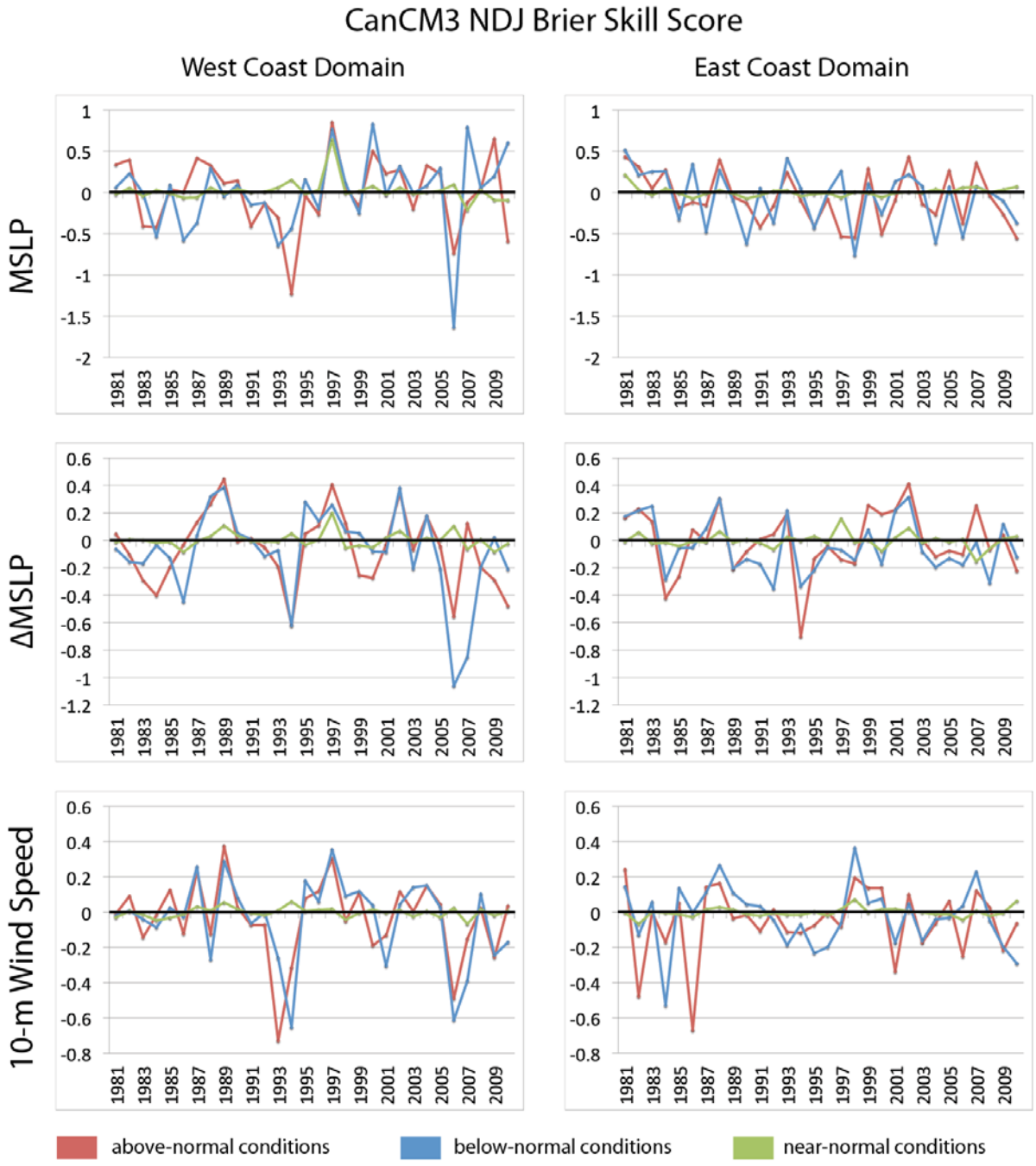

Figure C.15: As in Figure C.14, except for NDJ.

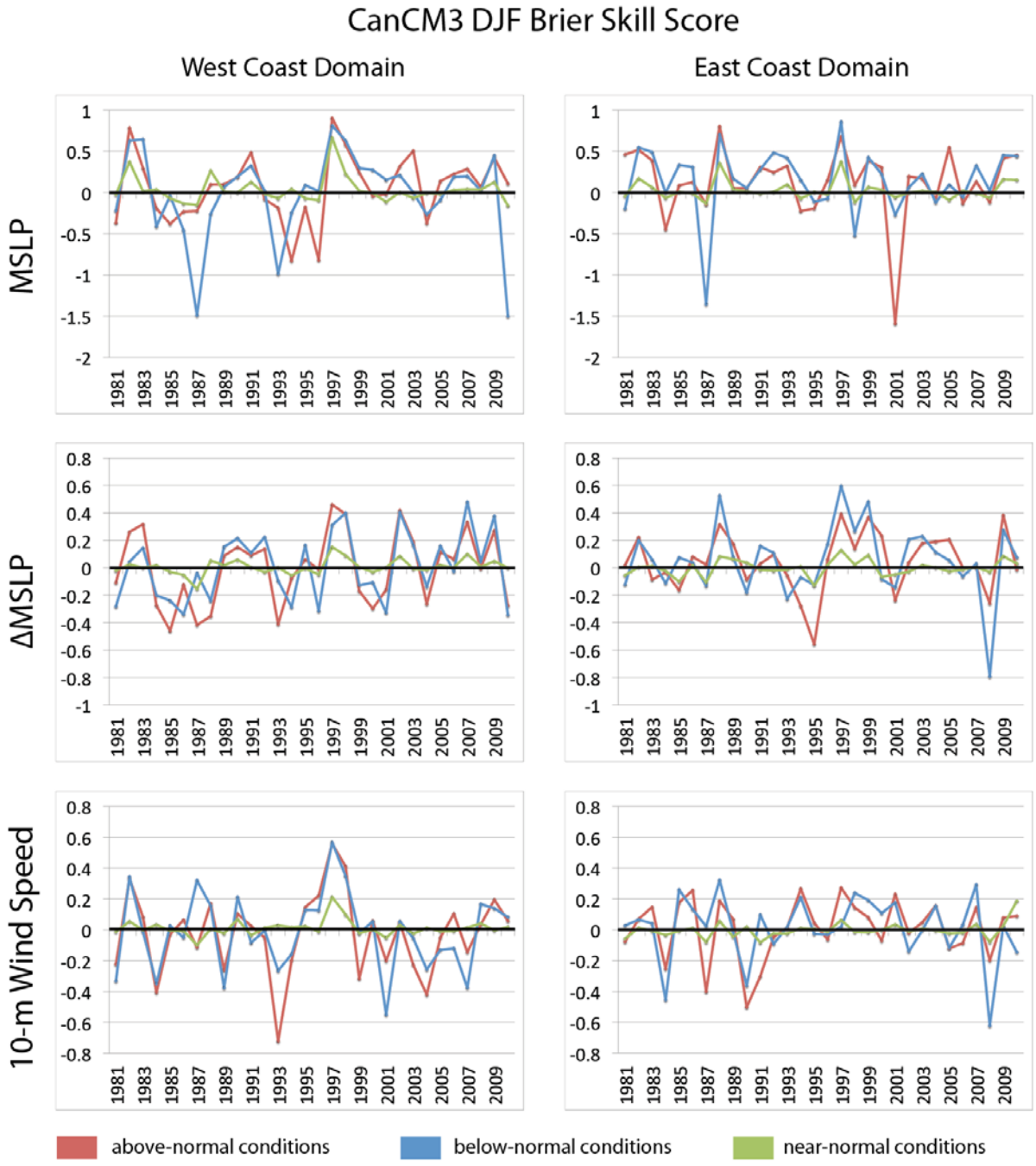

Figure C.16: As in Figure C.14, except for DJF.

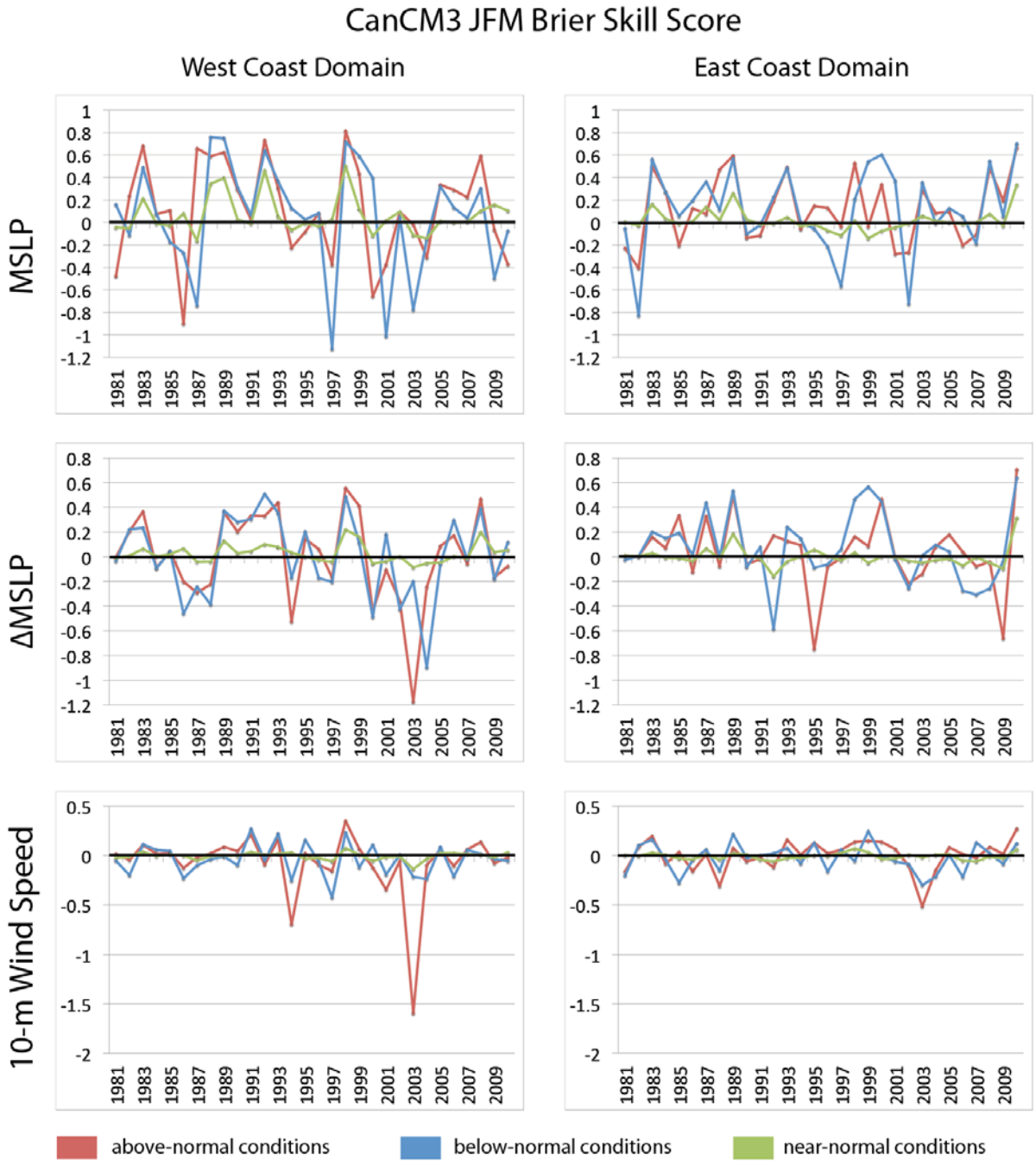

Figure C.17: As in Figure C.14, except for JFM.

C.3 Seasonal Prediction Skill of CanCM4

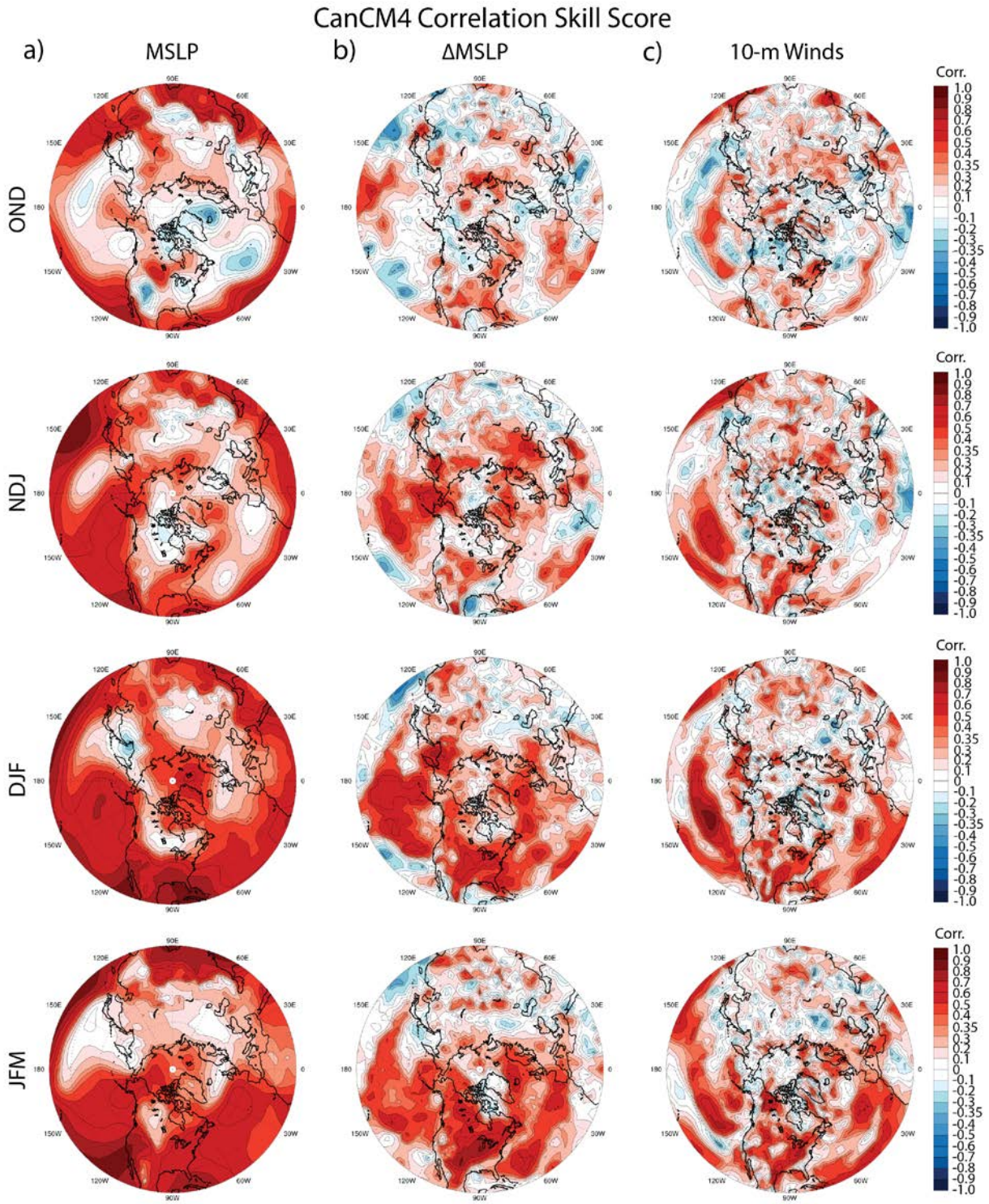

Figure C.18: CanCM4 correlation skill scores for the rolling 3-month cold seasons (OND, NDJ, DJF, JFM; top to bottom) for a) MSLP, b) ΔMSLP, and c) 10-m wind speed.

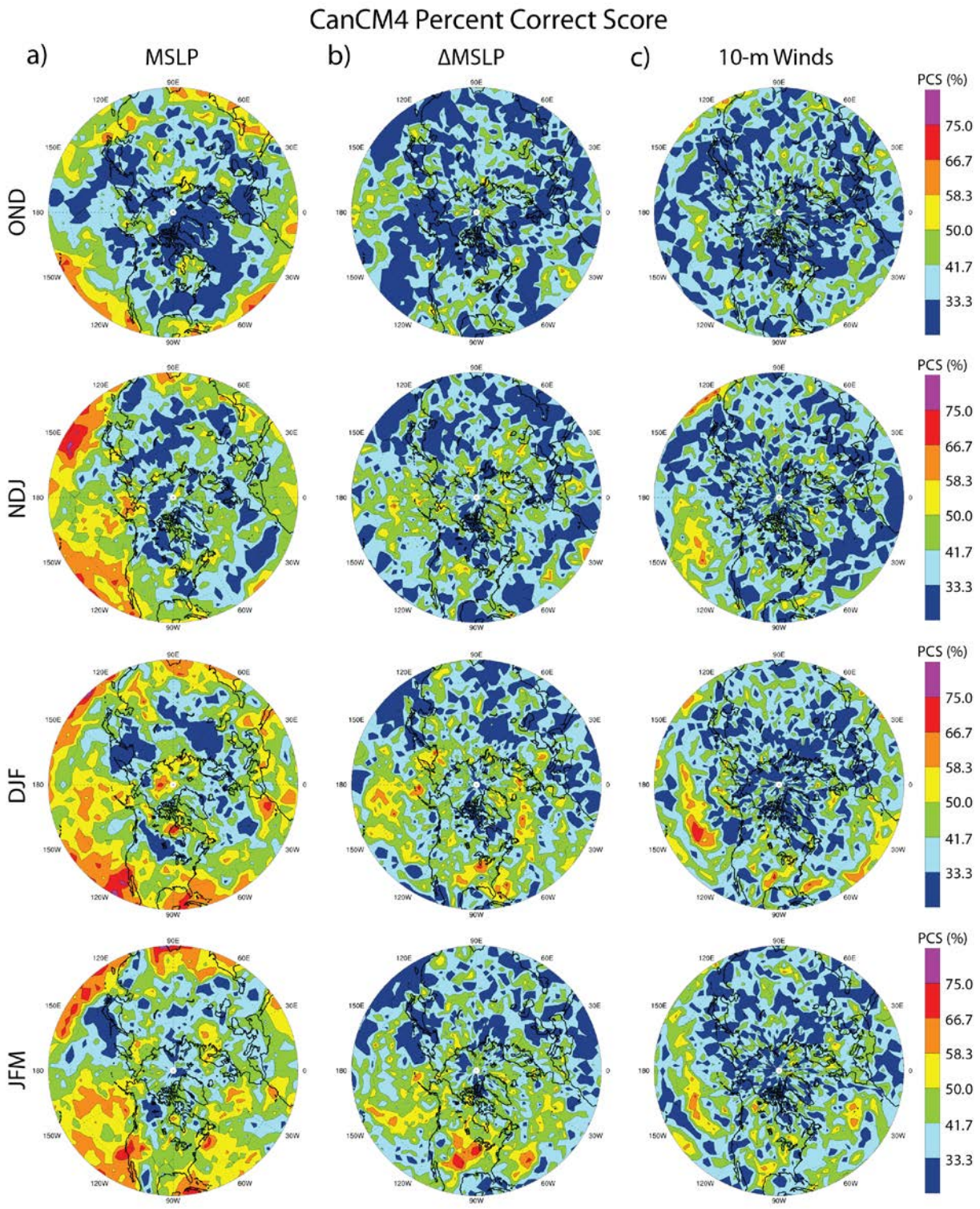

Figure C.19: CanCM4 percent correct scores for the rolling 3-month cold seasons (OND, NDJ, DJF, JFM; top to bottom) for a) MSLP, b) ΔMSLP, and c) 10-m wind speed.

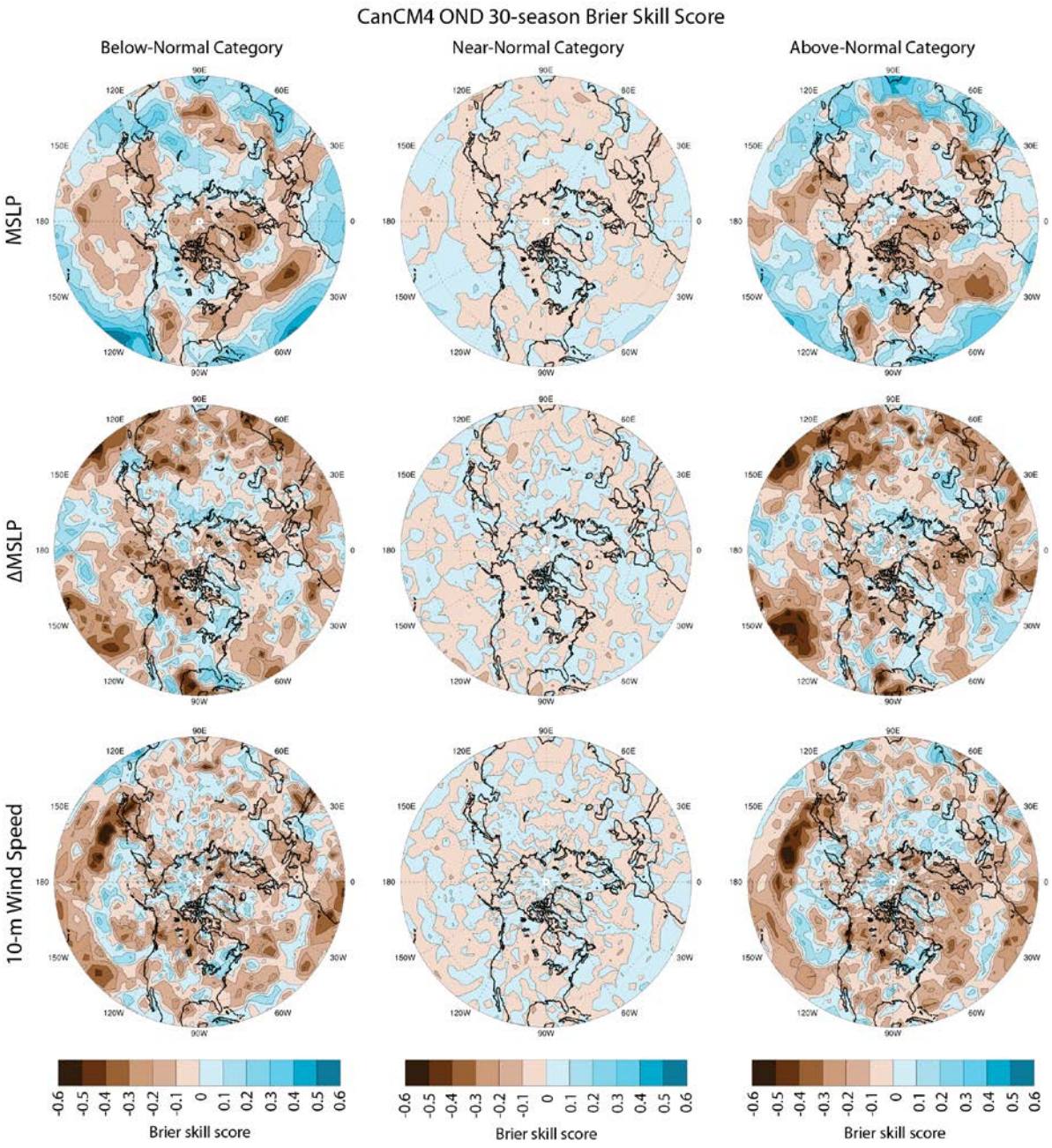

Figure C.20: Brier skill scores assessed over the 30-year seasonal CanCM4 hindcast sequences for the Northern Hemisphere (20°N-poleward) OND MSLP (top), ΔMSLP (middle), and 10-m wind speed (bottom) forecasts.

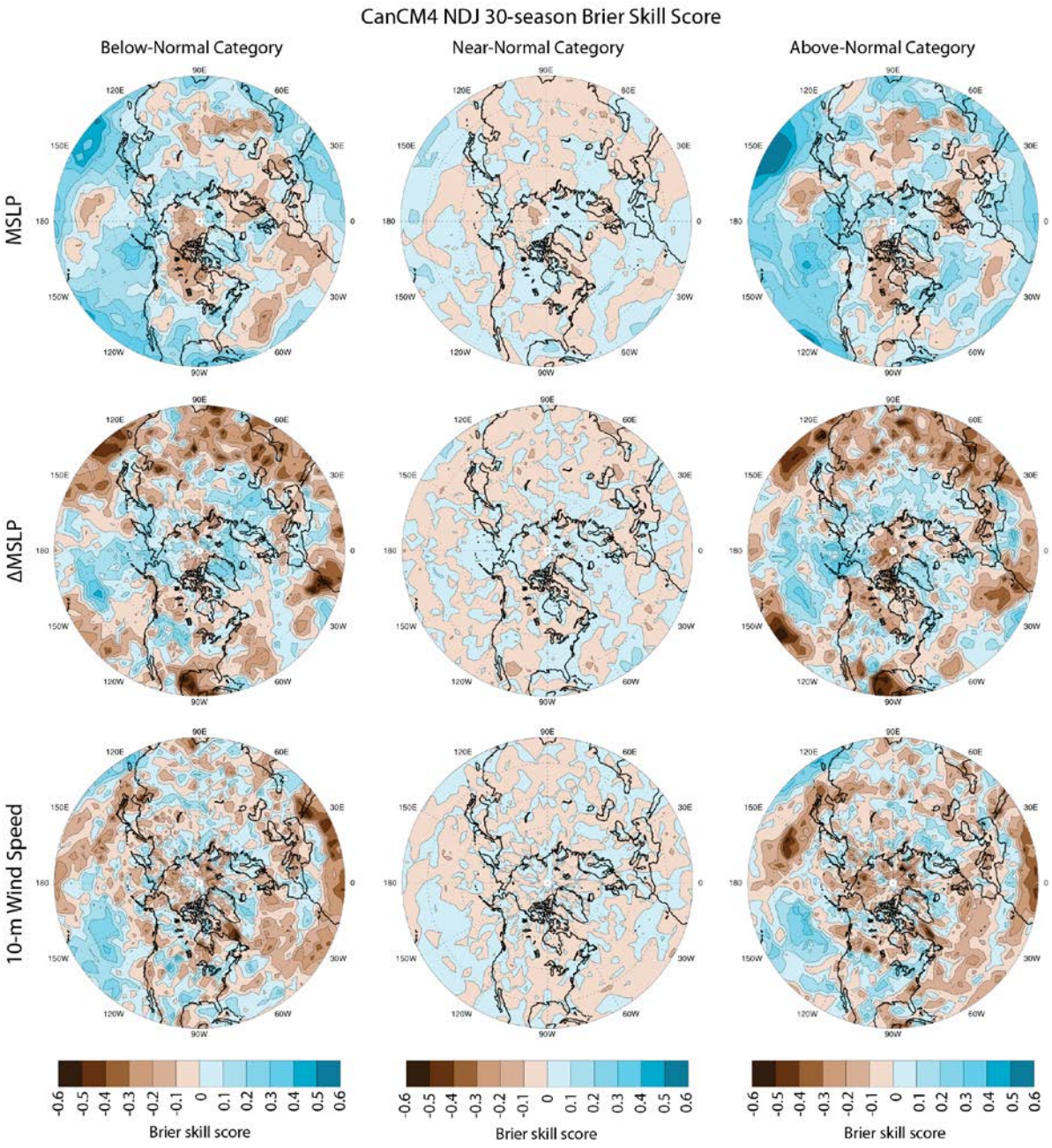

Figure C.21: As in Figure C.20, except for NDJ.

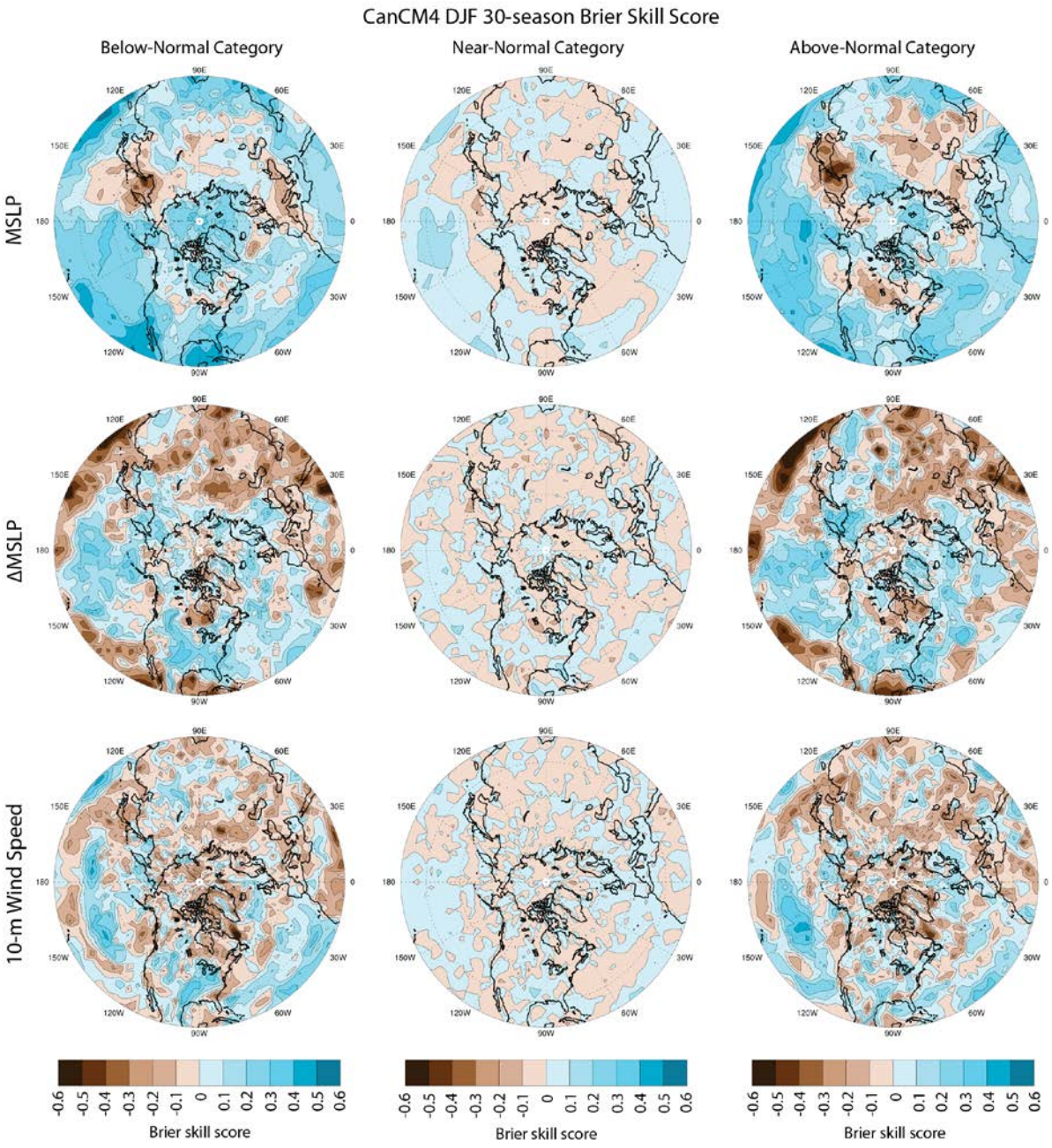

Figure C.22: As in Figure C.20, except for DJF.

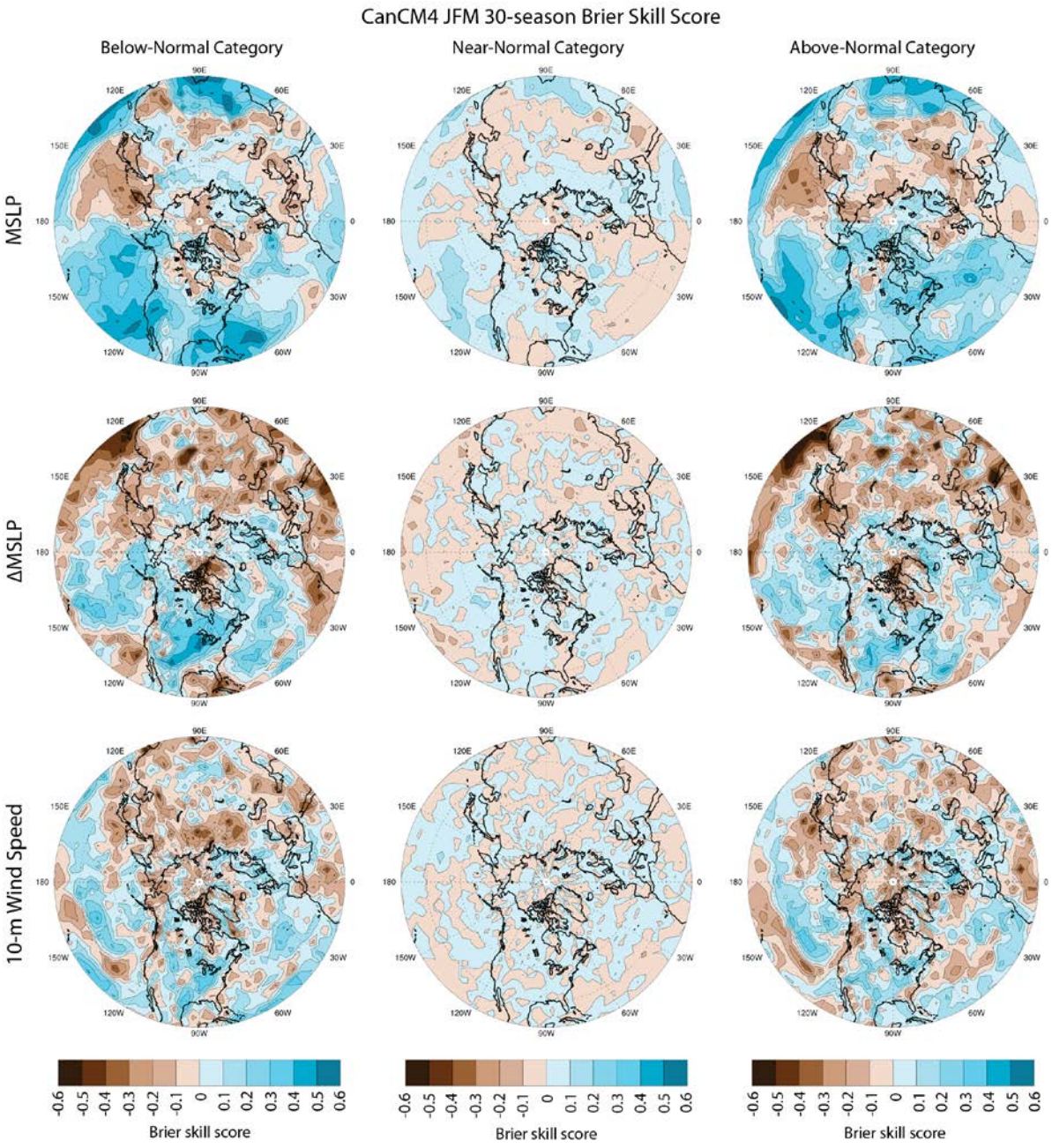

Figure C.23: As in Figure C.20, except for JFM.

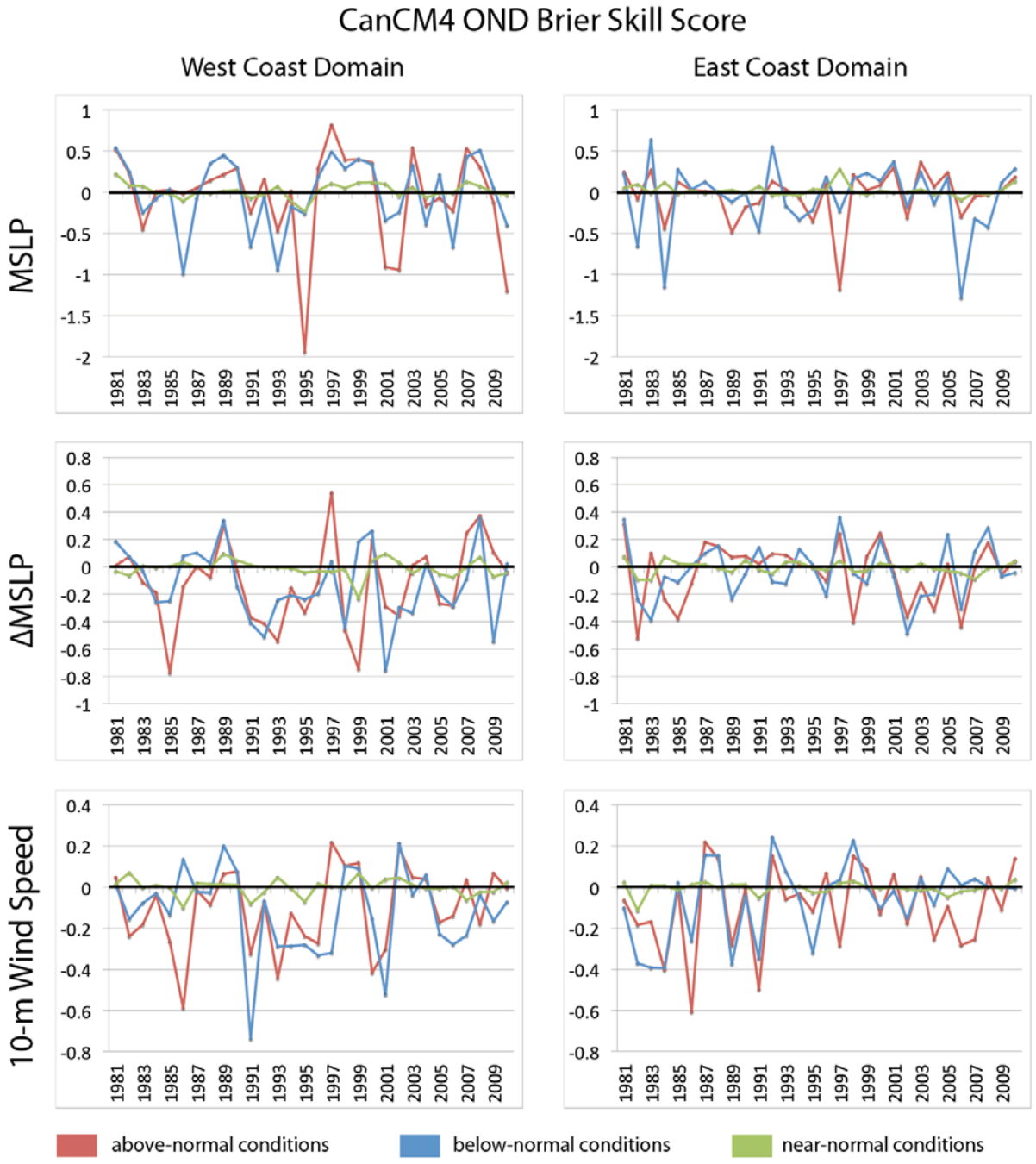

Figure C.24: Temporal variation in CanCM4 forecast performance as measured by the Brier skill scores assessed for the North American west and east coast study domains (Figure 6.1) for OND MSLP (top), ΔMSLP (middle), and 10-m wind speed (bottom) forecasts.

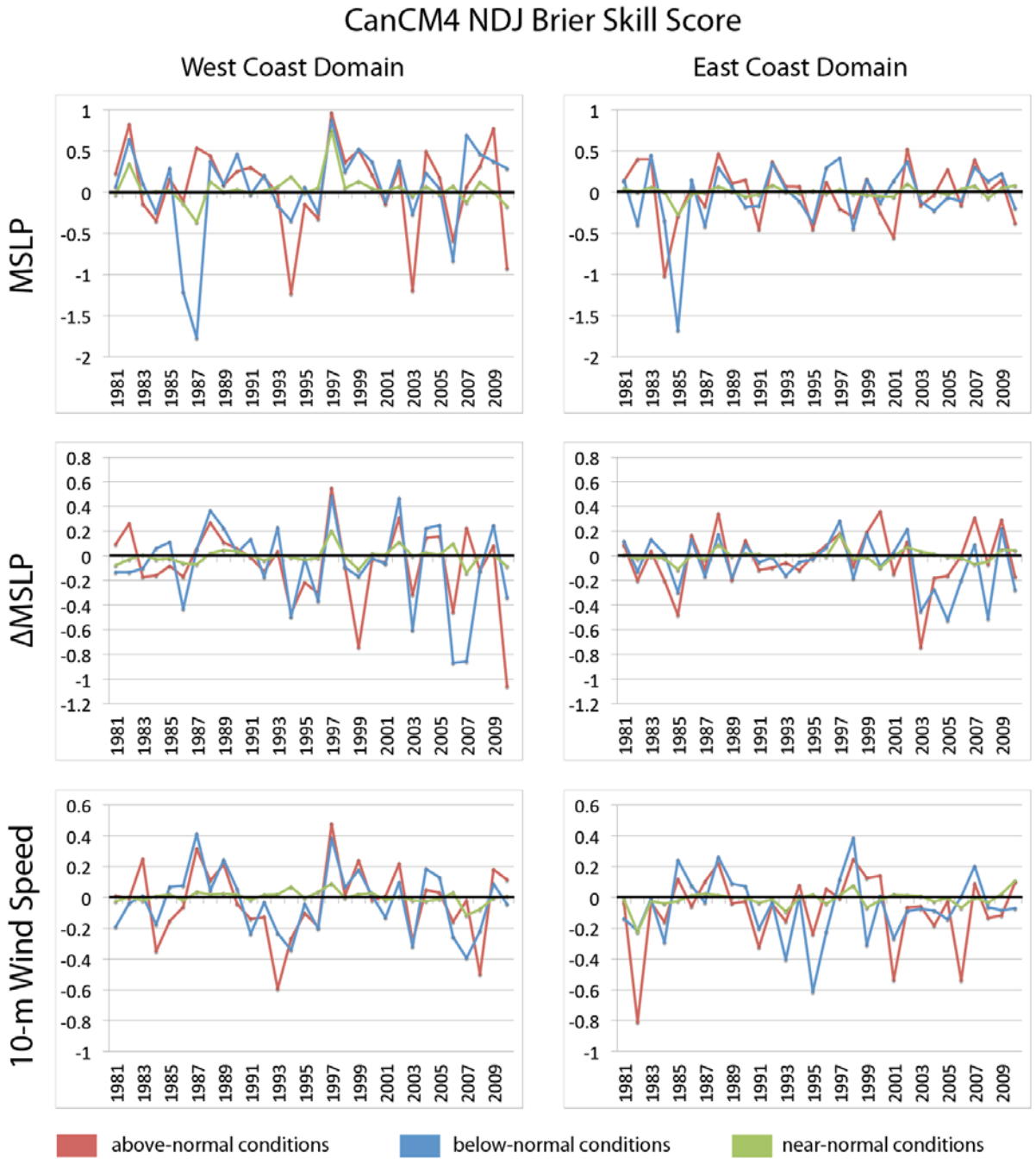

Figure C.25: As in Figure C.24, except for NDJ.

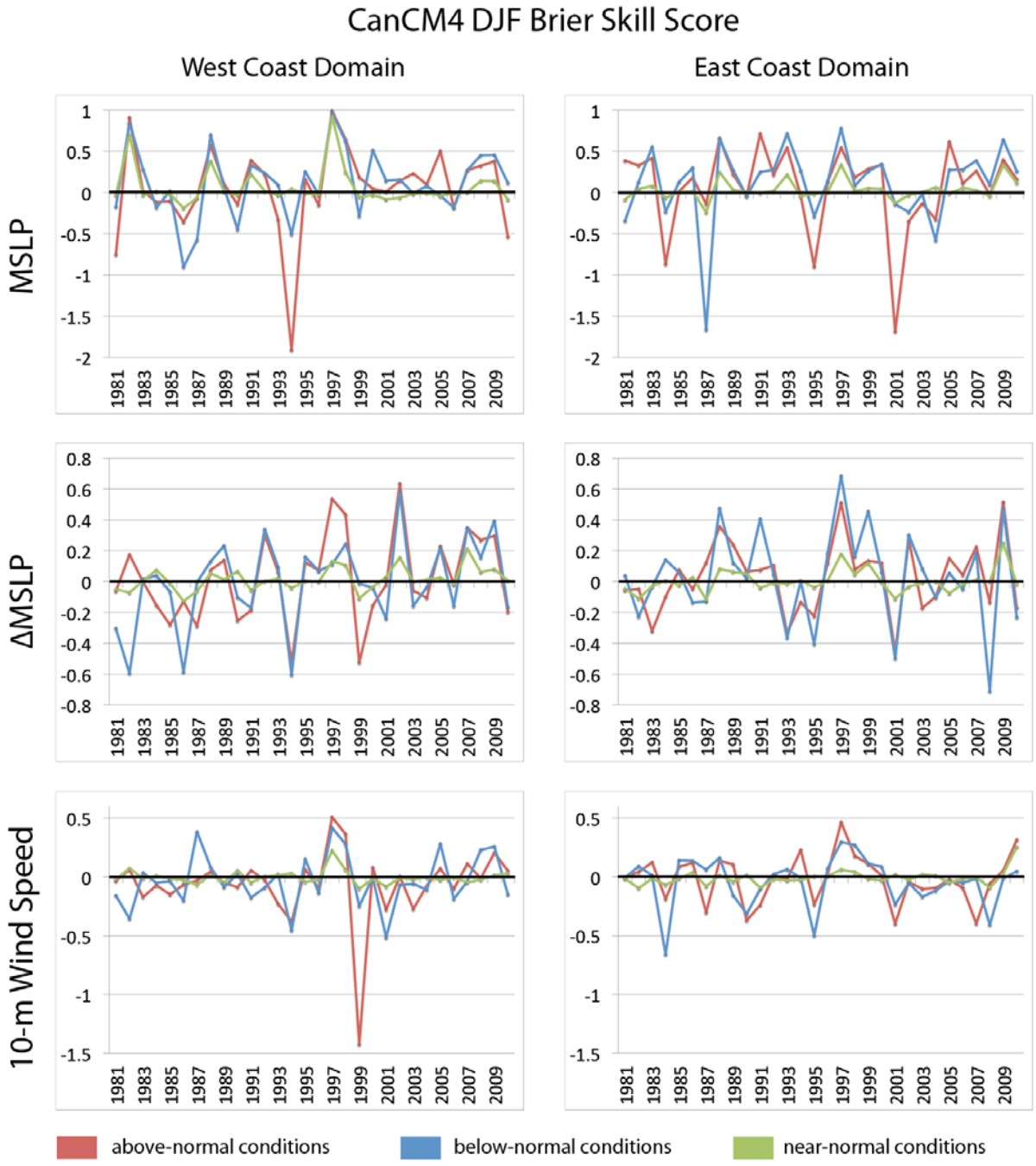

Figure C.26: As in Figure C.24, except for DJF.

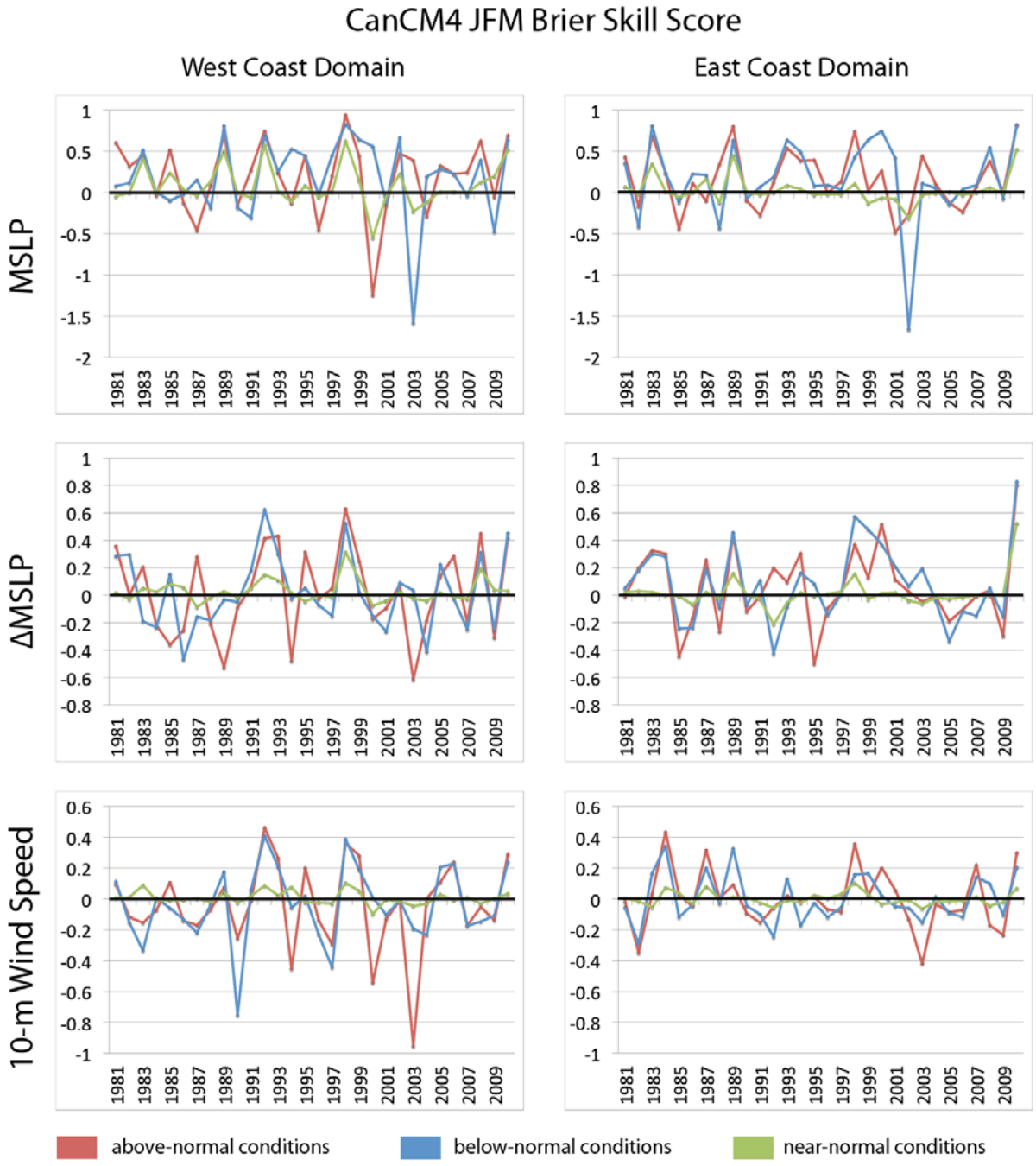

Figure C.27: As in Figure C.24, except for JFM.